



UNIVERSITY OF
BIRMINGHAM

Mechanistic understanding of the Rotating Membrane Emulsification
process towards the development of design and scale-up theory

By

DAVID MATTHEW LLOYD

A thesis submitted to

The University of Birmingham

For the degree of

DOCTOR OF ENGINEERING

School of Chemical Engineering
College of Engineering and Physical Sciences
University of Birmingham
August 2015

UNIVERSITY OF
BIRMINGHAM

University of Birmingham Research Archive

e-theses repository

This unpublished thesis/dissertation is copyright of the author and/or third parties. The intellectual property rights of the author or third parties in respect of this work are as defined by The Copyright Designs and Patents Act 1988 or as modified by any successor legislation.

Any use made of information contained in this thesis/dissertation must be in accordance with that legislation and must be properly acknowledged. Further distribution or reproduction in any format is prohibited without the permission of the copyright holder.

Abstract

The effect of processing and formulation parameters on the resulting oil-in-water emulsion microstructure has been studied for a recently developed process; rotating membrane emulsification. A broad range of surfactant and particle dispersions were explored to reveal the key drivers that determine the final average droplet size produced. The aim of the study was to understand initial droplet generation. Emulsion stability, whilst being a significant element in emulsification studies, is not considered here. By furthering the understanding of the processing mechanisms involved, this enabled development of theoretical models to estimate droplet size and extent of coalescence from first principles. In addition, the implications of process scale-up were studied. From this work, the very first design procedure for rotating membrane emulsification was derived and proposed.

The final emulsion microstructure is heavily dependent on the coupled interaction between the fluid flow behaviour of the two phases and interfacial phenomena. Careful selection of process parameters based on sufficient characterisation of properties such as interfacial tension and viscosity, can avoid the occurrence of droplet coalescence or dispersed phase jetting. These can have a detrimental effect on producing a carefully controlled microstructure on a repeatable basis. Of particular importance is the rate of surfactant adsorption at the oil/water interface. A unique approach of dispersing non-ionic, high HLB surfactants such as Tween 20 and Brij 97 within the oil phase has been found to significantly reduce droplet size. This discovery allows the process to be highly competitive with a rotor-stator high shear mixer and an ultrasonic probe at a fraction of the energy consumption. Pilot-scale operation of rotating membrane emulsification provided important insight into how one might design and therefore implement the process for an industrial purpose. It is proposed here that a suitable scale-up parameter would be the membrane surface velocity.

To Rachael

Acknowledgements

I would like to thank the following people:

My supervisors, Dr. Fotis Spyropoulos and Professor Ian Norton from the University of Birmingham for their help and guidance throughout my project.

Richard Greenwood for his encouragement, support and management of the Formulation Engineering EngD programme.

Patrick Mulqueen and Phil Taylor, alongside those from Syngenta (Jealott's Hill, UK) and the National Physical Laboratory (Teddington, UK) who have contributed to this work.

EPSRC and the Technology Strategy Board for their financial support.

My friends at the University of Birmingham for the good times.

My family (Mum, Dad, Chris and Nikki), my partner Rachael Swinney and her family (Adrian, Lesley, Rebecca and Hannah) for their amazing support, interest, encouragement and love throughout the EngD duration. I would not have completed this without you!

Table of Content

1. Introduction	1
1.1 Background to Research	2
1.1.1 Introduction to Emulsions	2
1.1.2 Challenges within Emulsification	3
1.1.3 Introduction to Project	5
1.2 Objectives	7
1.3 Business Case	8
1.4 Thesis Layout	10
1.5 Publications, Presentations & Awards	11
2. Literature Review	13
2.1 Emulsions and Emulsification	14
2.1.1 Fundamentals of Emulsion Formation	14
2.1.2 Emulsion Stability	20
2.1.3 The Physics of Conventional Emulsification	22
2.2 Membrane Emulsification	24
2.2.1 Process Development	25
2.2.2 Membrane Development	29
2.2.3 Droplet Formation Mechanisms	33
2.2.4 Fluid Flow Behaviour	41
2.3 Modelling of Membrane Emulsification Processing	47
2.4 Scale-up of Membrane Emulsification Processes	54
3. Materials and Methods	57
3.1 Chemical Components	58
3.1.1 Emulsions	58
3.1.2 Surfactants	58
3.1.2.1 Tween 20 (Polyoxyetheylene (20) Sorbitan Monolaurate)	59
3.1.2.2 Brij 97 (Polyethylene Glycol (10) Monooleyl Ether)	59
3.1.2.3 Sodium Dodecyl Sulphate	59
3.1.2.4 Hydrolysed Lecithin	60
3.1.3 Particles	60
3.1.3.1 Aerosil Silica	60

3.1.3.2 Ludox Silica	61
3.1.4 Surfactant/Particle Mixtures	61
3.2 Equipment	61
3.2.1 Emulsification Processes	61
3.2.1.1 Small-scale Rotating Membrane Emulsification	61
3.2.1.2 Pilot-scale Rotating Membrane Emulsification	64
3.2.1.3 Rotor-stator High Shear Mixer: The Silverson L4RT	68
3.2.1.4 Ultrasonic Emulsification: The Ultrasonic Vibracel Processor	68
3.2.2 Characterisation Equipment	69
3.2.2.1 Laser Diffraction Particle Size Analysis.....	69
3.2.2.2 Dispersed Phase Flux Measurement	72
3.2.2.3 Interfacial Tension Measurement	72
3.2.2.4 Rheology	75
3.2.2.5 Density	75
3.2.2.6 Temperature	75
3.2.2.7 Process Energy Consumption during Emulsification	76
4. Processing Effects using a Small-scale Rotating Membrane Emulsification Device	77
4.1 Introduction and Preliminary Studies	78
4.2 Effect of Transmembrane Pressure	83
4.2.1 On the resultant Droplet Size	83
4.2.2 On the Flux through the Membrane	89
4.3 Effect of Rotational Speed	92
4.4 Effect of Annular Gap Width	94
4.5 Effect of Shear Rate with Transmembrane Pressure	98
4.6 Viscosity Effects	99
4.6.1 Dispersed Phase Viscosity	100
4.6.2 Continuous Phase Viscosity	103
4.6.3 Viscosity Ratio	107
4.7 Conclusions	110
5. Formulation Effects using a Small-scale Rotating Membrane Emulsification Device	112
5.1 Introduction	113
5.2 Effect of Surfactant Type/Concentration	114
5.3 Effect of Transmembrane Pressure with Surfactant Type	121
5.4 Effect of Shear Rate with Surfactant Type	125

5.5 Effect of Particle Type/Concentration	127
5.6 Effect of Transmembrane Pressure with Particle Type	131
5.7 Effect of Shear Rate with Particle Type	133
5.8 Surfactant/Particle Mixtures	135
5.9 Effect of Surfactant Positioning	138
5.10 Pre-mix Rotating Membrane Emulsification	145
5.11 Conclusions	149
6. Theoretical Modelling and Process Comparison	151
6.1 Introduction	152
6.2 Model to Estimate the Probability of Coalescence	152
6.3 Application of the Force Balance Model to Predict Droplet Size	160
6.4 Process Comparison of the Basis of Production Rate	168
6.5 Process Comparison on the Basis of Energy Consumption	171
6.6 Conclusions	175
7. Operation using a Pilot-Scale Rotating Membrane Emulsification Device	177
7.1 Introduction	178
7.2 Effect of Transmembrane Pressure	179
7.3 Effect of Rotational Speed	181
7.4 Comparison with Small-scale Rotating Membrane Device	183
7.5 Effect of Surfactant Type/Concentration	188
7.6 Effect of Surfactant Positioning	189
7.7 Energy Considerations	191
7.8 Recommended Procedure for Process Design	193
7.9 Conclusions	197
8. Conclusions	199
9. Future Work	205
9.1 Operation as a Continuous Process	206
9.2 Effect of Temperature	206
9.3 Further Study of Surfactant Diffusion through an Interface	207
9.4 Bi-modal Emulsion Production	207

Appendix A208

References213

List of Figures

Fig. 2.1: A schematic representation of surfactant molecules at an interface	15
Fig. 2.2: A schematic representation of possible surfactant micelle structures	17
Fig. 2.3: A schematic illustrating various contact angles of a particle adsorbed at an O/W interface	19
Fig. 2.4: A schematic representation of an oil droplet positioned upon a membrane surface.....	30
Fig. 2.5: A schematic representation of the velocities across the horizontal plane of an RME configuration	35
Fig. 2.6: A schematic representation of droplet growth and detachment at a membrane surface, leading to creation of an emulsion	36
Fig. 2.7: Droplet deformation giving rise to spontaneous detachment and transformation	37
Fig. 2.8: A schematic representing droplet formation through dispersed phase jetting	39
Fig. 2.9: Mapping of the transitional point between dripping and jetting droplet formation mechanism	40
Fig. 2.10: Inclusion of Ohnesorge number in the mapping of the transitional point between dripping and jetting droplet formation mechanism	41
Fig. 2.11: A schematic diagram representing dispersed phase velocity change as a droplet grows at the membrane surface	44
Fig. 2.12: Possible alignments of Taylor vortices relative to a forming droplet	46
Fig. 2.13: Schematic (a) and magnitude (b) of forces acting on a droplet during cross-flow membrane emulsification (Schroder <i>et al.</i> , 1998). Within this figure, F_γ denotes the interfacial tension force, F_R is the viscous drag force, F_{BG} is the buoyancy force, F_I is the inertial force, F_D is the dynamic lift force and F_{stat} is the static pressure force	49
Fig. 2.14: Pore boundary condition and droplet simulation along minor and major axes; the basis of the surface evolver tool (Rayner <i>et al.</i> , 2004)	51
Fig. 2.15: Computational fluid dynamics (CFD) velocity profile of an oil droplet forming within an aqueous continuous phase (Abrahamse <i>et al.</i> , 2001)	52
Fig. 2.16: Visual representation of droplet formation (where T denotes the droplet formation time) using the lattice Boltzmann method (Van der Zwan <i>et al.</i> , 2009)	53
Fig. 2.17: The membrane area required to produce $20 \text{ m}^3 \text{ h}^{-1}$ of 30% disperse phase culinary cream for different membrane material properties. SPG: Shirasu Porous Glass, A11-3: ceramic $\alpha\text{-Al}_2\text{O}_3$ of increasing pore diameter standard deviation, m1-2: silicon nitride microsieve of increasing upper pore layer resistance (Gijsbertsen-Abrahamse <i>et al.</i> , 2004)	56
Fig. 3.1: A schematic diagram (a) and a photograph (b) of the small-scale rotating membrane emulsification system used within this thesis	63
Fig. 3.2: A schematic diagram (a) and a photograph (b) of the pilot-scale rotating membrane emulsification system used within this thesis	66
Fig. 3.3: A schematic diagram illustrating laser diffraction; the basis behind the Malvern Mastersizer model 2000 used to quantify droplet and particle diameters within this thesis	71
Fig. 3.4: A schematic diagram illustrating interfacial tension measurement with the Kruss Goniometer	73

Fig. 3.5: A schematic indicating the possible measurement configurations depending on the properties of the material used to form the droplet	73
Fig. 4.1: 2 Week stability data of 10 vol. % Sunflower Oil-in-water emulsions stabilised by 1 wt. % Tween 20 ..	79
Fig. 4.2: Droplet size distributions for an initial emulsion and after 1 hour of shear at a rate of 139.6 s^{-1} applied using the rotating membrane emulsification equipment without dispersed phase addition	80
Fig. 4.3: Bulk rheological measurements to compare dynamic viscosity values for a range of Sunflower Oil-in-water emulsions with the initial surfactant solution (i.e. pure continuous phase)	82
Fig. 4.4: The influence of transmembrane pressure on the mean droplet size for different rotational speeds. The emulsions are 10 vol. % sunflower oil stabilised by 1 wt. % Tween 20. The error bars represent one standard deviation of a triplicate of experimental runs	84
Fig. 4.5: Dynamic interfacial tension between sunflower oil and 1 wt. % Tween 20 solution. (a) shows the initial decrease whilst (b) shows the system equilibrium value. Note: Dotted line and solid line represent back-calculated and measured interfacial tension values respectively	88
Fig. 4.6: Influence of transmembrane pressure on the average dispersed phase flux (a) and active pore fraction (b) for a $6.1 \mu\text{m}$ pore diameter, hydrophilic SPG membrane	90
Fig. 4.7: The influence rotational speed on the mean droplet size at a transmembrane pressure of 0.5 bar. The emulsions are 10 vol. % sunflower oil stabilised by 1 wt. % Tween 20. The error bars represent one standard deviation of a triplicate of experimental runs	93
Fig. 4.8: Droplet size distributions for emulsions produced at a transmembrane pressure of 0.5 bar. The emulsions are 10 vol. % sunflower oil stabilised by 1 wt. % Tween 20	94
Fig. 4.9: The influence of gap width and rotational speed on the mean emulsion droplet size at 0.5 bar. The emulsions are 10 vol. % sunflower oil stabilised by 1 wt. % Tween 20. The error bars represent one standard deviation and where not visible are smaller than the symbols	95
Fig. 4.10: Relationship between droplet size and the shear rate at the membrane surface for the different gap widths and rotational speeds investigated, at 0.5 bar	96
Fig. 4.11: Relationship between mean emulsion droplet size and (continuous phase) Taylor number as a function of rotational speed, at a transmembrane pressure of 0.5 bar	97
Fig. 4.12: Relationship between mean emulsion droplet size and shear rate at a low (0.2 bar) and high (1.5 bar) transmembrane pressure	98
Fig. 4.13: The influence of transmembrane pressure on the mean droplet size for different oil viscosities. The emulsions are 10 vol. % silicone oil stabilised by 1 wt. % Tween 20. The error bars represent one standard deviation of a triplicate of experimental runs	100
Fig. 4.14: Dynamic interfacial tension between silicone oil of varying viscosity and 1% Tween 20 solution. (a) shows the initial decrease whilst (b) shows the system equilibrium value. Note: Dotted line and solid line represent back-calculated and measured interfacial tension values respectively	102
Fig. 4.15: Influence of transmembrane pressure on the dispersed phase flux for differing viscosity silicone oil through a $6.1 \mu\text{m}$ pore diameter, hydrophilic SPG membrane	103
Fig. 4.16: The influence of continuous phase viscosity and shear rate on the mean droplet size at 0.5 bar using a $6.1 \mu\text{m}$ pore diameter, hydrophilic SPG membrane	105
Fig. 4.17: Dynamic interfacial tension between sunflower oil and continuous phase containing variable concentration of glycerol and 1 wt. % Tween 20	106

Fig. 4.18: The influence of viscosity ratio on the mean droplet size stabilised by 1 wt. % Tween 20. The ratio was modified by using different viscosity silicone oils and varying the quantity of glycerol within the continuous phase. The error bars represent one standard deviation of a triplicate of experimental run	107
Fig. 5.1: Dynamic interfacial tension between sunflower oil and water with no surfactant present	116
Fig. 5.2: The effect of surfactant concentration on the mean droplet size for different surfactant types positioned within the aqueous continuous phase. The emulsions are 10 vol. % sunflower oil-in-water. The transmembrane pressure is 0.5 bar and the shear rate is 5.98 s^{-1} . The dotted lines are to guide the eye across the data set. The error bars represent one standard deviation of a triplicate of experimental runs	117
Fig. 5.3: Dynamic interfacial tension between sunflower oil and continuous phase containing variable concentration of surfactants: (a) Tween 20, (b) Brij 97, (c) SDS and (d) Lecithin	119
Fig. 5.4: The influence of transmembrane pressure on the mean droplet size for different surfactant types and concentrations. A shear rate of 5.98 s^{-1} is applied corresponding to a rotational speed of 1000 RPM and an annular gap width of 25 mm. The dotted lines are drawn to guide the eye across the data set. The error bars represent one standard deviation of a triplicate of experimental runs	122
Fig 5.5: The influence of shear rate on the mean droplet size for different surfactant types and concentrations. A transmembrane pressure of 0.5 bar is applied. The dotted lines are to guide the eye across the data set. The error bars represent one standard deviation of a triplicate of experimental runs	126
Fig. 5.6: The effect of particle concentration on the mean droplet size for different silica systems positioned within the aqueous continuous phase. The emulsions are 10 vol. % sunflower oil-in-water. The transmembrane pressure is 0.5 bar and the shear rate is 5.98 s^{-1} . The error bars represent one standard deviation of a triplicate of experimental runs	129
Fig. 5.7: Dynamic interfacial tension between sunflower oil and continuous phase containing variable concentration of silica particles: (a) Aerosil (b) Ludox	130
Fig. 5.8: The influence of transmembrane pressure on the mean droplet size for (a) Aerosil and (b) Ludox silica at a low and high concentration of particles. A shear rate of 5.98 s^{-1} is applied corresponding to a rotational speed of 1000 RPM and an annular gap width of 25 mm. The error bars represent one standard deviation of a triplicate of experimental runs	132
Fig 5.9: The influence of shear rate on the mean droplet size for (a) Aerosil and (b) Ludox silica at low and high concentrations of particles. A transmembrane pressure of 0.5 bar is applied. The error bars represent one standard deviation of a triplicate of experimental runs	134
Fig. 5.10: The effect of Tween 20 concentration on the mean droplet size for (a) Aerosil and (b) Ludox silica at a low and high concentration of particles. The transmembrane pressure is 0.5 bar. A shear rate of 5.98 s^{-1} is applied corresponding to a rotational speed of 1000 RPM and an annular gap width of 25 mm. The pH of the continuous phase is 2.0. The error bars represent one standard deviation of a triplicate of experimental runs	136
Fig. 5.11: Dynamic interfacial tension between sunflower oil and continuous phase containing either Ludox (particles), Tween 20 (surfactant) or a combination of the two. The pH was 2.0	138
Fig. 5.12: The influence of transmembrane pressure on the mean droplet size for different surfactant positions. A shear rate of 5.98 s^{-1} is applied corresponding to a rotational speed of 1000 RPM and an annular gap width of 25 mm. The dotted lines are drawn to guide the eye across the data set. The error bars represent one standard deviation of a triplicate of experimental runs	140
Fig. 5.13: Dynamic interfacial tension between distilled water and sunflower oil containing variable concentration of surfactants: (a) Tween 20, (b) Brij 97, (c) Lecithin	142

Fig. 5.14: The influence of shear rate on the mean droplet size for different surfactant positions. A transmembrane pressure of 0.5 bar is applied. The dotted lines are drawn to guide the eye across the data set. The error bars represent one standard deviation of a triplicate of experimental runs	143
Fig. 5.15: Images of droplet formation and initial detachment stages from a 1.8 mm diameter needle under quiescent continuous phase conditions. Sunflower oil, water and 1 wt. % Tween 20 were used in all cases. The surfactant positioning and injection rate between low (100 $\mu\text{l min}^{-1}$) and high (1000 $\mu\text{l min}^{-1}$) were varied as follows: (a) low & in water, (b) low & in oil, (c) high & in water, (d) high & in oil	144
Fig 5.16: The influence of pass number on mean droplet size using sunflower oil, distilled water and 1 wt. % Tween 20. Pass 0 denotes the initial emulsion droplet size adopting the conventional RME approach. Pass 1-3 denotes the extent of droplet break up as the initial emulsion is passed through the membrane repeatedly. A transmembrane pressure of 0.5 bar and shear rate of 5.98 s^{-1} is applied in all cases. The dotted lines drawn are to guide the eye across the data set. The error bars represent one standard deviation of a triplicate of experimental runs	146
Fig. 5.17: Volume fraction of oil within the final emulsion during process operation at a transmembrane pressure of 0.5 bar and a shear rate of 5.98 s^{-1} . The percentages represent the mass composition of the dispersed phase only. Note: the 90% sunflower oil and 10% Tween 20 data set is representative of the 1 wt. % Tween 20 (o) system	147
Fig. 6.1: A schematic representation of two droplets forming at adjacent active pores. In this case, $L_{x,a} < 2r_d$ indicating coalescence is likely due to droplet interface contact during expansion	154
Fig. 6.2: The basis for calculation of the average distance between pores across the membrane surface assuming a triangular array	155
Fig. 6.3: The probability of coalescence for active pores randomly distributed on the membrane surface as a function of theoretical droplet diameter	159
Fig. 6.4: A schematic representation of the forces acting on a droplet at the point of detachment from the membrane surface	163
Fig. 6.5: Relationship between droplet diameter and the magnitude of detachment and retaining forces based on the conditions listed in Table 6.3	164
Fig. 6.6: A more detailed breakdown of the acting forces on a droplet as it grows based on the conditions listed in Table 6.3	165
Fig. 6.7: Predicted droplet sizes compared to actual experimental data presented within Chapters 4 and 5. The parameters modified were (a) Transmembrane Pressure (b) Rotational Speed (c) Tween 20 concentration and (d) Interfacial Tension value	167
Fig. 6.8: The effect of processing time on the emulsion droplet size produced using: (a) Rotor-stator high shear mixer (HSM) at 6000 RPM and (b) Ultrasonic probe (SON) at 5.5 m s^{-1} tip speed	169
Fig. 6.9: The effect of varying processing time and subsequently the production rate on the emulsion droplet size produced. Power consumption: Rotating Membrane Emulsification (RME) = 16.4 W, Rotor-stator High Shear Mixer (HSM) = 70.9 W, Ultrasonic Probe (SON) = 102.2 W	171
Fig. 6.10: The effect of varying the process mechanical speed on the resulting emulsion droplet size. For the HSM (a), this was rotational speed of the rotor and for SON (b), this was the tip speed. The processing time (90 seconds) and batch size (110 ml) were kept constant	172
Fig. 6.11: The energy density utilised to produce emulsions containing 10 vol. % sunflower oil at a rate between 3.7 kg h^{-1} to 6.2 kg h^{-1} (depending on dispersed phase viscosity in case of RME)	173
Fig. 7.1: The effect of transmembrane pressure on the mean droplet size using a pilot-scale rotating membrane emulsification device. The emulsions are approximately 1 vol. % sunflower oil stabilised by 1 wt. % Tween 20	

within the continuous phase. The error bars represent one standard deviation of a triplicate of experimental runs	179
Fig. 7.2: Influence of transmembrane pressure on the dispersed phase flux at 1000 RPM for a 26 μm pore diameter, stainless steel membrane	181
Fig. 7.3: The influence rotational speed on the mean droplet size at a transmembrane pressure of 0.5 bar. The emulsions are 1 vol. % sunflower oil stabilised by 1 wt. % Tween 20 within the continuous phase. The error bars represent one standard deviation of a triplicate of experimental runs	182
Fig. 7.4: The effect of transmembrane pressure on the mean droplet size using a small-scale rotating membrane emulsification device with a stainless steel membrane. The rotational speed is 1000 RPM and the annular gap width is 25 mm. The emulsions are 1 vol. % sunflower oil stabilised by 1 wt. % Tween 20 within the continuous phase. The error bars represent one standard deviation of a triplicate of experimental runs	184
Fig. 7.5: The effect of transmembrane pressure on the mean droplet size for matched membrane surface velocity (a) and matched shear rate (b). The emulsions are 1 vol. % sunflower oil stabilised by 1 wt. % Tween 20 within the continuous phase. The error bars represent one standard deviation of a triplicate of experimental runs	186
Fig. 7.6: The effect of Membrane surface velocity (a) and Shear rate (b) on the mean droplet size produced. The emulsions are 1 vol. % sunflower oil stabilised by 1 wt. % Tween 20 within the continuous phase. The error bars represent one standard deviation of a triplicate of experimental runs	187
Fig. 7.7: The effect of surfactant concentration on the mean droplet size for different surfactant types positioned within the aqueous continuous phase. The emulsions are 1 vol. % sunflower oil in water. The transmembrane pressure is 0.5 bar and the shear rate is 89.1 s^{-1} . The error bars represent one standard deviation of a triplicate of experimental runs	188
Fig. 7.8: The effect of transmembrane pressure (a) and rotational speed (b) on the mean droplet size using a pilot-scale rotating membrane emulsification device. The emulsions are approximately 1 vol. % sunflower oil stabilised by 1 wt. % Tween 20 within the dispersed phase. The error bars represent one standard deviation of a triplicate of experimental runs	190
Fig. 7.9: The energy density utilised to produce emulsions containing ≈ 1 vol. % sunflower oil at a rate of 10 kg h^{-1} . A constant TMP of 0.5 bar is applied whilst the rotational speed is varied between 100-4000 RPM	192
Fig. A1: Membrane surface area required based on the selected Transmembrane Pressure	209
Fig. A2: Possible dimensions for a cylindrical membrane for the chosen surface area of 22.8 m^2	210

List of Tables

Table 2.1: Summary of membrane parameters and their effect on droplet diameter and dispersed phase flux. Symbols indicate parameter is; critically important (***) , important (**) or not important (*)	29
Table 2.2: Summary of processing and formulation parameters and their effect on droplet diameter and dispersed phase flux. Symbols indicate parameter is; critically important (***) , important (**) or not important (*)	34
Table 4.1: Density values for the silicone oils investigated	100
Table 4.2: Physical properties of solutions investigated when modifying continuous phase viscosity with glycerol	104
Table 4.3: Droplet size data for systems which share similar viscosity ratios and approximate IFT values	109
Table 5.1: Important physicochemical properties of the surfactants investigated	117
Table 5.2: Equilibrium interfacial tension values for systems investigated	122
Table 6.1: Parameter values applied within model of droplet coalescence	157
Table 6.2: Distance between active pores assuming an even distribution of these pores across the membrane surface, for a given active pore fraction	158
Table 6.3: Parameter values applied within the force balance model example	164
Table 7.1: Details of experimental configurations investigated across the small-scale and pilot-scale rotating membrane emulsification devices	185
Table A1: Possible solutions for membrane surface area required based on selected Transmembrane Pressure	210

Nomenclature

Symbols

Symbol	Unit	Definition
$A_{d,p}$	m^2	<i>Cross-sectional area of zone where coalescence occurs</i>
A_m	m^2	<i>Effective membrane surface area (covered by pores)</i>
A_n	m^2	<i>Cross-sectional area of droplet neck</i>
$A_{\Delta,d}$	m^2	<i>Area of triangular segment formed by adjacent pores</i>
$A_{\Delta,m}$	m^2	<i>Area of triangular segment formed by adjacent active pores</i>
ΔA	m^2	<i>Change in interfacial area</i>
Ca_c	-	<i>Capillary number of continuous phase</i>
Ca_d	-	<i>Capillary number of dispersed phase</i>
D	$m^2 s^{-1}$	<i>Diffusion coefficient</i>
$D_{4,3}$	μm	<i>Volume weighted mean diameter of droplet</i>
D_H	m	<i>Hydraulic diameter of channel</i>
d_d	m	<i>Droplet diameter</i>
d_p	m	<i>Membrane pore diameter</i>
d_1	m	<i>Membrane outer diameter</i>
E	J	<i>Energy of particle adsorption</i>
F_{BG}	N	<i>Buoyancy force</i>
F_c	N	<i>Centripetal force</i>
F_{DL}	N	<i>Dynamic lift force</i>
F_I	N	<i>Inertial force</i>
F_R	N	<i>Drag force</i>
F_{stat}	N	<i>Static pressure force</i>
F_γ	N	<i>Interfacial tension force</i>
ΔG	J	<i>Gibbs free energy</i>
g	$N kg^{-1}$	<i>Gravitational field strength</i>
H_i	-	<i>Hydrophilic group value</i>
h_1	m	<i>Membrane length</i>
J	$mol m^{-2} s^{-1}$	<i>Diffusion flux</i>
J_d	$L m^{-2} h^{-1}$	<i>Dispersed phase flux</i>
K	m^2	<i>Membrane permeability</i>

k_B	$m^2 \text{ kg s}^{-2} \text{ K}^{-1}$	<i>Boltzmann's constant</i>
k_x	-	<i>Wall correction factor for drag force</i>
k_y	-	<i>Lift coefficient for dynamic lift force</i>
k_1, k_2	-	<i>Coefficients to determine We_{crit}</i>
L_m	m	<i>Membrane wall thickness</i>
L_p	m	<i>Pore channel length</i>
$L_{x,a}$	m	<i>Distance between adjacent forming droplets</i>
M_d	kg	<i>Mass of dispersed phase added</i>
m	-	<i>Number of hydrophilic groups in surfactant molecule</i>
m_d	kg	<i>Mass of droplet</i>
n	-	<i>Number of lyophobic groups in surfactant molecule</i>
$n_{p,a}$	-	<i>Numbers of pores active on membrane surface</i>
$n_{p,ac}$	-	<i>Maximum number of pores active nearby to a forming droplet</i>
$n_{p,p}$	-	<i>Number of pores within close proximity to a forming droplet</i>
$n_{p,t}$	-	<i>Total number of pores on membrane surface</i>
n_1	RPM	<i>Number of rotations per minute</i>
Oh	-	<i>Ohnesorge number</i>
P_{active}	-	<i>Probability of a randomly chosen pore being active</i>
P_c	Pa	<i>Capillary pressure</i>
$P_{coalescence}$	-	<i>Probability of droplet coalescence</i>
P_d^0	Pa	<i>Pressure difference between dispersed and continuous phases</i>
P_{LP}^*	Pa	<i>Laplace pressure for non-spherical droplet</i>
ΔP	Pa	<i>Laplace pressure</i>
ΔP_{tm}	Pa	<i>Transmembrane pressure</i>
Q_d	$m^3 \text{ s}^{-1}$	<i>Volumetric flow rate of dispersed phase through membrane</i>
q_d	$m^3 \text{ s}^{-1}$	<i>Volumetric flow rate through a single pore channel</i>
Re	-	<i>Reynolds number</i>
Re_c	-	<i>Reynolds number of continuous phase</i>
r	m	<i>Radius of spherical particle</i>
r_d	m	<i>Droplet radius</i>
r_1	m	<i>Membrane outer radius</i>
r_2	m	<i>Emulsification vessel inner radius</i>
T	K	<i>Temperature</i>
Ta	-	<i>Taylor number</i>

$t_{crit,ref}$	s	<i>Droplet detachment time for $Ca_c = 1$</i>
t_d	s	<i>Droplet detachment time</i>
t_p	s	<i>Processing time</i>
We	-	<i>Weber number</i>
We_{crit}	-	<i>Critical Weber number</i>
We_d	-	<i>Weber number for dispersed phase</i>
$V_{crit,ref}$	m^3	<i>Droplet detachment volume for $Ca_c = 1$</i>
V_d	m^3	<i>Volumetric contribution of material during detachment</i>
V_{dr}	m^3	<i>Volume of droplet</i>
V_f	m^3	<i>Final droplet volume</i>
V_g	m^3	<i>Droplet volume at end of growth stage</i>
v_c	$m\ s^{-1}$	<i>Velocity difference between continuous phase/membrane surface</i>
v_d	$m\ s^{-1}$	<i>Velocity of dispersed phase</i>
$\overline{v_d}$	$m\ s^{-1}$	<i>Average dispersed phase velocity</i>
v_{dr}	$m\ s^{-1}$	<i>Tangential velocity of droplet</i>
x	m	<i>Diffusion length</i>
$x_{\Delta,a}$	-	<i>Number of triangular segments formed by active pores</i>
$x_{\Delta,p}$	-	<i>Number of triangular segments formed by all pores</i>

Greek letters

Symbol	Unit	Definition
α	-	<i>Fraction of pores active</i>
γ	N m^{-1}	<i>Interfacial tension</i>
$\dot{\gamma}$	s^{-1}	<i>Shear rate</i>
γ_{ow}	N m^{-1}	<i>Interfacial tension between oil and water</i>
γ_{so}	N m^{-1}	<i>Interfacial tension between solid particle and oil</i>
γ_{sw}	N m^{-1}	<i>Interfacial tension between solid particle and water</i>
ϑ	degree	<i>Contact angle</i>
μ_c	Pa s	<i>Dynamic viscosity of continuous phase</i>
μ_d	Pa s	<i>Dynamic viscosity of dispersed phase</i>
π	-	<i>Pi</i>
ρ_c	kg m^{-3}	<i>Density of continuous phase</i>
ρ_d	kg m^{-3}	<i>Density of dispersed phase</i>
τ	-	<i>Tortuosity factor for membrane</i>
τ_w	Pa	<i>Wall shear stress</i>
φ	-	<i>Membrane porosity</i>
φ_c	mol m^{-3}	<i>Surfactant molecule concentration</i>
ω_1	rad s^{-1}	<i>Angular velocity of membrane surface</i>

Abbreviations

Abbreviation	Definition
CFD	Computational Fluid Dynamics
CMC	Critical Micelle Concentration
FBM	Force Balance Model
HLB	Hydrophilic-Lypophilic Balance
HSM	Rotor-stator High Shear Mixer
IFT	Interfacial Tension
O/W	Oil-in-water
RME	Rotating Membrane Emulsification
RPM	Rotations Per Minute
SDS	Sodium Dodecyl Sulphate
SFO	Sunflower Oil
SON	Ultrasonic Probe
SPG	Shirasu-Porous-Glass
TBM	Torque Balance Model
TMP	Transmembrane Pressure
W/O	Water-in-oil
W/O/W	Water-in-oil-in-water
XME	Cross-flow Membrane Emulsification

Chapter 1:

Introduction

1.1 Background to Research

1.1.1 Introduction to Emulsions

An emulsion is defined as a mixture of two immiscible liquid phases with one finely dispersed within the other as droplets. Throughout the ages, emulsion systems have been utilised in many instances. Such is their versatile nature, they are ubiquitous within the modern world. Naturally occurring emulsions such as milk, rubber latex or plant saps have inspired the development of a whole range of man-made emulsion products. Products in a wide range of areas such as foods (ice cream, mayonnaise, salad dressing), agrochemicals (pesticides, herbicides), pharmaceuticals (creams, ointments), cosmetics (perfumes, lipsticks, moisturisers) and paints incorporate emulsion microstructures to induce physical, chemical and sensory attributes. Due to their multitude of uses, significant quantities of these systems are manufactured worldwide to meet consumer demand for such products. As with many colloidal systems, emulsions can be considered homogeneous at the macroscopic scale but heterogeneous at the microscale. They are generally white and opaque in appearance depending on the droplet size and the volume fraction of the dispersed phase. This is the result of the dispersed droplets diffracting light (Debye, 1947).

There are two common types of emulsion; Oil-in-water (O/W) emulsions and water-in-oil (W/O) emulsions contain oil and water droplets respectively. In addition, double emulsions can also be produced which utilise an emulsion as the dispersed phase; for example a water-in-oil-in-water (W/O/W) emulsion. Emulsions are typically termed depending on their droplet size with micro- or nano- (10-100 nm), mini- (10-1000 nm) or macro- (> 0.5 μm) emulsions possible.

Traditionally, emulsions have been produced by applying large quantities of energy to break down and disperse one of the phases. This can be achieved simply by shaking, whisking or beating a mixture of oil, water and a surfactant. However, to produce the small droplets required for use within an emulsion product, significant mechanical energy is required to increase interfacial area.

Processes such as rotor-stator mixers and high pressure homogenisers are generally employed to produce emulsions on an industrial scale. All of the emulsion ingredients are passed through areas of high energy dissipation which breaks down the dispersed phase into fine droplets due to turbulence within the flow. The extent of turbulence (i.e. fast and chaotic fluid movement) can be modified by the physical design of the process. For rotor-stator mixers, the design of the mixer impeller or the tank (e.g. inclusion of baffles) can alter the flow profile and hence alter the degree of droplet break up. For high pressure homogenisers, the orifice diameter of which a coarse pre-emulsion passes through can be modified to increase droplet break up in conjunction with the pressure drop across the orifice. Essentially, these processes are principally similar (imparting shear, turbulence and fluid cavitation to break up droplets) albeit different in their mechanical workings.

1.1.2 Challenges within Emulsification

The consumer market is becoming ever more demanding with a higher expectation that products can offer improved functionality. With further advancements in the development of unique emulsion structures (e.g. double emulsions, nano-emulsions, mono-dispersed droplet size emulsions), simple O/W or W/O emulsions formulated using conventional technologies are much less attractive than in the past. Such smart structures may impart useful properties to products including a longer shelf life, a well-controlled release rate of an active ingredient or a lowering of fat content without a loss of flavour (Vladislavjevic and Williams, 2005; Van der Graaf *et al.*, 2009). Products with these capabilities are only going to increase in popularity as society becomes more aware of adopting a healthy lifestyle.

Although well-understood, emulsification processes currently used within industry (e.g. homogenisers, rotor-stator mixers) are generally not suitable for formulating the complex emulsion structures needed within multi-functional products. Furthermore, these processes use large quantities of energy inefficiently. This is both environmentally and economically unsustainable. They also do not provide a high level of control over the droplet size distribution produced. A lack of

uniformity can trigger destabilisation mechanisms and thus be detrimental to the quality and shelf life of a product. Emulsions may vary from one operation to another which is not ideal for manufacture of a homogeneous product. Large quantities of surfactant are used to overcome this; these are costly ingredients within a formulation. The limitations of current technologies are accepted, but with a rising demand for higher quality products, they significantly limit the microstructures achievable. Thus, new technologies require developing to meet this demand.

Another important consideration within the manufacturing industry is energy consumption. For the majority of current emulsification technologies, the energy applied lies between a factor of 10-1000 times more than the theoretical energy required to produce the actual emulsion microstructure (Gijssbertsen-Abrahamse *et al.*, 2004). For rotor-stator mixers, only a small fraction of the power input is transferred to the fluid to induce mixing. The power loss is greater particularly under faster rotational speeds, higher viscosity systems or if the shear gap is small (Paul *et al.*, 2004). For the energy that is transferred, a large amount of this energy is used to break down droplets that have re-coalesced due to the inability of the surfactant to adsorb quickly enough. The need to repeatedly break down droplets in the hope they will be stabilised is obviously counterproductive. Manufacturers typically over-compensate for this by (over)loading their products with a much greater quantity of surfactant than is required to stabilise the emulsion interfacial area. Surfactants can be among the most expensive ingredients within a formulation but yet they are essentially being wasted. The remainder of the energy is dissipated as heat which can impart thermal stresses on the product. This may damage sensitive ingredients within the emulsion such as starches and proteins. It is easy to see how there is a cascade of energy loss throughout the process resulting in extremely low efficiency. Rhetorically speaking, in an age with rising energy cost and accelerated environmental damage, can we afford to be this reckless?

It is only within the past 25 years that research has shifted away from the well-established emulsion technologies towards the development of novel approaches. Generally, the objective is

unanimous; to produce emulsion droplets individually and precisely by ‘building’ or ‘growing’ them. Such bottom-up manufacturing approaches offer much greater control by comparison with turbulent break up. These can be divided into microfluidic approaches (e.g. microcapillary emulsification) and membrane emulsification approaches. For the former, the dispersed phase is added from the branch of a T-junction into the continuous phase by precisely modifying the ratio of the flow rates. Droplets are produced singularly which lends itself perhaps towards low volume, high precision processing rather than large-scale emulsion production. Well defined structures such as double emulsions or core/shell capsules can be produced in a single step since all the materials are intricately positioned where they are needed. Alternatively, membrane emulsification works by forcing dispersed phase through a porous structured material. The process can vary dramatically depending on the membrane used, as well as the means of which shear (to aid detachment) is applied to the membrane surface if at all. Microfluidic and membrane emulsification approaches are radically different to current emulsification technologies, with a much more conservative and hence efficient use of energy (Gijsbertsen-Abrahamse *et al.*, 2004).

1.1.3 Introduction to Project

A new process known as rotating membrane emulsification has been developed within the past 8 years. The dispersed phase is forced through a microporous material by the application of pressure such that individual droplets are produced at each pore channel. The movement of the membrane induces a number of forces to enable detachment of droplets at a controlled size. Such an approach solves a number of the problems experienced with current processing technologies (less energy consumption, low shear rates, uniform droplet sizes etc.). There is therefore increasing interest in exploiting the process to create specifically designed structures for a particular function.

However, challenges remain that may be holding back rotating membrane emulsification from being utilised to manufacture emulsions. Firstly, the process is complex and so there are unresolved phenomena that are not fully understood (Schadler and Windhab, 2006). Without this

understanding, it is difficult to predict how operation will form a particular emulsion microstructure (i.e. initial droplet size) based on the conditions and ingredients used. Exploration of the possibilities and limits of rotating membrane emulsification may not be realised without this knowledge. Secondly, the procedure on how to design and scale up rotating membrane emulsification is undefined since it has yet to be demonstrated at a scale similar to industrial scale manufacture. Even for established emulsification processes, scale up is based on experience and trial and error rather than a fundamental scientific understanding of the process (Paul *et al.*, 2004). Finally, stable droplet production using rotating membrane emulsification generally relies on slow addition of the dispersed phase (i.e. low dispersed phase flux). This is unsuitable if the aim is to produce large quantities of emulsion containing a well-controlled droplet size.

The aim of this thesis is therefore to further the fundamental understanding of the rotating membrane process. In particular, how the process behaves as one shifts from small-scale to pilot-scale operation. In turn, this should enable the creation of models that can predict the droplet size and dispersed phase flux, as well as outline procedure to design and scale up the process.

1.2 Objectives

The objectives of this thesis are:

- To further understanding of the process mechanisms involved during rotating membrane emulsification. In particular, to ascertain how the process can be controlled to achieve a desired initial droplet diameter or a rate of production.
- To optimise the process to be competitive with current emulsification technologies (rotor-stator high shear mixer, ultrasonic probe), producing similar droplet sizes at the high dispersed phase fluxes needed to be industrially viable.
- To demonstrate the capabilities of a pilot-scale rotating membrane emulsification device and to observe whether the process advantages seen with a small-scale device are upheld.
- To develop scale-up principles for rotating membrane emulsification through the evaluation of the pilot-scale device. This work should lay foundations on the approaches required to design and operate this equipment.

1.3 Business Case

Syngenta, who are the primary industrial collaborator within this study, are a multinational agribusiness that specialises in the development and manufacture of seeds and agrochemicals. They were formed in 2000 with the merger of Novartis Agribusiness and Zeneca Agrochemicals. In 2014, sales in crop protection products reached £7.3 billion with a global market share of 19.2%.

Emulsion systems are incorporated into many of their pesticide and herbicide products. The dependence on such products to help yield crops is only going to increase. Considering that the global population is growing at a rate of three people per second and on top of this, the land available for cultivation is decreasing by an area equal to a football pitch within the same second, maximising crop production for food security is extremely important. With 25% of crops being lost each year due to insects and weeds, agrochemicals are a necessary purchase by farmers in order to produce the food required to feed the population.

Syngenta have strived to gain an advantage over their competitors (BASF, Dow AgroSciences, DuPont) within this growing agrochemical sector (valued at approximately £38 billion) through the research and development of more sophisticated or 'smarter' emulsion structures. Such structures may provide enhanced properties to their products to offer multi-functional purposes. Examples include long term product stability, targeted and controlled release of segregated active ingredients and minimisation of potentially harmful active ingredients and surfactants within their products. Ultimately, these superior products have the potential to be more environmentally sustainable, more functional and therefore more marketable.

Conventional emulsification processes, whilst capable of formulating basic emulsion systems, may struggle to produce more intricate structures. Therefore, research into rotating membrane emulsification has been undertaken since it has been demonstrated to be capable of producing a very wide array of structures including nano-emulsions, double emulsions and shelled

structures. In addition, the rotating membrane process utilises a small fraction of the energy needed for current manufacturing processes; this would coincide with Syngenta's company strategy of minimising energy consumption and hence environmental impact. However, the procedure to design and operate this piece of equipment to meet the needs of a company such as Syngenta is undefined. Therefore, this piece of research can help shift the technology from being a simple small-scale process to one that is industrially viable for emulsification.

1.4 Thesis Layout

The thesis structure is as follows:

- The introduction to the thesis is discussed in **Chapter 1**
- **Chapter 2** presents the theoretical background to rotating membrane emulsification, alongside a review of the relevant work that has been conducted. This supports a number of ideas explored within this thesis.
- **Chapter 3** shows information on the materials and the methods used during the experimental work. The basis behind the characterisation of the emulsion structures produced is also described.
- **Chapter 4** discusses how the process parameters of rotating membrane emulsification at the small-scale alter the fluid flow behaviour and subsequently the emulsion structure.
- **Chapter 5** focuses on modifying the formulation parameters; specifically the surfactant or particle type and concentration, to impart different droplet interfacial behaviour during processing.
- In **Chapter 6**, a number of models relating to droplet-droplet interactions and prediction of the droplet size are derived and evaluated. Alongside this, the rotating membrane emulsification process is compared to a rotor-stator high shear mixer and an ultrasonic probe.
- Within **Chapter 7**, a pilot-scale rotating membrane device is tested and compared to a small-scale device, prior to discussion on how to approach the design and scale-up of the process.
- **Chapter 8** concludes the findings of the work conducted throughout the thesis. Suggestions and recommendations for future work are made within **Chapter 9**.
- The literature cited within this thesis is fully referenced in **Chapter 10**.
- An example of the proposed design procedure being applied is presented in **Appendix A**.

1.5 Publications, Presentations & Awards

The results and discussions within this thesis are published as follows:

Spyropoulos, F., Lloyd, D.M., Hancocks, R.D., Pawlik, A.K. (2014). Advances in membrane emulsification. Part A: recent developments in processing aspects and microstructural design approaches. *Journal of the Science of Food and Agriculture*, 94 (4) 613-627.

Spyropoulos, F., Lloyd, D.M., Hancocks, R.D., Pawlik, A.K. (2014). Advances in membrane emulsification. Part B: recent developments in modelling and scale-up approaches. *Journal of the Science of Food and Agriculture*, 94 (4) 628-638.

Lloyd, D.M., Norton, I.T., Spyropoulos, F. (2014). Processing effects during rotating membrane emulsification. *Journal of Membrane Science*, 466 8-17.

Lloyd, D.M., Norton, I.T., Spyropoulos, F. (2015). Process optimisation of Rotating Membrane Emulsification through the study of surfactant dispersions. *Journal of Food Engineering*, 166 316-324.

The results and discussions within this thesis were presented as follows:

Lloyd, D.M., Spyropoulos, F., Norton, I.T. (April 2012-2014), The engineering principles of rotating membrane emulsification. *The 9th-11th Annual EngD Formulation Engineering Conference*, Birmingham, United Kingdom (oral presentation).

Lloyd, D.M., Norton I.T., Spyropoulos, F. (April 2014), Food-grade emulsion production using a low energy rotating membrane technology. *The 8th European Workshop on Food Engineering and Technology*, Quakenbrück, Germany (oral presentation).

Spyropoulos, F., Lloyd, D.M., Norton, I.T. (June 2015). A microstructural approach to optimising membrane emulsification: surfactant diffusion through the oil/water interface. *The 12th International Congress on Engineering and Food*, Quebec City, Canada (poster presentation).

The research presented was awarded the following:

The 'Peter Bongers Prize', awarded at the 10th Annual EngD Formulation Engineering Conference (April 2013) for the best presentation by an EngD student.

The 'Julius-Maggi Research Award', awarded by Nestlé at the 8th European Workshop on Food Engineering and Technology (April 2014) for the best presentation by a doctoral or post-doctoral researcher.

Chapter 2:

Literature Review

This chapter reviews the current theory and understanding behind both conventional emulsification techniques and more specifically membrane emulsification. Evolution of the membrane process from its initial form to a variation in guises such as rotating membrane emulsification is discussed alongside the merits of each. Current understanding of the important process mechanisms is introduced in conjunction with how selection of processing, formulation and membrane parameters can produce a wide range of micro-structural products. Finally, modelling techniques used to reinforce underlying theory are summarised which in turn will aid the development of approaches to design and scale up membrane emulsification processes.

Elements of the discussion contained within this chapter have been published within:

Spyropoulos, F., Lloyd, D.M., Hancocks, R.D., Pawlik, A.K. (2014). Advances in Membrane Emulsification. Part A: Recent developments in processing aspects and microstructural design approaches. *Journal of the Science of Food and Agriculture*, 94 (4) 613-627.

Spyropoulos, F., Lloyd, D.M., Hancocks, R.D., Pawlik, A.K. (2014). Advances in Membrane Emulsification. Part B: Recent developments in Modelling and Scale-up approaches. *Journal of the Science of Food and Agriculture*, 94 (4) 628-638.

2.1 Emulsions and Emulsification

2.1.1 Fundamentals of Emulsion Formation

To disperse the two immiscible liquids into an emulsion, mechanical energy is typically applied in the presence of an interfacial stabiliser known as a surfactant. The process of forming emulsions is known as emulsification or homogenisation. The applied energy in the form of shear is used to deform and eventually break down droplets, increasing the interfacial area. However, droplet break up is naturally resisted by the internal pressure of the droplet, which is known as the Laplace pressure. This is defined as the pressure difference at the convex and concave side of the droplet interface and is caused by the surface tension. The applied energy needs to therefore be greater than the Laplace pressure in order to break up the droplet. However, this break up can be facilitated by a surfactant adsorbing to lower the interfacial tension and hence the Laplace pressure. This is quantified within Eq. 2.1 assuming a spherical droplet:

$$\Delta P = \frac{2\gamma}{r_d} \quad (\text{Eq. 2.1})$$

where ΔP is the Laplace pressure, γ is the interfacial tension and r_d is the droplet radius. The interfacial tension is defined as the work required to alter the shape of an interface. An interface is defined as the narrow region between two separate phases. It is an important factor in determining emulsion formation, stability and physicochemical properties including viscosity etc. The interfacial tension is measured as a force per unit length parallel to the interface; usually expressed as mN m^{-1} .

A surfactant (also known as an emulsifier) is a 'surface active agent' capable of adsorbing at the interface between oil and water to stabilise droplets. Many of the traditionally used surfactants to stabilise emulsion systems were extracted from natural sources. Classic examples include lecithin from egg yolk or proteins from milk. However, with advancements both in understanding and the technology to synthesise chemical materials, a whole catalogue of surfactants both natural and man-made are available for use. Other examples include various polysorbates, phospholipids, mono-

diglycerides etc. The role of the surfactant is to lower the interfacial tension between the two phases (to facilitate formation) and then to stabilise the formed droplets against coalescence. This can be controlled to an extent by selection of the appropriate type and concentration. Surfactants are amphiphilic molecules, usually consisting of a hydrophobic tail group which has affinity to the non-polar, organic phase and a hydrophilic head group which has affinity to the polar, aqueous phase. Because of this structure, they tend towards the oil/water interface so each group can sit either side of the interface. This minimises unfavourable contact between the two phases as can be observed in Fig. 2.1. The gradual accumulation of surfactant molecules alters the molecular interactions at the interface, enabling the system to be more thermodynamically stable (by reducing the Gibbs free energy). This is a dynamic process and hence the value of interfacial tension will decrease as a function of time to reach an equilibrium value.

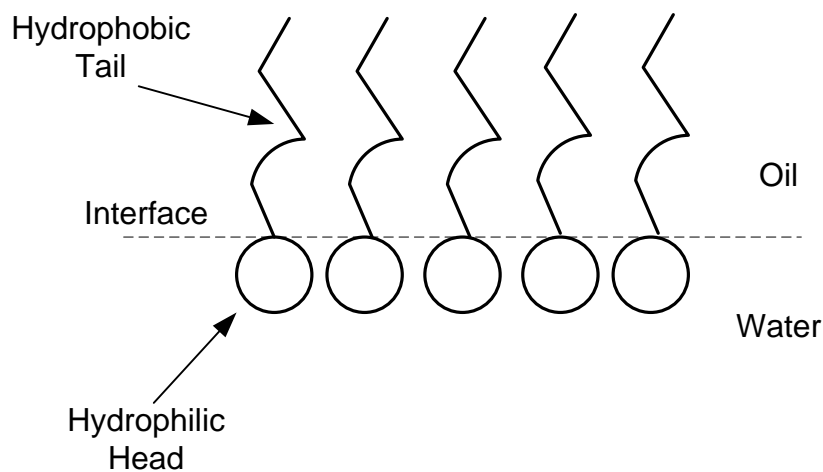


Fig. 2.1: A schematic representation of surfactant molecules at an interface.

The type of hydrophilic head group can determine whether the surfactant is anionic (negatively charged), cationic (positively charged), zwitterionic (both positively and negatively charged) or non-ionic, depending on the capability of the surfactant to dissociate within an aqueous phase. The ability of a surfactant to stabilise a particular system can be quantified by the hydrophilic-lipophilic balance (HLB) number; essentially a ratio of the molecular weight of the hydrophilic head part to the lipophilic tail. It can be used as a rough guide of the surfactants suitability. For example, high HLB

values (8+) are suitable for O/W emulsion formation whilst low values (3-6) are preferable for W/O emulsions (Griffin, 1949; Griffin, 1954). The further away from the threshold HLB value of 7, the more powerful the surfactant. The HLB number can be calculated using the Davies' method as:

$$HLB = 7 + \sum_{i=1}^m H_i - n \times 0.475 \quad (\text{Eq. 2.2})$$

where m is the number of hydrophilic groups in the molecule, H_i is a predetermined value for each hydrophilic group and n is the number of lipophilic groups in the molecule. Whether a surfactant stabilises an O/W or W/O emulsion depends on its solubility within each phase. The Bancroft rule states that 'the phase in which the surfactant is more soluble constitutes the continuous phase' (Bancroft, 1912). For this reason, O/W emulsions are typically stabilised by high HLB surfactants positioned within the aqueous continuous phase and vice-versa.

Beyond a certain concentration, surfactant molecules form self-assembled structures called micelles instead of existing as individual molecules or monomer. Hence, this point is termed the critical micelle concentration (CMC). Micelles (typically consisting of 50-200 surfactant molecules) form in order to lower the free energy of the system. If positioned within an aqueous environment, the hydrophobic tail group of a surfactant molecule will congregate towards the centre of the micelle structure, whilst the hydrophilic head groups will point outwards. If positioned within an organic environment, the reverse effect will occur with hydrophilic head groups congregating towards the centre. In some cases, vesicles or bilayers may form. These are each represented schematically in Fig. 2.2.

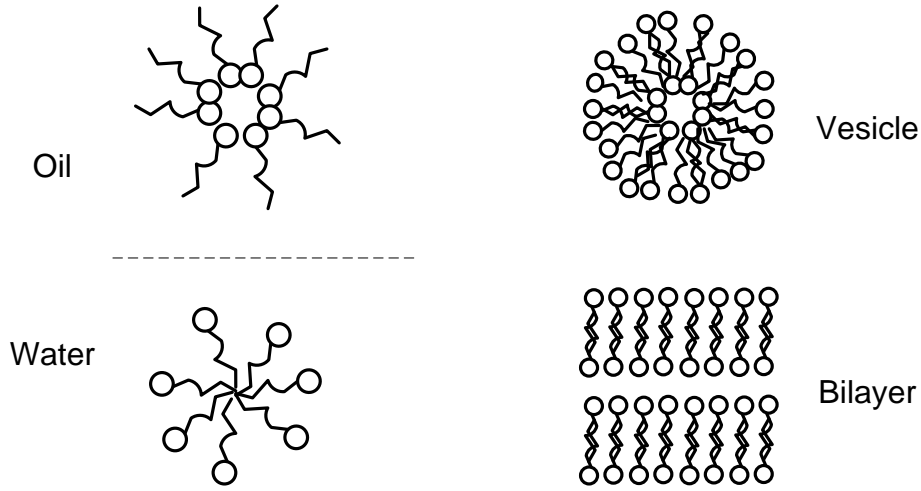


Fig. 2.2: A schematic representation of possible surfactant micelle structures.

In order for surfactant to adsorb at the droplet interface, the micelle must first be transported within the bulk phase to a region nearby to the droplet, which is known as the sub-surface. Under quiescent i.e. stationary fluid flow conditions, surfactant is transferred by diffusion. This is determined by the concentration gradient and the molecular diffusion coefficient; Fick's Law (Eq. 2.3). The diffusion coefficient is inversely proportional to the bulk phase viscosity and the surfactant molecule characteristic length as stated by the Stokes-Einstein equation (Eq. 2.4):

$$J = -D \frac{\partial \phi_c}{\partial x} \quad (\text{Eq. 2.3})$$

$$D = \frac{k_B T}{6\pi\mu r} \quad (\text{Eq. 2.4})$$

where J is the diffusion flux, D is the diffusion coefficient, ϕ_c is the surfactant molecule concentration, x is the diffusion length, k_B is Boltzmann's constant, T is the absolute temperature, μ is the viscosity and r is the characteristic length of the spherical particle. If fluid is flowing, a mechanism to aid transport of the surfactant provided by the motion of the fluid is known as advective transport. Advection depends on the fluid velocity and the concentration of surfactant and is more dominant than diffusion especially during most emulsification processes. However, the two mechanisms of diffusion and advection do combine to provide an overall convective transport.

Upon reaching the sub-surface, micelles dissociate into individual surfactant molecules. However, it is more likely that individual molecules already free within the bulk will adsorb first and the micelle dissociation will simply replenish the free molecules available for adsorption, to remain in equilibrium. As such, the concentration of surfactant that is able to adsorb will not change with further increase in the overall concentration beyond the CMC; a minimum interfacial tension value will be obtained. However, if the micelle dissociation rate is slow relative to the rate of adsorption, there will be occurrences where there is minimal surfactant available for adsorption which will hinder the rate of interfacial tension reduction. Furthermore, the rate of surfactant adsorption will decrease with greater occupation of surfactant at the interface. An equilibrium is established as surfactant desorbs from the droplet surface at the same rate that free surfactant adsorbs from the sub-surface with no net change at the interface.

In addition to surfactants, colloidal particles can also be used to stabilise emulsions via a mechanism known as Pickering stabilisation. Examples include silica, clay, calcium carbonate and fat or ice crystals. More recently, specially designed amphiphilic particles known as 'Janus' particles have been produced (Glaser *et al.*, 2006). The concept of particle stabilised emulsions was demonstrated by Pickering (1907) for plant spraying applications. Unlike surfactants, particles are irreversibly adsorbed at the interface and provide a strong mechanical barrier against destabilisation mechanisms. The adsorption process is triggered by the collision of particles with the unoccupied droplet interface with sufficient energy (Manga *et al.*, 2012). The energy to remove a particle from the interface once adsorbed is very high. As such, droplets colliding in the emulsion bulk do not contain enough kinetic energy to displace the particle and coalesce. However, most particles are not amphiphilic so they do not significantly alter the interfacial tension to enable easier droplet formation. Therefore, the primary benefit of using particles is associated with enhanced stability. Interest in these systems has accelerated within the last 30 years or so in conjunction with advancements in nanoparticle technology. Particles are required to be at least one order of magnitude smaller than the droplet in order to pack around the interface. For example, droplets of 1

μm in diameter need to be stabilised by particles $< 100 \text{ nm}$. The strength of the adsorption is a function of both the particle size but also the contact angle between the particle and each phase (Levine *et al.*, 1989) as calculated by Eq. 2.5 and shown in Fig. 2.3:

$$E = \pi r^2 \gamma (1 \pm \cos\theta)^2 \quad (\text{Eq. 2.5})$$

where E is the adsorption energy, r is particle radius, γ is the interfacial tension and θ is the contact angle of the particle at the interface. The plus or minus sign depends on whether the particle is removed into the oil or water phase respectively.

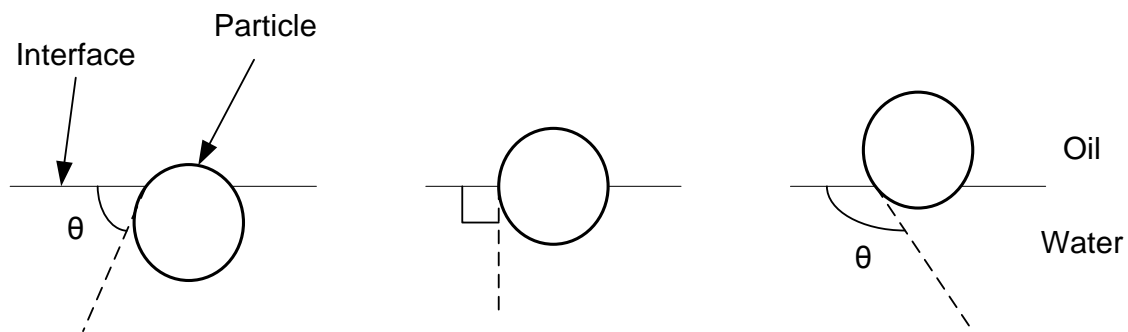


Fig. 2.3: A schematic illustrating various contact angles of a particle adsorbed at an O/W interface.

As can be seen from Fig. 2.3, the wettability of the particle alters the position of the particle at the interface and subsequently the energy of adsorption. The maximum energy is achieved when the contact angle equals 90° i.e. the particle wets both phases equally. For O/W production, generally a contact angle of $60\text{-}80^\circ$ is favourable (measured relative to the water phase). Wetting can be quantified by the Young's equation which is essentially a force balance between the particle/oil/water interface at the contact line (Tadros, 2005):

$$\gamma_{SW} + \gamma_{OW} \cos\theta - \gamma_{SO} = 0 \quad (\text{Eq. 2.6})$$

where γ_{SW} is the interfacial tension between the solid particle and water, γ_{OW} is the interfacial tension between oil and water and γ_{SO} is the interfacial tension between the solid particle and oil. If the contact angle is too small ($< 60^\circ$) or too large ($> 130^\circ$), it is likely that the particle will remain at

the bulk phase rather than adsorb at the interface. In terms of the particle size, small particles are able to adsorb faster since they require less energy. They also provide more effective packing and surface coverage of the interface. On the other hand, larger particles attach with more energy and form a thicker interface. Thus, this imparts greater droplet stability (Binks, 2002).

Emulsion droplets can be stabilised by mixtures of surfactants and particles. The droplet sizes produced using just particles tend to be relatively large due to the high interfacial tension value. However, surfactant only systems do not necessarily provide as effective an interfacial stability mechanism. There are therefore opportunities to apply the benefits of each material rather than each component in isolation (Pichot *et al.*, 2010). It is highly probable there are going to be forms of interactions between the surfactants and the particles depending on the ratio of the two; for example surfactants may alter the wettability of the particles (Binks *et al.*, 2007), promote particle aggregation within the continuous phase (Binks and Rodrigues, 2007) or displace particles from the interface altogether.

2.1.2 Emulsion Stability

The stability of emulsions refers to the ability of an emulsion to retain its properties over an arbitrary period of time without significant change. This primarily relates to the droplet size distribution evolution. Emulsions are thermodynamically unstable systems since increasing the interfacial area subsequently increases the Gibbs free energy. This is a directly proportional relationship as shown by Eq. 2.7.

$$\Delta G = \gamma \Delta A \quad (\text{Eq. 2.7})$$

where ΔG is the change in Gibbs free energy. γ is the interfacial tension and ΔA is the change in interfacial area. However, emulsion systems are kinetically stable since a minimum value of ‘activation’ energy is required before an emulsion can reach its most thermodynamically favourable state (i.e. complete separation of the two phases). Thus, an emulsion can remain stable despite

being thermodynamically unfavourable; this is termed metastable. The constant motion of particles due to intermolecular or external forces will potentially result in particle interactions and hence mechanisms of instability. Conflictingly, nano-sized droplets (<100 nm) move randomly due to Brownian motion so these systems are not susceptible to destabilisation mechanisms (hence they are thermodynamically stable). This allows nano-emulsions to be stable for many years without any change (McClements, 2011).

There are a number of different destabilisation mechanisms, which can have a detrimental effect on the properties of a product. Firstly, gravitational separation can occur. Due to density differences between the two phases under the action of gravity, a concentrated layer of droplets can form either at the top or bottom of the emulsion. If the droplets have lower density than the continuous phase (typically O/W systems) then this movement is called creaming whilst the opposite is sedimentation. Whilst gravitational separation does not alter the droplet size, it can promote other forms of destabilisation mechanisms by compacting droplets close together such that interactions are more likely. It can be limited if the densities are very similar, droplets are small or the continuous phase is highly viscous. Secondly, constant movement of droplets results in collisions within the bulk phase, which depending on their nature can cause droplets to move away separately, aggregate together as a cluster of droplets (flocculation) or as a single droplet (coalescence). In the case of flocculation, the droplets are still individual entities. The rate and strength of flocculation can be controlled by considering the electrostatic and steric colloidal interactions possible. Depending on the strength of these interactions between the droplets, the process can be reversible or irreversible. Flocculation can also increase emulsion viscosity which may be advantageous for obtaining certain properties within a product. In the case of coalescence, external forces cause two droplets merge together to form a larger droplet. This process is always irreversible. Two droplets become sufficiently close such that the thin film of continuous phase between the droplets ruptures, allowing dispersed phase material to flow between them. With a thicker film, the collision is weaker since this film acts as a physical barrier. If coalescence occurs to enough of an extent, phase

separation occurs resulting in two distinct layers of material. For O/W emulsions, this may typically be a layer of free oil on top of the denser continuous phase. Coalescence therefore needs to be limited to achieve stable emulsion production; this is possible through selection of a suitable surfactant that is able to adsorb quickly and provide a sufficient steric (if a large molecule) or electrostatic (if ionic) repulsive mechanism. Consideration of the operating conditions may also be employed i.e. reducing the collision energies through less energy input or increased viscosity. The final destabilisation mechanism possible is Ostwald ripening. This is a thermodynamically driven process. Laplace pressure differences between droplets of varying size, cause smaller droplets (of high Laplace pressure) to migrate towards larger ones (low Laplace pressure). As a consequence, small droplets disappear as large droplets grow. Whilst Ostwald ripening is only a major process for droplets smaller than 10 μm , the growth caused by this mechanism may induce other destabilisation mechanisms (Walstra, 2003).

2.1.3 The Physics of Conventional Emulsification

As highlighted previously, emulsions are typically produced by breaking up droplets into smaller entities using a 'top-down' approach. Examples include high pressure homogenisers and high-shear rotor stator mixers. The discussion will focus on the latter case although both rely on the principle of shear to break up the droplets. Fluid enters the mixer head from the underside. The rotation of a rotor impeller at high speeds between 10-50 m s^{-1} generates shear (approximately 20000-100000 s^{-1}) between the rotor and the stator screen (Paul *et al.*, 2004). As a consequence, the fluid experiences radial and tangential shear flow inside the stator. The fluid then passes through holes within the stator screen. Variation of the surface properties of this screen (e.g. the inclusion of specific diameter holes) can further enhance the production of turbulence compared to smooth surfaces. The primary operating parameter within mixing processes is the power draw. This is defined as the amount of energy required to generate fluid movement by agitation within a given time period. For a fixed geometry system, the droplet diameter produced is based on a function of

rotational speed and mixing time, as well as the dynamic balance between droplet break up and re-coalescence (since these both occur simultaneously). The forces involved in breaking up droplets are referred to as viscous or frictional forces and are imparted by fluid flow parallel to the droplet surface. Additionally, inertial forces due to pressure fluctuations within the fluid act perpendicular to the droplet surface. The presence and magnitude of each of these disruptive forces depends on the Reynolds number (Re) of the system. For emulsification, operation occurs predominately within either the turbulent-viscous ($Re = 4000$) or turbulent-inertial regime ($Re = 40000$) rather than laminar-viscous flow ($Re < 2300$). The production of turbulent eddies within the flow, each containing varying amount of energy depending on their size, promotes droplet break up. The largest eddies (comparable to the impeller diameter in size) transfer energy to gradually diminishing eddies until reaching the smallest size achievable; known as the Kolmogorov length scale. Droplets existing at a size greater than the Kolmogorov length scale are broken up by inertial forces whilst if they are smaller, they are broken up by viscous forces (Walstra and Smulders, 1998). The cohesive force holding a droplet together and preventing break up is the interfacial tension force. Therefore, the feasibility of droplet break up relies on the disruptive forces to overcome the cohesive force. This can be numerically characterised by the Weber number (We) which is the ratio of these respective forces. If $We > 1$, droplet break up occurs. An additional process complexity is that droplets can re-coalesce as a consequence of frequent droplet collisions induced by agitation. Surfactant is required to adsorb much faster than the collision time in order to prevent coalescence. It is therefore clear that a minimum droplet size limit will be reached when; (i) the shear applied is insufficient to overcome the Laplace pressure and break droplets up further, (ii) the collision time is very fast due to greater numbers of droplets within the bulk, (iii) all free surfactant within the system has been exhausted. Furthermore, this suggests that emulsion production adopting a break up approach has a number of inherent disadvantages.

Ensuring uniform energy dissipation (i.e. all turbulent eddies are identical in size) is extremely difficult. As a consequence, there is a lack of control over the droplet size distribution with

wide distributions produced. This may lead to Ostwald ripening which has a detrimental effect on the quality of the product, limiting its lifespan. Process reproducibility is also poor, so each batch may vary significantly in droplet size; this is not ideal if one is required to manufacture a homogeneous product. Secondly, droplet break up processes impart very high shear stresses on the emulsion microstructure. This may therefore be unsuitable for materials or structures that are susceptible to damage by shear (e.g. double emulsions, proteins, high dispersed phase volume fraction emulsions). Currently, these limitations are accepted gracefully by manufacturers. However, the nature of the process may restrict the development of more unique structures in future, of which the limitations will be problematic.

2.2 Membrane Emulsification

Membrane emulsification is a novel process that has been developed over the past 25 years. It was initially introduced by Tadao Nakashima in 1988 at a meeting for the Chemical Engineering Society of Japan in conjunction with a new type of membrane material (Shirasu Porous Glass; SPG). The first set of experimental data for membrane emulsification was published in 1991 (Nakashima *et al.*, 1991) with the process subsequently patented in 1994 (Nakashima *et al.*, Inventors U.S. Pat. No. 5326484). Within this patent, it was detailed that the process involves a tubular SPG membrane with continuous phase flowing through the centre and dispersed phase pressurised from outside-to-inside. Thus, this was the inception of cross-flow membrane emulsification (XME). Nakashima and colleagues produced Kerosene-in-water emulsions stabilised by a variety of surfactants (SDS, Tween 20 and PGPR). A key feature was the ability of the process to produce mono-dispersed emulsions using SPG membranes with span values of less than 0.5. The exact reason has been debated within literature. Most authors suggest the reason to be due to the narrow pore size distribution (Cheng *et al.*, 2006; Pawlik and Norton, 2013) although the SPG membrane surface consists of asymmetric pore openings (Vladisavljevic *et al.*, 2007) which makes this hypothesis unclear. Alternatively, the resultant droplet formation mechanisms induced by such pore openings is suggested to be

responsible (Yasuno *et al.*, 2002; Rayner *et al.*, 2005). In the case of Nakashima, the Kerosene droplets ranged between 300 nm to 40 μm ; a ratio of between 3-8 times the pore diameter. This ratio has since been suggested to be wider, between 2-15 times and depending on a multitude of factors related to the membrane material properties, the process conditions and the formulation used (Joscelyne and Tragardh, 2000; Charcosset, 2004).

Clearly, selection of the appropriate membrane has a strong influence on the emulsion structure by determining the droplet formation process. Once the droplet has detached from the membrane surface, no further change in size should be experienced either due to turbulent break up or coalescence. This is the basis of membrane emulsification. However, the process has been further developed leading to a wide variety of approaches to impart shear at the membrane surface. These innovations have served to allow for formulation of a wide array of micro-structural products. Alongside basic emulsions, double emulsions (van der Graaf *et al.*, 2005; Pawlik and Norton, 2012) nano-emulsions (Oh *et al.*, 2011) and structures for encapsulation purposes including microspheres, microcapsules and microbeads (Vladisavljevic and Williams, 2005) have all been produced. As the demand within society for specialised products (e.g. low fat foods; achievable via double emulsion production and stabilisation) or for products that have been manufactured in a sustainable manner (e.g. low energy consumption) increases, it is highly probable that a greater interest will be taken in membrane emulsification since it has the potential to meet these demands.

2.2.1 Process Development

Membrane emulsification can be undertaken using a wide range of approaches. Whilst cross-flow membrane emulsification (XME) was the first membrane emulsification process to be developed, it is not considered the simplest of the subset of processes due to the flow of continuous phase across the membrane surface. Instead, membrane emulsification can be operated with a quiescent continuous phase. Known as dead end membrane emulsification, it is very similar to emerging processes such as microchannel emulsification (Kobayashi *et al.*, 2011) and Edge-based

Droplet Generation; EDGE (Dijke *et al.*, 2009). Droplet detachment occurs spontaneously in the absence of shear induced by the continuous phase. Generally, the droplets produced are quite large due to the absence of force that induces earlier detachment such as the drag force. Applying some degree of shear at the membrane surface is beneficial for producing smaller droplets. This can be achieved either by moving the continuous phase or moving the membrane to induce a relative velocity difference between the attached droplet and the continuous phase. For the former, movement of fluid is achieved using a re-circulating pump for XME (Peng and Williams, 1998) or a mechanical stirrer for stirred cell membrane emulsification (Kosvintsev *et al.*, 2008; Egidi *et al.*, 2008; Oh *et al.*, 2011). In the latter case, the membrane can be vibrated (Zhu and Barrow, 2005; Kelder *et al.*, 2007) or rotated (Schadler and Windhab, 2006; Yuan *et al.*, 2009; Pawlik and Norton, 2012) to move the attached droplet at a faster velocity than the continuous phase adjacent to the membrane surface. Finally, an alternative approach in which coarse emulsions were passed through membrane materials was recently introduced, known as pre-mix membrane emulsification (Vladisavljevic *et al.*, 2004a; Nazir *et al.*, 2011). Rather than adopting the conventional approach, droplets are broken down within the internal structure of the membrane rather than forming from individual pore channels. It is predictable that with such a wide array of process designs, membrane emulsification is yet to undertake its completely optimised form. Common problems include low dispersed phase flux, membrane fouling, droplet coalescence or break up during/after formation. These will now be discussed further for a number of the process developments prior to outlining why rotating membrane emulsification (RME) has been considered the most favourable.

As highlighted, the XME process utilises a pump to flow continuous phase and flow it across the surface of the membrane. This generates shear that acts on droplets to cause detachment from the pore outlet at a size smaller than would be achievable purely spontaneously (as with dead end membrane emulsification). The continuous phase is continuously re-circulated to gradually increase the amount of dispersed phase until the required volume fraction is reached. This therefore means that droplets formed at the very beginning of the process are passed repeatedly through the pump

which may cause break up or coalescence (Kato, 1997; Dragosavac *et al.*, 2008). Additionally, the dispersed phase flux with XME has been found to be low, particularly when using typical membrane materials such as SPG and ceramics (these have a high resistance to flow due to their internal structure). A typical flux value would be within the region of 10-100 L m⁻² h⁻¹ to produce droplets of 1-10 µm (Joscelyne and Tragardh, 2000). Combining the issues with droplet-droplet interactions within the bulk with long operation times, XME can damage the microstructure of an emulsion. This was not a problem with the simpler dead end process which has no moving parts. Furthermore, the energy consumption of dead end membrane emulsification is low even compared to other membrane emulsification techniques (Lambrich and Schubert, 2005). However, high concentrations of surfactant are required to reduce the interfacial tension force sufficiently to detach droplets and compensate for a lack of drag force. Instead of these possible configurations, rotating the membrane is an innovation that can potentially overcome these problems.

Rotating Membrane Emulsification (RME) is a relatively new approach to produce emulsions which has been developed over the past 8 years (Schadler and Windhab, 2006; Vladisavljevic and Williams, 2006). As such, there are very few studies investigating this process so the effects of various parameters on the emulsion structure are unclear. The concept of RME was developed from applications within membrane filtration which utilised rotating disks and cylinders to dynamically separate materials (Bouzerar *et al.*, 2000; Lee and Lueptow, 2001). Two leading groups pioneered initial research into RME; a research group in Switzerland led by Prof. Erich Windhab and one in Leeds (UK) which was led by Prof. Richard Williams. Each group rotated micro-engineered metal, tubular membranes within a continuous phase vessel to produce emulsions. However, the philosophies driving the research were different. Windhab and co-workers focussed on producing small emulsion droplets at high surface shear. This was achieved by using a 100 mm diameter, nickel foil tube with pores of 1-5 µm produced by etching combined with plasma enhanced chemical vapour deposition. The membrane was rotated at speeds up to 8000 RPM within a vessel only 1-2 mm wider in diameter (Schadler and Windhab, 2006). On the other hand, Williams and co-workers

aimed to form mono-disperse droplets by using a narrower diameter (10 mm), stainless steel tube with laser-drilled pores of 100-150 μm (Vladisavljevic and Williams, 2006; Aryanti *et al.* 2009; Yuan *et al.*, 2009). Regardless of approach, rotating the membrane negates the requirement of a pump to continuously re-circulate the continuous phase. As such, Vladisavljevic and Williams (2006) suggested RME to be highly suitable for the production of fragile particles as well as viscous emulsions for this reason. In addition, the rotational motion (which imparts shear on the droplet) ensures droplets do not flow directly parallel across the surface of the membrane which may promote coalescence phenomena. As with many of the membrane emulsification processes, low dispersed phase flux to produce small droplets was the rate limiting step and thus a problem needing solving.

The apparent flaw for 'direct' membrane emulsification processing resulted in the development of an alternative approach; pre-mix membrane emulsification, which uses a coarse emulsion as the dispersed phase rather than pure material. Since the viscosity is likely to be much lower, much higher fluxes are achievable. For example, Suzuki *et al.* (1998) recorded fluxes of $13 \text{ m}^3 \text{ m}^{-2} \text{ h}^{-1}$ through $1 \mu\text{m}$ pore diameter polytetrafluoroethylene (PTFE) membranes and an applied TMP of 15 bar. Nazir *et al.* (2011) achieved fluxes up to $1600 \text{ m}^3 \text{ m}^{-2} \text{ h}^{-1}$ using a low porosity (0.05) nickel sieve with $13.2 \mu\text{m}$ pores and a TMP of 2 bar. Vladisavljevic *et al.* (2004) observed values of up to $37 \text{ m}^3 \text{ m}^{-2} \text{ h}^{-1}$ using a $10.7 \mu\text{m}$ SPG membrane combined with a TMP of 3 bar. All of these values are typically at least two orders of magnitude higher than emulsification with direct XME or RME. The basis of pre-mix membrane emulsification is that large droplets are disrupted within pore channels through a combination of localised shear forces, interfacial tension effects and steric hindrance of droplets (Vladisavljevic *et al.*, 2004). This causes droplets to elongate and compress in a similar manner to high pressure homogenisation and hence can be considered a modified approach to typical droplet break up processing. Although unclear as to how these combined forces exactly act on the droplet (Nazir *et al.*, 2010), it is known that increasing the pore fluid velocity (through applying a higher TMP) or the membrane resistance to flow (smaller pores, greater thickness)

increases the shear force and subsequently the extent of break up. This process is typically repeated numerous times, narrowing the droplet size distribution curve in conjunction with minimising the droplet size. Pre-mix membrane emulsification is also very energy efficient since there are no moving parts (if used alongside a dead end approach). However, the requirement for multiple passes rather than a single, slower pass of pure dispersed phase may result in the energy savings being lost. The major drawback to emulsification using this approach is due to membrane fouling (van der Zwan *et al.*, 2008; Trentin *et al.*, 2009). The process is still within uncharted territory with regards to the theoretical understanding and without readily available membrane materials that minimise fouling (or that can be easily and sufficiently cleaned). For these reasons, it was decided that RME has shown the most promise but requires detailed exploration.

2.2.2 Membrane Development

Arguably, the most important aspect within membrane emulsification processing is the membrane itself. A membrane is defined as an interfacial barrier or area that can separate at least two different phases and select material passing through it. Selection of the material to-be-used is one of the most critical stages for design and operation of membrane emulsification. A table of membrane factors influencing the emulsion microstructure and dispersed phase flux as compiled by Gijssbertsen-Abrahamse *et al.* (2004) is shown:

Table 2.1: Summary of membrane parameters and their effect on droplet diameter and dispersed phase flux. Symbols indicate parameter is; critically important (***), important (**) or not important (*)

Parameter	Effect on Droplet Dia.	Effect on Flux
Average pore diameter	***	***
Shape of pore outlet	**	**
Wettability	***	*
Porosity	**	***
Thickness	*	***

Droplets are usually between a ratio of 2-15 times the pore diameter although typically a factor of 5 for SPG membranes. For non-SPG membrane types, this ratio can be as high as 50. It is therefore apparent that selection of the pore diameter governs the range of droplet sizes that can be produced. A uniform pore size distribution is also important for production of mono-disperse droplets (Peng and Williams, 1998). The shape of the pores can also be modified to enhance droplet formation from conventional circular pores, to oblong (Kobayashi *et al.*, 2002), square (Yuan *et al.*, 2009) and even unusual shapes such as stars. For example, Yuan *et al.* (2009) found that horizontally aligned rectangular pores produced droplets twice as fast as vertically aligned or cylindrical pores in lieu of easier droplet detachment even under low shear rate operation. In terms of the dispersed phase flux, this is also strongly determined by membrane properties such as the pore diameter, porosity, thickness etc. Membranes can come in a variety of sizes and shapes; typically as cylindrical tubes or flat disks. Their surfaces may be hydrophilic, hydrophobic or non-charged; this may be modified by pre-soaking the membrane within an acidic solution or an organic silane for example. It is essential that the dispersed phase does not wet (i.e. spread across) the membrane surface (wall contact angle $< 90^\circ$) so typically the membrane is soaked in the material to-be-used as the continuous phase (Gijsbertsen-Abrahamse *et al.*, 2004). The concept of contact angle is shown by Fig. 2.4. Spreading of the dispersed phase and therefore shifting of the three-phase contact line may promote coalescence between adjacent pores. This may also be promoted if surfactant adsorbs to the membrane surface, as well as possible fouling.

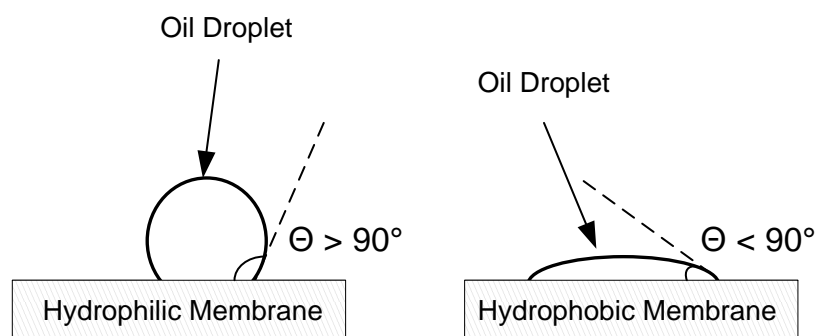


Fig. 2.4: A schematic representation of an oil droplet positioned upon a membrane surface.

When considering the behaviour of the material, a number of assumptions are typically made; an idealised membrane material would consist of identical, perfectly spherical, non-interacting pores. In reality, the internal pore network can be complex so neighbouring pores play an important role during droplet formation. If adjacent droplets interact with each other at the membrane surface, this could result in coalescence occurring. As such, there is an optimum membrane porosity (based on the droplet to pore diameter ratio) which ensures droplet-droplet contact is avoided whilst maximising membrane permeability and hence the flux. Based on all pores being active (i.e. dispersed phase passing through each one) and equal pore spacing, Abrahamse *et al.* (2002) recommended a maximum porosity of 0.015 for 5 μm pores producing droplets of 33 μm in diameter. This transcends to a pore spacing of at least 10 times the pore diameter. Appreciation of this concept can allow for the development of carefully engineered membranes to meet requirements for a given application. The membranes must also be durable to withstand high temperatures and chemicals needed for cleaning processes, as well as strong to withstand forces induced by the application of pressure or a rotating motion. With membrane replacement costs likely to be reasonably high, work needs to be undertaken to produce membranes with a longer lifespan beyond the current estimate of 5 years (Charcosset, 2009). In their present form, materials such as SPG, ceramic, polymer and metallic membranes do not meet all of the aforementioned criteria.

SPG (Shirasu-porous-glass) membranes are the most commonly investigated within membrane emulsification processing. They are a type of glass material produced by the phase inversion of $\text{CaO-Al}_2\text{O}_3\text{-B}_2\text{O}_3\text{-SiO}_2$; a volcanic ash from Kyushu Island, Japan. The material was developed and patented by Nakashima *et al.* (Inventors U.S. Pat. No. 4657875) and is typified by a very narrow pore size distribution. Subsequently, this allows SPG membranes to produce very mono-disperse droplet sizes compared to other membrane types (Vladisavljevic *et al.*, 2004b). They are extremely well characterised predominately through the work of Vladisavljevic using liquid permeability, Hg (Mercury) porosimetry, SEM imaging and high resolution X-ray microtomography

(Vladisavljevic *et al.*, 2005; Vladisavljevic *et al.*, 2007). From this work, it is revealed that SPG membranes contain a series of tortuous, non-circular and randomly distributed pores that are interconnected within the material structure as a network or 'maze'. They are available in a range of pore sizes between 0.05-30 μm . The porosity varies almost randomly between 0.5-0.6 with an average of 0.56. However, the percentage of pores active is below 10% (Schroder *et al.*, 1998; Vladisavljevic *et al.*, 2007) so the effective porosity is much lower. Due to the increased resistance to flow caused by the interconnection of pores, a tortuosity factor was introduced to characterise the pore channel length. For example, a tortuosity factor of 1 indicates perfectly cylindrical pores perpendicular to the membrane surface as such the channel length equals the membrane thickness. For SPG membranes, the tortuosity factor has been experimentally determined with values of 1.28 (Vladisavljevic *et al.*, 2005) and 1.32 (Nakashima and Shimizu, 1993) suggested. Alongside their low active pore fractions, SPG membranes are fragile (despite being able to withstand TMPs up to 25 bar) so are therefore unsuitable for many food or pharmaceutical applications as well as for use at an industrial scale.

Ceramic membranes have been investigated by a number of authors (Williams *et al.*, 1998; Matos *et al.*, 2013; Hancocks *et al.*, 2013). Typically, their structure consists of an inner ceramic substrate which provides strength to the material with a thin, outer microporous ceramic coating or 'skin'. Examples include ZrO_2 on a TiO_2 support substrate (Matos *et al.*, 2013) or $\alpha\text{-Al}_2\text{O}_3$ (Lepercq-Bost *et al.*, 2010). The pore size is altered by modifying the voids between ceramic particles as part of a sintering process although this is difficult to control. Ceramic membranes generally demonstrate higher active pore fractions of around 40-60% (Lepercq-Bost *et al.*, 2008) but lower porosity than for SPG (between 0.3-0.4). Additionally, the support layer is thicker for ceramic membranes than for SPG membranes; around 2 mm compared to 20-30 μm respectively. This increases the resistance to flow significantly due to frictional losses which causes ceramic membranes to have low permeability. Their fragile nature also eliminates them from use in an industrial environment. On the other hand, polymer materials such as polypropylene (Suzuki *et al.*, 1998) and polycarbonate track-etched

membranes (Tangirala *et al.*, 2007) may be more favourable due to their higher fluxes and availability in large surface areas (Kobayashi *et al.*, 2002).

It is undoubted that membranes manufactured from metals have the most potential. Examples of such membranes may include laser-drilled stainless steel, etched nickel foil or micro-machined silicon nitride microsieves. In the latter case, microsieves are flat disks consisting of an inner thin film layer of pores and an outer support layer with terraces. They were initially developed for filtration and particle separation applications (Kuiper *et al.*, 1998) but later adopted for emulsification. They are very capable of producing mono-disperse droplets since each pore is almost identical, to an even lower tolerance than for glass or ceramic membranes. Furthermore, they are extremely thin (a couple of microns) so very high fluxes are achievable (Wagdare *et al.*, 2010) and fouling is unlikely. Since their pores are straight and perpendicular to the surface, the active pore fraction is close to 100% with a tortuosity factor of 1. Generally, metal membranes can be carefully designed in such a way to ensure sufficient pore spacing and with unique pore shapes (Yuan *et al.*, 2009) to aid droplet detachment (Kobayashi *et al.*, 2002). They are generally more robust, durable and versatile than other membrane types allowing for much harsher cleaning treatments. For microsieves, they are difficult and expensive to produce. Furthermore, they are fragile since they are so thin which may result in them rupturing under high TMPs. Until recently, other processes to produce metal membranes (e.g. laser drilling) lacked the precision and accuracy needed to produce small, mono-disperse pore sizes. However, advances in metal processing have enabled opportunities for realistic, cost-effective solutions to be created in future.

2.2.3 Droplet Formation Mechanisms

The mechanisms determining the size produced during droplet formation are important to understand in order to control membrane emulsification processes. These are dependent on a combination of processing and formulation parameters (Table 2.2) as well as the membrane parameters (Table 2.1) discussed within the previous section.

Table 2.2: Summary of processing and formulation parameters and their effect on droplet diameter and dispersed phase flux. Symbols indicate parameter is; critically important (***) , important (**) or not important (*)

Parameter	Effect on Droplet Dia.	Effect on Flux
Wall shear stress	***	*
Transmembrane pressure	***	***
Temperature	*	**
Continuous phase viscosity	**	*
Dispersed phase viscosity	**	***
Surfactant type/conc.	***	**

Current theory states that the size of which a droplet grows to and subsequently detaches from the membrane surface is governed by the point of force imbalance. This idea was introduced by Peng and Williams (1998). A high speed camera observed droplet formation from a single capillary tube (diameters ranging from 5-200 μm) into a perpendicular flowing continuous phase (similar concept to XME). The force balance approach can be applied to a membrane (rather than a single capillary tube) provided there are no interactions between adjacent droplets (e.g. coalescence or perturbation of the downstream continuous phase velocity). Generally, as a droplet becomes larger, the magnitude of the detachment forces increases to overcome the retention force (interfacial tension) holding the droplet in position. The interfacial tension force is affected directly by the surfactant adsorption behaviour, but more specifically the rate and extent of interfacial tension reduction over time. For example, with a fast reduction in interfacial tension droplets can detach earlier to be smaller sizes. Of the detachment forces, the most significant is the drag force which is induced by a velocity difference between the attached droplet and the continuous phase. For XME, the drag force is induced by the continuous phase flowing across the membrane surface. In the case of RME, the droplet moves faster than the continuous phase ($v_r > v_{cr}$). These ideas are shown schematically in Fig. 2.5.

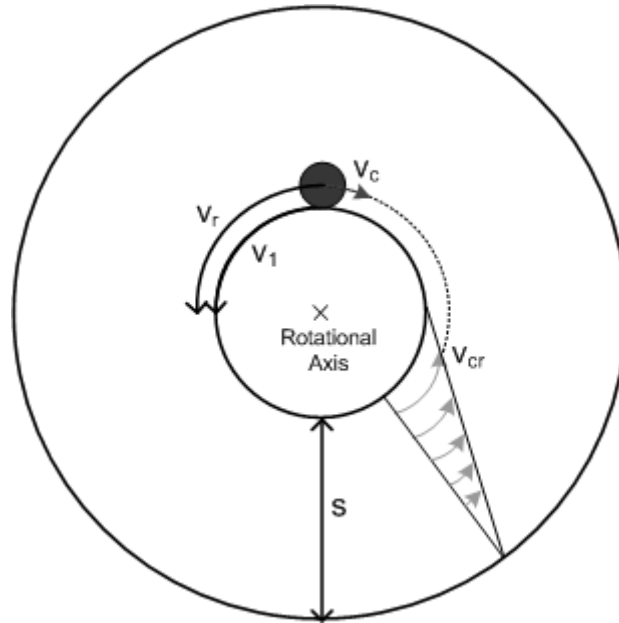


Fig. 2.5: A schematic representation of the velocities across the horizontal plane of an RME configuration.

Another important detachment force is the buoyancy force particularly if droplets are large or there are significant differences in density between the two phases. The inertial, dynamic effect of pressure and dynamic lift forces are typically orders of magnitudes lower (Schroder *et al.*, 1998). Steric droplet interaction without coalescence can give rise to a ‘push-off’ force that may also aid droplet detachment (Egidi *et al.*, 2008; Kosvintsev *et al.*, 2008). Yuan *et al.* (2009) discussed the possibility of a viscous retaining force that hinders droplet detachment. The equations defining each of these forces will be discussed in greater detail within Chapter 6 of the thesis as part of the application of a theoretical model for RME.

Once the point of which the detachment forces overcome the retention force, a droplet will begin to detach from the membrane surface. However, Peng and Williams (1998) also suggested that dispersed phase material will still be contributed to the droplet volume even after force imbalance. Material is added to the droplet via the droplet neck (Scheele and Meister, 1968) which therefore implies that the droplet size is determined by a two stage mechanism as shown by both Eq. 2.8 and Fig. 2.6:

$$V_f = V_g + V_d = V_g + q_d t_d \quad (\text{Eq. 2.8})$$

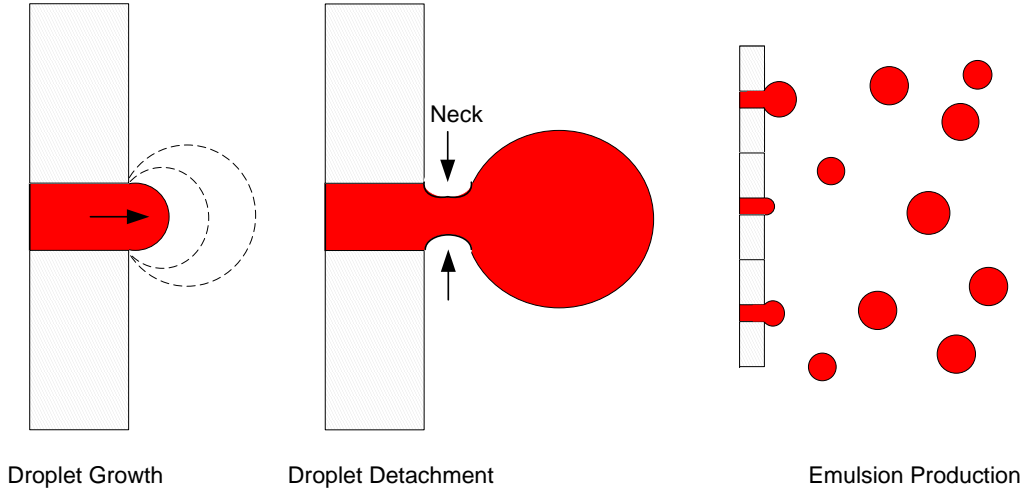


Fig. 2.6: A schematic representation of droplet growth and detachment at a membrane surface, leading to creation of an emulsion.

where V_f is the final droplet volume, V_g is the droplet volume at the end of the growth stage, V_d is the volumetric contribution of material during detachment, q_d is the volumetric flow rate through a single pore channel and t_d is the droplet detachment time. Increasing the TMP would increase both the rate of droplet growth (as it expands) and also the amount of volume contributed as the droplet detaches. If the interfacial area of a droplet expands quickly such that it approaches the rate of surfactant adsorption, insufficient interfacial coverage may lead in higher interfacial tension values (and therefore larger droplets) (Schroder *et al.*, 1998). Eq. 2.8 was extended by Van der Graaf *et al.* (2006) since the formation process was seen to scale with continuous phase capillary number (Ca_c) alongside two coefficients. This is presented in Eq. 2.9:

$$V_f = V_{crit,ref} Ca_c^m + t_{crit,ref} Ca_c^n q_d \quad (\text{Eq. 2.9})$$

where $V_{crit,ref}$ and $t_{crit,ref}$ are the droplet volume at the point of detachment and droplet detachment time respectively (for $Ca_c = 1$), m and n are coefficients which lie between -0.75 to -1.5 assuming no pore distortion effects. To summarise, droplets reach a size in which the detachment forces begin to

exceed the retention forces (the 'droplet growth' stage). Additional material is then added to the droplet depending on the dispersed phase flux and the droplet detachment time (the 'droplet detachment' stage).

Despite the above droplet formation procedure being widely accepted, questions were asked as to how a droplet could be deformed when its Laplace pressure far surpasses the magnitude of the shear stress (drag force) causing the detachment (Rayner *et al.*, 2004). It was postulated by Sugiura *et al.* (2001) that droplet detachment may be induced by interfacial energy rather than hindered by it. A droplet may become deformed (rather than detach directly) due to the forces acting upon it. This results in the droplet increasing its surface area to volume ratio, which from the perspective of Gibbs free energy is a higher energy state. In an attempt to reach its more thermodynamically stable spherical form, a droplet detaches itself from the dispersed phase at the pore outlet whilst simultaneously transforming into a sphere. Hence, this mechanism is known as Spontaneous Transformation-based Droplet Formation and is represented by Fig. 2.7.

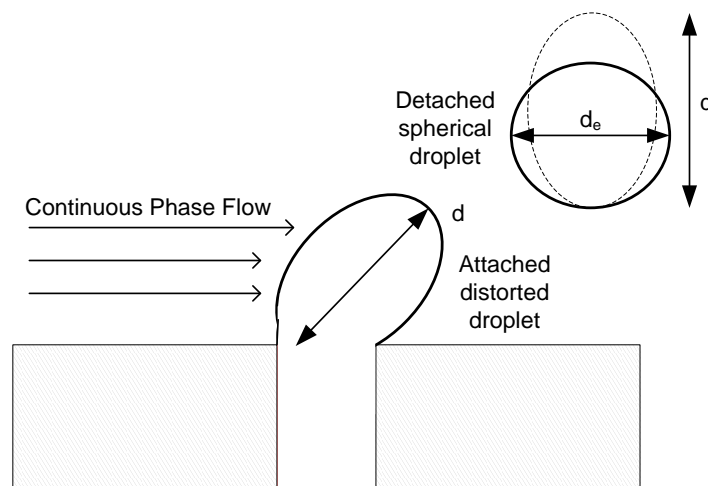


Fig. 2.7: Droplet deformation giving rise to spontaneous detachment and transformation.

The mechanism may be triggered by the use of non-circular pores (e.g. SPG membranes, silicon nitride microsieves) if the dispersed phase wets the pore edges causing droplet deformation. Furthermore, for high IFT systems the differences in energy state between a deformed and a

completely spherical droplet are greater. There is therefore a more significant driving force causing droplet detachment to achieve the lower energy state, spherical form. From a Laplace pressure perspective, a deformed droplet has at least one smaller radius of curvature resulting in a higher internal pressure (aiding detachment since material moves from high to low pressure). Spontaneous transformation-based droplet formation was also concluded to be the droplet formation mechanism in the case where droplet sizes were smaller than expected (Kukizaki, 2009; Matos *et al.*, 2013). Essentially, this idea was adopted for the 'push-off' force value which entails adjacent droplets pushing against each other (with small pore spacing distances) but without coalescing (Egidi *et al.*, 2008; Kosvintsev *et al.*, 2008). This causes an elongation of the droplets which is also energetically unfavourable.

Finally, it is known that if the dispersed phase velocity within the membrane pore is sufficiently high, or the IFT between the dispersed and continuous phases is low, the processes of individual droplet formation described above do not occur. Instead, the dispersed phase is injected into the continuous phase as a liquid jet. This jet breaks up chaotically at a certain length where it is unstable due to Rayleigh instabilities. This mechanism is highlighted schematically in Fig. 2.8. The individual droplet formation mechanisms are therefore referred to as 'dripping' whilst formation of droplets at a distance greater than the droplet diameter away from the membrane surface is known as 'jetting'. Alternatively, the term 'continuous outflow' may also be used to describe jetting phenomena (Kukizaki, 2009).

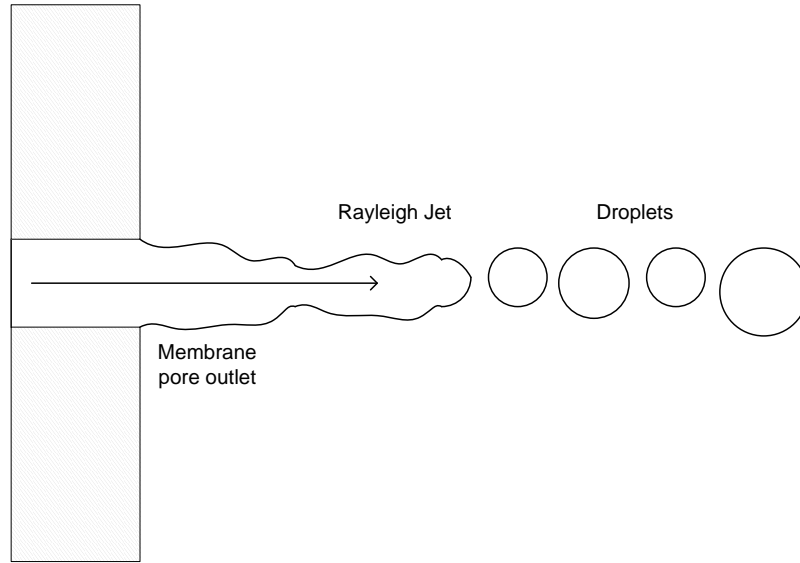


Fig. 2.8: A schematic representing droplet formation through dispersed phase jetting.

Jetting is generally considered unfavourable if the objective is to produce mono-disperse droplets in a controlled manner. However, it may be appropriate to operate with jetting to maximise the dispersed phase flux. It is potentially a compromise between droplet size homogeneity and the emulsion production rate although recent effort has been made to control jet fragmentation (Santos *et al.*, 2015). The occurrence of the jetting mechanism can be predicted by considering dimensionless numbers that characterise the systems flow behaviour. Initially, Sugiura *et al.* (2002) suggested as a rough estimation that a Capillary number (Eq. 2.10) of 0.056 must not be exceeded in order to produce droplets in a controlled manner.

$$Ca_d = \frac{\mu_d \bar{v}_d}{\gamma} \quad (\text{Eq. 2.10})$$

where Ca_d is the dispersed phase Capillary number, μ_d is the dispersed phase viscosity, \bar{v}_d is the average dispersed phase velocity and γ is the interfacial tension. Pathak (2011) expanded the idea with jetting also being a function of the Weber number (Eq. 2.11).

$$We_d = \frac{d_a \rho_d \bar{v}_d^2}{\mu_d} \quad (\text{Eq. 2.11})$$

where We_d is the dispersed phase Weber number, d_d is the droplet diameter and ρ_d is the density of the dispersed phase. Simulations were performed using a Computerised Fluid Dynamics (CFD) software package. The Weber number was modified between 0.009-1.82 by changing the dispersed phase velocity, whilst the continuous phase capillary number was altered by its velocity and IFT value between 0.004-0.008. This enabled the transitional point between dripping and jetting to be mapped in a way shown in Fig. 2.9 and defined by Eq. 2.12.

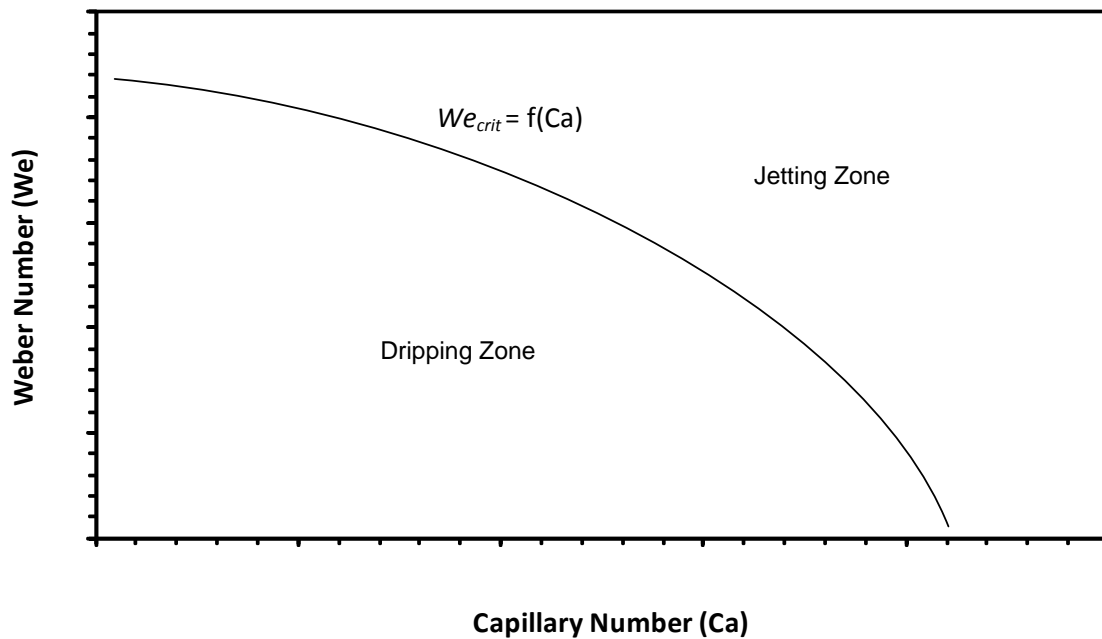


Fig. 2.9: Mapping of the transitional point between dripping and jetting droplet formation mechanism.

$$We_{crit} = k_1 \{1 + k_2 Ca_c^2 - [(1 + k_2 Ca_c^2)^2 - 1]^{0.5}\}^2 \quad (\text{Eq. 2.12})$$

where We_{crit} is critical Weber number, k_1 and k_2 are coefficients determined to be 1.188 and 3455 respectively for the system investigated (Pathak, 2011). Meyer (2010) discussed the idea that the transitional point is not the same for all fluids on the We and Ca space (i.e. Fig. 2.10). The transitional point was found by Ambravaneswaran *et al.* (2004) to be lower values of We or Ca with increasing Ohnesorge number (Eq. 2.13)

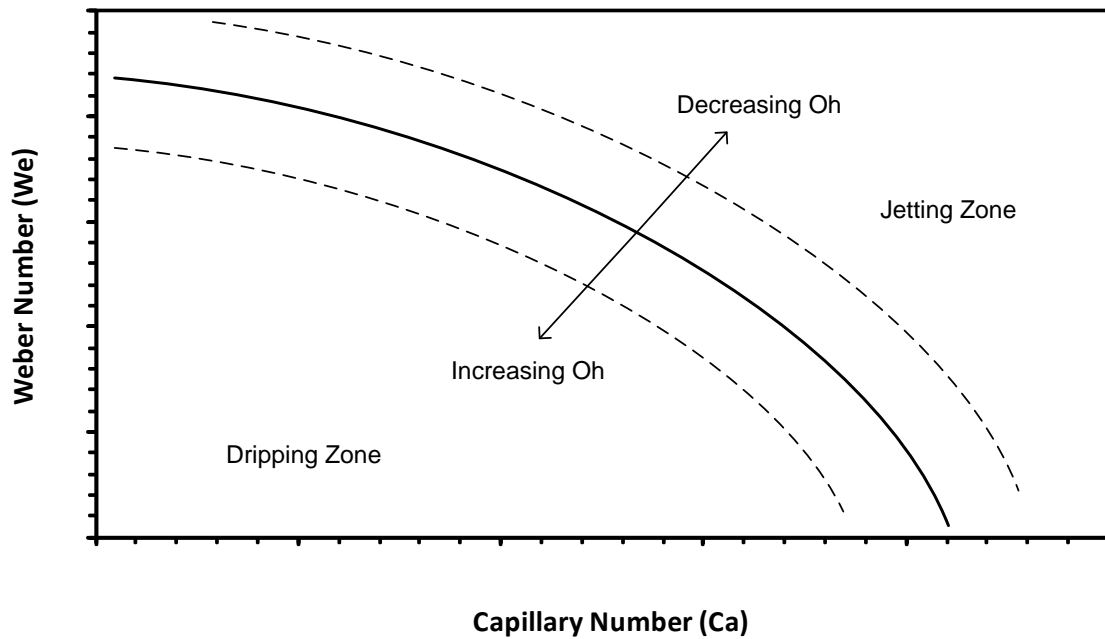


Fig. 2.10: Inclusion of Ohnesorge number in the mapping of the transitional point between dripping and jetting droplet formation mechanism.

$$Oh = \frac{\mu_c}{(\rho_c d_d \gamma)^{0.5}} \quad (\text{Eq. 2.13})$$

where Oh is the Ohnesorge number, μ_c is the continuous phase viscosity and ρ_c is the density of the continuous phase.

2.2.4 Fluid Flow Behaviour

Consideration of the flow behaviour of either the dispersed or continuous phase is important in order to understand membrane emulsification processing. More specifically, this relates to the dispersed phase permeating through the membrane material and the continuous phase flow pattern within the emulsification vessel. The dispersed phase flow behaviour strongly governs the droplet growth rate and the subsequent rate of emulsion production. On the other hand, the continuous phase predominately determines the point of droplet detachment (due to acting detachment forces) and thus the size. Ultimately, the flow behaviour of either phase is explained by equations commonly used within fluid mechanics.

For the dispersed phase, the movement of material through a single channel can be quantified by the Hagen-Poiseuille equation assuming steady-state laminar flow of incompressible fluid:

$$q_d = \frac{\pi d_p^4}{128 \mu_d L_p} \Delta P_{tm} \quad (\text{Eq. 2.14})$$

where d_p is the pore diameter and ΔP_{tm} is the transmembrane pressure. The pore channel length (L_p) is calculated using Eq. 2.15:

$$L_p = L_m \tau \quad (\text{Eq. 2.15})$$

where L_m is the membrane wall thickness and τ is a tortuosity factor which is 1.0 for straight-through pores and 1.28 for SPG (Vladisavljevic *et al.*, 2005). The laminar flow condition is often met since the pore channels tend to be within the micro-scale and thus the Reynolds number of the fluid is very low. However, since membrane emulsification relies on droplet production from multiple pore channels (using a porous bed), Darcy's law is more suitable for predicting the flux behaviour:

$$Q_d = \frac{-K A_m \Delta P_{tm}}{\mu_d L_p} \quad (\text{Eq. 2.16})$$

where Q_d is the volumetric flow rate of dispersed phase through the membrane and A_m is the membrane surface area. The permeability (K) is calculated using an equation suggested by O'Brien *et al.* (2007) adapted from the Carman-Kozeny equation:

$$K = \alpha d_p^2 \phi^{1.5} \quad (\text{Eq. 2.17})$$

where α is the fraction of pores active and ϕ is the membrane porosity. However, these equations cannot be blindly used to estimate the flux and therefore the emulsion production rate. As mentioned in section 2.2.2, membrane materials such as SPG and ceramics demonstrate variable effective porosity as pores activate with increasing TMP. This means that the TMP not only increases the driving force and therefore the flow rate, but also increases the membrane permeability. As such, the flux increases exponentially rather than in a linear fashion. For metallic membranes, this

occurs to less of an extent so the permeability does not drastically change. The extent of pore activation depends on the properties of the specific membrane tested (this may differ slightly for each one). Therefore, the fraction of pores active under a given TMP has to be determined experimentally.

A minimum TMP is required for the dispersed phase to be able to permeate the membrane structure and form a droplet. Therefore, the above equations are only applicable presuming the TMP is above this critical value; known as the capillary pressure. This is defined as:

$$P_c = \frac{4\gamma\cos\theta}{d_p} \quad (\text{Eq. 2.18})$$

where P_c is the capillary pressure and θ is the contact angle between the dispersed phase and the capillary wall. The capillary pressure is also affected by tortuosities within the pores, irregular shaped pore openings and surface wettability effects so the minimum TMP may need to be slightly higher. It is recommended to operate with a TMP between 1-10 times larger than the capillary pressure (ideally 1-5) in order to produce small, stable droplets (Nakashima *et al.*, Inventors U.S. Pat. No. 5326484) since the interfacial tension force is dominant (Sugiura *et al.*, 2001). However, to maximise the dispersed phase flux, the TMP must be as high as possible, but without jetting occurring. This may also be achievable by lowering the dispersed phase viscosity via heating, but this may promote droplet instability (Boyd *et al.*, 1972). It was also suggested the dispersed phase flux could be increased by applying surfactant within the dispersed phase (Katoh *et al.*, 1996), pre-soaking the membrane in continuous phase (Wu *et al.*, 2006) or using non-circular pores (Yuan *et al.*, 2009). The occurrence of dispersed phase jetting flow behaviour upon exiting the pore can be determined by evaluating the dimensionless Reynolds, Weber and Ohnesorge numbers as discussed in section 2.2.3. The velocity term can be estimated by dividing the volumetric flow rate by the cross-sectional area of the pore channel or calculated by using the Fanning equation (for steady laminar flow in a tubular pipe):

$$v_d = \frac{d_p^2}{32\mu_d L_p} \Delta P_{tm} \quad (\text{Eq. 2.19})$$

where v_d is the dispersed phase fluid velocity within the pore channel. However, the velocity is an approximation since it has been shown to fluctuate during droplet formation (Abrahamse *et al.*, 2001). As the droplet expands, the Laplace pressure decreases (Schroder *et al.*, 1998), resulting in more of the applied pressure being used to force material through the membrane channel (increase in pore fluid velocity). With the formation of a droplet neck, the velocity decreases sharply as the pressure drop across the droplet neck is high. This is represented schematically:

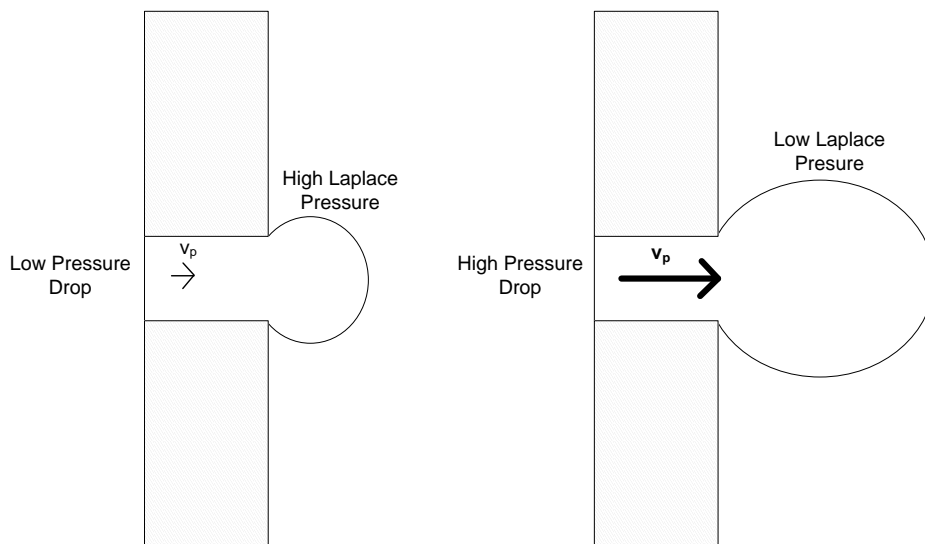


Fig. 2.11: A schematic diagram representing dispersed phase velocity change as a droplet grows at the membrane surface.

For the continuous phase, the flow behaviour depends on the membrane emulsification configuration used. For XME, the behaviour can be quantified simply by the Reynolds number within the cross-flow channel as shown by Eq. 2.20:

$$Re_c = \frac{\rho_c v_c D_H}{\mu_c} \quad (\text{Eq. 2.20})$$

where Re_c is the continuous phase Reynolds number, v_c is velocity of the continuous phase and D_H is the hydraulic diameter of the channel. Generally, membrane emulsification is operated within laminar flow with streamlines moving parallel to the membrane surface (to ensure uniform droplet

production). However, the flow behaviour for RME is more complex since it involves two coaxial cylinders in which one rotates at a specified angular velocity relative to the other (Lathrop *et al.*, 1992). As such, radial mixing rather than axial mixing occurs (Baier *et al.*, 2000). A dimensionless Taylor number (Ta) quantifying rotating fluid flow therefore also requires consideration (Taylor, 1923) alongside an alternative expression for Reynolds number:

$$Re_c = \omega_1 r_1 (r_2 - r_1) \frac{\rho_c}{\mu_c} \quad (\text{Eq. 2.21})$$

$$Ta = Re_c \sqrt{\frac{2(r_2 - r_1)}{r_1 + r_2}} \quad (\text{Eq. 2.22})$$

where ω_1 is the angular velocity of the membrane surface, r_1 and r_2 are the radii of the membrane and outer vessel respectively. The movement of the membrane can generate inertial instability within the flow; known as Taylor vortices. Their development depends on factors such as the membrane surface angular velocity, the annular gap width between the membrane surface and the emulsification vessel wall and the continuous phase viscosity. As the Taylor number exceeds 41.3 (Schadler and Windhab, 2006), the behaviour shifts from simple laminar-couette flow to laminar flow with vortices. Beyond a Taylor number of 400, the flow is turbulent with formation of unsteady, non-symmetric vortices known as Wavy vortices. The development of Taylor vortices as seen by Schadler and Windhab (2006) is advantageous for producing small droplet sizes; the droplet to pore size ratio decreased from 6.15 to 1.81 in their presence. Eisner (2007) suggested the flow profile could directly affect the droplet formation process depending on the alignment of Taylor vortices as shown in Fig. 2.12:

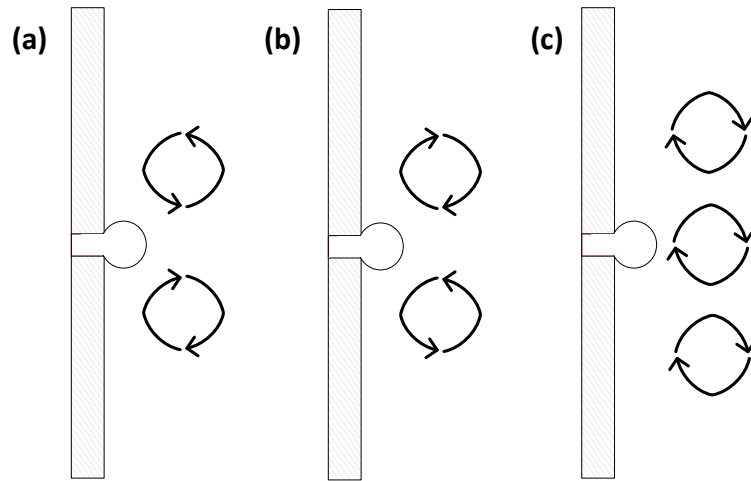


Fig. 2.12: Possible alignments of Taylor vortices relative to a forming droplet.

In case (a), the droplet is forming at the outflow of the vortex (flow away from membrane surface) which helps to pull droplets into the continuous phase. For case (b), droplet production occurs within the inflow of the vortex (towards the membrane surface) holding droplets at the membrane surface for longer. In case (c), the flow is tangential to the droplet which will induce detachment due to shear. The angular velocity of the vortex roughly equates to the velocity of the membrane surface; this flow is insufficient to destabilise emulsions due to droplet coalescence within the bulk (van Boekel and Walstra, 1981).

The shear rate at the membrane surface is also often used as a means to characterise the behaviour of the process. This is typically converted into a wall shear stress value by multiplying by the continuous phase viscosity demonstrated at a given shear rate. For RME, the shear rate was derived by Vladisavljevic and Williams (2006) for a concentric cylinder setup as:

$$\dot{\gamma} = \frac{\pi r_1^2 n_1}{15(r_2^2 - r_1^2)} \quad (\text{Eq. 2.23})$$

$$\tau_w = \mu_c \dot{\gamma} \quad (\text{Eq. 2.24})$$

where $\dot{\gamma}$ is the shear rate, n_1 is the number of rotations per minute and τ_w is the wall shear stress. Greater shear generally results in the production of mono-dispersed droplets of diminishing size until their diameter becomes independent of the shear (Joscelyne and Tragardh, 2000). The shear rates are generally very low (such that it is unlikely droplet break up will occur). Control of the droplet size at a given TMP is achieved by modifying the shear rate (rather than the viscosity) to impart more detachment force and hence earlier detachment. This is because viscosity effects are more complicated; for example, the continuous phase viscosity may limit surfactant diffusion or prevent formation of Taylor vortices.

Finally, the importance of a dimensionless Capillary number for the continuous phase (Ca_c) was introduced (Lepercq-Bost *et al.*, 2008). This included an interfacial tension value alongside consideration of the velocity within a cross-flow channel as shown in Eq. 2.25:

$$Ca_c = \frac{\mu_c v_c}{\gamma} \quad (\text{Eq. 2.25})$$

Beyond a Capillary number of 0.5, droplet size was unaffected with a constant droplet to pore size ratio of 3. Operation at the threshold Capillary number was therefore suggested to be the optimum point in terms of energy efficiency.

2.3 Modelling of Membrane Emulsification Processes

In order for membrane emulsification to progress from the small scale towards an industrially viable emulsion manufacturing method, the process requires the development of scale up approaches and appropriate modelling systems. Such models will enable predictions of how input parameters (e.g. TMP, shear rate, membrane pore size) determine the output of the process (e.g. droplet size, production rate). In essence, this would give manufacturers a significant element of control over the final properties of the emulsion product (Schroder and Schubert, 1999; Charcosset *et al.*, 2004). However, the process is highly complex, governed by a large number of interacting

processing, formulation and membrane parameters (Vladisavljevic *et al.*, 2004b; De Luca *et al.*, 2007). As such, modelling approaches require much focus as to explain and predict their influence on micro-structural design.

At the most basic level, empirical models have been developed from experimental data although these generally demonstrate parameter trends rather than mathematically justify the final droplet size. Algebraic force balance models (FBM) and torque balance models (TBM) consider the physics of detachment and remain the most widely adopted technique. Other more complex approaches such as surface free energy minimisation models, multi-dimensional fluid dynamics (CFD) and lattice Boltzmann simulations require the use of computers to predict the aforementioned droplet formation mechanisms and fluid flow behaviour. Ideally, the modelling technique should be reliable but also easy to use and therefore each method has advantages and limitations.

The idea of FBMs and TBMs were first introduced by Peng and Williams (1998) when they suggested (as discussed within section 2.2.3) that a droplet will begin to detach due to an imbalance of forces acting upon it. The difference between the two techniques is primarily down to the point of reference, with the TBM considering moments around the leading point of the pore circumference in the direction of detachment. On the other hand, the FBM is based around the contact line at the membrane surface. However, both rely on the concept that detachment forces (e.g. drag, buoyancy) overcome the adhesive force of interfacial tension. A schematic of the forces is represented within Fig. 2.13 (a) whilst their magnitude is presented in Fig. 2.13 (b):

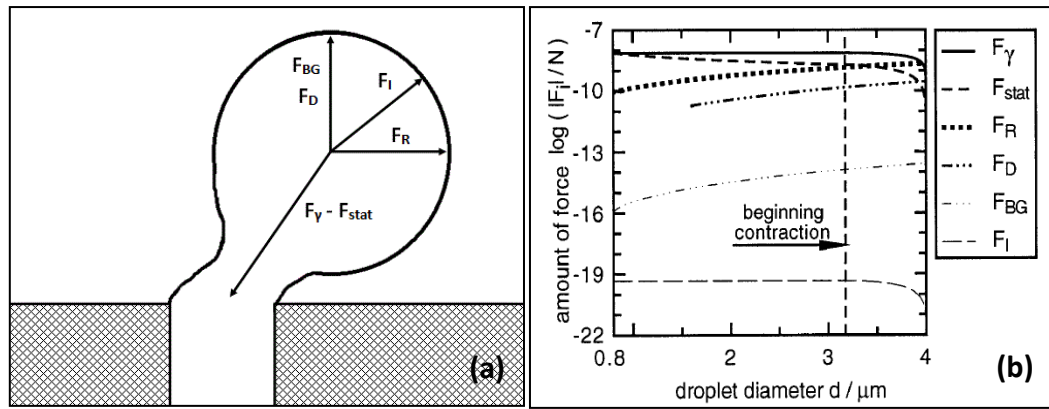


Fig. 2.13: Schematic (a) and magnitude (b) of forces acting on a droplet during cross-flow membrane emulsification (Schroder *et al.*, 1998). Within this figure, F_Y denotes the interfacial tension force, F_R is the viscous drag force, F_{BG} is the buoyancy force, F_I is the inertial force, F_D is the dynamic lift force and F_{stat} is the static pressure force.

It is clear that modification of processing parameters alters the magnitude of each force as a function of droplet size and thus changes the point of which imbalance and therefore detachment occurs. Initial attempts used equilibrium rather than dynamic interfacial tension values which led to some inaccuracy with the static models. De Luca *et al.* (2004) improved the TBM to account for this by substituting different values of interfacial tension with respect to time; solutions could be found numerically over theoretical droplet formation times. Reasonable accuracy was achieved at large pore sizes above $5.5 \mu\text{m}$. Further development by De Luca and Drioli (2006) introduced a FBM that considers distortion of the droplet due to continuous phase flow. In this work, the behaviour of advancing and receding contact angles were calculated numerically as a function of droplet size. The critical droplet diameter of which detachment began was recorded as the smallest of multiple solutions corresponding to one of droplet contact angles reaching a value of 0 or π radians.

Timgren *et al.* (2010) successfully developed a FBM to predict droplet size taking into account droplet deformation during the growth and detachment stages. This was achieved through alteration of the perpendicular drag and lift force coefficients (Timgren *et al.*, 2008). Previous models adopted coefficient values of 1.7 and 0.761 respectively. However, these values did not consider the attachment between a forming droplet and dispersed phase within the pore, but rather the droplet

as a rigid spherical entity. Through modelling and iterative calculation of the deformation angle of a droplet using CFD, the point of force imbalance could be solved. A drag force coefficient of 2.6 was found to correspond better to the systems behaviour. Similarly, a much larger value of 2.0 was appropriate for the lift force coefficient since the coefficient asymptotes once the dispersed phase Reynolds number falls below 50. Overall, a significant reduction in error was demonstrated between calculated and simulated droplet sizes even in the case of low shear rates.

The limitations of the model are that the transfer of material via the droplet neck during detachment is not accounted for; droplets are assumed to detach instantaneously upon force imbalance. Secondly, spontaneous transformation-based droplet formation is not considered (Rayner *et al.*, 2004). As a consequence, the model can sometimes over-predict the droplet diameter. This is prominent particularly for high interfacial tension systems and if very small, tortuous or non-circular pore openings are used. This can play a pivotal role in droplet distortion and the consequential detachment process. Finally, the models generally do not account for the movement and adsorption of surfactant(s). The differences in dynamic behaviour of fast adsorbing surfactants such as SDS and those that are slower (e.g. Tween 20) are not discriminated. Greater error is experienced if the interfacial tension decreases very quickly (Timgren *et al.*, 2010). Whilst these models remain less accurate than the more rigorous computational techniques, they are useful for process optimisation studies and serve as a rough estimation of droplet size (De Luca *et al.*, 2008). Calculations can be performed quickly since very few equations require solving, facilitating their use. They also offer great versatility since many parameters can be altered at once. However, the models are based around a number of assumptions namely droplet coalescence negligence. Reliability may be increased by removing or relaxing assumptions to take droplet interaction and pore effects into account.

Rayner *et al.* (2004) developed an alternative modelling technique which accounted for droplet detachment being induced by interfacial energy rather than by forces acting upon it (Sugiura

et al., 2001) i.e. spontaneous transformation-based droplet formation mechanism. A ‘surface evolver’ tool was developed to model the droplet shape as it formed and represented it as a triangular tessellation of surfaces as shown in Fig. 2.14.

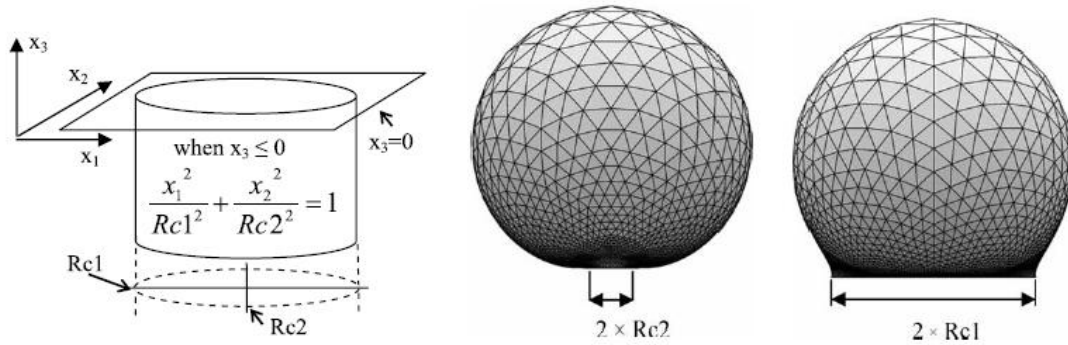


Fig. 2.14: Pore boundary condition and droplet simulation along minor and major axes; the basis of the surface evolver tool (Rayner *et al.*, 2004).

The original model assumed a stationary continuous phase and therefore negated the effects of drag force on droplet shape. Furthermore, the interfacial tension was taken as a static rather than dynamic driving force. Nevertheless, good agreement with experimental data was seen. Rayner *et al.* (2005) improved the model by considering the coupling effect between the rate of droplet inflation and the surface coverage by the surfactant, and hence interfacial tension. The increase in size during the detachment stage was also accounted for. This modelling technique was capable to overcome some of the issues encountered with FBM and TBM since it could be applied to quiescent conditions and non-spherical pore geometries. The limitations of the model primarily relate to the longer calculation times required, but also inaccuracy due to possible membrane wetting effects.

Another useful modelling approach uses CFD to simulate droplet formation on two dimensional planes. This has enabled development of the simpler models by providing insight into the physics of the process, but also as a means of validating model predictions. Abrahamse *et al.* (2001) successfully demonstrated the use of CFD for membrane emulsification. A droplet was theoretically formed from a single cylindrical pore within a laminar flow continuous phase as

represented in Fig. 2.15.

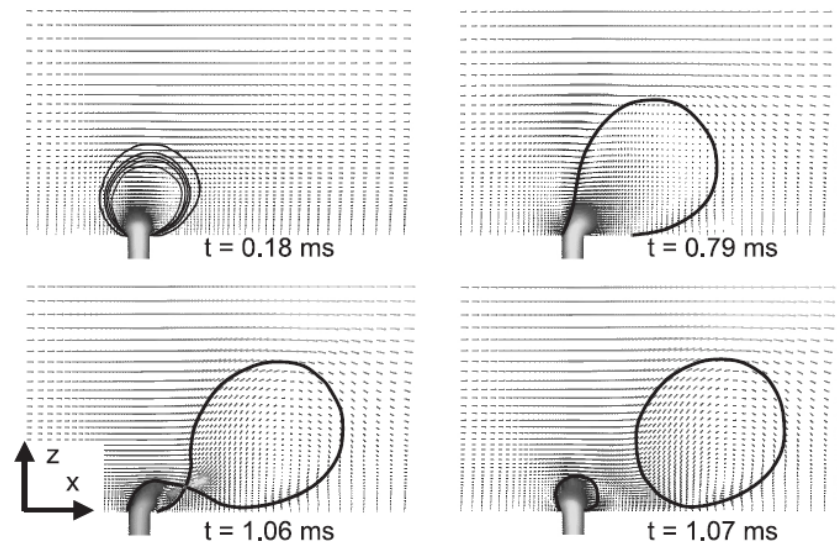


Fig. 2.15: Computational fluid dynamics (CFD) velocity profile of an oil droplet forming within an aqueous continuous phase (Abrahamse *et al.*, 2001).

The primary aim of the study was to observe the pressure drop across the pore channel, and the subsequent dispersed phase fluid velocity changes as a droplet is produced. As mentioned previously, these values fluctuated drastically over time despite a constant applied pressure (1.3 bar) and interfacial tension value (30 mN m^{-1}). This was due to the Laplace pressure decrease as the droplet inflated, followed by significant frictional losses from flow via the neck; this would have been difficult to measure experimentally. Where CFD particularly excels is for modelling flow behaviour of multiple forming droplets. The technique can account for complexities that simplified models do not address, including consideration of pore activation and droplet-droplet interactions. The main drawback apart from long calculation times, is the need for the system to be very clearly defined in terms of its physics. Also, CFD has yet to be demonstrated to account for wetting of the membrane surface. Despite this, CFD can achieve a decent level of prediction accuracy for two dimensional planes.

Finally, simulations have been performed through adoption of the lattice Boltzmann method (Van der Graaf *et al.*, 2006; Van der Zwan *et al.*, 2009) as seen in Fig. 2.16. This approach relies on kinetic gas theory to predict how hypothetical particles move and collide on a lattice. These particles

can be considered to represent segments of fluid and therefore model the process from both a physical and thermodynamic perspective. Generally the other models could only invoke the former which is why difficulties arose when accounting for the dynamic behaviour of surfactants.

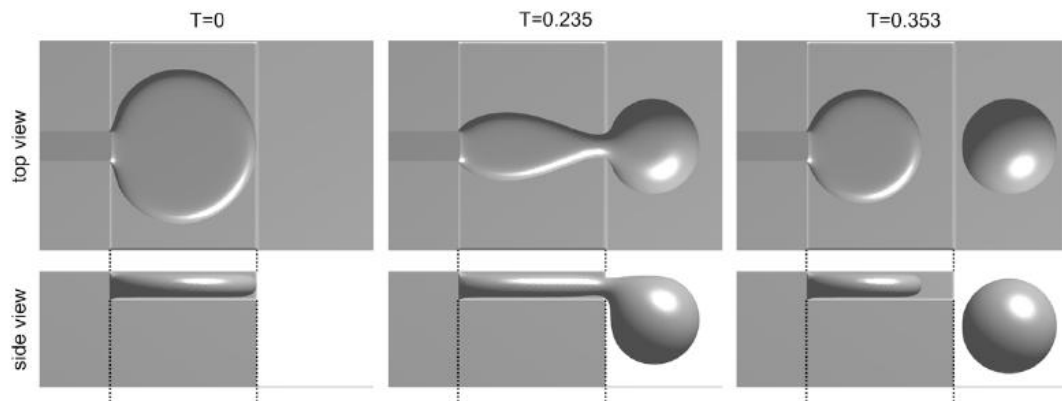


Fig. 2.16: Visual representation of droplet formation (where T denotes the droplet formation time) using the lattice Boltzmann method (Van der Zwan *et al.*, 2009).

Van der Graaf *et al.* (2006) compared simulated and experimental data using this technique with a T-shaped microchannel. Interestingly, the wetting of the membrane surface is also accounted for; another limitation hindering other techniques. It was concluded that good agreement was found for predicted and actual droplet sizes. Importantly, they also found that the volume contribution during the growth and detachment stages depended on the continuous phase Capillary number as well as the dispersed phase flux. The primary limitation again is the long times required for the software to obtain a solution.

In conclusion, membrane emulsification can be modelled using a variety of techniques. There is usually a trade off between the speed and ease of calculations against their accuracy as assumptions are gradually removed. Selection of the appropriate modelling technique depends on the level of precision required, as well as the amount of resource available to the user i.e. computational power, time. Within this thesis, modelling was undertaken by solving algebraic equations within a force balance model (FBM). This was achieved via iteration using Microsoft Excel.

2.4 Scale-up of Membrane Emulsification Processes

Membrane emulsification has been highlighted to offer many advantages over conventional processing methods. This is predominantly associated with low energy consumption and the intricate level of control, capable of producing unique, high-value products. However, unlike processes such as rotor-stator mixers or homogenisers, engineers do not know how to design or up-scale membrane emulsification equipment. There is no known procedure as to how one would approach this problem. Furthermore, demonstration within literature of membrane emulsification at the pilot-scale (or larger) is extremely limited. Williams *et al.* (1998) did demonstrate an industrial scale XME device to be capable of formulating O/W emulsions both within batch and semi-continuous mode. 1.2 kg h⁻¹ of emulsion containing 25 wt. % mineral oil (Marcol 172) as the dispersed phase was achieved. A ceramic membrane of 60 cm length, 3.5 mm inner diameter and 0.5 µm pore diameter was used and a TMP of 1.4 bar was applied. Aside from this, there are almost no other examples in open literature of membrane emulsification being operated at a large scale. Only one company (Morina Milk Industry, Japan) has been reported to use membrane emulsification to manufacture their product (Nakashima *et al.*, 2000). It could be speculated that this was a risky decision to deviate from trusted technologies to a relatively unknown one without clear design and operation guidelines.

Considering the general configuration of the process, there are multiple, fundamentally different approaches that can potentially be adopted. A number of authors have theorised that through modulation i.e. using multiple membrane tubes, production rate requirements could be satisfied by overcoming typically low dispersed phase fluxes (Williams *et al.*, 1998; Joscelyne and Tragardh, 2000; Charcosset, 2009). However, very little discussion has been focussed on the alternative approach; simply using a higher membrane surface area in conjunction with larger vessels (the approach used within this thesis). Up-scaling a single membrane may be cheaper from a capital cost perspective rather than purchasing multiple membrane tubes. There is no doubt that

parallelisation could be applied to membrane emulsification processes. Such an approach has been utilised within the field of microfluidics, but primarily within the context of filtration rather than emulsification (Hansson *et al.*, 2012). Either multiple membrane tubes could be positioned within a single emulsification vessel or alternatively, individual membrane/vessel units could be implemented. Challenges may lie in ensuring the shear at the membrane surface or pressure driving force is uniform across all membranes. For example, the latter could possibly be difficult to achieve due to frictional losses within the pipe work upstream of each membrane. It was observed that even subtle variations in the TMP or shear could vastly alter the micro-structural properties of an emulsion (Abrahamse *et al.*, 2002; Vladisavljevic *et al.*, 2004b).

Gijsbertsen-Abrahamse *et al.* (2004) suggested that the priority in terms of up-scaling should be focussing research towards the design of membranes which have specific properties to overcome flux limitations. The authors considered a hypothetical scenario of which culinary cream of 30% dispersed phase containing droplets of 1-3 μm required manufacture at a rate of $20 \text{ m}^3 \text{ h}^{-1}$. A range of membrane materials were considered including SPG, ceramic $\alpha\text{-Al}_2\text{O}_3$ and metallic microsieve membranes of variable properties. The pore size of the respective materials was selected as 0.2 μm in order to meet the droplet size requirements. Three design scenarios were postulated; to minimise membrane area, to produce mono-dispersed droplet sizes or to allow stable emulsion production with TMP fluctuation. It was concluded that a microsieve of surface area 1 m^2 was the optimum membrane material regardless of the design criteria as shown in Fig 2.17.

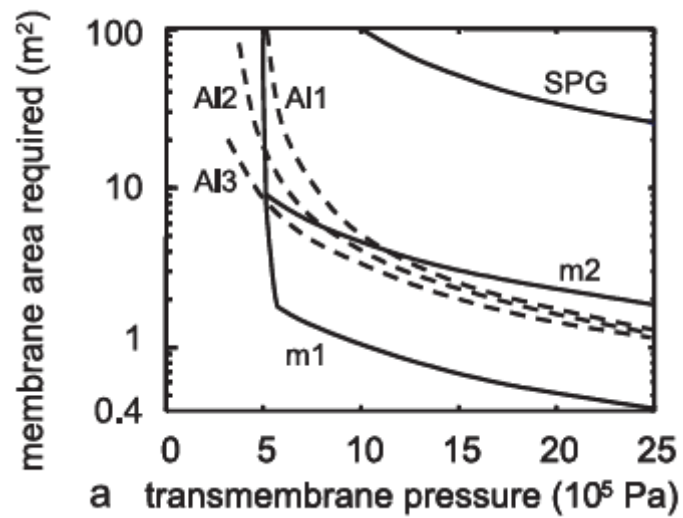


Fig. 2.17: The membrane area required to produce $20 \text{ m}^3 \text{ h}^{-1}$ of 30% disperse phase culinary cream for different membrane material properties. SPG: Shirasu Porous Glass, Al1-3: ceramic $\alpha\text{-Al}_2\text{O}_3$ of increasing pore diameter standard deviation, m1-2: silicon nitride microsieve of increasing upper pore layer resistance (Gijssbertsen-Abrahamse *et al.*, 2004)

The approach used by Gijssbertsen-Abrahamse and co-workers perhaps suggests that selection of the appropriate membrane material (pore size, porosity etc.) could be the first major step in the design process for membrane emulsification.

Chapter 3:

Materials and Methods

This chapter details the range of materials, equipment and operating procedures used for the experimental work presented in this thesis.

3.1 Chemical Components

3.1.1 Emulsions

All emulsions were oil-in-water (O/W) systems produced using Milli Q water as the continuous phase and either commercially available sunflower oil or silicone oil (Sigma Aldrich, UK) as the dispersed phase. Sunflower oil has a density of 919 kg m^{-3} and a viscosity of 0.066 Pa s at 20°C . Silicone oil had variable density and viscosity values depending on the one selected. The quantity of dispersed phase within the emulsion was expressed as vol. %.

Water has a density of 998 kg m^{-3} and a viscosity of 0.001 Pa s at 20°C .

Emulsions were stabilised either using a surfactant, particles or a mixture of both. These are expressed as wt. % of the whole emulsion system.

In some cases, Glycerol (supplied by Sigma Aldrich, UK) of varying quantity between 1-87.5 wt. % was used to modify the continuous phase viscosity. Glycerol has a density of 1260 kg m^{-3} and viscosity of 1.408 Pa s at 20°C .

3.1.2 Surfactants

All surfactant systems were produced through adding a pre-calculated mass of surfactant to a known mass of dispersion media (either water or oil) and applying magnetic stirring until the surfactant had dissolved. This was undertaken at a slightly elevated temperature of 40°C to increase the speed of the process. However, all the systems were cooled to 20°C prior to their use during emulsification. Large batch sizes between 0.5-5 L were produced in order to minimise any human error during weighing.

3.1.2.1 Tween 20 (Polyoxyethylene (20) sorbitan monolaurate)

Tween 20 was supplied by Sigma Aldrich (UK). It is a non-ionic surfactant commonly used with food products since it has a low toxicity and imparts high emulsion stability. It has the molecular formula of $C_{58}H_{114}O_{26}$ and a molecular mass of $1227.5 \text{ g mol}^{-1}$. In appearance, it is described as a transparent yellow liquid. It has a density of approximately 1100 kg m^{-3} . Tween 20 favours the production of O/W emulsions since it has a high hydrophilic-lipophilic balance (HLB) value of 16.9. It was used in concentrations between 0.01-10 wt. % positioned either within the continuous phase or the dispersed phase. The critical micelle concentration (CMC) within the continuous phase is 0.07 g L^{-1} .

3.1.2.2 Brij 97 (Polyethylene glycol (10) monooleyl ether)

Brij 97 was supplied by Fluka Chemie GmbH (Switzerland). It is a non-ionic surfactant with the molecular formula of $C_{20}H_{40}O_2$ and a molecular weight of 357 g mol^{-1} . In appearance it is described as a very pale yellow liquid/semi-solid at room temperature. Brij 97 has a density of approximately 1000 kg m^{-3} . With a HLB value of 12.4, it is effective at stabilising O/W emulsions. It is used in concentrations between 0.01-1 wt. % positioned either within the continuous phase or the dispersed phase. The CMC within the continuous phase is 0.29 g L^{-1} .

3.1.2.3 Sodium Dodecyl Sulphate

Sodium Dodecyl Sulphate (SDS) was supplied by Fisher Scientific (UK). It is an anionic surfactant with the molecular formula of $NaC_{12}H_{25}SO_4$ and a molecular mass of 288.4 g mol^{-1} . It is provided in a form of a fine white powder. SDS has a density of 1010 kg m^{-3} . It is extremely effective at stabilising O/W emulsions since it has a very high HLB value is 40 and therefore it is incorporated within many detergent and cleaning products. It is used in concentrations between 0.01-5 wt. % positioned within the continuous phase only (it is insoluble within oil). The CMC within the continuous phase is 2.4 g L^{-1} .

3.1.2.4 Hydrolysed Lecithin

Hydrolysed Lecithin derived from soy beans was acquired from Cargill (Minnesota, USA). It is a phospholipid with a molecular formula of $C_{40}H_{80}NO_8P$ and a molecular mass of 678 g mol^{-1} . In appearance it is described as a very viscous, dark brown liquid. It has a density value of 1030 kg m^{-3} . Hydrolysed Lecithin has a low HLB value of approximately 5 which indicates it prefers to stabilise water-in-oil (W/O) emulsions. However, it is still capable of (briefly) stabilising O/W emulsions. It is used in concentrations between 0.01-1 wt. % positioned either within the continuous phase or the dispersed phase. The CMC within the continuous phase is 0.61 g L^{-1} .

3.1.3 Particles

All continuous phase particle suspensions were produced by adding a pre-calculated mass of particles to Milli Q water. The pH was then adjusted using hydrochloric acid solution (HCl at a concentration of 5 wt. %) or sodium hydroxide solution (NaOH at a concentration of 5 wt. %) to a value of 2. These chemicals were both purchased from Sigma Aldrich (UK). Within the work of Pichot *et al.* (2009), a pH of 2 was identified to be the optimum value for emulsification since operating at its iso-electric point of the particle encourages aggregation which in turn enhances stability against coalescence. The particles were then dispersed using a high intensity ultrasonic vibracell processor (Jencons-PLS, UK). The batch size was kept constant at 500 ml in order to ensure uniform dispersion during sonication.

Two forms of silica (silicon dioxide) particles were investigated. These both have the same generic molecular formula of SiO_2 , molecular weight of 60.1 g mol^{-1} and density of 2200 kg m^{-3} .

3.1.3.1 Aerosil Silica

Aerosil (A200) Silica was purchased from Evonik (Germany). These particles are hydrophilic fumed silica particles of high purity silicone dioxide content (greater than 99.9 wt. %). Aerosil is

supplied as a fine white powder of particle size 12 nm and a specific surface area of 200 m² g⁻¹. Once dispersed at a pH of 2, the particle size of the aggregates is 190 nm. The concentration of particles varied between 0.01-2 wt. %.

3.1.3.2 Ludox Silica

Ludox AM Colloidal Silica was purchased from Sigma Aldrich (UK). These particles are provided pre-dispersed within a surfactant-containing solution at a high particle concentration of 30 wt. %. This therefore required dilution with water before pH adjustment and sonication. The unidentified surfactant within the solution is incorporated to keep the particles finely dispersed. Ludox was characterised on a Zetasizer (Malvern Instruments, UK) to have a particle size of approximately 21 nm. The concentration of particles varied between 0.1-30 wt. %.

3.1.4 Surfactant/Particle Mixtures

Continuous phase systems with varying ratios of Tween 20 and either Aerosil Silica or Ludox Silica were produced using the same procedure as detailed within section 3.1.3. Instead of Milli Q water, surfactant solution was used which was produced following the steps outlined in section 3.1.2. The particles were added to the surfactant solution prior to pH adjustment and sonication.

3.2 Equipment

3.2.1 Emulsification Processes

3.2.1.1 Small-scale Rotating Membrane Emulsification

For the small-scale Rotating Membrane Emulsification (RME) device, the membrane material most extensively investigated (Chapters 4-6) was a hydrophilic, Shirasu Porous Glass (SPG) membrane of 6.1 µm pore diameter. This was purchased from SPG Technology Co. (Japan) as 250 mm long, 10 mm outer diameter tubes (8 mm inner diameter) which were subsequently cut using a

diamond file into 45 mm sections. This gave the membrane an effective surface area of 14.1 cm². Alternatively, a stainless steel membrane with laser drilled pores was also investigated (Chapter 7). A readily available metal tube of 60 mm length and 10 mm outer diameter was processed along a 50 mm section by Laser Micromachining Limited (UK) producing pores of 25 μm diameter, a pore spacing of 0.5 mm and an effective surface area of 15.7 cm². The short membrane tubes were bonded using a resistant epoxy resin or welded to a female threaded ferrule at one end whilst the other end was capped to dead-end the system. The membrane tube was then mounted on a male threaded shaft fed through a commercially available IKA Eurostar Digital overhead stirrer to provide rotational motion. PTFE tape was placed on the threaded shaft to prevent leaking of the dispersed phase at the joint. The membrane was then submerged in continuous phase to apply shear at the membrane surface induced by the relative velocities of the membrane and continuous phase. The continuous phase was contained within an emulsification vessel of variable diameter between 20-100 mm diameter which altered the emulsion batch size between 20-360 g. A schematic of the small-scale rotating membrane apparatus is presented in Fig. 3.1 (a) alongside a photograph in Fig. 3.1 (b).

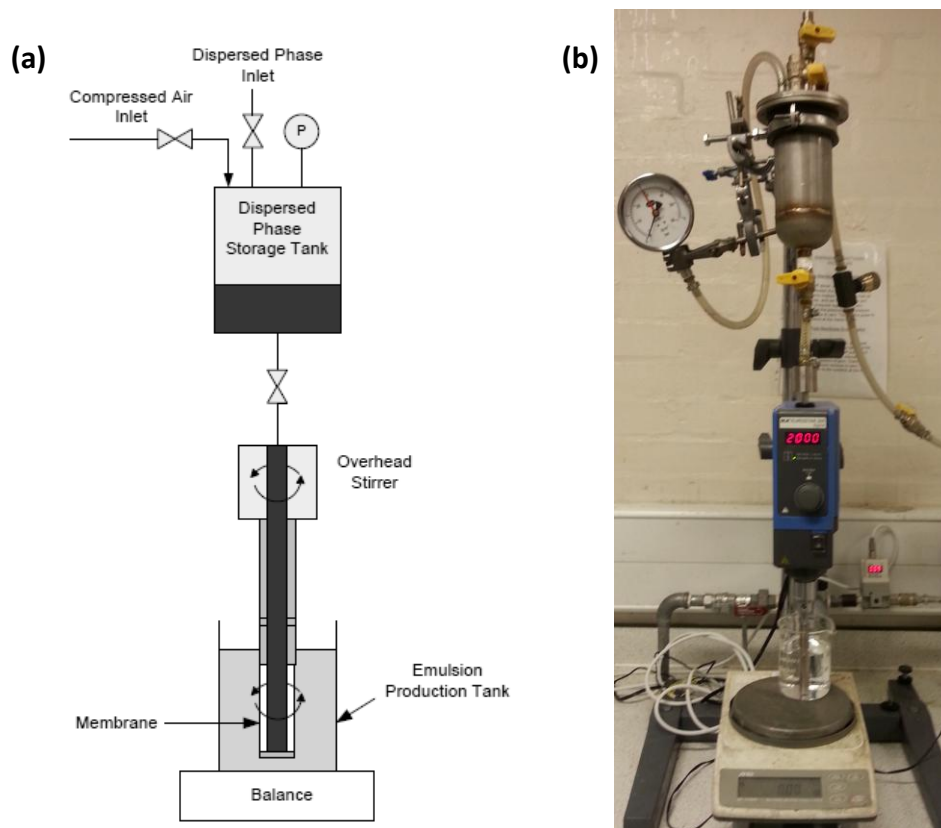


Fig. 3.1: A schematic diagram (a) and a photograph (b) of the small-scale rotating membrane emulsification system used within this thesis.

Before operating the RME device, the membrane to be investigated was soaked in continuous phase (surfactant solution) and cleaned within an ultrasonic bath (Model B2210E, Branson, Switzerland) for 3 hours. This was done to remove any air or oil trapped within the internal structure of the membrane, replacing these materials with continuous phase. Occasionally (typically once a week), a more thorough cleaning procedure was required. In this case, the membrane was sonicated in ethanol for 3 hours before drying in an oven at 60°C for 12 hours (overnight). Finally, the membrane was sonicated within continuous phase for 3 hours as before. For cleaning during operation, after a triplicate of experimental runs (at a given set of conditions), the membrane was detached and sonicated for 1 hour within continuous phase. The 3 hour cleaning treatment was only undertaken generally at the end of the day in preparation for experimental work the day afterwards.

The standard operating procedure was as follows. The dispersed phase storage tank was manually filled with the dispersed phase material to be used via the dispersed phase inlet valve. This was filled to a maximum working volume of 450 ml (capacity of tank = 482.5 ml) before closing this inlet valve. Once the membrane was attached, submerged within continuous phase and rotating at a constant speed between 100-2000 rotations per minute (RPM), the dispersed phase storage tank was pressurised using compressed air. This was achieved by altering the set-point on a pressure regulator between 0.1-1.8 bar combined with the opening of the compressed air inlet valve. The set-point is the 'transmembrane pressure' value quoted since the membrane capillary pressure (≈ 0.03 bar) and hydrostatic pressures (≈ 0.002 bar) of the respective phases are relatively small. Finally, the valve between the dispersed phase storage tank and the membrane tube was opened, allowing dispersed phase to permeate through the membrane into the continuous phase as individual droplets. RME was operated as a semi-batch process, with the mass increase observed over time using a weighing balance. Once the mass of dispersed phase equating to a fixed volume fraction was obtained, the dispersed phase tank was depressurised and the valve to the membrane tube closed simultaneously. Measuring the time of operation allowed for the rate of mass addition and hence the dispersed phase flux to be found. The RME equipment was then shut down by switching off the overhead stirrer prior to removal of the emulsion sample away for storage and measurement (within less than 8 hours).

3.2.1.2 Pilot-scale Rotating Membrane Emulsification

For the pilot-scale RME device, the membrane investigated was a large laser drilled stainless steel tube of 26 μm pore diameter. Its dimensions were 62 mm outer diameter (60 mm inner diameter) and length 400 mm. A small section of the tube was milled to reduce the wall thickness from (1 to 0.1 mm). A 50 mm length of this thinner section was laser drilled with pore spacing of 0.5 mm as a square array. This pore array was skewed by 1° to ensure adjacent pores to not follow the same horizontal trajectory path as the membrane rotates. The effective membrane surface area was

therefore 97.4 cm² with comparable properties to the small-scale laser drilled stainless steel membrane (pore size, porosity etc.). The pilot-scale RME device was mechanically designed and constructed by Het Stempel (Netherlands) according to specifications devised through discussions at the University of Birmingham. These were stated as a maximum TMP of 4 bar, rotational speed of 4000 RPM and batch size volume of 12 litres. RME has been recently commercialised by companies such as Kinematica although the scale is still relatively small in comparison to this device; < 12 L h⁻¹ with a continuous phase volume of 400 ml (Eisner, 2007). Essentially, the fundamental principles of the equipment are the same as the small-scale device; a membrane mounted on a motor-driven rotating shaft with dispersed phase pressurised through it into an emulsification tank containing continuous phase. Obviously the sealing and coupling mechanisms are more complex and therefore consideration of the mechanical workings of the process is beyond the scope of this research. The primary focus here is towards the understanding of emulsification process mechanisms and design based on input variables (TMP, rotational speed etc.) and output variables (droplet size, dispersed phase flux). As a visual representation, both a schematic and a photograph of the process are presented in Fig. 3.2.

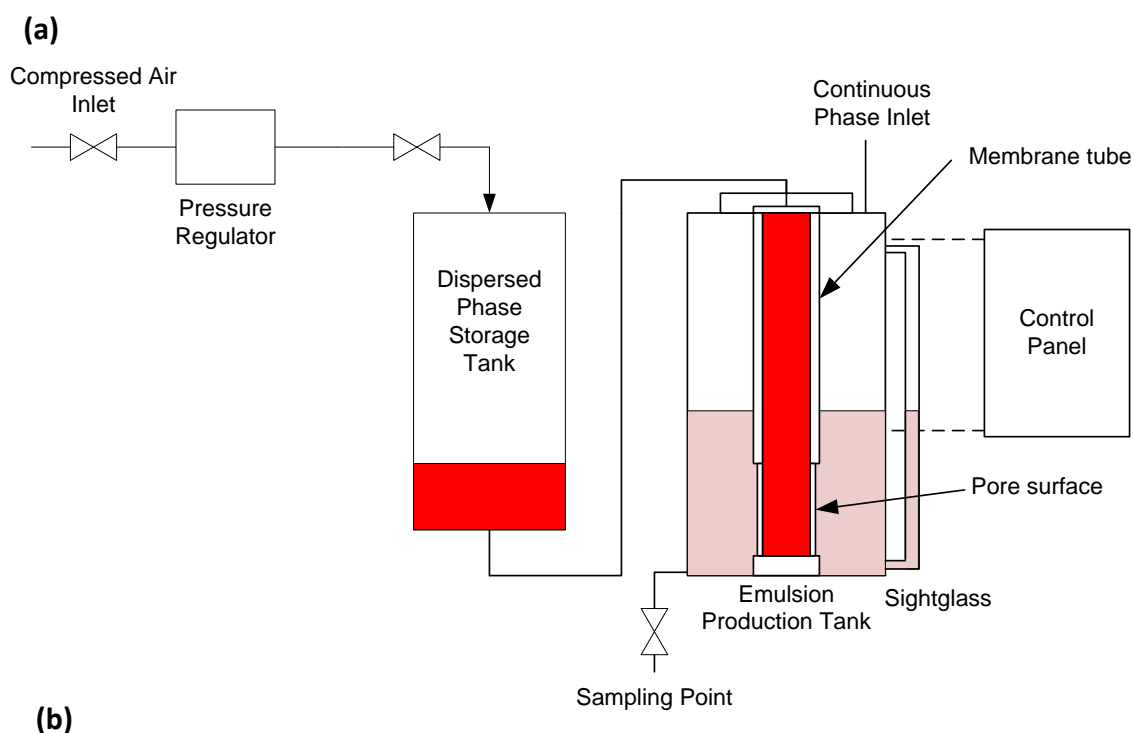


Fig. 3.2: A schematic diagram (a) and a photograph (b) of the pilot-scale rotating membrane emulsification system used within this thesis.

Prior to assembly of the pilot-scale device (undertaken monthly), the porous section of the membrane tube was sonicated firstly within Milli Q water and then within continuous phase solution for 3 hours to remove any possible trapped air or dispersed phase material. Since it was impractical

to deconstruct and then rebuild the equipment between each experimental run (this took around half a day), only the membrane surface and emulsification tank were cleaned by using 10 litres of dilute surfactant solution followed by the same volume of Milli Q water at a rotational speed of 2000 RPM for 5 minutes. These were subsequently drained from the emulsification tank removing any residual waste material. Since the pore channels are straight-through and relatively short in length (0.1 mm), it was assumed that fouling within the pore would be unlikely since the residence time is low. Furthermore, since the emulsion systems produced were dilute (< 1 vol % of dispersed phase), sample contamination between experimental runs would also be improbable considering the cleaning process used 20 litres of material (any dispersed phase would be extensively diluted).

The standard operating procedure was as follows. The dispersed phase tank was manually filled during the assembly stage to a known height of liquid. Based on the usual dispersed phase tank geometry, it was determined using a volumetric flask that 100 ml of dispersed phase correlates to 13 mm of liquid height. The emulsification tank was filled to a volume of 8 litres (marked height on sight glass) using a gear pump (Cole-Parmer, UK) to transfer liquid from two 5 litre batches of continuous phase. The rotational speed was set on the control panel of the RME device. The cooling jacket of the emulsification vessel was set to 20°C which was then left for 10 minutes to equilibrate the temperature of the system. The seal cooling system was set to 1°C to ensure it didn't melt under high rotational speeds due to friction. Both of these cooling systems were necessary to ensure this frictional heating did not conduct throughout the stainless steel vessel increasing the emulsification temperature. The required TMP was controlled by a pressure regulator using compressed air. Upon opening the compressed air valve to the dispersed phase tank, this compressed the dispersed phase within the storage tank (altering the liquid height) but also starting the process. The new height was recorded and the process was operated until 1 vol. % of dispersed phase was added; this equated to roughly 10.5 mm of dispersed phase liquid height (\approx 80 ml). Once this had been added, the dispersed phase was depressurised and the valve was closed. The rotational speed of the membrane was then set to zero and the emulsification tank was drained. Multiple samples were analysed from the same

batch at 2 litre intervals to check consistency throughout the emulsion bulk (this did not dramatically vary but was accounted for within the data presented).

3.2.1.3 Rotor-Stator High Shear Mixer: The Silverson L4RT

Emulsions were also produced using a high shear rotor-stator mixer (Silverson Machines Ltd., UK) to offer a process comparison with the small-scale RME device. The 4 vane rotor impeller and screen diameters were 21 mm and 22 mm respectively whilst the screen holes were 1 mm in diameter. Batch sizes between 110-360 ml were investigated within this thesis. A range of rotational speeds between 2000-10000 RPM were used (constant mixing time = 1.5 minutes). Additionally, the mixing time was also varied between 10 seconds and 10 minutes (at constant speed = 6000 RPM). For operation of the process, the dispersed and continuous phases were both positioned immediately within a vessel prior to emulsification. The mixer head was lowered to a positional central within the tank and just below the initial oil/water interface. The rotor speed was increased starting the process. This was then decreased back to zero after a fixed time had elapsed and the sample was retained for analysis. During this process, the temperature was not controlled resulting in thermal energy losses from the equipment (due to process inefficiency) heating the emulsion sample. However, the heat loss to the environment was minimised using tin foil in order to quantify the process inefficiency.

3.2.1.4 Ultrasonic Emulsification: The Ultrasonic Vibracell Processor

An ultrasonic probe (Jencons-PLS, UK) was used to formulate emulsions to further the process comparison study. A 12 mm diameter tip was oscillated at amplitudes between 20-95% of its maximum amplitude of 114 μm (for a time of 1.5 minutes). The frequency was constant at 20 kHz in all cases. This therefore altered the tip velocity between 1.8 m s^{-1} to 8.7 m s^{-1} . The sonication time was also investigated between 10 seconds and 10 minutes (at a constant amplitude of 60%). Again, the dispersed and continuous phases were introduced within a single vessel immediately before

emulsification occurred. The ultrasonic probe was centralised within the tank with the edge of the tip just below the oil/water interface. Upon inputting the percentage amplitude and operating time on the control panel, the ultrasonic probe device was switched on to begin the emulsification process. Once completed, the probe was removed away from the emulsification vessel and the emulsion was stored until analysed. During the process, the temperature was not controlled and so the emulsion sample was heated up by the high energy input of the process. Aluminium foil was used to reduce heat losses to the atmosphere, in order to quantify the thermal energy generated during the process.

3.2.2 Characterisation Equipment

3.2.2.1 Laser Diffraction Particle Size Analysis

The primary method for analysing the emulsion droplet sizes produced was by laser diffraction using a Malvern Mastersizer model 2000 (Malvern Instruments Ltd., UK). The emulsions were measured using a Hydro SM manual small volume dispersion unit to obtain a size distribution curve. The equipment was repeatedly flushed with Milli Q water at a stirring speed of 3500 RPM until the laser light intensity received by the detector was at least 77 %. Once clean, the emulsion sample was gently re-dispersed (as appropriate) by inverting a number of times. The dispersion unit was filled with Milli Q water and set to 1500 RPM to ensure sufficient dispersion (without droplet breakup). The emulsion sample was then added via a pipette. Once the laser obscuration was within the green range indicating a measurable degree of laser 'interference', a triplicate measurement was taken which was averaged. The refractive index used for water at 20°C was 1.33. For sunflower oil and silicone oil, the refractive indices used were 1.47 and 1.40 respectively. For the particle stabilised emulsions, it is assumed that there is complete coverage of the droplet interface by particles. As such, the refractive index used was for silica particles (1.46). The error is likely to be minimal since it is very close to the refractive index of the sunflower oil which was the dispersed phase used.

The droplet size measured by the equipment is the volume weighted mean diameter or ' $D_{4,3}$ '. This is defined in Eq. 3.1 as:

$$D_{4,3} = \frac{\sum n_i d_i^4}{\sum n_i d_i^3} \quad (\text{Eq. 3.1})$$

where n_i is the number of droplets and d_i is the droplet size within a specific size class (since the distribution curve is split into vertical bands). There are alternative forms of diameter value that can be quoted including the surface weighted mean diameter ($D_{3,2}$) or the volume median diameter (D_{50}). Within this thesis, the $D_{4,3}$ value was chosen as the representative emulsion droplet diameter as this was the value measured directly by the Mastersizer and therefore was more accurate. Unless otherwise stated after this point, the droplet 'diameter' or 'size' will refer specifically to the $D_{4,3}$ value. In addition to this diameter, a measure of the size distribution variation (poly-disparity) is also used which is known as the span value. This is defined as:

$$\text{Span} = \frac{D_{90} - D_{10}}{D_{50}} \quad (\text{Eq. 3.2})$$

where D_n denotes the volume diameter of which n% of the volume distribution is below this value. A lower span value indicates a more uniform distribution curve although there is no absolute definition of what span value is considered 'mono-dispersed' in literature.

As mentioned, the equipment is fundamentally dependent on the principle of laser diffraction. Emulsions droplets or solid particles pass through a laser beam; a source of coherent, intense, monochromatic light. This induces light scattered in all directions (Rayleigh scattering) at an angle depending on their size and the refractive index. For example, large droplets scatter at small angles with greater intensity and vice versa. The laser diffraction process can be described using both the Fraunhofer Approximation and Mie Theory. For the former, the droplets can be considered as opaque discs that scatter light at narrow angles. The refractive index difference between the droplet and the surrounding medium is considered infinite and all droplet sizes scatter light equally effectively. This allows the Fraunhofer Approximation to accurately determine the size for large

droplet sizes ($> 50 \mu\text{m}$). For smaller droplet sizes below $50 \mu\text{m}$, these are characterised by Mie Theory which assumes a homogenous sample of spherical droplets, dilute enough such that diffracted light can be measured prior to any further 'interference'. Mie Theory is able to predict both the extent of scattering based on differences in the refractive indices and the degree of absorption and subsequent refraction of light by the droplet. This therefore is highly suitable for emulsion systems where the measured droplets can be small ($< 50 \mu\text{m}$) and transparent. Using both the Fraunhofer Approximation and Mie Theory enables a range of sizes between 100 nm and 2000 microns to be measured by this technology. The interactions between the light and the sample are measured by a variety of detectors including focal plane detectors (for small scatter angles $< 10^\circ$), large angle detectors (10° to 90°) and back scatter detectors (100° to 135°). A schematic of the equipment is shown in Fig. 3.3:

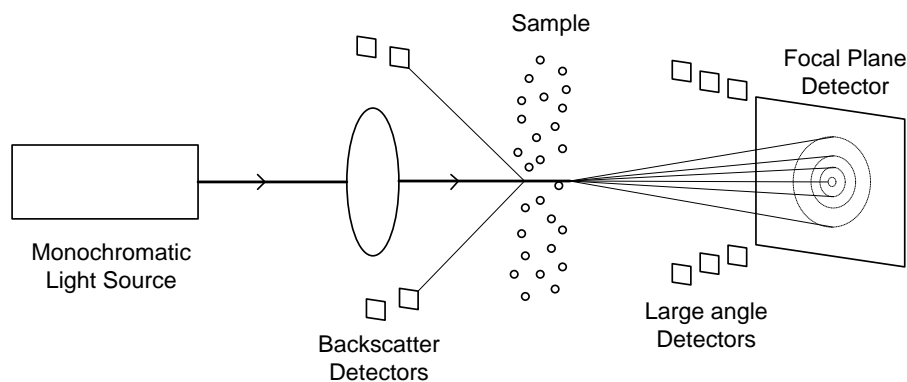


Fig. 3.3: A schematic diagram illustrating laser diffraction; the basis behind the Malvern Mastersizer model 2000 used to quantify droplet and particle diameters within this thesis.

The main advantages of using laser diffraction for the droplet size analysis as opposed to other techniques (e.g. microscopy) are:

- Quick to quantify multiple droplet sizes without image analysis
- Does not require calibration. Only the correct refractive indices are needed
- Measurements can be made rapidly within a couple of minutes of emulsion formation
- Only a small quantity of sample is required (typically a few millilitres)

However, there are a few limitations of laser diffraction. Firstly, it is assumed that the droplets (or particles) measured are completely spherical entities. In reality, droplets might be deformed within the flow at an orientation that alters the extent of diffraction giving an erroneous measurement. Secondly, laser diffraction is difficult to accurately measure if the refractive indices of the dispersed and continuous phases are very similar. Therefore, care and consideration is required both during the application of laser diffraction and interpretation of the droplet size data generated.

3.2.2.2 Dispersed Phase Flux Measurement

During emulsion production, the change in mass of the emulsification vessel due to oil addition was recorded as a function of time. Therefore, the dispersed phase flux value can be obtained using:

$$J_d = \frac{M_d}{\rho_d A_m t_p} \quad (\text{Eq. 3.3})$$

where M_d is the mass of dispersed phase added, ρ_d is the density of the dispersed phase, A_m is the effective membrane surface area and t_p is the processing time. The units of flux are generally expressed as a volume of material per unit area per unit volume. Within this thesis, the unit $\text{L m}^{-2} \text{h}^{-1}$ is used for the dispersed phase flux values.

3.2.2.3 Interfacial Tension Measurement

The interfacial tension (IFT) between oil/water was measured predominately using an EASYDROP Contact Angle Measuring System (Kruss GmbH, Germany), referred to as a Goniometer, which employs the pendant drop method. A droplet of organic material (with or without oil-soluble surfactant) or aqueous solution (with or without water-soluble surfactant) was produced via a controllable syringe unit which took approximately less than 3 seconds to form. This occurred whilst the syringe needle (of 1.8 mm diameter) was submersed within the alternate phase contained within a 40 x 40 x 30 mm glass cuvette. A Monochrome interline CCD camera observed the shape of the

droplet at a rate of 25 frames per second. The associated software monitors and analyses the shape of the droplet over time, based on the known density values of each phase. In turn, this calculates the IFT between the two phases (using the Laplace equation) by accounting for buoyancy force effects on the droplet shape. A schematic of the equipment can be seen in Fig. 3.4.

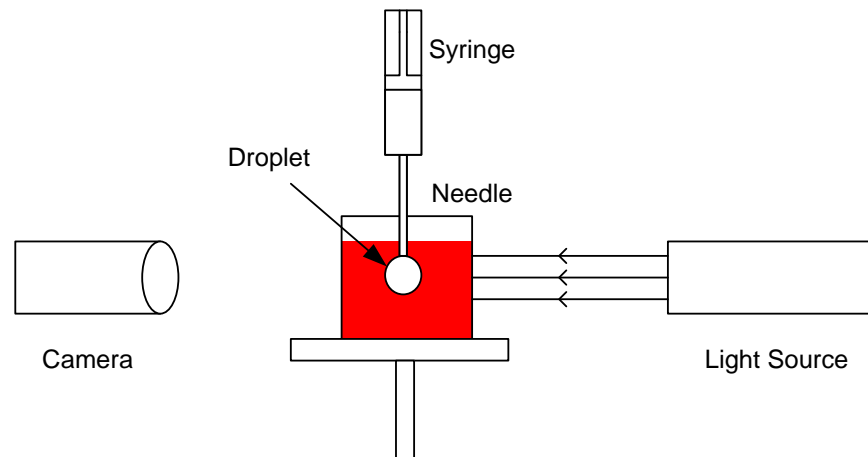


Fig. 3.4: A schematic diagram illustrating interfacial tension measurement with the Kruss Goniometer.

In the majority of cases, an oil droplet was formed within an aqueous solution in order to emulate the RME research producing O/W emulsions. However, in some cases the phases were reversed if the aqueous solution was too opaque (e.g. lecithin solutions, Aerosil dispersions). A U-shaped syringe needle was used to produce oil droplets since the buoyancy force acts to move droplets upwards and away from the needle once detached. This is shown schematically in Fig. 3.5.

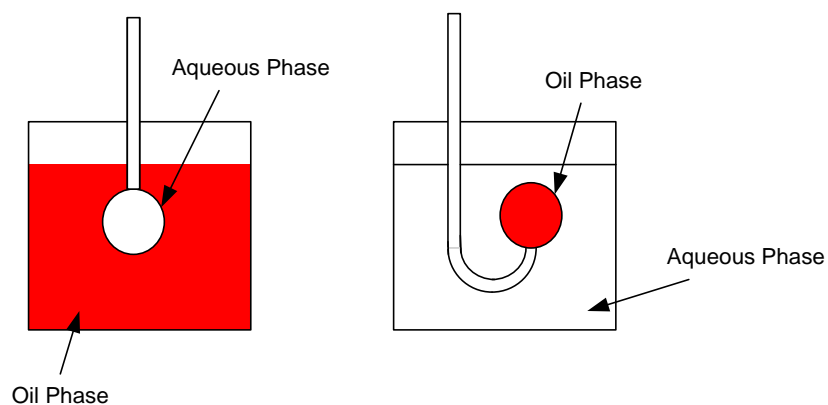


Fig. 3.5: A schematic indicating the possible measurement configurations depending on the properties of the material used to form the droplet.

Once an individual measurement had been completed, the glass cuvette was cleaned with distilled water and then dried. When required, the syringe needle was flushed repeatedly with oil or water (without surfactant) to prevent contamination when altering the material used to create the droplet.

A range of measurement approaches were utilised with the Goniometer. In all cases, the measurement temperature was at 20°C. To determine the equilibrium IFT, a triplicate series of measurements were performed for a time of 30 minutes with IFT measurements taken at 30 second intervals. For a more detailed observation of the IFT immediately upon droplet formation, IFT values were measured at the shortest time intervals possible (≈ 0.2 seconds) for a period of one minute. This was performed ten times to provide confidence in the rate behaviour of the systems investigated. Since there was an inherent 3.5 second time delay between forming the droplet and beginning the measurement, this was accounted for i.e. measurement time of 0 seconds was altered to 3.5 seconds. A logarithmic function was then applied to this data to obtain an equation connecting IFT with time. This allowed for the IFT to be back-calculated for times less than 3.5 seconds as an estimation of the IFT value within a time period similar to droplet formation during RME.

The primary advantages of using the Goniometer to measure the IFT are:

- Measurements can be taken quickly and easily
- Only the density values of the respective phases are required
- It is a crude representation of the membrane emulsification process
- It can provide a visual demonstration of droplet formation and evolution of its shape
- Only requires small quantities of the dispersed and continuous phases

The limitations of the Goniometer relate mainly to the difficulty of the software to identify the interface if both phases are opaque or if they have a similar refractive index. Additionally, both a high resolution camera and a smooth capillary needle (to form an axisymmetric droplet) are required to perform accurate measurements.

3.2.2.4 Rheology

The bulk viscosity was measured using a Bohlin Gemini HR Nano (Malvern Instruments, UK) with the concentric cylinder C25 DIN 53019 geometry at 20°C. Initially, a cone-and-plate geometry was used since it applies a uniform shear field across the whole sample. However, this led to inaccuracies particularly when measuring very low viscosity fluids since the gap did not remain filled. Instead, the concentric cylinder geometry was used since fluid could be contained within the outer cylinder. In addition, the configuration is conceptually similar to the RME process i.e. an inner rotating cylinder within an outer stationary cylinder. Viscosity measurements of emulsions or their constituent ingredients were undertaken across a range of shear rates between 0.1 s^{-1} and 1000 s^{-1} to investigate behaviour under shear rates similar to both the small-scale ($0.6\text{-}139.6 \text{ s}^{-1}$) and pilot-scale ($2.2\text{-}89.1 \text{ s}^{-1}$) RME equipment during emulsification.

3.2.2.5 Density

Density values for the dispersed and continuous phase materials were generally acquired via material data sheets. In some cases (e.g. for surfactant solutions), the average density was calculated by considering the mass fraction of each component. If no density information was available, 25 ml of material was placed within a volumetric flask and then its mass was recorded. The density was then calculated by dividing the recorded mass by the volume.

3.2.2.6 Temperature

Within Chapter 6, the emulsion temperature was measured immediately upon formation to quantify the process energy wasted as thermal energy. This was undertaken using a commercially available digital thermometer. In order to minimise heat losses to the environment, the emulsification vessel was insulated with tin foil such that it could be considered a closed system.

3.2.2.7 Process Energy Consumption during Emulsification

The energy consumed during process operation was calculated firstly by measuring the power draw using a commercially available plug-in energy meter at a given equipment rotational speed. Ten measurements were recorded whilst the membrane or impeller was fully submerged within distilled water and then a 10 vol. % sunflower oil-in-water emulsion (representing the two extremes of viscosity). These values were averaged to find the rate of energy consumption in Joules per second, which when multiplied by the processing time gives the energy consumed to operate the process.

Chapter 4:

Processing Effects using a Small-scale Rotating Membrane Emulsification Device

This chapter furthers current understanding on how processing variables influence fluid flow behaviour, and consequently the observed droplet size and dispersed phase flux during rotating membrane emulsification for batch sizes less than 0.36 kg.

Data and discussions contained within this chapter have been published within:

Lloyd, D.M., Norton, I.T., Spyropoulos, F. (2014). Processing effects during rotating membrane emulsification. *Journal of Membrane Science*, 466 8-17.

4.1 Introduction and Preliminary Studies

The aim of this chapter is to gain insight into how the O/W emulsion droplet size and production rate are affected by the flow behaviour of the dispersed phase (flow through the membrane) and continuous phase (flow within the processing vessel) during Rotating Membrane Emulsification (RME). It is well known that the key processing parameters are the transmembrane pressure (TMP; which forces the dispersed phase to permeate through the membrane material and form individual droplets) and the shear rate (which acts to detach droplets from the membrane surface). What is important to consider is that these can be selected and altered by the operator allowing for flexibility if one wanted to produce smaller droplets for example. It is therefore fundamentally important that these parameters, and more specifically the influence they have on droplet formation mechanisms, are well understood. However, there is a lot of deliberation within literature which means the design and operation procedures for RME lack clarity. The following chapter is therefore designed to evaluate these processing effects in order to further understanding of RME.

Prior to exploration of the processing effects that can occur, a number of key variables had to be selected. In particular, these relate to formulation parameters (such as surfactant type, concentration, volume fraction etc.) which will be discussed further in Chapter 5. The membrane parameters were also kept constant. Sunflower oil (SFO) was chosen as the dispersed phase since it is readily available, cheap and safe to use. Dragosavac *et al.* (2008) stated that SFO is a suitable dispersed phase material when performing membrane emulsification with hydrophilic Shirasu-Porous-Glass (SPG) membranes because it does not contain any triglycerides that specifically would adsorb to the membrane and cause wetting of dispersed phase across the membrane surface. The non-ionic surfactant Tween 20 was used within the continuous phase because it is reasonably effective at stabilising O/W emulsions and also any electrostatic effects between forming droplets and the membrane surface are eliminated (compared to anionic SDS for example). At 1 wt. %, the

concentration is well above the CMC and therefore emulsions remain stable far beyond the timescale between emulsion formation and droplet size analysis (typically < 8 hours). This is highlighted in Fig. 4.1 below where a range of formed droplet sizes stabilised by 1 wt. % Tween 20 were measured immediately after formation and 2 weeks later after storage at 20°C.

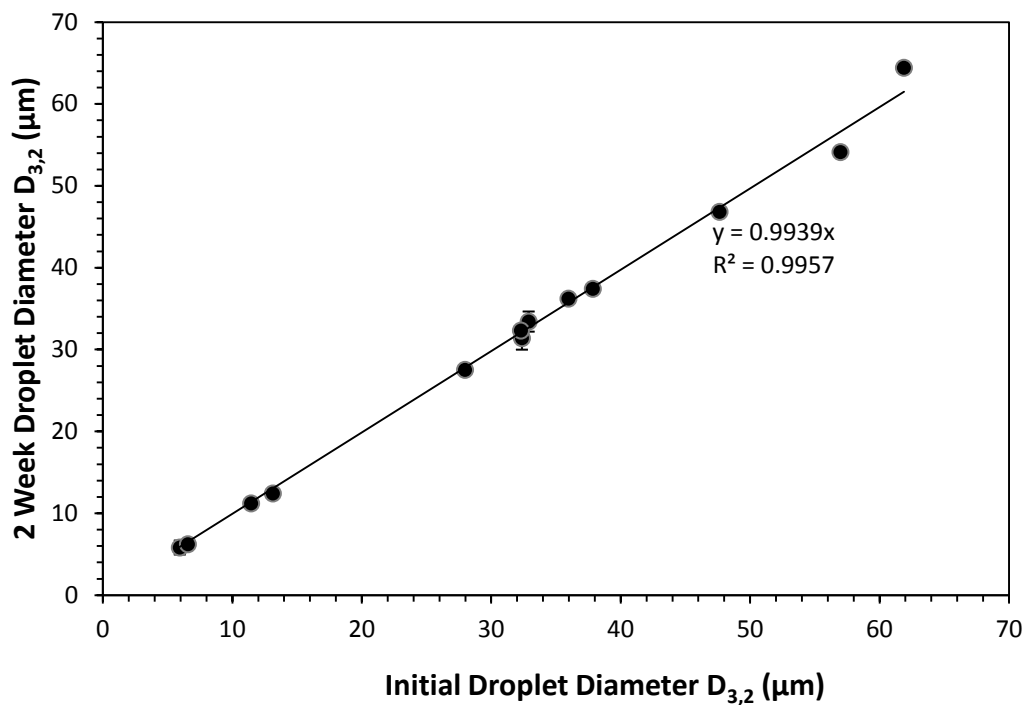


Fig. 4.1: 2 Week stability data of 10 vol. % Sunflower Oil-in-water emulsions stabilised by 1 wt. % Tween 20.

It is clear that there is a negligible difference in droplet size after 2 weeks (gradient very close to 1) except in the case where larger droplet sizes had been produced (>60 µm). This is likely to be due to minor destabilisation mechanisms perhaps induced by creaming. However, considering the time between droplet formation and measurement during the remainder of this study is less than 8 hours and hence a much shorter timescale, it is reasonable to suggest that the measured droplet size and the droplet size upon formation are the same.

Another important consideration for RME that required brief investigation was whether the emulsion properties changed during processing time. This was to ensure that droplet formation

remains a homogeneous process from start to finish as the RME process is being operated. For example, it could be hypothesised that under the highest shear rates achievable during RME, droplets may break up in the bulk continuous phase. This would not only add a layer of complexity in deciphering why droplets achieve a certain size under a given set of conditions, but also undermines the nature of RME (to build-up droplets individually in a controlled manner). Fortunately, this was ruled out by subjecting an emulsion of large droplet size (104 μm , stabilised by 1 wt. % Tween 20) to the highest shear rate achievable with the RME setup (139.6 s^{-1}) for a period of 1 hour which is far longer than typical operation times (< 5 minutes depending on the applied TMP). For this experiment, no additional dispersed phase was added via the membrane, but the membrane was rotated at the maximum speed of 2000 RPM within a 20 mm diameter vessel to impart shear on the already formed emulsion. As can be seen in Fig. 4.2, there is minimal difference between the two droplet distribution curves which implies that droplets do not break up once they have detached from the membrane surface. Furthermore, the likelihood of droplet break up is reduced further if the droplets are smaller (due to their Laplace pressure), less shear is applied (e.g. at lower RPM) or the processing time is shorter.

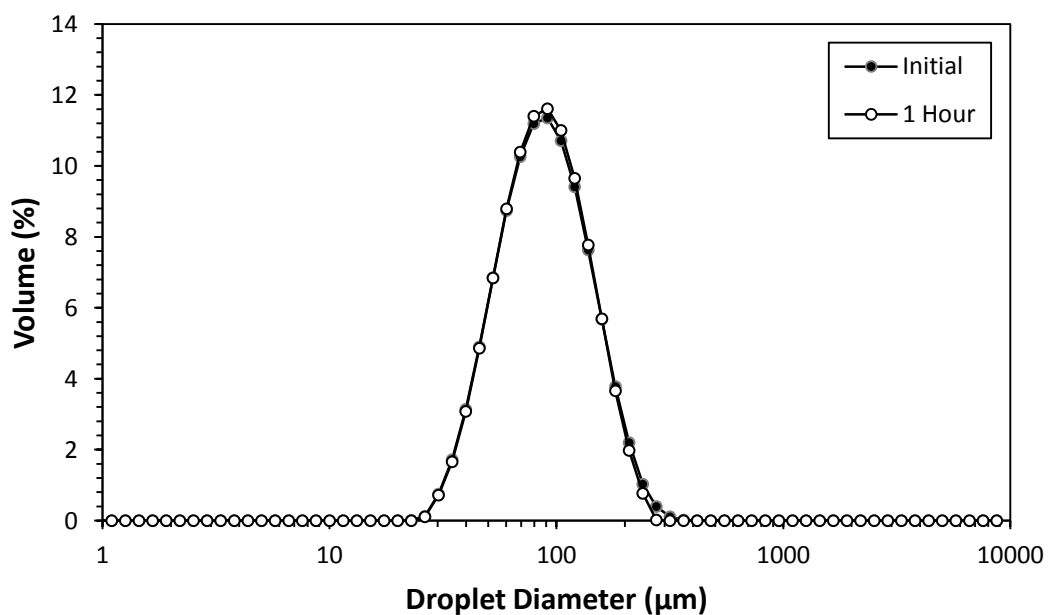


Fig. 4.2: Droplet size distributions for an initial emulsion and after 1 hour of shear at a rate of 139.6 s^{-1} applied using the rotating membrane emulsification equipment without dispersed phase addition.

One final consideration is that since the dispersed phase is gradually added to the continuous phase over time, it could also be hypothesised that the viscosity may vary and so droplets formed towards the end of process operation experience a different drag force to those formed within pure surfactant solution at the very beginning. A dispersed phase volume fraction of 10% was chosen for a number of reasons. Firstly, the majority of emulsion based products are non-dilute systems, so the aim was to ensure the research would be applicable if one wanted to formulate emulsions with RME to replicate those used in actual products. Secondly, production of these systems did not take too long or occur too quickly so this was beneficial from a practical point of view. Finally, these emulsions were concentrated enough to be easily measured during droplet size analysis without large quantities of emulsion required (particularly when the emulsion droplets are large and diffraction occurs to less of an extent). In order to investigate the extent of viscosity modification during processing, emulsions containing 5 v/v % and 10 v/v % dispersed phase (which represent the midpoint and endpoint of the process respectively) were compared to 1 wt. % Tween solution (i.e. 0 v/v % dispersed phase) using a Rheometer. It can be observed from Fig. 4.3 that viscosity appears to be independent of the dispersed phase volume fraction (for dilute systems) or range of droplet diameters considered. Shear thinning behaviour occurs under low shear rates ($<1 \text{ s}^{-1}$) with the value then tending to approximately the viscosity of water. Importantly, this indicates that the drag force acting on droplets forming towards the end of the process is going to be almost (if not) identical to the force acting on droplets at the beginning (as per findings by Schadler and Windhab, 2006). It is noteworthy that the sudden increase in viscosity around 60 s^{-1} is due to vortex formation within the Rheometer resulting in erroneous values upon further increase in shear. Thus, these values were ignored from calculations.

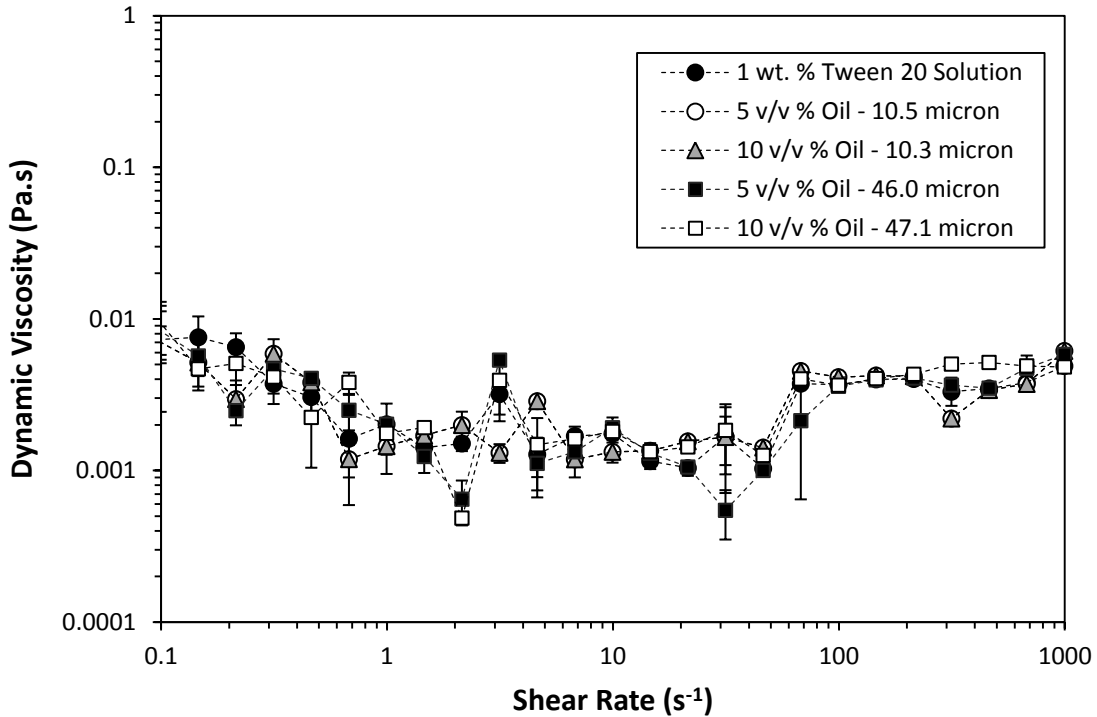


Fig. 4.3: Bulk rheological measurements to compare dynamic viscosity values for a range of Sunflower Oil-in-water emulsions with the initial surfactant solution (i.e. pure continuous phase).

The membrane used within this chapter and a large portion of this thesis is a Shirasu-porous-glass (SPG) membrane of 6.1 μm pore diameter. SPG membranes are very capable of producing uniform droplet sizes with highly repeatable results due to their extremely narrow pore size distributions (Vladisavljevic *et al.*, 2007). This is important because it therefore allows droplet formation mechanisms induced by a particular set of processing conditions to be studied. Use of an intermediate size pore diameter and relatively high TMPs (up to 57 times higher than the capillary pressure) was deliberate because the motivation behind the research was aiming towards high production rate emulsion production rather than forming the narrowest droplet size distribution achievable. However, variations caused by membrane and formulation parameters have been minimised where possible in order to obtain the lowest error and hence repeatable results. These preliminary findings provide confidence that the processing effects are meaningful observations

rather than being an artefact caused by the experimental methodology. The effect of processing parameters will now be discussed further.

4.2 Effect of Transmembrane Pressure

4.2.1 On the resultant droplet size

Fig. 4.4 shows the resulting droplet size of the emulsion at different TMPs (between 0.1 to 1.8 bar) across a range of rotational speeds (100, 1000 and 2000 RPM). Predominantly, the TMP used within most other studies tends to be no more than 2 or 3 times the critical capillary pressure. In this study, much higher TMPs are investigated up to 57 times the capillary pressure as the aim was to obtain high(er) throughput of dispersed phase. The trend observed in general was that with increasing pressure, the droplet size decreased to a minimum before gradually increasing upon further pressure application. This behaviour is more prominent when the rotational speed, and hence the shear rate is low (i.e. 100 RPM). It is highly likely that to some extent coalescence is a contributing factor to the relatively large droplet sizes under these processing conditions, since these droplet sizes vary between 8.6-17.2 times larger than the pore diameter i.e. the upper end of the ratio values suggested by other authors (Charcosset, 2009; Joscelyne and Tragardh, 2000). Furthermore, droplet size distribution span values across the whole data set range dramatically between 0.720 to 2.210 depending on processing conditions.

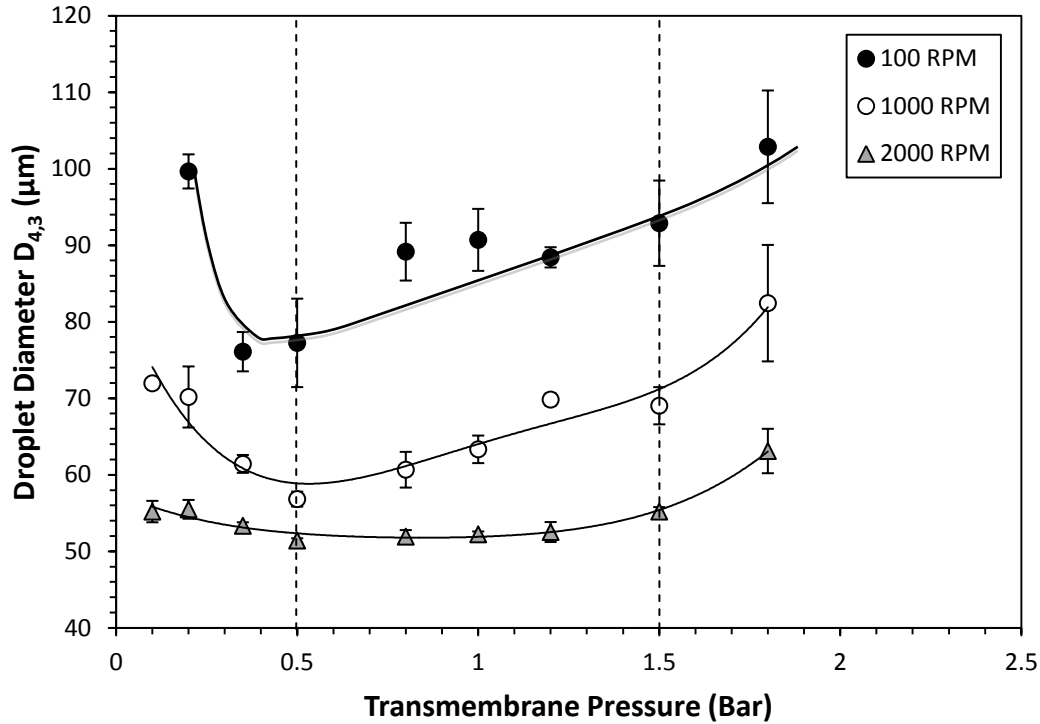


Fig. 4.4: The influence of transmembrane pressure on the mean droplet size for different rotational speeds. The emulsions are 10 vol. % sunflower oil stabilised by 1 wt. % Tween 20. The error bars represent one standard deviation of a triplicate of experimental runs.

Within the literature, the effect of TMP in membrane emulsification is contentious with the majority suggesting the droplet size increases with increasing TMP (Katoh *et al.*, 1996; Schroder *et al.*, 1998; Peng and Williams, 1998; Christov *et al.*, 2008). Abrahamse *et al.* (2002) and Matos *et al.* (2013) found the droplet size to decrease with increasing TMP. Within this study, it is observed that there is an initial decrease followed by an increase agreeing with the work of Vladislavjevic *et al.* (2004b). It is therefore logical to suggest that there are multiple, competing factors affecting the droplet size produced. A droplet size increase with increasing pressure is attributed to higher IFT values at small droplet formation times due to depletion of surfactant adsorbed at the rapidly expanding interface (Schroder *et al.*, 1998). It has also been suggested that there is significant mass transfer of dispersed phase via the droplet neck during detachment (Peng and Williams, 1998) although the pressure does not directly alter the point that a droplet begins to detach since the inertial force is considered negligible. On the other hand, explanations for size decrease are that

steric hindrance aids detachment of droplets from the membrane surface as a 'push off' force (Abrahamse *et al.*, 2002; Egidi *et al.*, 2008; Kosvintsev *et al.*, 2008) and formation occurs from smaller diameter pore channels that were previously inactive at lower pressure due to their higher capillary pressures (Vladisavljevic *et al.*, 2004b). The data presented here in Fig. 4.4 can be essentially divided into three regions with regards to TMP; a droplet decrease to a minimum (<0.5 bar), a gradual increase in droplet size (0.5-1.5 bar) and then a rapid increase with poly-dispersed droplet sizes formed (>1.5 bar). The exact transitional point between the regions depends on the rotational speed so approximations are stated to enable clarity during the discussion. Although not observed for the experimental conditions studied for systems shown in Fig. 4.4, in the later parts of this chapter and for systems of higher IFT values, the existence of a fourth region, in which a droplet size plateau is observed, will be proposed.

At pressures <0.5 bar the droplet size decreases with the extent depending on the rotational speed. At 100 RPM, this decrease is significant (22.5%, from 99.6 μm to 77.2 μm) whilst at 2000 RPM the decrease is almost negligible (6.9%, from 55.5 μm to 51.4 μm). The droplet size distribution span values follow a similar trend decreasing from 1.786 to 1.058 at 100 RPM whilst at 2000 RPM they decrease from 0.784 to 0.722. The observed decrease in droplet diameter with increasing rotational speeds is explained by the higher drag force aiding earlier detachment with increasing rotational frequency. In the case of 0.1 bar TMP and 100 RPM, the emulsion phase separated completely. It is unlikely that such a dramatic destabilisation between 0.1 and 0.2 bar could be explained purely by the activation of smaller pores on the surface forming smaller droplets as postulated by Vladisavljevic *et al.* (2004b). Furthermore, if steric hindrance to aid droplet detachment as suggested by Abrahamse *et al.* (2002) is the explanation then surely a dramatic droplet size decrease would also be experienced (but without complete phase separation) at the higher rotational speeds. Therefore, it is proposed that droplet coalescence at the membrane surface would explain the trends.

With an increase in TMP, the droplet formation time will decrease and thus droplets spend less time at the membrane surface i.e. where there is a higher risk for droplet coalescence (Lepercq-Bost *et al.*, 2010). Furthermore, the magnitude of the linear momentum and dynamic effect of pressure forces will increase, slightly aiding both detachment and displacement away from the membrane surface. If droplets remain nearby to the membrane surface and are not swept away into the bulk continuous phase, coalescence events between them and the forming droplet (at the membrane surface) would not be inconceivable (due to longer droplet contact times). This would eventually lead to formation of a more poly-dispersed emulsion (i.e. greater droplet size distribution span values). Coalescence would be promoted when an increase in active pore fraction leads to droplets forming more closely together, increasing the likelihood of contact between droplet interfaces. However the distance between active pores across the membrane surface is on average over 100 μm (number of pores estimated from Vladisavljevic *et al.*, 2005, assuming a triangular tessellation of evenly distributed pores; this is discussed further in Chapter 6) meaning contact even at higher pressures is unlikely. It appears longer droplet formation times implicit to low shear rates and low pressures pose a higher risk of coalescence, hence production of larger droplet sizes and even phase separation can occur. However, this can be avoided with careful process operation, a fast adsorbing surfactant (Vladisavljevic and Schubert, 2002; Kobayashi *et al.*, 2002) or sufficient pore spacing (Abrahamse *et al.*, 2001).

As the pressure is increased between 0.5-1.5 bar, the extent of droplet size increases gradually, but dependency on the rotational speed is still observed. At 100 RPM, an increase of 20.3% (up to 92.9 μm) is observed whilst at 2000 RPM the increase is 7.3% (up to 55.2 μm). It is hypothesised that the effect of coalescence is now minimised (since droplets spend less time at the membrane surface) and as such, the droplet size is determined by the dispersed phase mass transfer rate as the droplet detaches from the membrane surface and thus on the TMP. This theory was discussed within the work of Peng and Williams (1998) in which the final droplet size was suggested to consist of volumetric contributions from both the growth and detachment stages. The growth

volume depended on the size needed for the detachment forces to overcome the interfacial tension force. However, the detachment volume scaled linearly with dispersed phase flux with a greater contribution towards the final volume if the flux was high or the detachment time was long (which they observed under low shear conditions). At a low rotational speed, the droplet detachment time is likely to be longer compared to higher speeds (since lower magnitude of force to displace droplets from the membrane surface) and as such the mass transfer of dispersed phase during detachment is more significant. With high rotational speeds, the droplet detachment time approaches close to zero meaning any variation in volumetric flow rate (determined by TMP) does not significantly influence the volumetric contribution during detachment. The final droplet volume is likely to coincide with the growth volume which will be smaller due to dominating drag force and presence of Taylor vortices compared to at low speed.

Finally, at pressures >1.5 bar the droplet size begins to increase rapidly and erratically (as shown by the large error bars). Evaluation of the Capillary number (using Eq. 2.10) suggests there is a likely change in the droplet formation mechanism from dripping to jetting. For jetting to occur, either the dispersed phase velocity within the pore has to be high or the interfacial tension (IFT) has to be low. The IFT value for 1 wt. % Tween 20 and SFO is shown in Fig. 4.5. The complete line represents almost continuous measurement of the IFT whilst the dotted line is back-calculated from the dynamic rate since there was an inherent 3.5 s time delay between droplet formation and IFT measurement. Droplet formation and detachment typically occurs within a couple of seconds (Abrahamse *et al.*, 2002) so using the equilibrium IFT value would be a significant underestimation (De Luca *et al.*, 2004). For example, the IFT varies between 10.7 mN m^{-1} at 0.01s and 7.7 mN m^{-1} at 2 s (Fig. 4.5 [a]) - values much higher than the equilibrium value of 4.8 mN m^{-1} (Fig. 4.5 [b]).

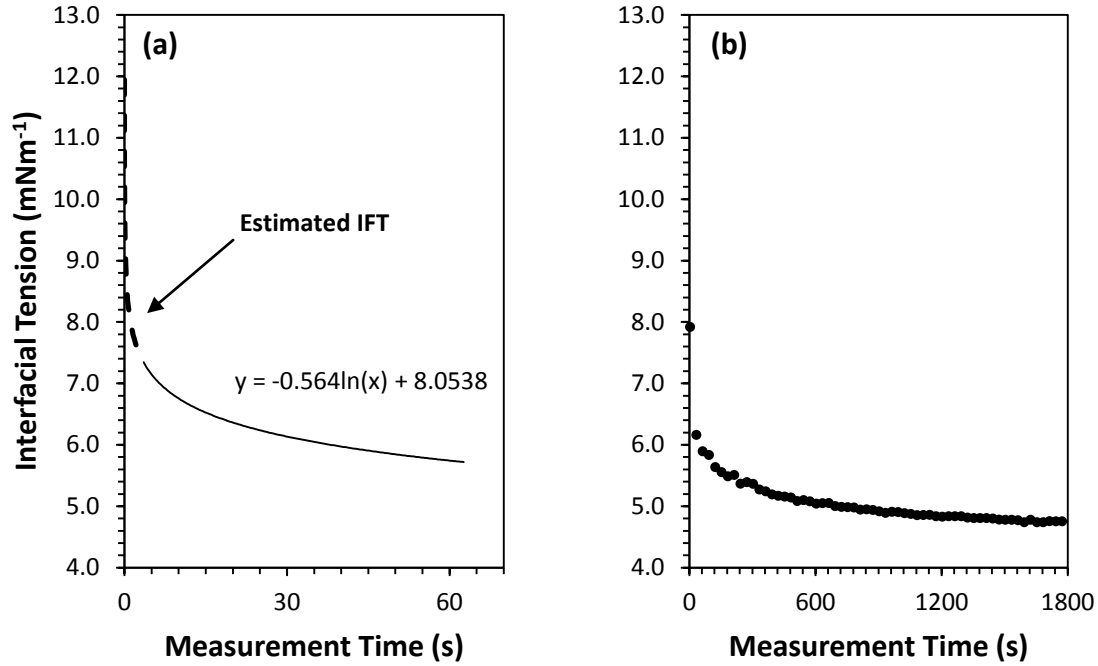


Fig. 4.5: Dynamic interfacial tension between sunflower oil and 1 wt. % Tween 20 solution. (a) shows the initial decrease whilst (b) shows the system equilibrium value. Note: Dotted line and solid line represent back-calculated and measured interfacial tension values respectively.

At pressures beyond 1.5 bar, the dispersed phase velocity exceeds 0.0023 m s^{-1} (calculated using Eq. 2.19) so evaluating for the Capillary Number with SFO of measured viscosity 0.066 Pa s equates to values greater than 0.014. Thus, the Capillary Number is tending towards the approximate threshold of 0.056 suggested by Sugiura *et al.* (2002) as the jetting point. At low droplet formation times that are achieved with high pressure (van der Graaf *et al.*, 2004) or high rotational speed, detachment will occur in a period of higher IFT which minimises the Capillary number slightly. However, the velocity increase induced by higher pressure is far more influential compared to any slight differences in the IFT. Using this logic, this would explain why the droplet size increases more erratically at 100 RPM compared to 2000 RPM as the lower drag force allows sufficient time for the IFT value to tend more towards the equilibrium value (increasing Capillary Number). Pathak (2011) reported that a higher continuous phase Weber number, which in this case would be induced by a higher rotational speed, could also induce jetting by ‘pulling’ the dispersed phase from the pore

opening. However, for this configuration the Weber number did not dramatically vary compared to the Capillary number since the continuous phase velocity is low.

What is clear is that the TMP has differing effects on the droplet size depending on the amount of shear applied through rotation. Both a decrease following by an increase in droplet size, as well as an almost single increase has been demonstrated within this study across the range of the pressures investigated. This may possibly explain the variation in observations for this parameter within the literature.

4.2.2 On the flux through the membrane

The dispersed phase flux is defined as the volumetric flow rate of the material across a specific membrane surface area. The rate limiting step of RME is the addition of dispersed phase to the continuous phase. This means that if the flux is high, the dispersed phase is added faster and therefore less time has to pass before the desired volume fraction is reached. Intrinsically, the production rate of the emulsion is greater which may be beneficial if RME is used as a manufacturing process. High dispersed phase flux is also potentially favourable because longer processing times can lead to the energy advantage over conventional processes being lost (since rotating the shaft for RME or re-circulation through the pump in XME requires energy input, albeit relatively low) (Joscelyne and Tragardh, 2000). However, if the dispersed phase flux is too high then jetting may occur as discussed in the previous section. It is therefore apparent that manipulation of the TMP is generally a balancing act between the level of control on the droplet formation process versus the throughput.

From the same experimental data shown in Fig. 4.4, the dispersed phase flux was also measured (as a mass flow rate). This was converted into flux using the density and membrane surface area (which were 919 kg m^{-3} and 14.1 cm^3 respectively) with the findings presented in Fig.

4.6 (a). Knowledge of the flux is important to correlate the TMP to the demonstrated permeability of the membrane, which for SPG membranes is known to vary depending on the pressure applied.

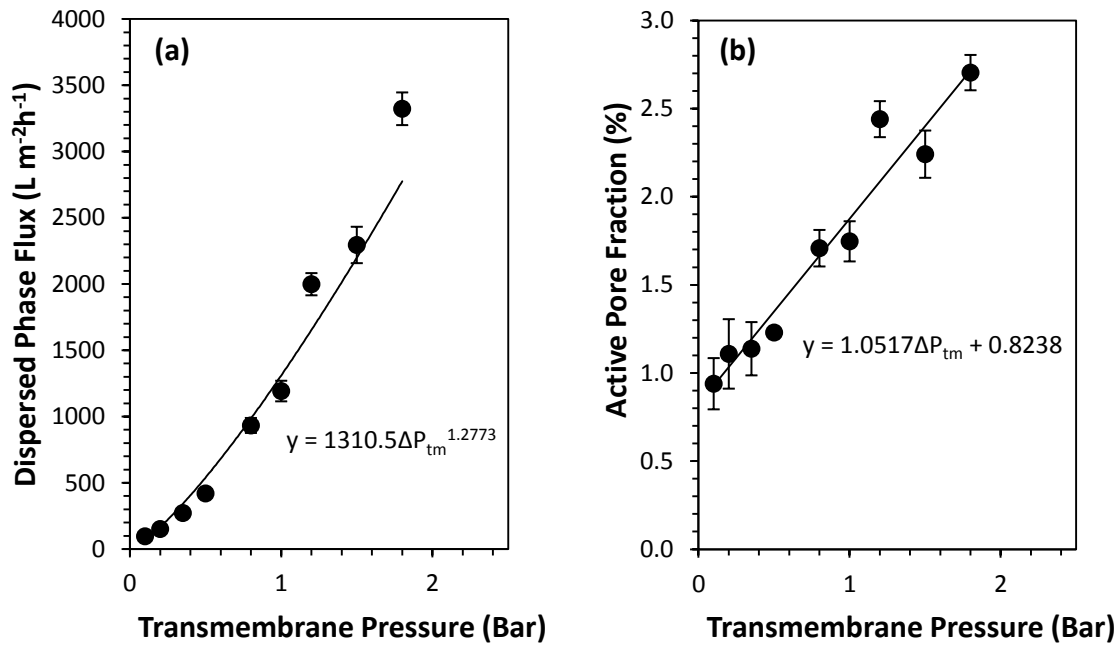


Fig. 4.6: Influence of transmembrane pressure on the average dispersed phase flux (a) and active pore fraction (b) for a 6.1 μm pore diameter, hydrophilic SPG membrane

As expected, with increasing pressure the dispersed phase flux also increases as determined by Darcy's law. Typical values of 100-200 L m⁻² h⁻¹ are achieved at 0.2 bar compared to 2000-2600 L m⁻² h⁻¹ at 1.5 bar. This relationship shows an exponential increase in flux due to increased pore activation of the SPG membrane when greater pressure is applied. If a membrane consists of multiple interconnected, tortuous pore channels of varying cross-sectional area, it is the wider channels that will activate first since there is less resistance to flow followed by the narrower ones (increasing the overall permeability). Vladisavljevic *et al.* (2004b) found the flux of water was proportional to the TMP to the power of a value between 2.3-2.7 when using SPG membranes. However, a value of 1.28 is demonstrated within this work which is likely to be because the dispersed phase used is of higher viscosity and has different wetting properties within the membrane structure. In all cases, the percentage of pores active increased in a linear manner and

ranged between 0.9-2.7% (Fig. 4.6 [b]) which is similar to values quoted in previous literature (Vladisavljevic *et al.*, 2004b; Vladisavljevic and Schubert, 2002). Lepercq-Bost *et al.* (2008, 2010) observed a hysteresis effect with both droplet diameter and dispersed phase flux as the TMP increased and then decreased. Pores activated under high TMP conditions then remained active at a lower TMP. Whilst being logical that this could happen if one altered TMP mid-experiment, this was not observed possibly due to differences in membrane cleaning protocols.

The active pore fraction was calculated by firstly evaluating the demonstrated permeability (K) of the SPG membrane at a given TMP (ΔP_{tm}); combining Darcy's law with an expression for volumetric flow rate per unit membrane surface area:

$$J_d = \frac{K\Delta P_{tm}}{\mu_d L_p} = \frac{M_d}{\rho_d A_m t_p} \quad (\text{Eq. 4.1})$$

$$K = \frac{\mu_d L_p M_d}{\Delta P_{tm} \rho_d A_m t_p} \quad (\text{Eq. 4.2})$$

where J_d is the dispersed phase flux, M_d is the mass of dispersed phase added, μ_d is the dispersed phase viscosity, ρ_d is the dispersed phase density, A_m is the membrane surface area and t_p is the processing time. The pore channel length (L_p) is estimated as the membrane thickness multiplied by a tortuosity factor of 1.28 for SPG membranes (Vladisavljevic *et al.*, 2005). Using this value within an expression of permeability given by O'Brien *et al.* (2007) allows for the active pore fraction (α) to be estimated:

$$K = \alpha d_p^2 \phi^{1.5}$$

$$\alpha = \frac{K}{d_p^2 \phi^{1.5}} \quad (\text{Eq. 4.3})$$

where d_p is the pore diameter and ϕ is the membrane porosity which is assumed to be approximately 0.56. This value was obtained by averaging all SPG porosities measured within the work of Vladisavljevic *et al.* (2005) since porosity varied randomly between 0.5 and 0.6. The flux also

appeared to be hindered under higher rotational speeds. As an example, at 1.8 bar the flux at 100 RPM was $3600 \text{ L m}^{-2} \text{ h}^{-1}$, but at 2000 RPM it was lower at $3100 \text{ L m}^{-2} \text{ h}^{-1}$. This may be the consequence of the inward acting centripetal force acting on the dispersed phase within the pore channel. If this hypothesis is the case, it is likely the active pore fraction will be slightly higher than calculated.

4.3 Effect of Rotational Speed

The effect of varying the rotational speed of the membrane between 100 and 2000 RPM on droplet size is shown in Fig. 4.7. As mentioned at the beginning of this chapter, another key parameter (alongside the TMP) is the shear rate applied at the membrane surface. This can be manipulated either by altering the rotational speed, the membrane outer diameter or the distance between the membrane surface and the emulsification vessel wall (termed the annular gap width). The shear rate equation between two concentric cylinders of which the inner cylinder is rotating and the outer is stationary was derived by Vladislavjevic and Williams (2006):

$$\dot{\gamma} = \frac{\pi r_1^2 n_1}{15(r_2^2 - r_1^2)} \quad (\text{Eq. 4.4})$$

It is clear that the shear rate ($\dot{\gamma}$) increases linearly with increasing rotational speed (n_1) assuming the radii of the membrane (r_1) and the emulsification vessel are constant. Within this experiment, the annular gap width was kept at 25 mm which varied the shear rate between 0.60 s^{-1} and 12.0 s^{-1} . The TMP was also kept constant at 0.5 bar to minimise as much as possible the effects of coalescence or jetting which would complicate the discussion.

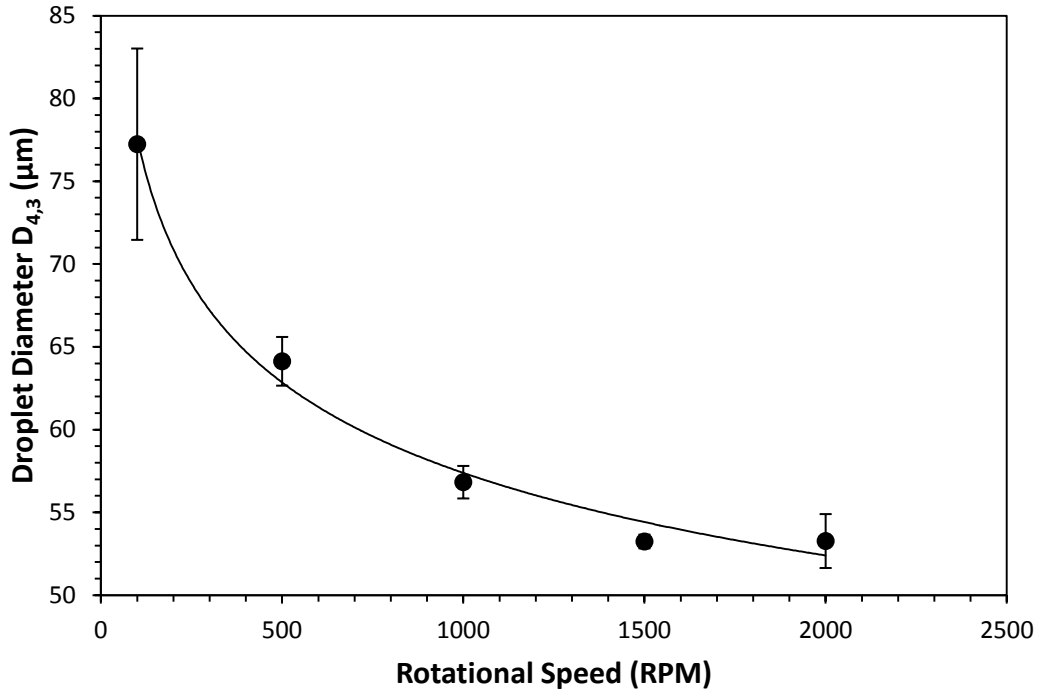


Fig. 4.7: The influence rotational speed on the mean droplet size at a transmembrane pressure of 0.5 bar. The emulsions are 10 vol. % sunflower oil stabilised by 1 wt. % Tween 20. The error bars represent one standard deviation of a triplicate of experimental runs.

With increasing rotational speed, the droplet size decreases until it reaches a size almost independent of the speed (i.e. an exponential decay relationship). For example, as the speed increases from 100 to 500 RPM, the droplet size reduces significantly from 77.2 μm to 64.1 μm (a decrease of 17.0%). In contrast, the droplet sizes produced at 1000 and 2000 RPM are 56.8 μm and 53.3 μm respectively (a smaller decrease of 6.2% across a wider range). As the rotational speed increases, the magnitude of the inward acting centripetal force becomes more significant (compared to the drag force) to therefore hold the less dense dispersed phase at the membrane surface. Within literature, there is unanimous agreement that increasing the shear rate results in droplets experiencing more drag force and therefore detaching earlier at a smaller size. This was irrespective of the method used to apply that shear whether that be by rotational motion of the membrane (Pawlik and Norton, 2013; Schadler and Windhab, 2006; Yuan *et al.*, 2009) or increase of the continuous phase flow velocity by pumping (van der Graaf *et al.*, 2004; Spyropoulos *et al.*, 2011; Vladisavljevic *et al.*, 2004b) or stirring (Egidi *et al.*, 2008; Dragosavac *et al.*, 2008). At the lowest

speed of 100 RPM, the large error bar can be attributed to coalescence at the membrane surface resulting in inconsistency during the droplet formation process (Kobayashi *et al.*, 2002). This is evident when examining the droplet distribution curves in Fig. 4.8 with a less homogeneous droplet size (wider distribution curve) at 100 RPM compared to 2000 RPM, corresponding to span values of 1.593 and 0.733 respectively. It can be seen that smaller daughter droplets are formed under low speed which can be a by-product of coalescence phenomena (Charles and Mason, 1960).

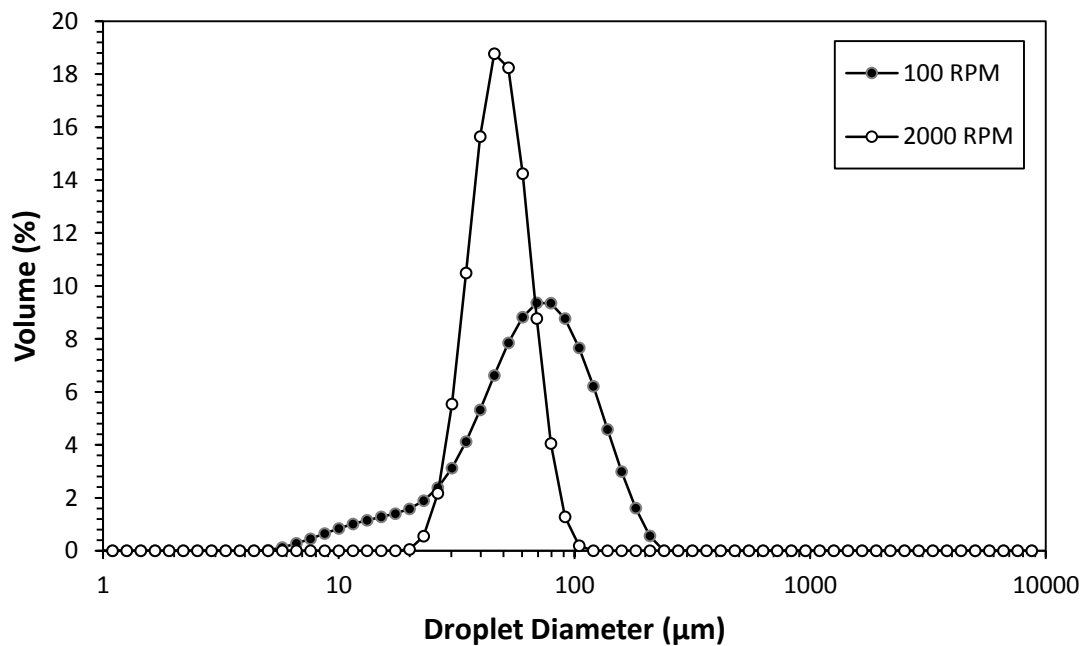


Fig. 4.8: Droplet size distributions for emulsions produced at a transmembrane pressure of 0.5 bar. The emulsions are 10 vol. % sunflower oil stabilised by 1 wt. % Tween 20.

4.4 Effect of Annular Gap Width

The annular gap width (the distance between the membrane surface and the emulsification vessel wall) is another parameter that requires consideration during the process design and operation stages. As shown in Eq. 4.4, the system geometry plays an important role in determining the shear rate at the membrane surface with higher shear rates achievable if the annular gap width is narrow (Vladisavljevic and Williams, 2006). Furthermore, the continuous phase flow behaviour is

strongly influenced by the annular gap width and membrane rotational speed as discussed in section 2.2.4. A series of transitions in the flow profile may occur depending on the Reynolds and Taylor numbers, which therefore requires consideration.

A range of emulsification vessel diameters ranging between 20 and 100 mm were explored at low (100 RPM), intermediate (1000 RPM) and high (2000 RPM) rotational speeds with the results displayed in Fig. 4.9. Again, a TMP of 0.5 bar was applied to minimise coalescence or jetting. It can be observed that the annular gap width influences the droplet diameter but primarily when operating with a low rotational speed. However, re-plotting the same data as a function of shear rate highlights a much clearer relationship as seen in Fig. 4.10.

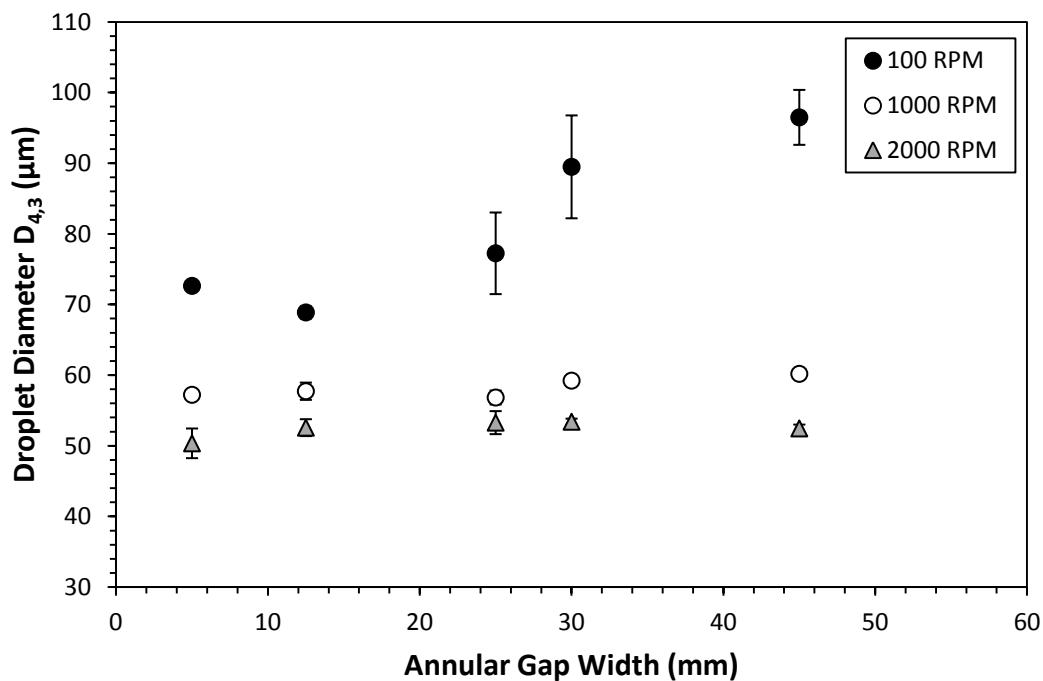


Fig. 4.9: The influence of gap width and rotational speed on the mean emulsion droplet size at 0.5 bar. The emulsions are 10 vol. % sunflower oil stabilised by 1 wt. % Tween 20. The error bars represent one standard deviation and where not visible are smaller than the symbols.

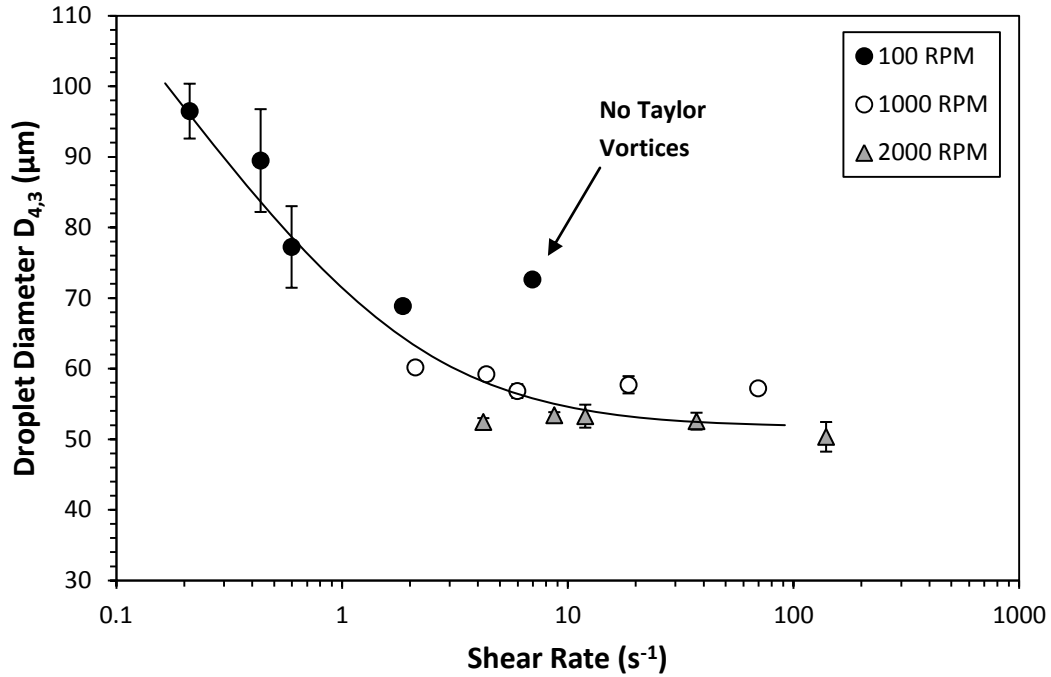


Fig. 4.10: Relationship between droplet size and the shear rate at the membrane surface for the different gap widths and rotational speeds investigated, at 0.5 bar.

With a rotational speed of 100 RPM, the shear rate at the membrane surface varied across a range of 0.21-6.98 s⁻¹. Increasing the gap size between 12.5-45 mm, the droplet size increased almost linearly from 68.9 μm to 96.5 μm. This is attributed to low shear rates indicating droplets grow much larger before experiencing sufficient drag force that induces detachment. With a wider outer vessel, the velocity gradient of the continuous phase in the radial direction is reduced. Therefore, droplets need to protrude further to encounter a significant velocity difference between the membrane surface and the continuous phase. Coalescence may also be a factor at the lowest shear rates as the probability of droplet-droplet interactions on the membrane surface increases with larger droplets. Within this range of gap sizes, vortices are produced as the Taylor number exceeds the critical value of 41.3 as shown in Fig. 4.11. However in the case of the 5 mm gap, vortices are not present since the calculated Taylor number for this configuration is 26. The small gap inhibits the development of these vortices such that the system is simple laminar Couette flow. Thus, a larger than expected droplet size of 72.6 μm is obtained despite the higher shear rate as

seen in Fig. 4.10; This is consistent with the findings by Schadler and Windhab (2006) under low rotation speeds (<5000 RPM) and a 0.5 mm annular gap width.

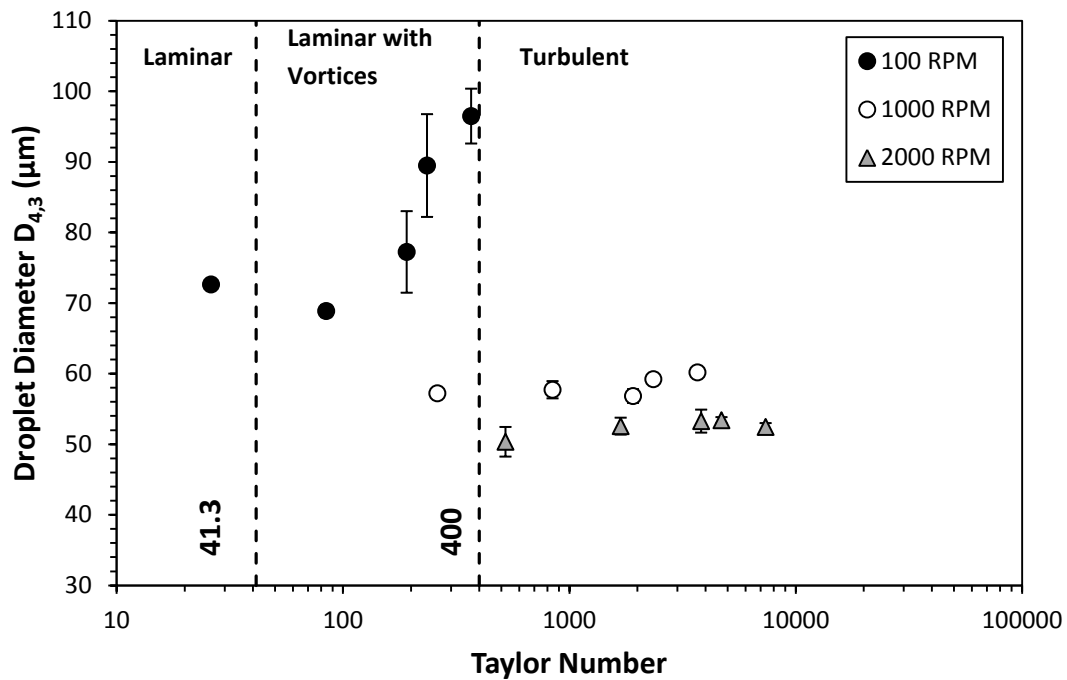


Fig. 4.11: Relationship between mean emulsion droplet size and (continuous phase) Taylor number as a function of rotational speed, at a transmembrane pressure of 0.5 bar.

Increasing the membrane rotational speed to an intermediate level of 1000 RPM, this broadened the shear rate range experienced by droplets at the membrane surface between $2.12\text{-}69.8\text{ s}^{-1}$. The droplet size remained relatively constant ($56.8\text{-}60.2\text{ }\mu\text{m}$) regardless of the shear rate applied. This suggests that with the rotating membrane system, as with previous findings with Cross-flow Membrane Emulsification (XME), the droplet size tends to a value that is independent of the shear rate applied. However, droplet sizes produced at 1000 RPM were smaller than those produced at 100 RPM because of higher shear rates alongside the presence of Taylor vortices. The flow regime of the continuous phase in all cases apart from with a 5 mm gap was turbulent although in this specific case, there is no difference in droplet size below the threshold of turbulent flow (Taylor number of 400).

At 2000 RPM, shear rates of 4.2-139.6 s^{-1} were generated across the range of gap widths investigated and turbulent flow was present in all cases ($Ta > 400$). Droplets were consistently 50.3-53.4 μm in diameter suggesting the size was again independent of the shear rate applied.

4.5 Effect of Shear Rate with Transmembrane Pressure

In the previous section, a range of shear rates were applied between 0.21-139.6 s^{-1} at a fixed TMP of 0.5 bar. It is apparent that there is a relationship between TMP, rotational speed and the annular gap size on the droplet size produced during RME. Therefore, a low (0.2 bar) and high (1.5 bar) TMP were also investigated to consider all three variables. The results are shown in Fig. 4.12.

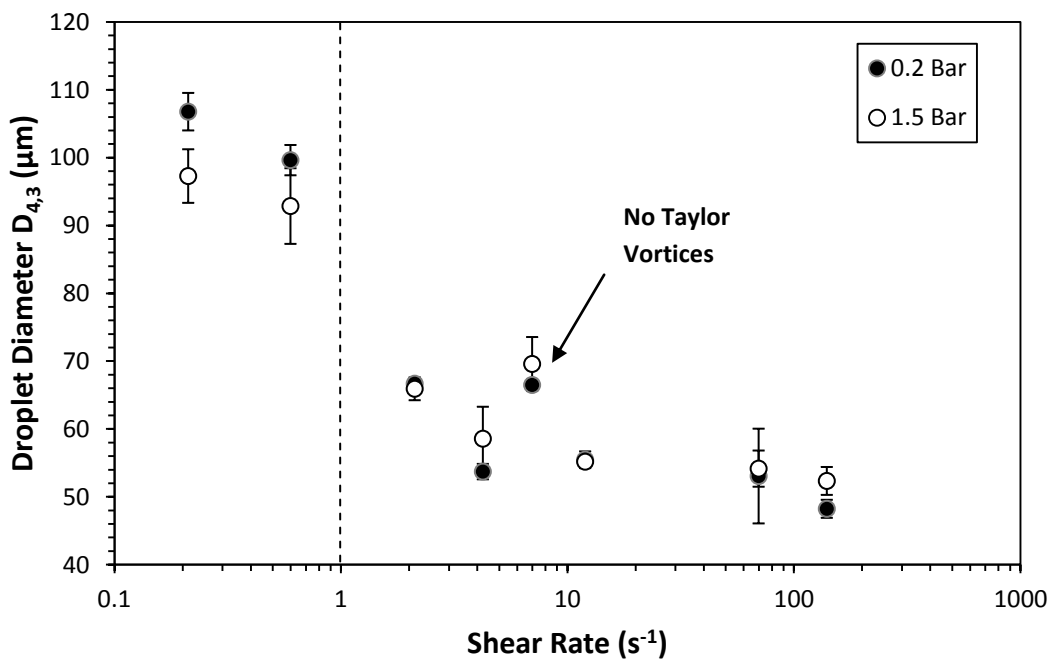


Fig. 4.12: Relationship between mean emulsion droplet size and shear rate at a low (0.2 bar) and high (1.5 bar) transmembrane pressure.

At shear rates below $\approx 1s^{-1}$, it can be seen that droplets formed under low TMP conditions are approximately 7-10 μm larger than those formed at high TMP. The difference can be explained by considering coalescence phenomena; in the case of 0.2 bar the droplets spend a longer time

forming at the membrane surface and so are more prone to coalescence. For 1.5 bar, droplets form much faster although the membrane would demonstrate a higher active pore fraction so droplets would be forming closer together. This therefore suggests that time at the membrane surface is important, considering that low TMP just above the capillary pressure should theoretically yield the smallest droplets (Spyropoulos *et al.*, 2011). With the shear rate above $\approx 1 \text{ s}^{-1}$, the droplet diameters are relatively similar with perhaps a low TMP being slightly favourable to formation of smaller droplets. In this instance, the interface is formed slowly at 0.2 bar allowing surfactant sufficient time to adsorb to lower the IFT. The interfacial tension force holding the droplet at the membrane surface is therefore lower so droplets can grow to a smaller size, but still experience sufficient drag force to enable detachment. Furthermore, less dispersed phase material is added to the droplet during the detachment stage since the flux is lower. Again, in the absence of Taylor vortices developing (in the case of 6.98 s^{-1} i.e. 100 RPM and 5 mm gap) within the continuous phase flow, a sudden 'jump' in the droplet size can be observed irrespective of the TMP applied. This therefore confirms that this effect is induced by the continuous phase flow profile rather than the dispersed phase flow behaviour.

4.6 Viscosity Effects

It is well established that fluid flow behaviour is related not only to the energy input (whether this be achieved by pressure, agitation, gravity etc.) but the resistance to flow of the fluid itself i.e. its viscosity. Until now, processing effects have been investigated using SFO as the dispersed phase and 1 wt. % Tween 20 solution. However, investigation into the behaviour of differing viscosity systems gives a further insight into the flow behaviour induced by altering process variables. Viscosity tends to be inherent to the ingredients selected to formulate the emulsion rather than being controlled directly during operation. To some extent this would be achievable through thermal control, for example the dispersed phase viscosity could be lowered by heating to increase the dispersed phase flux. However, this may have a detrimental effect on the emulsion stability so generally this is avoided. For this study, a range of silicone oils and glycerol concentrations are

explored to alter the dispersed and continuous viscosities respectively and hence clarify their effects on droplet size and dispersed phase flux.

4.6.1 Dispersed Phase Viscosity

A range of different viscosity silicone oils were used to form O/W emulsions under varying TMP and a fixed shear rate of 5.98 s^{-1} (1000 RPM and 25 mm gap). The dynamic viscosity of these oils varied between 0.012-0.085 Pa s with their properties listed in Table 4.1. As can be seen in Fig. 4.13, the dispersed phase viscosity has an influence on the measured droplet size.

Table 4.1: Density values for the silicone oils investigated.

Dispersed Phase	Density (kg m^{-3})
Silicone Oil (0.012 Pa s)	930
Silicone Oil (0.023 Pa s)	950
Silicone Oil (0.085 Pa s)	960

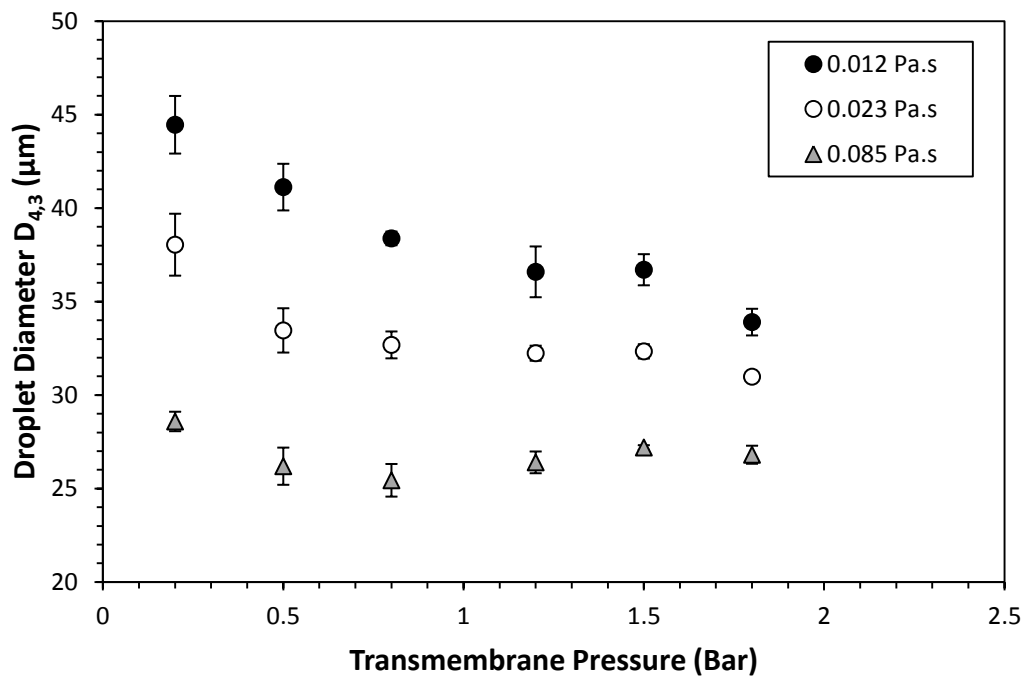


Fig. 4.13: The influence of transmembrane pressure on the mean droplet size for different oil viscosities. The emulsions are 10 vol. % silicone oil stabilised by 1 wt. % Tween 20. The error bars represent one standard deviation of a triplicate of experimental runs

With increasing TMP, the droplet size decreased to a minimum with the extent depending on the viscosity. For the lowest viscosity silicone oil (0.012 Pa s), the decrease between 0.2-1.8 bar was 23.8% (from 44.5 μm to 33.9 μm) whereas for the highest viscosity oil (0.085 Pa s), the decrease was 6.3% (from 28.6 μm to 26.8 μm). Generally, the droplet sizes were the largest for the 0.012 Pa s oil agreeing with a number of authors (Kobayashi *et al.*, 2005; Vladislavljevic *et al.*, 2008). On the other hand, Yuan *et al.* (2009) implied a higher viscosity dispersed phase would produce larger droplets because of the presence of a viscous force holding droplets at the membrane surface (directly proportional to viscosity). Perhaps the trend seen here is because the lower resistance to flow enables greater mass transfer during the detachment stage. Furthermore, it was suggested that the drag coefficient adopted (typically 1.7 for a rigid sphere; O'Neil, 1964) was a possible variable within force balance models (Timgren *et al.*, 2008). It is proposed here that a higher viscosity dispersed phase droplet potentially resembles a rigid sphere more closely than a lower viscosity equivalent and therefore experiences greater drag to aid detachment. The density differences between the silicone oils (listed in Table 4.1) also alter the point of detachment with higher density droplets (approaching that of the continuous phase) less susceptible to being held at the membrane surface by the centripetal force.

In contrast with Fig. 4.4 shown in section 4.2.1, only two distinct regions are observed; an initial droplet size decrease that may possibly be attributed to coalescence, followed by a plateau in the size. The latter region was typically observed within microchannel emulsification and is known as the 'size-stable zone' (Kukizaki, 2009; Kobayashi *et al.*, 2003). The prominence of this region depends on high IFT values which cause non-spherical, deformed droplets to transform back to spheres by detaching in a bid to minimise their interfacial free energy – known as 'spontaneous transformation-based droplet formation' (Sugiura *et al.*, 2001). As can be seen by Fig. 4.14, the IFT between silicone oil and 1 wt. % Tween 20 solution is higher than for SFO (Fig. 4.5) since there are no triglyceride impurities and hence the 'size-stable zone' is not apparent in Fig. 4.4. A more viscous silicone oil also has a higher IFT value due to high molecular weight siloxane chains having greater Van der Waals'

forces between them and hence a greater cohesive energy (Conley, 1996). Upon further pressure increase (beyond the 1.8 bar maximum TMP studied here), it is predicted the droplet size will begin to increase as the volumetric contribution during detachment becomes significant and eventually droplet production through a jetting mechanism will occur. However, these latter two regions (unlike in Fig. 4.4) are not observed here. Despite the high dispersed phase velocity achievable with 0.012 Pa s silicone oil ($0.0015\text{-}0.014\text{ m s}^{-1}$ across the pressure range, calculated using Eq. 2.19), the high IFT during detachment (between 18.8 mN m^{-1} at 0.01 s and 13.1 mN m^{-1} at 2 s) ensures the Capillary number (calculated using Eq. 2.10) does not exceed 0.010 implying the IFT is the dominating factor in droplet formation (Kukizaki, 2009).

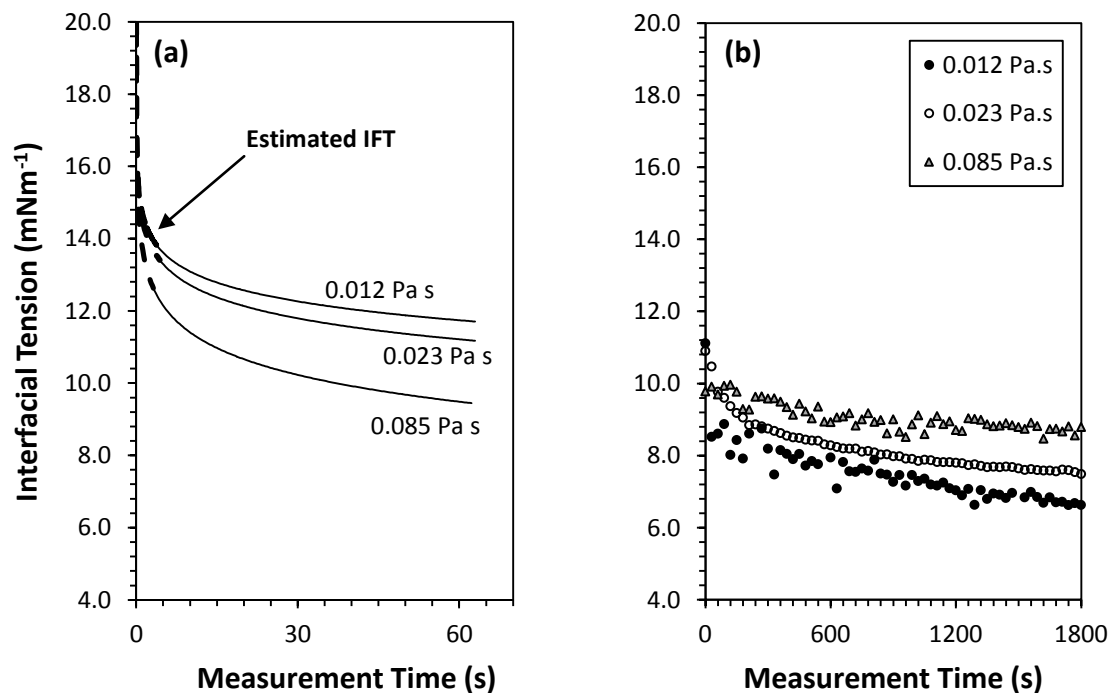


Fig. 4.14: Dynamic interfacial tension between silicone oil of varying viscosity and 1% Tween 20 solution. (a) shows the initial decrease whilst (b) shows the system equilibrium value. Note: Dotted line and solid line represent back-calculated and measured interfacial tension values respectively.

The dispersed phase flux for the respective silicone oils is presented in Fig. 4.15. As expected, higher flux values are achieved with the lower viscosity dispersed phase since there is less resistance to flow. In this case, flux values between $470\text{-}12500\text{ L m}^{-2}\text{ h}^{-1}$ were measured for the 0.012

Pa s silicone oil compared to 50-1200 L m⁻² h⁻¹ for the 0.085 Pa s oil. The exponential coefficient ranges between 1.43-1.49 with increasing viscosity; the 0.012 Pa s silicone oil has the lowest surface tension allowing it to permeate more readily through the tortuous pore channels previously inactive at lower pressure. This may be a similar effect to one observed by Yuan *et al.* (2009) where with increasing wettability of a more viscous dispersed phase (0.23 Pa s), they obtained similar fluxes to unmodified dispersed phase of lower viscosity (0.049 Pa s).

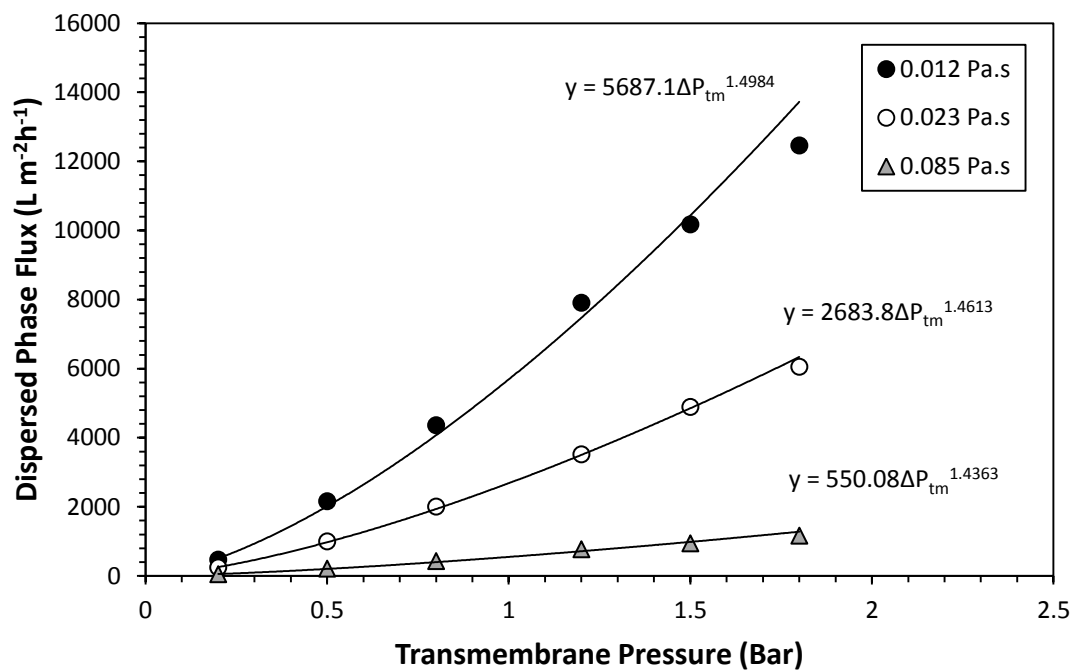


Fig. 4.15: Influence of transmembrane pressure on the dispersed phase flux for differing viscosity silicone oil through a 6.1 μm pore diameter, hydrophilic SPG membrane.

4.6.2 Continuous Phase Viscosity

The viscosity of the continuous phase was modified by added varying quantity of glycerol between 1 wt. % to 50 wt. %. This was achieved by blending the glycerol with water prior to surfactant addition. As can be seen by the data shown in Table 4.2, use of glycerol not only altered the viscosity and density as expected, but the IFT as well. Identifying a viscosity modifier to form Newtonian solutions whilst not demonstrating surface activity, proved to be challenging. It was

decided the former was the priority in order to impart a constant shear stress during operation (at a given shear rate) to produce the most uniform droplet size. The IFT decreases at higher glycerol concentrations since glycerol interacts with the hydrogen bonding in the continuous phase to lower the cohesive forces and hence the surface tension. Yilmaz *et al.* (1999) suggested that glycerol can be considered as a ‘co-emulsifier’. Irrespective of the mechanism, the IFT needs accounting for during the discussion. For this experiment, the TMP was fixed at 0.5 bar and the shear rate was modified between 0.60-104.7 s⁻¹ by varying both the rotational speed and annular gap width. The results are presented in Fig. 4.16.

Table 4.2: Physical properties of solutions investigated when modifying continuous phase viscosity with glycerol.

	Ratio of Glycerol : Water (wt. %)	Equilibrium IFT w/ SFO & 1% Tween 20 (mN m⁻¹)	Viscosity w/ 1% Tween 20 (Pa s)	Density w/ 1% Tween 20 (kg m⁻³)
Increasing Viscosity ↓	1 : 99	4.7	0.00186	1001.6
	10 : 90	4.1	0.00226	1025.0
	25 : 75	3.5	0.00332	1063.9
	50 : 50	2.4	0.00916	1128.7

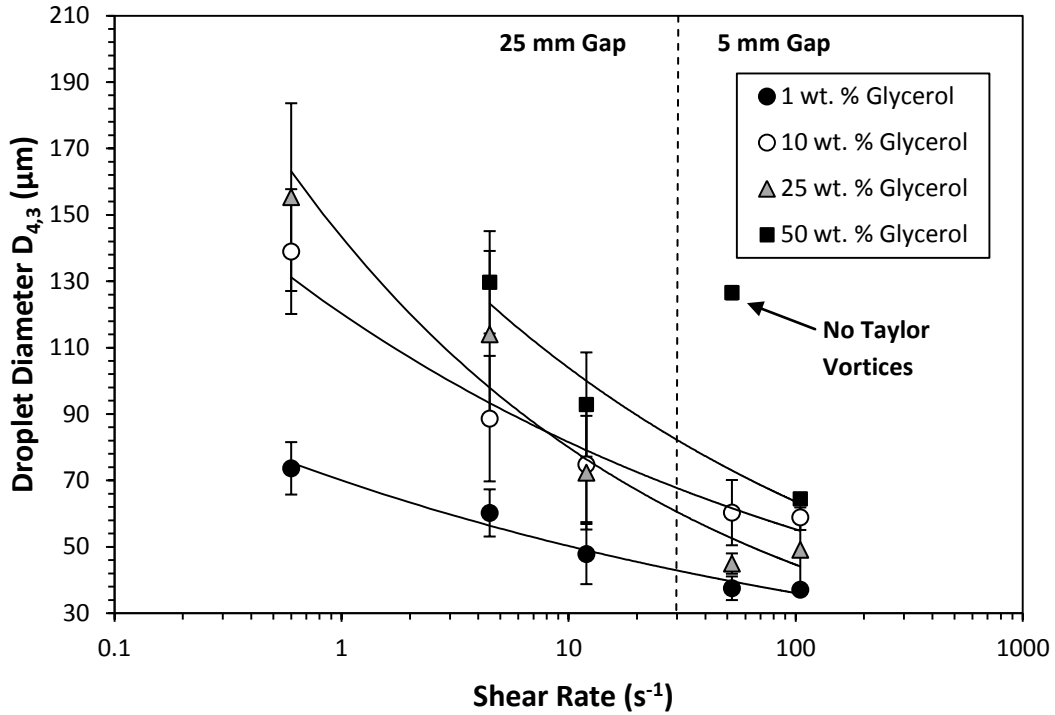


Fig. 4.16: The influence of continuous phase viscosity and shear rate on the mean droplet size at 0.5 bar using a 6.1 μm pore diameter, hydrophilic SPG membrane.

The viscosity of the continuous phase has previously been shown to affect the droplet size with a rotating membrane configuration (Aryanti *et al.*, 2009; Pawlik and Norton, 2013; Vladislavljevic and Williams, 2006). In these studies, the droplet size decreased when using a more viscous continuous phase since the drag force increases in a directly proportional manner. It was therefore expected that investigation of this parameter by thickening the continuous phase with glycerol would provide a similar trend. As can be seen, surprisingly the smallest droplet sizes (37.1-73.6 μm) were achieved with the lowest viscosity continuous phase of 1 wt. % glycerol compared to 25 wt. % glycerol (450-155 μm). Additionally, differentiating the power curve functions shows the droplet size decreases much more rapidly for high viscosity systems up to 25-50 wt. % glycerol where the curves are parallel. This is despite the IFT retaining the droplet at the membrane surface being slightly higher for low glycerol concentrations. Matos *et al.* (2013) observed larger droplets when using more viscous continuous phase attributing this to surfactant diffusion being hindered by

the higher viscosity, resulting in coalescence. From Fig. 4.17, there is no evidence that surfactant diffusion is limited by viscosity as the initial rate of IFT decrease is quick for higher viscosity systems. This effect may be hidden by the glycerol surface activity in this case.

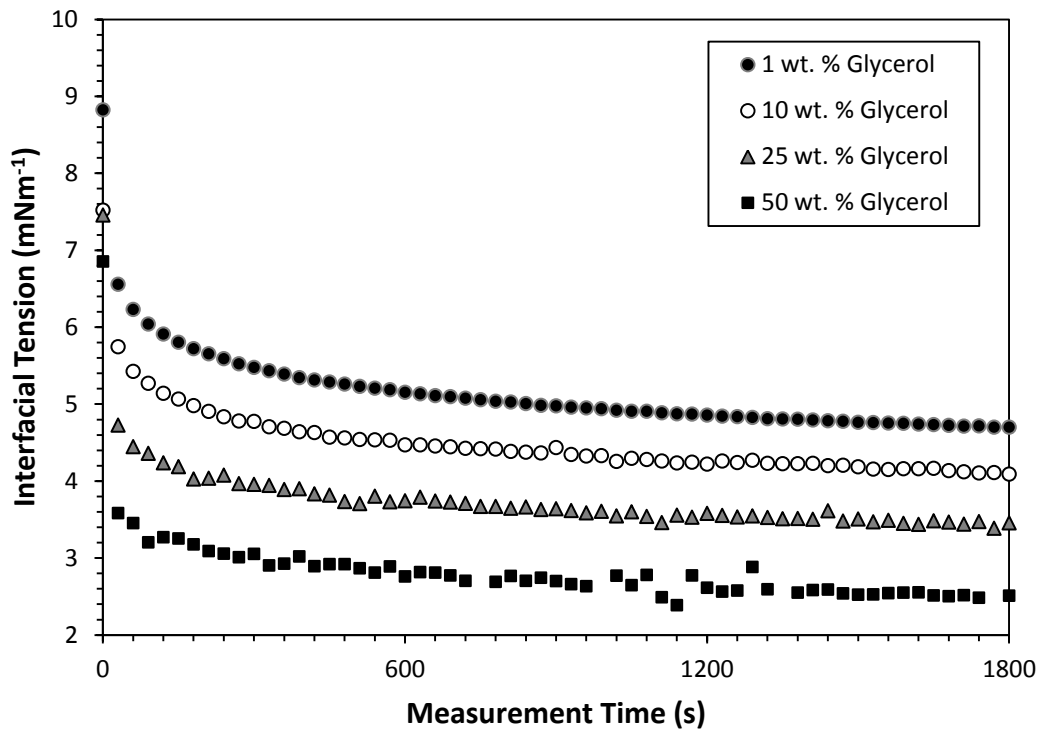


Fig. 4.17: Dynamic interfacial tension between sunflower oil and continuous phase containing variable concentration of glycerol and 1 wt. % Tween 20.

The droplet size observations (from Fig. 4.16) may therefore perhaps be explained by considering the movement of droplets within the continuous phase. With a more viscous continuous phase, droplets cannot easily move away from the membrane surface towards the outer edge of the emulsification vessel since their movement is hindered by viscosity and density effects (SFO droplets less dense than continuous phase). As a consequence, detached droplets remain within the vicinity of forming droplets increasing the likelihood of coalescence. This would explain why complete phase separation is observed in the case of 50 wt. % glycerol under a shear rate of 0.60 s^{-1} . Also, very viscous solutions are more laminar within a concentric cylinder setup and as such may not develop Taylor vortices to sweep droplets away. This can be seen in the case of 50 wt. % glycerol and an

applied shear rate of 52.4 s^{-1} (which corresponds to 750 RPM and a 5 mm gap size). Under these conditions, the Taylor number is 31 and hence the droplet size is much larger than expected ($127 \mu\text{m}$). Overall, the droplet size decrease is rapid for more viscous solutions upon increasing the shear rate. As coalescence effects are negated, the higher drag force allows droplets to detach much earlier from the membrane surface. It is therefore predicted that further shear rate modification $\gg 104.7 \text{ s}^{-1}$ that droplet sizes will be smaller for higher viscosity continuous phase systems.

4.6.3 Viscosity Ratio

Finally, the effect of viscosity ratio was studied under fixed processing conditions (TMP = 0.5 bar, shear rate = 5.98 s^{-1}). A slightly broader range of silicone oils (0.007-0.085 Pa s) and glycerol concentrations (1-75 wt. %) were used in order to explore viscosity ratios between 0.16 to 45.7. Droplet sizes between $35.2\text{-}69.2 \mu\text{m}$ were produced as shown in Fig. 4.18.

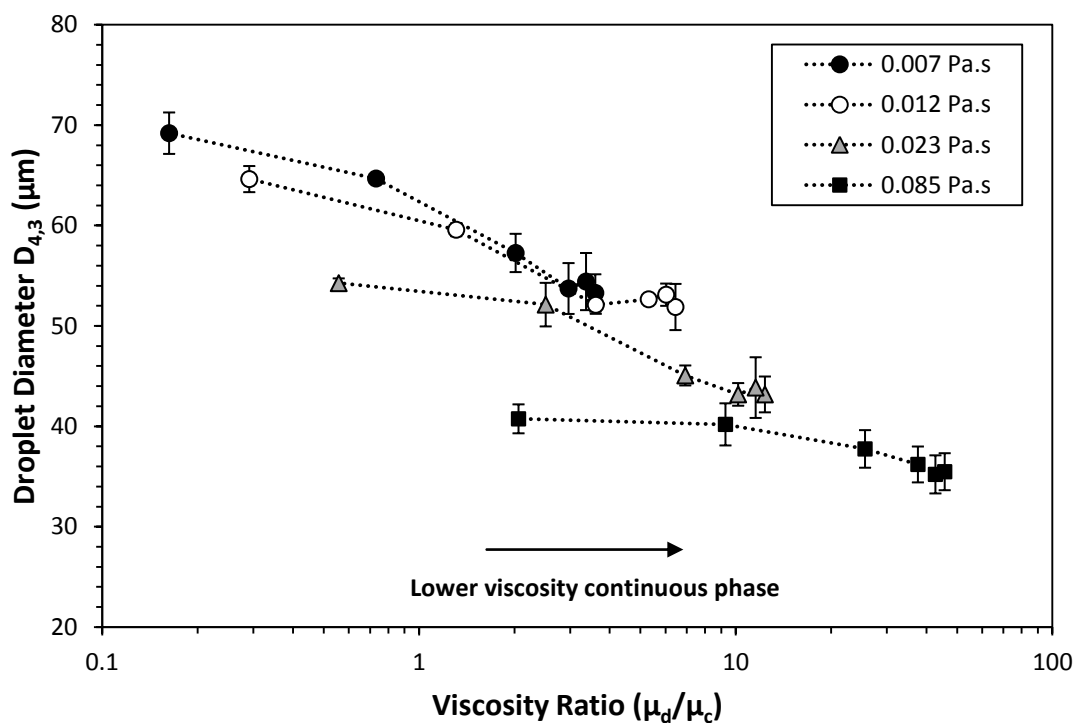


Fig. 4.18: The influence of viscosity ratio on the mean droplet size stabilised by 1 wt. % Tween 20. The ratio was modified by using different viscosity silicone oils and varying the quantity of glycerol within the continuous phase. The error bars represent one standard deviation of a triplicate of experimental run.

As a general observation, a lower viscosity dispersed phase produced larger droplets as seen in section 4.6.1. It is suggested that this is due to more viscous oil droplets acting as rigid entities having a higher drag coefficient so they experience more drag force. A lower density difference between the two phases will mean the droplet is influenced less by the inward acting centripetal force. The higher viscosity dispersed phase also has a lower dispersed phase flux so less material will be transferred to the droplet during the detachment stage (Kukizaki, 2009). Beyond a viscosity ratio of 1, the droplet size decreases with this explained within section 4.6.2 by the continuous phase hindering the movement of droplets away from the membrane surface at high viscosity. This theory is possibly supported by observations here as more dense material (e.g. 0.085 Pa s silicone oil) is able to overcome the flow resistance within the continuous phase since it has greater momentum upon detachment. As a consequence, the droplet size does not increase as dramatically with increasing continuous phase viscosity compared to a dispersed phase of lower density (e.g. 0.007 Pa s silicone oil). Kukizaki (2009) and Christov *et al.* (2008) both observed a decrease in droplet diameter with increasing viscosity ratio with smaller droplets produced when using a lower viscosity continuous phase and higher viscosity dispersed phase. The data therefore agrees with those findings presented. Kukizaki (2009) also suggested the droplet size was independent of viscosity ratio at a TMP of 1.1 times the capillary pressure of the membrane pore channel. In this case, the TMP was kept constant rather than altered to account for lower IFT systems reducing the capillary pressure required. However, there is a slight suggestion this is the case at a fixed ratio above the capillary pressure. Droplet size and viscosity ratio data clusters around areas which may have a similar approximate IFT based on measurements made within sections 4.6.1 and 4.6.2. Some examples are shown in Table 4.3 in which the TMP is roughly 15.2 times the capillary pressure calculated from Eq. 2.10.

Table 4.3: Droplet size data for systems which share similar viscosity ratios and approximate IFT values.

Dispersed Phase Viscosity (Pa s)	Continuous Phase Viscosity (Pa s)	Dispersed Phase IFT^a (mN m⁻¹)	Continuous Phase IFT^b (mN m⁻¹)	Average IFT^c (mN m⁻¹)	Viscosity Ratio	Droplet Diameter (μm)
0.012	0.00332	6.6	3.5	5.1	3.61	52.1
0.023	0.00916	7.5	2.4	5.0	2.51	52.1
0.023	0.00226	6.6	4.1	5.4	10.18	43.2
0.085	0.04125	8.8	1.7	5.3	9.28	40.2

(a) Measured between silicone oil and 1 wt. % Tween 20.

(b) Measured between sunflower oil and varying glycerol content with 1 wt. % Tween 20.

(c) Rough approximation of average value between measurements from (a) and (b).

A more rigorous study of viscosity ratio accounting for TMP and IFT (to keep the ratio of TMP above the capillary pressure constant) would be required in order to sufficiently prove that the droplet size does not change at a given viscosity ratio.

4.7 Conclusions

The effect of TMP, shear rate, dispersed and continuous phase viscosity on the final droplet size and flux has been investigated for a RME system. O/W emulsion droplets of average diameter 23.4-217 μm have been produced using an SPG membrane of 6.1 μm pore diameter. In this chapter, a number of complex processing effects have been discussed through consideration of the fluid flow and IFT behaviour of the two phases.

Considering the dispersed phase flow behaviour effects on droplet size, four distinct regions can be seen across the range of TMPs investigated. Firstly, a decrease in size across low pressures (at approximately <0.5 bar) which is attributed to coalescence at the membrane surface during long droplet formation times. Secondly, a plateau in size known as the 'size-stable' zone which occurs due to the spontaneous transformation-based droplet formation mechanism in systems with high IFT (i.e. with silicone oils). Thirdly, an eventual increase in droplet size as significant mass is transferred via the droplet neck during detachment. The volumetric contribution during this stage depends primarily on the droplet detachment time at the dispersed phase flux and thus can become negligible at increased rotational speeds (>1000 RPM). This is due to higher drag force to ensure earlier detachment from the membrane surface. It is also suggested that viscous dispersed phase droplets may experience a higher drag coefficient since they resemble more rigid spheres; an assumption within drag force calculations. Finally, if the IFT is low and dispersed phase flux (or more specifically the pore fluid velocity) is sufficiently high, jetting of the dispersed phase may occur (approximately >1.5 bar). In this case, the Capillary number defining this flow behaviour approaches the threshold value of 0.056 that is previously suggested in literature.

The flux through the membrane increases with high pressure and low dispersed phase viscosity as defined by Darcy's law. Values between 50-12500 $\text{L m}^{-2} \text{h}^{-1}$ were measured for oil viscosities between 0.012-0.085 Pa s across applied TMPs between 0.1-1.8 bar. For SPG membranes, this relationship between flux and pressure is exponential rather than directly proportional since

membranes demonstrate a variable permeability. The percentage activation of tortuous pore channels depends on the applied TMP. The calculated values for active pore fraction ranged between 0.5-2.7% coinciding with previous findings for SPG membranes.

The continuous phase flow behaviour also determines the droplet size produced primarily by altering the drag force acting on the droplet. By increasing the shear rate (through higher rotational speeds and narrower annular gap widths), the droplet size tends to a minimum independent of the applied shear as commonly observed within cross-flow membrane emulsification. In this case, higher RPM imparts greater centripetal force which dominates over the effect of increasing shear. Another key consideration is where Taylor vortices can form and in their absence below a critical Taylor number of 41.3, droplet sizes are significantly larger. This is possible particularly for low speed, narrow gap or high viscosity continuous phase systems. Finally, if there is a significant density difference between the two phases (dispersed phase being typically lower for O/W systems) or if the aqueous continuous phase viscosity is high, there is a potential for droplets to not be displaced sufficiently away from the membrane surface but remain within the vicinity of other forming droplets. This is likely to increase coalescence phenomena, which is generally unfavourable during emulsification processing.

Chapter 5:

Formulation Effects using a Small-scale Rotating Membrane Emulsification Device

This chapter furthers current understanding on how interfacial phenomena determined by the formulation can control the droplet size during rotating membrane emulsification for batch sizes less than 0.36 kg.

Data and discussions contained within this chapter are to be published within:

Lloyd, D.M., Norton, I.T., Spyropoulos, F. (2015). Process optimisation of Rotating Membrane Emulsification through the study of surfactant dispersions. *Journal of Food Engineering*, 166 316-324.

Spyropoulos, F., Lloyd, D.M., Norton, I.T. (June 2015). A microstructural approach to optimising membrane emulsification: surfactant diffusion through the oil/water interface. *The 12th International Congress on Engineering and Food*, Quebec City, Canada (poster presentation).

5.1 Introduction

The aim of this chapter is to investigate how O/W emulsion droplet size is affected by the interfacial behaviour of the material used to stabilise the droplets. A range of materials are used from conventional surfactants (e.g. Tween 20, Brij 97), particles (silica) and mixtures of the two. As discussed earlier in this thesis, surfactants are commonly used to lower the tension between the oil/water interface to facilitate droplet break up (high-shear processing) or droplet detachment (membrane processing). Surfactants and particles can stabilise the droplet interface to prevent coalescence through steric or electrostatic repulsive mechanisms. Therefore, selection of a suitable surfactant/particle type and concentration is a key consideration in order to produce an emulsion microstructure of desired properties (e.g. a specific droplet size or a narrow droplet size distribution).

Within many formulations, surfactants in particular remain some of the most costly components and therefore minimising consumption of these would be positive from a manufacturer's perspective since the product would be more profitable. On the other hand, insufficient amount of surfactant/particles can reduce the efficiency of the emulsification process and have a detrimental effect on properties such as emulsion stability. Typically, manufacturers over-compensate by using a much higher concentration than required; this is not very effective with a large quantity of material remaining 'wasted' in the bulk continuous phase rather than at the interface. Membrane emulsification is able to use surfactant more efficiently since the interfacial area is gradually increased, potentially allowing surfactant sufficient time to adsorb. However, this generally coincides with low dispersed phase flux and therefore the rate of production is slow compared to other processes used in industry. It is therefore a dilemma if the intention is to produce small, mono-dispersed droplets at a rate that is competitive with current emulsification technologies. The key to solving this challenge is by ensuring rapid adsorption of surfactant/particles to ensure early droplet detachment and stabilisation of the interface against coalescence. At

present, conventional approaches may lead to membrane coalescence in the majority of cases irrespective of the surfactant type(s) and concentrations used (Wagdare *et al.*, 2010; Abrahamse *et al.*, 2002).

This chapter considers dynamic interfacial behaviour of the oil/water system for a range of material types and concentrations using a rotating membrane emulsification (RME) setup. Processing parameters such as the transmembrane pressure (TMP) and shear rate are also investigated to explore the coupled behaviour between the rate of generation of the interface versus the rate of adsorption kinetics of the surfactant/particles used. Subsequently, a novel approach to ensure rapid adsorption of surfactant is presented namely through positioning of high hydrophilic-lipophilic balance (HLB), non-ionic surfactants within the dispersed phase rather than their common positioning within the continuous phase. This is compared to a pre-mix membrane emulsification setup which is considered favourable for high production rate processing. The study will therefore further understanding of the RME process and allow for optimisation to reduce droplet size and surfactant/particle consumption whilst maximising production rate simultaneously.

5.2 Effect of Surfactant Type/Concentration

The surfactant used plays an essential role in the stabilisation and detachment of droplets during RME. The major retaining force acting to hold droplets at the membrane surface during formation is the interfacial tension (IFT) force. If this is able to be reduced significantly and quickly through rapid adsorption of surfactant, droplets detach from the membrane surface earlier and therefore have grown to less of an extent. A surfactant's ability to migrate towards, adsorb and stabilise an oil/water interface depends on intrinsic physicochemical properties such as its affinity towards the interface (roughly quantified by the hydrophile-lipophile balance; HLB) and its molecular weight. Concentration of surfactant is also a very important formulation variable during emulsification. Firstly, the greater the interfacial area of the emulsion system, the more surfactant is required to stabilise that interface so by that logic, higher concentrations can produce smaller

droplets or stable emulsions of higher dispersed phase volume fractions. Secondly, operation below a threshold concentration known as the critical micelle concentration (CMC) means the surfactant moves within the bulk phase as individual molecules (or monomer) which would be depleted over time as they adsorb at the oil/water interface. Above the CMC, micelle formation occurs so the amount of free surfactant molecules in the bulk phase remains in dynamic equilibrium. As surfactant molecules enter the sub-surface prior to adsorption at the droplet interface, these molecules are replenished by the dissociation of surfactant micelles. Theoretically, further increase of the surfactant concentration above the CMC results in greater numbers of micelles (rather than individual monomer available for adsorption) and as such the extent of IFT decrease is not dramatically affected. Finally, the concentration of surfactant alters the transport through the bulk phase by diffusion and convection with these processes promoted with a higher quantity of surfactant. In turn, this enhances the rate of IFT decrease (Schroder *et al.*, 1998) which can facilitate early droplet detachment. Selection of the surfactant type and concentration is clearly just as important as how the RME process is operated, hence these formulation parameters also require rigorous investigation. It is worth highlighting that even in the absence of surfactant (Fig. 5.1), there is a gradual decrease in IFT (to 23.2 mN m^{-1}) between SFO and water due to surface active impurities within the oil. These impurities are triglycerides, namely saturated palmitic and stearic acids, monounsaturated oleic acid and polysaturated linoleic acid (Garces *et al.*, 2009).

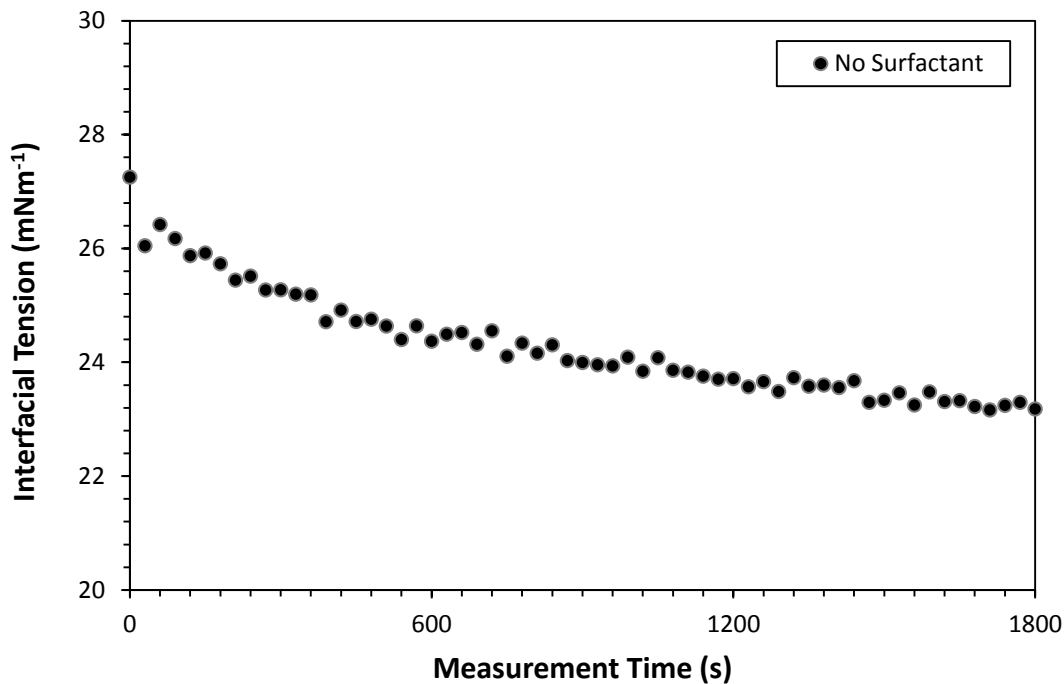


Fig. 5.1: Dynamic interfacial tension between sunflower oil and water with no surfactant present.

Four surfactants were identified to explore a range of properties that can affect the interfacial behaviour. Tween 20 and Brij 97 were selected as two differing non-ionic surfactants. Sodium dodecyl sulphate (SDS) was also investigated since it is anionic and extremely effective at stabilising O/W emulsions. Finally, hydrolysed lecithin (a phospholipid derived from soy beans) was chosen as an alternative since whilst more suited to W/O emulsion stabilisation, is also capable of stabilising O/W. Important surfactant properties are listed in Table 5.1. A range of concentrations were used between 0.01 wt. % and a maximum of 10 wt. % depending on the observed solubility within the aqueous continuous phase. 10 vol. % of sunflower oil (SFO) in water emulsions were produced under fixed processing conditions; TMP = 0.5 bar, shear rate = 5.98 s^{-1} . The results are presented in Fig. 5.2.

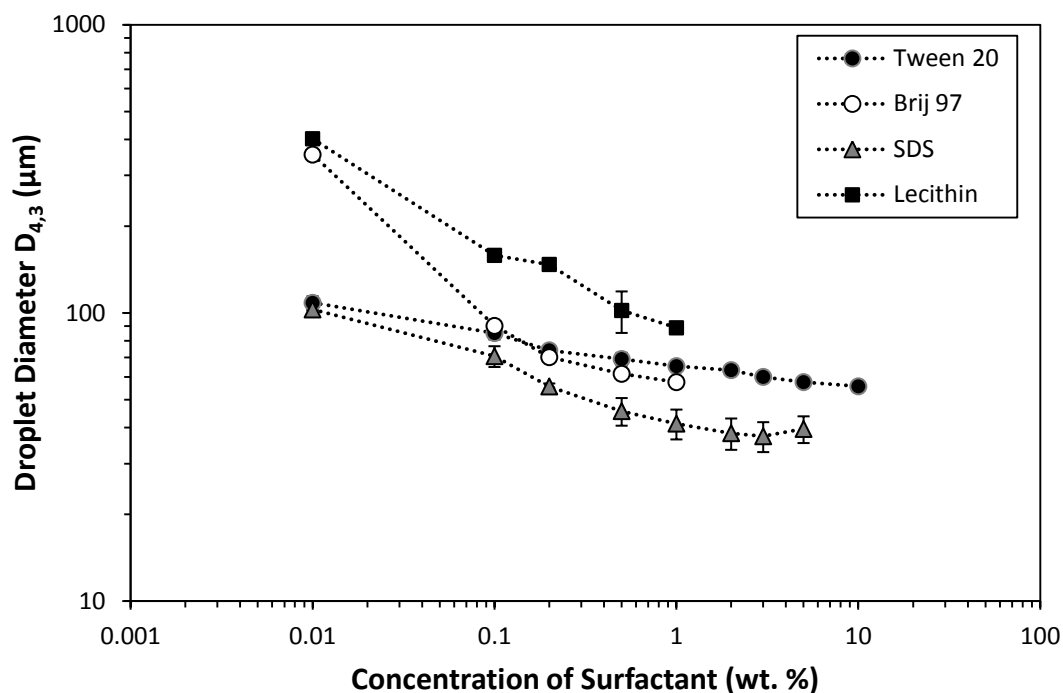


Fig. 5.2: The effect of surfactant concentration on the mean droplet size for different surfactant types positioned within the aqueous continuous phase. The emulsions are 10 vol. % sunflower oil-in-water. The transmembrane pressure is 0.5 bar and the shear rate is 5.98 s^{-1} . The dotted lines are to guide the eye across the data set. The error bars represent one standard deviation of a triplicate of experimental runs.

Table 5.1: Important physicochemical properties of the surfactants investigated.

Surfactant	HLB Value	Molecular Weight	CMC	
		(g mol^{-1})	(g L^{-1})	(wt. %)
Tween 20	16.9	1228	0.07	0.006
Brij 97	12.4	357	0.29	0.026
SDS	40	288	2.4	0.218
Hydrolysed Lecithin	5	678	0.61	0.055

It is clear that an increasing concentration of surfactant leads to a decrease in droplet diameter. Furthermore, the most significant variation in droplet size occurs at very low concentrations. For example, as the concentration of Tween 20 is increased from 0.01-0.1 wt. %, the droplet size reduces by 21.5% from 108 μm to 81.5 μm . Increasing the concentration further to 0.2 wt. % results in only a 12.8% decrease in size to 74.2 μm . This agrees with most findings in literature that the droplet size decreases with increasing surfactant concentration until the diameter becomes independent of the concentration (van der Graaf *et al.*, 2004; Christov *et al.*, 2008; Spyropoulos *et al.*, 2011). Using a higher surfactant concentration reduces the IFT much quicker and to a greater extent resulting in early droplet detachment (Lepercq-Bost *et al.*, 2008) Despite the presence of surface active SFO impurities, these would only have a minor effect on IFT considering surfactant is much more dominant in determining the IFT due to faster occupation of the interface. This is true even at very low concentrations as can be observed in Fig. 5.3. For example, 0.01 wt. % Brij 97 reduces the IFT to 5.4 mN m^{-1} which is much lower than without any surfactant.

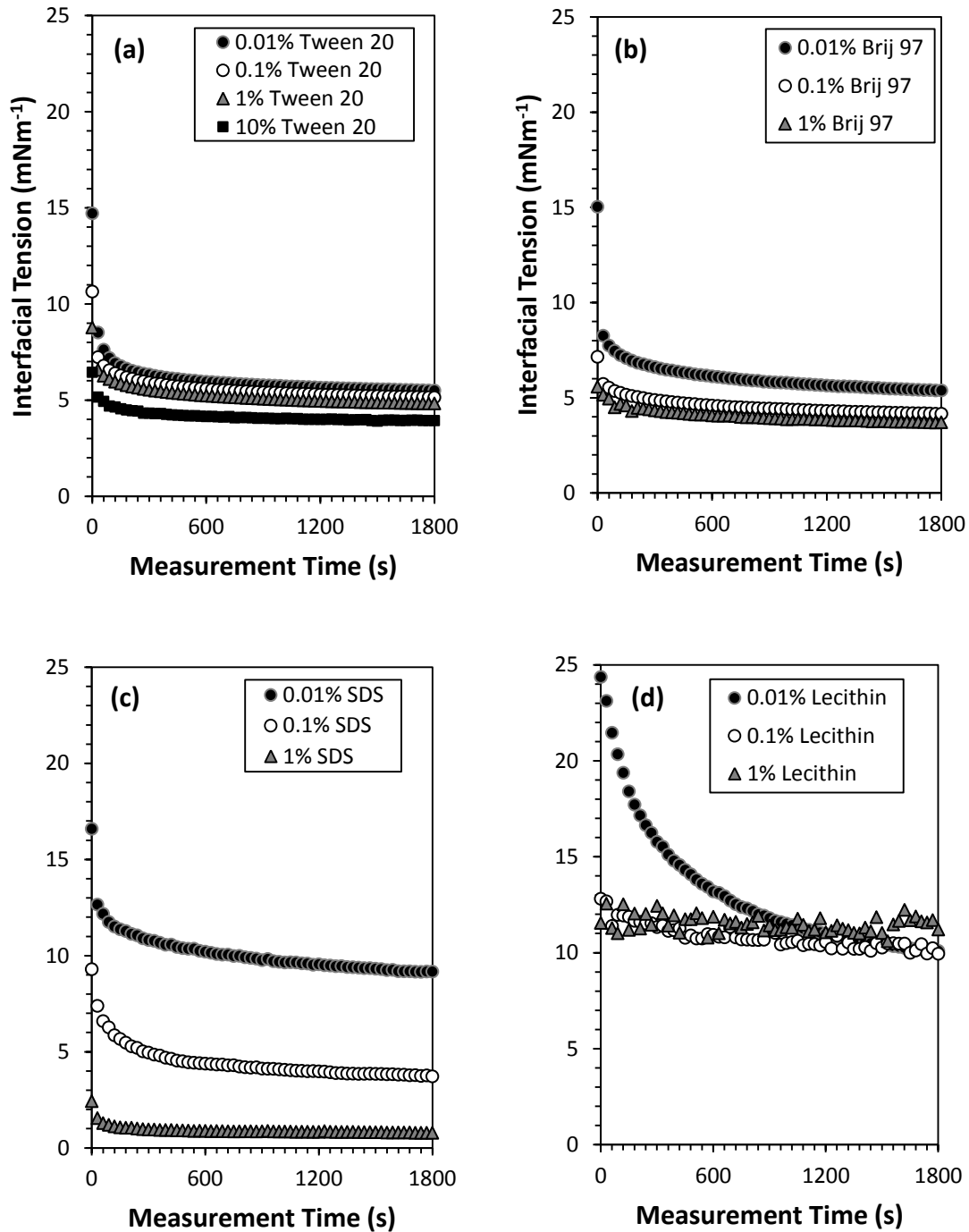


Fig. 5.3: Dynamic interfacial tension between sunflower oil and continuous phase containing variable concentration of surfactants: (a) Tween 20, (b) Brij 97, (c) SDS and (d) lecithin.

Focussing on properties of the emulsions produced (Fig. 5.1), very large droplets ($>100\ \mu\text{m}$) are formed at low concentrations ($<0.1\ \text{wt.}\ \%$) especially if the surfactant is not very effective (i.e. lecithin) or the concentration is below the CMC (i.e. Brij 97). It is highly likely this is due to a

combination of dominant retention forces (Vladisavljevic *et al.*, 2008) and coalescence at the membrane surface (Lepercq-Bost *et al.*, 2010) instigated by insufficient droplet coverage and/or slow rate of transport and subsequent adsorption. Coalescence has been observed in literature even in cases of high surfactant concentration e.g. 4 wt. % Tween 20 (Wagdare *et al.*, 2010) very effective surfactant systems e.g. 2 wt. % SDS (Lepercq-Bost *et al.*, 2010) or under optimised process conditions e.g. SDS just above the capillary pressure (Christov *et al.*, 2008). Under these circumstances, large poly-dispersed droplets were formed and droplets were observed to be partially 'sticking' to the surface of the membrane – this was also apparent within this experiment (as well as under low TMP and low shear rate conditions to be discussed further in sections 5.3 and 5.4).

Comparing the differences between surfactants, it can be seen from Fig. 5.2 that SDS produces the smallest droplet sizes (39.6-103 μm). The adsorption dynamics of SDS are much faster than most other surfactants (Schroder *et al.*, 1998; Wagdare *et al.*, 2010) particularly when operating with a concentration above the CMC (>0.22 wt. %) as shown in Fig. 5.3 (c). SDS is capable of reducing the IFT to a significant extent as characterised by its very high HLB number of 40 (Table 5.1). Furthermore, SDS is anionic so once adsorbed at the droplet interface, electrostatic repulsive forces between adjacent droplets will reduce the extent of coalescence. The negatively charged membrane surface will also repel droplet interfaces covered by SDS to perhaps additionally aid detachment. In contrast, systems using lecithin produced extremely large droplets (88.8-402 μm). Lecithin does not decrease IFT to as much as an extent as the other surfactants (low HLB value of 5) with equilibrium values above 10.0 mN m^{-1} (Fig. 5.3 [d]). Also, the rate of IFT reduction is very gradual since lecithin much first dissociate from vesicles (rather than micelles) formed in the bulk solution prior to adsorption at the forming droplet interface. This essentially lowers the effective concentration of free lecithin able to stabilise the droplet. Hence, this combination of factors consequently results in droplets requiring to grow to large diameters before experiencing sufficient detachment forces to overcome the higher retention forces. For Brij 97, a very large droplet size was

produced when operating below the CMC (354 μm at a concentration of 0.01 wt. %). Above the CMC of 0.03 wt. %, droplet sizes of between 57.5-90.1 μm were produced. Across the same concentration range for Tween 20 (0.1-1 wt. %), the droplet diameter varied between 65.4-85.1 μm . Brij 97 despite having a lower HLB value than Tween 20 (12.4 and 16.9 respectively), produced smaller droplets because its molecular weight is much lower. This means the Brij 97 molecules (357 g mol^{-1}) can move more freely throughout the bulk continuous phase compared to heavier Tween 20 molecules (1228 g mol^{-1}) which are hindered by hydrodynamic resistance forces (e.g. drag). Hence, Brij 97 can reduce the IFT faster (Fig. 5.3 [b]) and enable earlier droplet detachment compared to Tween 20 (Fig. 5.3 [a]).

5.3 Effect of Transmembrane Pressure with Surfactant Type

The TMP has been seen within the previous chapter to strongly influence both the droplet size produced but also the dispersed phase flux. If the TMP was too low and there was insufficient drag force, droplets were seen to be large due to coalescence. On the other hand, if the TMP was too high and the IFT was sufficiently low, again large droplets were produced of a poly-dispersed size distribution. Hence, the microstructure of the emulsion depends on the TMP but also the capability of the surfactant to reduce IFT and stabilise against coalescence. These two parameters therefore require studying in tandem to understand the time element of surfactant adsorption versus the interfacial expansion rate (as per Rayner *et al.*, 2004). A variety of low (0.1 wt. %) and high (1 wt. %) surfactant concentrations were investigated. A TMP range between 0.2 and 1.5 bar was used whilst operating at a shear rate of 5.98 s^{-1} .

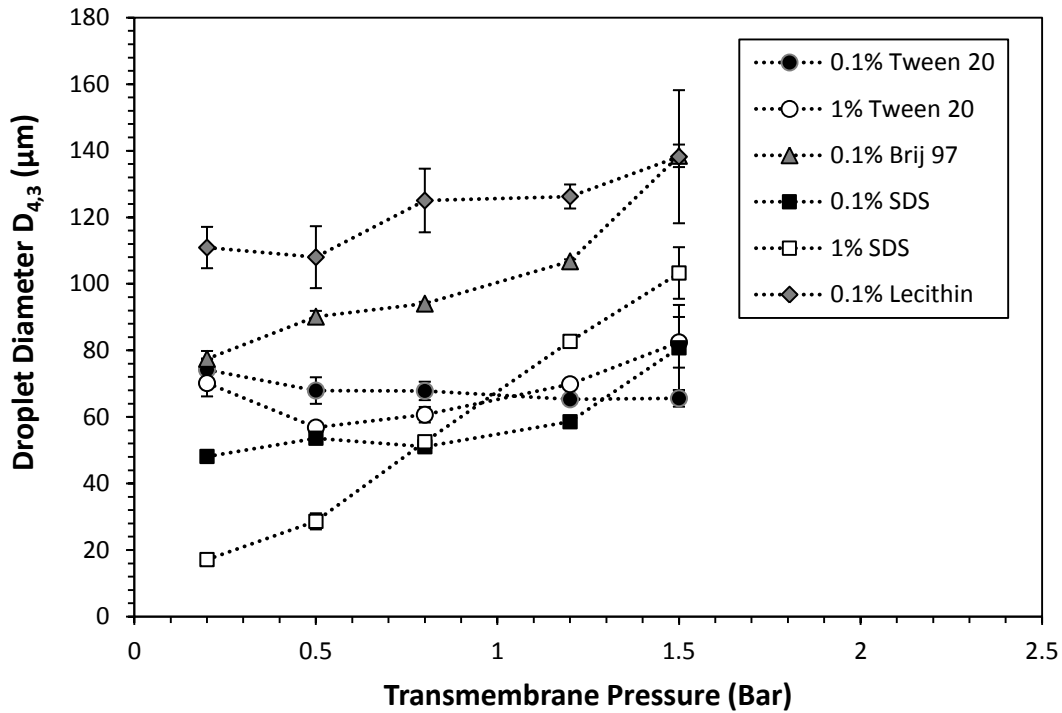


Fig. 5.4: The influence of transmembrane pressure on the mean droplet size for different surfactant types and concentrations. A shear rate of 5.98 s^{-1} is applied corresponding to a rotational speed of 1000 RPM and an annular gap width of 25 mm. The dotted lines are drawn to guide the eye across the data set. The error bars represent one standard deviation of a triplicate of experimental runs.

Table 5.2: Equilibrium interfacial tension values for systems investigated.

Low Concentration (0.1 wt. %)	Equilibrium IFT w/ SFO (mN m^{-1})	High Concentration (1 wt. %)	Equilibrium IFT w/ SFO (mN m^{-1})
Tween 20	5.1 ± 0.1	Tween 20	4.8 ± 0.1
Brij 97	4.2 ± 0.1	SDS	0.8 ± 0.1
SDS	3.7 ± 0.5		
Lecithin	10.0 ± 1.0		

Fig. 5.4 shows the effect of TMP on the resultant droplet diameter for a variety of surfactant types and concentrations in which the surfactant is dissolved within the continuous phase. What is clear is that there is a variance in the behaviour of the trend across the TMP range depending on both the type of surfactant used and whether a low or high concentration is used. For just the low concentration systems, Tween 20 exhibits a decrease across the pressure range investigated (from

74.2 μm to 65.6 μm). The systems containing Brij 97, SDS and lecithin follow a steady increase in droplet size with increasing pressure; this is expected in the absence of coalescence with diffusion being fast relative to the rate of interfacial expansion (van der Graaf *et al.*, 2004). Additionally, more mass is transferred to the droplet during the detachment stage (Peng and Williams, 1998). Furthermore, droplets detach in a period of higher IFT if the droplet forms very quickly (e.g. under high TMP). What separates the behaviour of Tween 20 from the other surfactants can be explained again by considering the physicochemical properties associated with each of the surfactants used (as shown in the previous section in Table 5.1). It might be expected that Brij 97 and Tween 20 exhibit slightly different behaviour across the pressure range as Brij 97 molecules can adsorb much faster than Tween 20 (Fig. 5.3) to prevent coalescence (hence only an increase in size with TMP). The surface coverage of the surfactant needs to be quicker than the rate of interfacial expansion in order to prevent coalescence upon droplet-droplet interactions. On the other hand, Brij 97 is a less effective surfactant (compared to Tween 20) at stabilising O/W emulsions as indicated by the HLB value, droplet diameters between 77.5 μm to 139 μm are formed which are larger than those observed with Tween 20. SDS being an anionic surfactant of very high HLB value indicates it is a very effective surfactant for stabilising forming oil droplets at the membrane surface and enabling detachment. A combination of electrostatic repulsive forces between adjacent forming droplets (that have adsorbed SDS molecules at their interface) and low IFT values (Table 5.2) enabling droplets to detach earlier during formation virtually eliminate coalescence events and produce the smallest droplets (between 48.1 μm to 58.6 μm \geq 1.2 bar). Lecithin is a zwitterionic phospholipid with a low HLB value and hence is more effective at stabilising W/O emulsions. A unique characteristic of lecithin is its ability to form an elastic-like interface (Dimitrov *et al.*, 1978) which may in turn prevent coalescence. The largest droplet diameters are formed (111 μm to 138 μm) since lecithin does not reduce the IFT to as great an extent as the other surfactants. Furthermore, the rate of decrease is slow since the lecithin must first dissociate from vesicles formed in the bulk solution prior to adsorption at the forming droplet interface. This essentially lowers the effective

concentration of free lecithin to stabilise the droplet since vesicle dissociation is the rate limiting step. Hence this combination of factors imply that droplets have to grow to much larger sizes in order to experience sufficient detachment force to overcome the higher retention forces (Spyropoulos *et al.*, 2014). As a general observation, the droplet size average across the data set corresponds with the HLB value of the surfactant with higher values leading to smaller droplets. This agrees with findings by a number of other authors (Ban *et al.*, 1994; Spyropoulos *et al.*, 2011; Pawlik and Norton, 2013; van der Graaf *et al.*, 2004; Kukizaki, 2009).

Focussing on the high surfactant concentration systems, slightly different behaviour is exhibited by the Tween 20 and SDS systems than observed at 0.1 wt. %. It is expected that increasing surfactant concentration generally enables formation of smaller droplet sizes since there are more surfactant molecules available for adsorption across a greater dispersed phase surface area and so the IFT is lower (Schroder *et al.*, 1998). For example, at 0.5 bar the droplet diameters of 0.1 wt. % and 1 wt. % of Tween 20 are 67.9 μm and 56.8 μm respectively. Similarly for SDS, these values are 53.6 μm and 28.6 μm respectively. However, there is a stark contrast in the behaviour of these systems across the pressure range. Tween 20 demonstrates a decrease followed by a plateau and then a slight increase which was not observed at the low concentration. The plateau region (referred to previously as the size-stable zone) is attributed to droplet formation due to a spontaneous transformation in its shape in order to lower its Gibbs free energy (Sugiura *et al.*, 2001; Rayner *et al.*, 2004). Such a phenomenon is more prevalent for high(er) IFT system since they are more thermodynamically unstable. Therefore, with an increase in surfactant concentration to 1 wt. % and hence lower IFT, the region of which this phenomenon potentially occurs becomes much narrower and so an eventual increase in droplet size upon further increase in TMP is observed. In the case of SDS, beyond 0.5 bar the droplet size increases extremely rapidly from 28.6 μm to 103 μm . Beyond 1.2 bar, the droplet sizes produced are much larger than those formed at low concentration. It is therefore expected that there is a change in the droplet formation mechanism from dripping to jetting which is inherent to high pressures and low IFT systems (Sugiura *et al.*, 2002). This suggests

that whilst lowering the IFT is beneficial if one wanted to produce smaller droplets, it limits the ability to operate at higher throughputs of dispersed phase whilst still forming droplets in a controlled way. Across all experiments conducted, the dispersed phase flux was unaffected by the surfactant system used since the TMP was well above the minimum capillary pressure.

5.4 Effect of Shear Rate with Surfactant Type

The shear rate applied can impact on the droplet formation process in two ways during RME. Operating with a range of rotational speeds and/or annular gap widths alters the drag and centripetal force, and therefore the initial size at the end of the droplet growth stage. Additionally, the hydrodynamic behaviour of the continuous phase induced by these process parameters can alter the transport mechanisms of the surfactant. For example, if the rotational speed is high, this may aid movement of surfactant molecules throughout the bulk phase by advection. The study of shear rate against surfactant type is essentially considering the ratio of inertial forces to capillary forces i.e. altering the point of droplet imbalance.

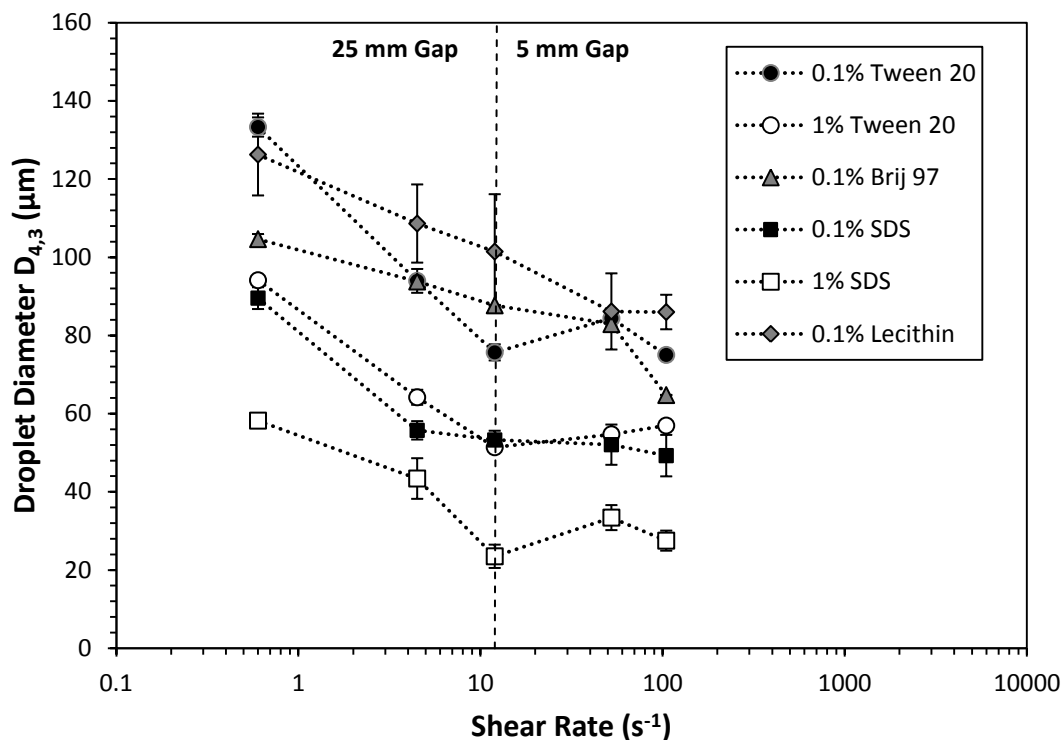


Fig 5.5: The influence of shear rate on the mean droplet size for different surfactant types and concentrations. A transmembrane pressure of 0.5 bar is applied. The dotted lines are to guide the eye across the data set. The error bars represent one standard deviation of a triplicate of experimental runs.

The effect of altering the shear rate at the membrane surface between $0.6\text{--}104.7\text{ s}^{-1}$ (whilst applying a TMP of 0.5 bar) for different surfactant systems is shown in Fig. 5.5. Generally, increasing the shear rate through higher rotational speeds and/or narrower annular gap widths leads to formation of smaller droplet sizes. The drag force is greater so droplets detach earlier from the membrane surface. This will also occur if the IFT can be reduced to low values quickly so the magnitude of the IFT force is smaller e.g. when using SDS (Kobayashi *et al.*, 2002). It is therefore unsurprising that the 1 wt. % SDS system (which has the lowest IFT) produces the smallest droplet sizes between $27.5\text{ }\mu\text{m}$ and $58.2\text{ }\mu\text{m}$ followed by 0.1 wt. % SDS ($49.3\text{ }\mu\text{m}$ to $89.5\text{ }\mu\text{m}$) and 1 wt. % Tween 20 ($57.0\text{ }\mu\text{m}$ to $94.1\text{ }\mu\text{m}$). Furthermore, with higher rotational speeds which subsequently increase the Reynolds and Taylor numbers of the continuous phase, the transport of surfactant towards the interface is aided by a combination of diffusion and convection. As observed with the

effect of TMP in Fig. 5.4, lecithin since it has a low HLB value produces the largest droplet sizes. The significant error bars when using lecithin also indicates droplet formation is quite erratic perhaps due to variant effects that the shear has on deforming the elastic interface which may subsequently promote forms of droplet-droplet interactions (Lepercq-Bost *et al.*, 2010; Dragosavac *et al.*, 2008; Egidi *et al.*, 2008) or alter the velocity profile locally to the membrane surface (Timgren *et al.*, 2009). Overall, the lower the IFT value, the less influence shear has on droplet diameter due to the relative ease droplets can detach even at low shear rates agreeing with findings by Lepercq-Bost *et al.* (2008).

5.5 Effect of Particle Type/Concentration

Emulsion droplet interfaces can also be stabilised by solid particles in what is termed as a 'Pickering' emulsion. This is an area of growing interest because the use of particles provides greater stability against coalescence either during production or long-term storage. For instance, Midmore (1998) produced very concentrated paraffin oil-in-water emulsions up to 81 vol. % stabilised by Ludox silica. The droplet size of the emulsion did not change over a 3 month period. Particles irreversibly adsorb to form a very strong physical barrier that prevents droplet interfaces coalescing (once adsorbed) due to steric stabilisation mechanism. There have also been advancements in recent years in the manufacture of nanoparticles, which are highly suitable for emulsion stabilisation. Ideally, the particles used need to be at least an order of magnitude smaller than the desired droplet size range in order to pack effectively around the oil/water interface. For example, particles of 10-100 nm would be needed to stabilise a droplet of approximately 1 μm .

Whilst Pickering emulsions have been extensively investigated by a large number of researchers (Binks and Lumsdon, 1999; Guillot *et al.*, 2009; Pichot *et al.*, 2012), there are very limited studies of their use during membrane emulsification (and more specifically RME). Conventionally, high energy mechanical processes are used to provide the particles sufficient energy to adsorb (Manga *et al.*, 2012) since this energy is much higher than for surfactant systems. In this instance,

the low energy RME process is investigated. Varieties of colloidal silica particles were chosen since they were readily available and reasonably homogeneous in size (≈ 12 nm). However, operating at a pH of 2.0 (the iso-electric point of silica) enabled different degrees of flocculation (due to attractive van der Waals forces) and hence varied the size of the aggregates. Therefore, it is a two stage mechanism as particles flocculate within the bulk phase prior to adsorption at the interface as multilayers of particles (Hassander *et al.*, 1989). Aerosil silica was measured to be around 190 nm whilst Ludox silica was smaller at approximately 21 nm. The size of the flocs determines the energy of adsorption (Eq. 2.5) with larger aggregates requiring more energy to adsorb which prolongs the adsorption time. Furthermore, the ability of the particles to pack effectively around a spherical interface is governed by the ratio of the droplet and the particle used. For example, smaller particles can potentially pack more effectively around a given droplet diameter with less void space between adjacent particles.

The effect of increasing concentration of silica for Aerosil (between 0.01-2 wt. %) and Ludox (0.1-30 wt. %) to stabilise a dispersed phase volume fraction of 10 vol. % of SFO is shown in Fig. 5.6. The processing conditions were a TMP of 0.5 bar and a shear rate of 5.98 s^{-1} . The pH of the continuous phase was 2.0 so as mentioned the aggregates of Aerosil and Ludox were 190 nm and 21 nm respectively.

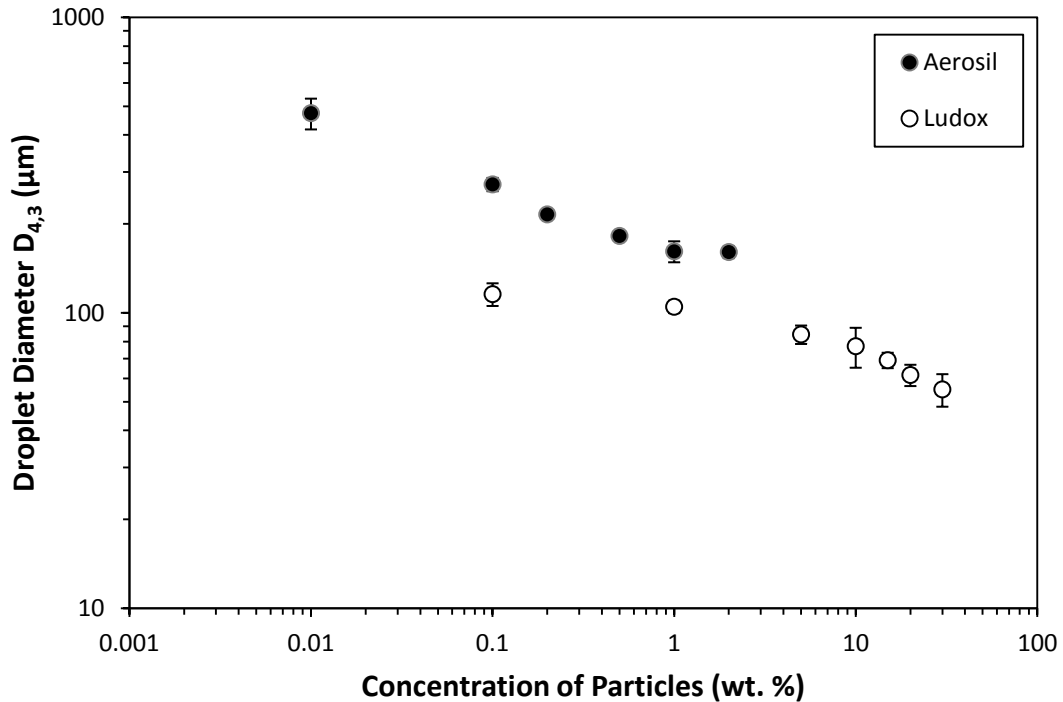


Fig. 5.6: The effect of particle concentration on the mean droplet size for different silica systems positioned within the aqueous continuous phase. The emulsions are 10 vol. % sunflower oil-in-water. The transmembrane pressure is 0.5 bar and the shear rate is 5.98 s^{-1} . The error bars represent one standard deviation of a triplicate of experimental runs

There are two clear observations that can be made. Firstly, increasing the concentration of particles results in the production of smaller droplet sizes. This is expected because with more particles available within the continuous phase, the probability of collisions that lead to the particle adsorbing at the forming droplet interface increases. This reduces the extent of droplet coalescence at the membrane surface as there is less un-stabilised interface. Secondly, the droplets stabilised by Aerosil are significantly larger than those stabilised by Ludox. For example, at 0.1 wt. % the droplet diameter for Aerosil and Ludox stabilised emulsions were 272 and 116 μm respectively. At 1 wt. %, these sizes reduced to 162 and 105 μm . It is important that the adsorption kinetics of the particle is fast to prevent coalescence (Manga *et al.*, 2012). Aerosil aggregates are an order of magnitude larger than Ludox so both the movement throughout the continuous phase (due to drag) and adsorption (high energy required) are slow processes. Furthermore, the Aerosil cannot pack as effectively around the interface if the droplet curvature is too great. These reasons enhance the likelihood of

coalescence when using Aerosil. Studying the IFT data for Aerosil and Ludox (Fig. 5.7), the IFT is much higher than for surfactant systems and very close to the IFT between SFO and water without surfactant (Fig. 5.2).

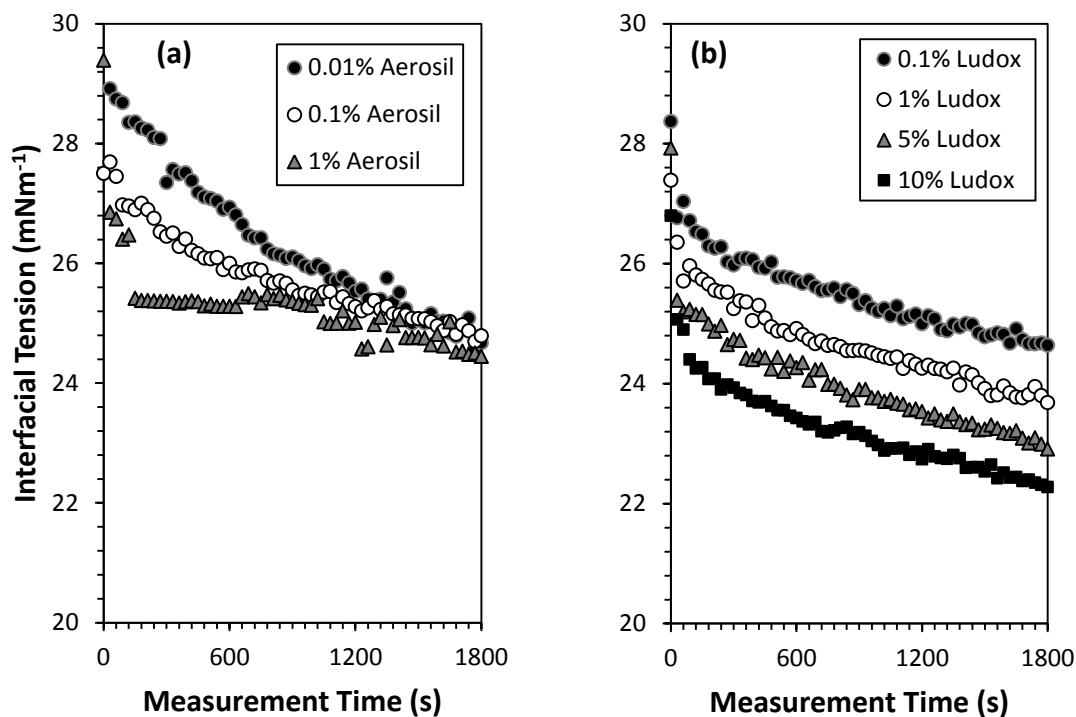


Fig. 5.7: Dynamic interfacial tension between sunflower oil and continuous phase containing variable concentration of silica particles: (a) Aerosil (b) Ludox.

The high IFT values (and hence the retention force) would explain why droplets are significantly larger than surfactant systems under corresponding process conditions (Fig. 5.2). For example, the equilibrium IFT values of 1 wt. % Tween 20 and 1 wt. % Aerosil are 4.8 mN m⁻¹ and 24.4 mN m⁻¹ respectively; a ratio of 5.1. However, the droplet size produced by these systems was 65.4 μm and 162 μm; a ratio of 2.5. This therefore suggests that the difference is not purely due to IFT differences but behaviour of the interface. Tween 20 forms an interface only a couple of nanometres in thickness which is a lower energy barrier against coalescence. The Ludox systems demonstrate a slightly lower IFT due to surface active materials added by the manufacturer within the concentrated

Ludox solution that are used to keep the silica dispersed during storage. Certainly for the Aerosil systems, a decrease in IFT can be observed suggesting that particles do adsorb at the oil/water interface (albeit very slowly), agreeing with some authors (Kutuzov *et al.*, 2007; Du *et al.*, 2010; Kim *et al.*, 2010; Manga *et al.*, 2012) but disagreeing with others (Vignati *et al.*, 2003; Drelich *et al.*, 2010; Pichot *et al.*, 2012). The exact effect that particles have on the IFT is a contentious issue within literature. Brian and Chen (1987) argued that adsorption of particulate flocs would be unlikely to alter IFT since this process would not interfere with oil/water interactions at a molecular level. In contrast, Levine *et al.* (1989) predicted as part of a theoretical model that the IFT would decrease as the contact angle for the particle approaches 90° (for which the particle is wetted by both oil/water phases). However, Pichot *et al.* (2012) measured the contact angle for Aerosil silica at a pH of 2.0 to be very close to 90° so therefore the IFT data in Fig. 5.7 validates the model proposed by Levine *et al.* (1989).

5.6 Effect of Transmembrane Pressure with Particle Type

The rate that particles collide with and subsequently adsorb at the droplet interface plays an important role as seen in the previous section. However, another key consideration is the rate of interfacial expansion of the droplet. This is manipulated by altering the TMP to control the dispersed phase flux. It is well established that high TMPs lead to rapid expansion of the interface and hence shorter droplet formation times. This may have consequences for the emulsification process if particle adsorption is too slow so this therefore requires investigation. The TMP was varied between 0.2 and 1.5 bar for both a low and high concentration of particles. The shear rate was constant at 5.98 s⁻¹.

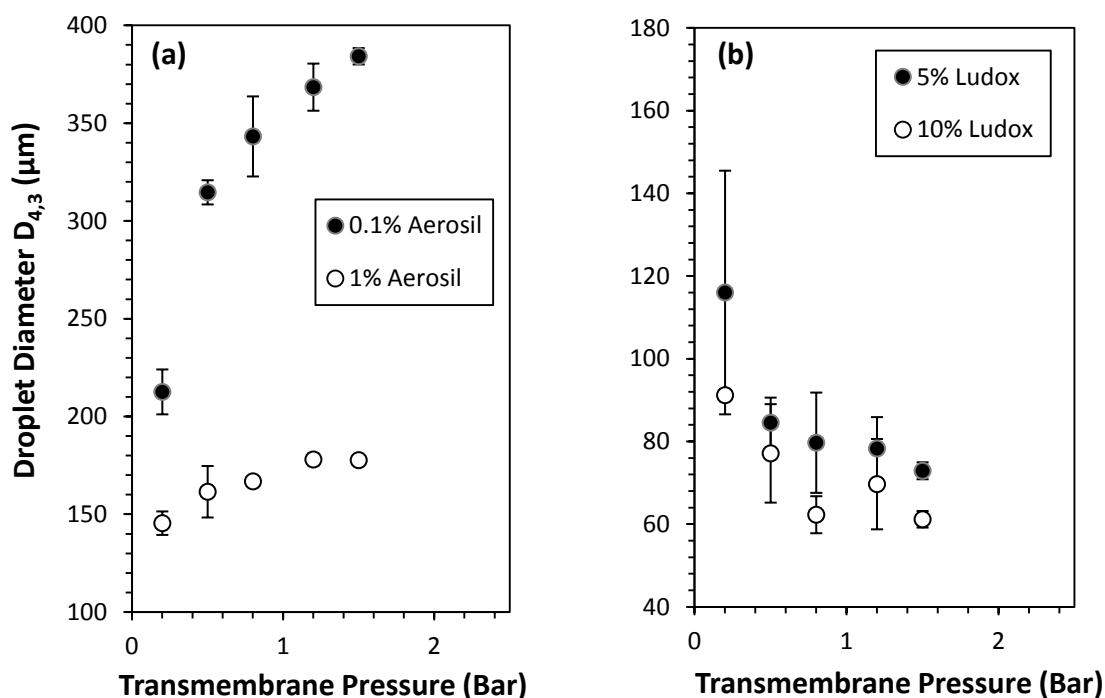


Fig. 5.8: The influence of transmembrane pressure on the mean droplet size for (a) Aerosil and (b) Ludox silica at a low and high concentration of particles. A shear rate of 5.98 s^{-1} is applied corresponding to a rotational speed of 1000 RPM and an annular gap width of 25 mm. The error bars represent one standard deviation of a triplicate of experimental runs.

Fig. 5.8 shows the relationship between TMP and droplet size differs depending on whether Aerosil or Ludox silica is used. Focussing on Fig. 5.8 (a), much larger droplets were produced if the TMP was high or the concentration of particles was low. For 0.1 wt. % Aerosil, the droplet diameter increased by 44.7% across the TMP range from 213 μm to 384 μm . For 1 wt. %, the increase was to less of an extent (18.2%) from 145 μm to 178 μm . With a higher concentration of particles, the likelihood of particles adsorbing to stabilise the droplet interface is much greater. Furthermore, the system can stabilise smaller droplets even if the relative expansion is high (i.e. at 1.5 bar). Unlike in the case of Tween 20 as shown in section 5.3, coalescence is negated to an extent by the creation of a thick (>190 nm), rigid interface of particles. A decrease in droplet diameter is not observed. In contrast, Fig. 5.8 (b) shows the droplet size to reduce with increasing TMP. Again, the high concentration of particles produced the smallest droplet diameters. At 5 wt. % Ludox, the droplet

size decreases by 37.2% from 116 μm to 72.9 μm and for 10 wt. % Ludox, the size decrease is 32.9% (from 91.2 μm to 61.2 μm). The probability of particles colliding with the droplet interface is much higher in the case of Ludox as there are more particles by at least three orders of magnitude compared to the Aerosil systems. Additionally, these Ludox particles diffuse faster and require less energy to adsorb since their radius is an order of magnitude smaller (Eq. 2.5) so the collisions are more likely to be successful. This therefore suggests that the rate of particle adsorption is likely to be in excess to the rate of interfacial expansion. The formation of a thinner interface with Ludox silica aggregates (≈ 21 nm) may not be able to provide a significant steric stabilisation mechanism to prevent coalescence. Less energy is required to displace the particles from the interface compared to Aerosil. As a consequence, higher pressures reduce the time that droplets potentially spend in contact with adjacent forming droplets to minimise coalescence. Overall, the Ludox silica produced the smallest droplet sizes because of its availability for adsorption (and hence coverage of the interface) alongside lower IFT values as shown in Fig. 5.7.

5.7 Effect of Shear Rate with Particle Type

Modification of the shear rate (by changing the rotational speed of the membrane and annular gap width) can potentially play an even more critical role when operating RME to produce Pickering emulsions. The frequency and energy of particle collisions with the forming droplet interface is not only governed by the particle size or concentration but by the hydrodynamic behaviour of the continuous phase. For example, it would be expected that under turbulent flow conditions, particles would move throughout the continuous phase with higher velocity and hence greater kinetic energy. For surfactant systems, these are small amphiphilic molecules (rather than large particle aggregates) that are attracted to the interface and so the transport of surfactant is more reliant on diffusion than convection. The hydrodynamics of RME when using particles therefore plays a dual role in providing particles and energy for adsorption but also inducing

detachment forces such as drag. The shear rate ranged between 0.6-104.7 s^{-1} whilst the TMP was kept constant at 0.5 bar.

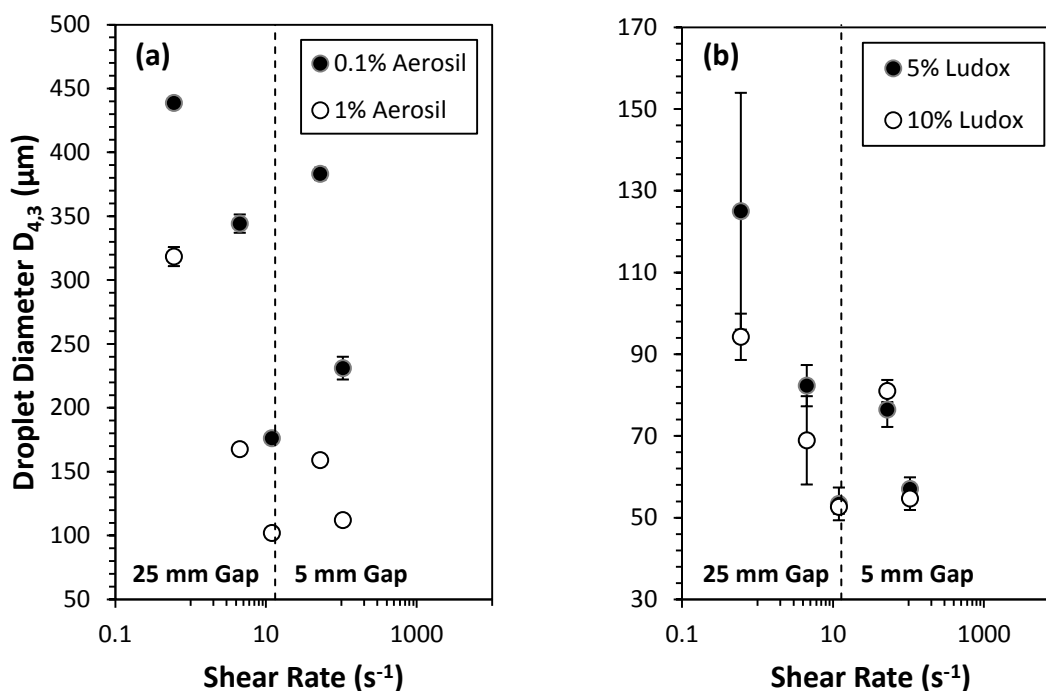


Fig 5.9: The influence of shear rate on the mean droplet size for (a) Aerosil and (b) Ludox silica at low and high concentrations of particles. A transmembrane pressure of 0.5 bar is applied. The error bars represent one standard deviation of a triplicate of experimental runs.

There are two interesting observations that can be made from Fig. 5.9. Firstly, for a fixed annular gap width, increasing shear through higher rotational speeds led to the formation of smaller droplet diameters. For example, 1 wt. % Aerosil produced 439 μm at 100 RPM (shear rate = 0.6 s^{-1}) and 176 μm at 2000 RPM (shear rate = 12.0 s^{-1}). This is due to the higher drag force (Manga *et al.*, 2012) alongside faster movement of silica particles within the continuous phase induced by the fluid flow behaviour. Secondly, the droplet size is seen to suddenly increase as the annular gap width is reduced to impart higher shear rates; this was not the case for surfactant systems as seen in Fig. 5.5 previously. With the reduction of the annular gap width, the Reynolds and Taylor numbers of the systems are lower despite the higher shear rate at the membrane surface. As a consequence, the flow is less chaotic and so particles collide less frequently and energetically with the forming

interface. Coalescence is more likely with insufficient coverage and so the sudden increase in size occurs.

5.8 Surfactant/Particle Mixtures

There have been very few studies on the stabilisation of emulsion droplets using both surfactants and particles. The key function of the surfactant is to lower the IFT quickly whilst for the particle, its main purpose is to provide stability against coalescence (Whitby *et al.*, 2008; Midmore, 1998). Therefore, it seems logical that by positioning both surfactants and particles at the droplet interface, this may offer both these functions for the emulsion system. This was observed to be the case within the work of Pichot *et al.* (2009, 2010) for high shear processing. For RME; a process that can be susceptible to coalescence at the membrane surface, a combination of surfactants and particles may be capable of preventing this phenomena occurring.

A high and low concentration of Aerosil and Ludox silica particles within the continuous phase was combined with varying quantity of Tween 20 (also within the continuous phase). This essentially altered the ratio between the two components. The processing conditions were fixed at a TMP of 0.5 bar and a shear rate of 5.98 s^{-1} . The emulsion droplet sizes as a function of Tween 20 concentration (0.01-2 wt. %) are shown in Fig. 5.10.

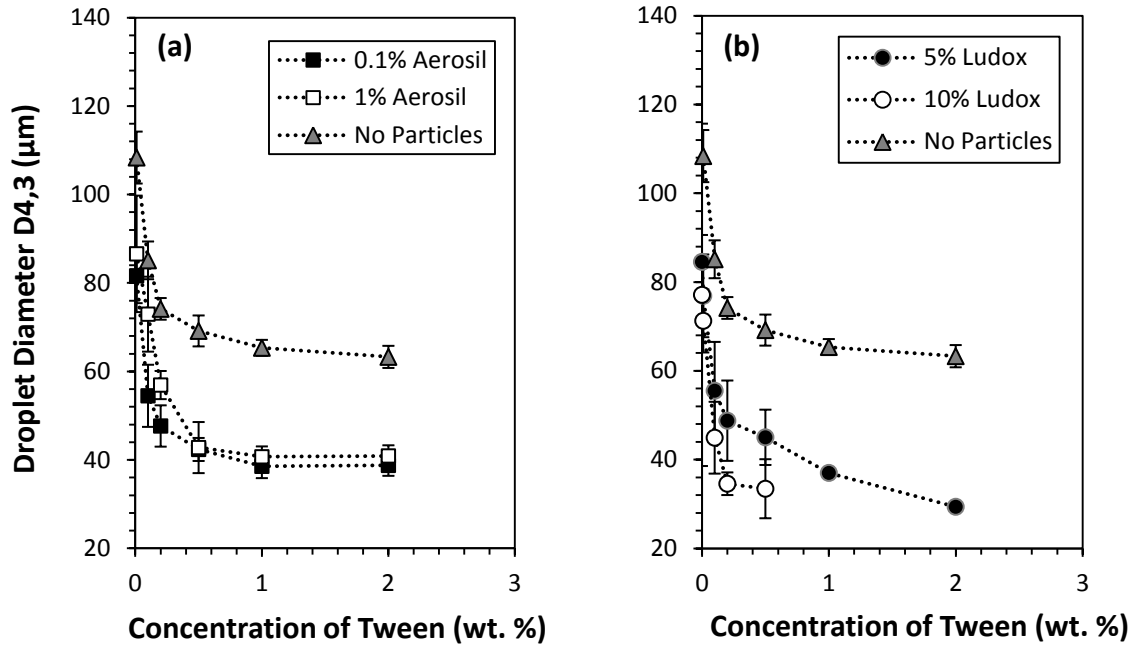


Fig. 5.10: The effect of Tween 20 concentration on the mean droplet size for (a) Aerosil and (b) Ludox silica at a low and high concentration of particles. The transmembrane pressure is 0.5 bar. A shear rate of 5.98 s^{-1} is applied corresponding to a rotational speed of 1000 RPM and an annular gap width of 25 mm. The pH of the continuous phase is 2.0. The error bars represent one standard deviation of a triplicate of experimental runs.

It is evident that increasing the concentration of Tween 20 within the system results in a decrease of droplet diameter. This coincides with findings discussed within section 5.1 that higher surfactant concentration decreases the IFT at a faster rate, resulting in earlier droplet detachment from the membrane surface. In the absence of any silica particles at all, droplets stabilised solely with Tween 20 were generally much larger than in their presence. As the concentration of Tween 20 increases from 0.01 wt. % to 2 wt. %, the droplet diameter decreases by 41.6% from $108 \mu\text{m}$ to $63.3 \mu\text{m}$. In the presence of 1 wt. % Aerosil for example, the droplet size decreases to a much greater extent (by 74.7% from $162 \mu\text{m}$ to $40.9 \mu\text{m}$). At very low concentrations of Tween 20 ($\approx 0.01 \text{ wt. \%}$), the droplet interface is primarily stabilised by the particles which impart higher IFT values and hence droplets are larger than with just Tween 20. With increasing concentration of surfactant, there is a threshold of which the interface is stabilised by both surfactants and particles which can impart greater stability against coalescence than Tween 20 independently. As a consequence, the droplet sizes are smaller. The proposed mechanism by Pichot *et al.*, (2010) is competitive adsorption of both

surfactant and particles. The surfactant generally adsorbs first to stabilise the initial interface (since it is amphiphilic, smaller and therefore more mobile). Following this, the particle then adsorbs more slowly either at exposed or 'naked' areas of the droplet interface but also to the adsorbed surfactant. At very high concentrations of surfactant, it is likely the surfactant will dominate with the particle unable to adsorb quickly enough. However, the droplet diameter does not tend towards the sizes produced by the surfactant only system even if this is the case. It is also probable some of the surfactant adsorbs to the surface of the particles and is therefore unavailable for adsorption to the droplet interface; this would be noticeable at low surfactant concentration where the proportion 'lost' to particle surfaces would be high (Pichot *et al.*, 2012). The IFT data shown in Fig. 5.11 (using 5 wt. % Ludox as an example) supports these ideas. It can be seen that the IFT values of 0.01 wt. % Tween 20 in the presence of particles are much higher than in their absence. The Ludox can compete with the rate of the adsorption of the Tween 20 (and so the IFT curve is closer to the 5 wt. % Ludox data without surfactant). Additionally, the 'effective' concentration of Tween 20 in the continuous phase may be lower due to adsorption to the particle surface resulting in a greater IFT value. At a much higher concentration of surfactant (1 wt. %), the Ludox particles cannot compete with the rate of surfactant adsorption. Consequently, the IFT values of 1 wt. % Tween 20 irrespective of the presence or absence of particles are almost the same since the effect of surfactant adsorbing to the particle surface is negligible (compared to that in the continuous phase). In the case of Aerosil silica which is much larger (and hence has a lower surface area), the presence of surfactant dominates adsorption to the droplet interface. Differences in IFT with or without particles are less pronounced since there is less surface area that may be coated by the Tween 20.

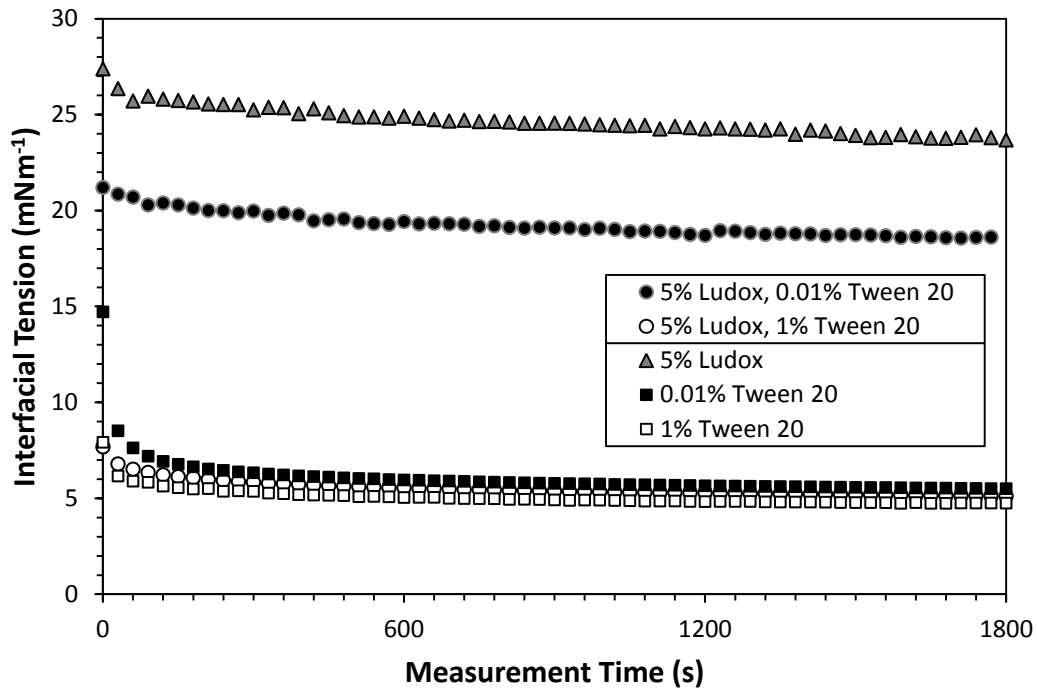


Fig. 5.11: Dynamic interfacial tension between sunflower oil and continuous phase containing either Ludox (particles), Tween 20 (surfactant) or a combination of the two. The pH was 2.0.

5.9 Effect of Surfactant Positioning

Within sections 5.1 to 5.3 in which the surfactant was dissolved within the continuous phase, a wide range of droplet sizes were produced. Considering just the non-ionic surfactants (Tween 20 and Brij 97), the droplet size ranged from between 51.4 μm to 354 μm . Given the pore diameter of the SPG membrane was 6.1 μm , this means the droplet size to pore size ratio varied between 8.4 to 58.1, which is at the upper end (and beyond) of the ratio values suggested by other authors (Joscelyne and Tragardh, 2000; Charcosset, 2009). Since the hydrodynamics of RME are generally quite mild by comparison to the XME setup, the transport of surfactant to the forming droplet interface relies primarily on diffusion (and to a lesser extent convection). It can therefore be concluded that with the surfactant in the continuous phase, the transport and subsequent adsorption of surfactant is too slow and thus coalescence to some extent occurs in most cases. This is supported by observations within the work of Wagdare *et al.* (2010) in which 4 wt. % Tween 20

and 1 wt. % SDS were unable to single-handedly prevent coalescence of SFO droplets produced from a silicon nitride membrane. For SDS, the surfactant is able to stabilise droplet interfaces more effectively, but is prone to jetting except under low TMP conditions where the pore fluid velocity is minimised (Fig. 5.4). This raises two fundamentally important questions. Firstly, 'how can small droplets be produced quickly and in a controlled manner?' and similarly 'how can rapid adsorption of surfactant be ensured to minimise droplet coalescence in this process?'

Interestingly, a recent article by Gassin *et al.* (2013) considered the effects of the transfer of amphiphilic molecules across an O/W interface on the IFT between the two phases. They supported earlier findings (Ferrari *et al.*, 1997; Ligierrri *et al.*, 1997) that the IFT of a system could decrease below the equilibrium value at least in the initial stages depending on the partition coefficient of the surfactant and the kinetic rate to achieve adsorption equilibrium. This approach relies on surfactants that can be soluble in both aqueous and organic phases. Therefore, the use of non-ionic surfactants such as Tween 20 and Brij 97 and the zwitterionic surfactant lecithin are facilitated whilst SDS is excluded since it is insoluble in oil. It was hypothesised that by allowing surfactant to diffuse through a forming droplet interface during RME, this would cause earlier detachment of droplets due to lower than expected IFT values whilst simultaneously limiting coalescence by enhancing the rate of adsorption. Thus, the process would be operated much more efficiently.

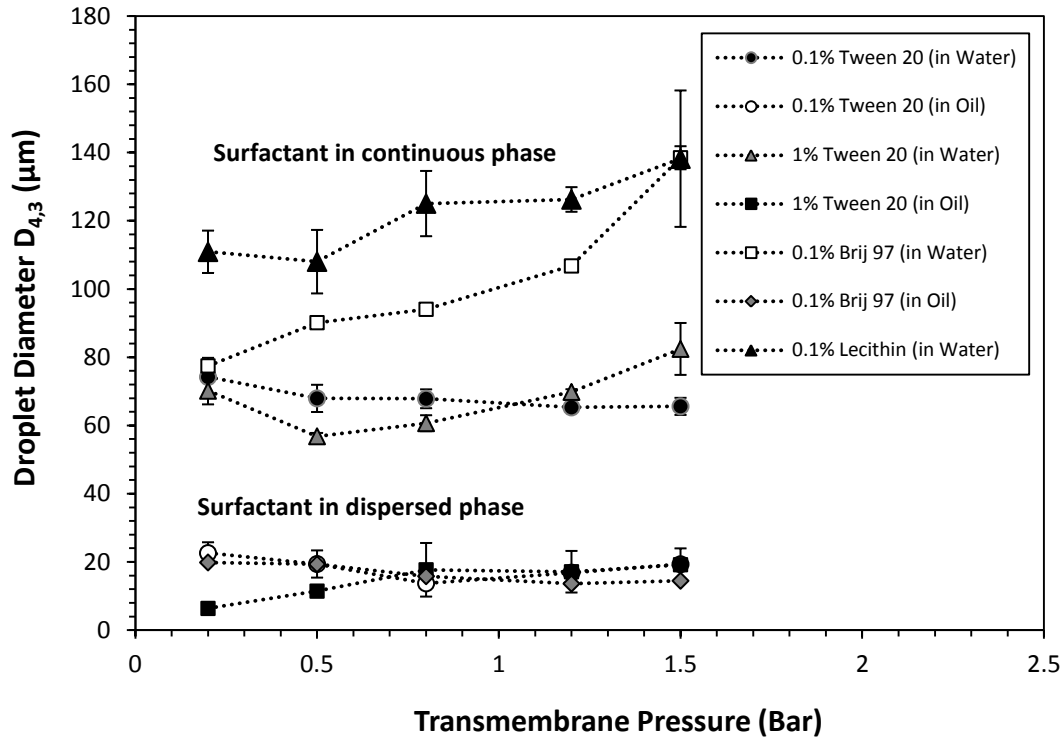


Fig. 5.12: The influence of transmembrane pressure on the mean droplet size for different surfactant positions. A shear rate of 5.98 s^{-1} is applied corresponding to a rotational speed of 1000 RPM and an annular gap width of 25 mm. The dotted lines are drawn to guide the eye across the data set. The error bars represent one standard deviation of a triplicate of experimental runs.

What can be observed in Fig. 5.12 are significant differences in the droplet size depending on the positioning of the surfactant. For example, emulsions formed by using 0.1 wt. % Tween 20 and Brij 97 positioned within the oil phase (o) are at least 3 times smaller than those formed with surfactant within the conventional aqueous phase for the same formulation/processing conditions. In this case, the droplet size to pore size ratio is much lower than previously observed, between 2.2 and 3.7. With 1 wt. % Tween 20 (o) and 0.2 bar TMP, a ratio as low as 1.1 is achieved. Furthermore, 0.1 wt. % Tween 20 (o) produces smaller droplets than a higher concentration of surfactant (1 wt. %) within the continuous phase (w). These two surfactants preferentially move towards being within the water phase and so by diffusing out of the oil droplet to move into an aqueous environment, the IFT is seen to drop below equilibrium as shown by Fig. 5.13. As an example, the IFT of 0.1 wt. % Tween 20 (o) reaches 1.7 mN m^{-1} after 30 minutes but within water (Fig. 5.3) the value is 5.1 mN m^{-1} . It is

anticipated that if left for a long enough period, the IFT values of the systems will converge to the same point. However, the RME process relies on droplet formation and detachment within the first few seconds (in which the two phases are introduced) and thus a rapid decrease in IFT is beneficial. In the case of lecithin, this surfactant partitions in favour of being within the oil phase and is therefore 'reluctant' to diffuse out of the droplet and stabilise the forming interface. As a consequence, emulsions formed with lecithin in oil destabilised almost immediately most likely due to significant coalescence at the membrane surface (agreeing with findings by Wagdare *et al.*, 2010). In terms of the effects of TMP, very little variation is seen between 0.2 and 1.5 bar when Tween 20 and Brij 97 are positioned within the oil phase ($< 9 \mu\text{m}$). Since the timescale for droplet formation and detachment is likely to be much shorter (since droplets are smaller), any variations within dispersed phase flow will not drastically alter the volume contributed during detachment (Peng and Williams, 1998). For these systems, jetting does not occur because although the IFT is low, the slight increase in viscosity from blending 0.1 or 1 wt. % of surfactant into the 10 vol. % dispersed phase rather than the 90 vol. % of continuous phase leads to a lower dispersed phase pore fluid velocity such that the jetting point is not reached. It is likely further increase in TMP beyond 1.5 bar, the jetting point may be reached.

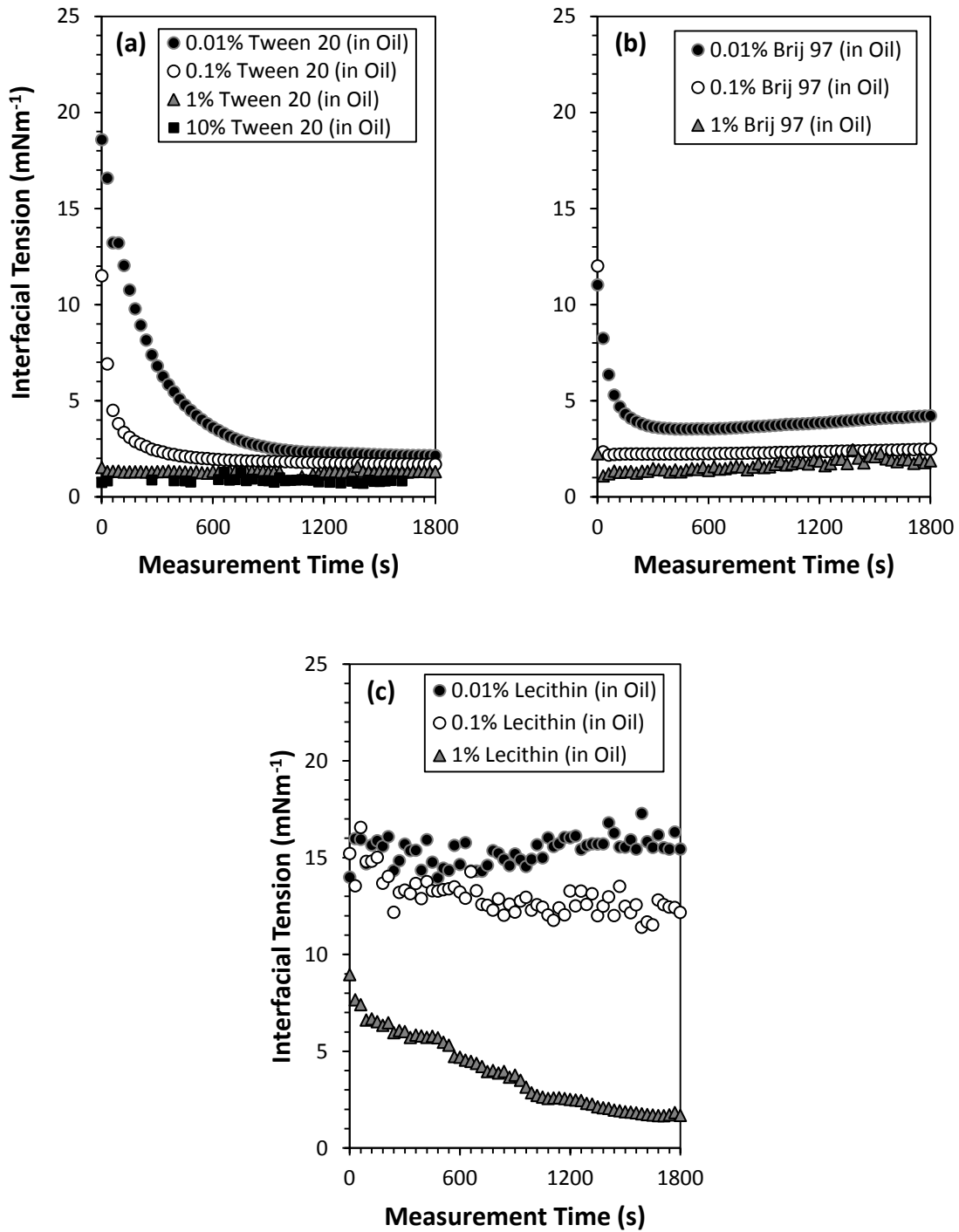


Fig. 5.13: Dynamic interfacial tension between distilled water and sunflower oil containing variable concentration of surfactants: (a) Tween 20, (b) Brij 97, (c) Lecithin.

The effect of shear rate at the membrane surface on droplet diameter when considering the surfactant position is presented in Fig. 5.14. Since the IFT of the non-ionic surfactant systems within oil is much lower than when in water, droplets are less resistant to shear and therefore detach

earlier as smaller sizes. Only a small decrease is seen with increasing shear rate from 0.6 s^{-1} to 104.7 s^{-1} . For example, when using 0.1 wt. % Brij 97 (o), the droplet size varies between $15.2 \mu\text{m}$ to $21.5 \mu\text{m}$ ($6.3 \mu\text{m}$ increase) compared to the more dramatic variation when within the aqueous phase ($64.8 \mu\text{m}$ to $105 \mu\text{m}$; $40.2 \mu\text{m}$ increase). This emphasises that if the aim is produce small droplet diameters, this can be achieved using less surfactant and less energy input if operating under minimal shear rates with Tween 20 or Brij 97 within the dispersed phase.

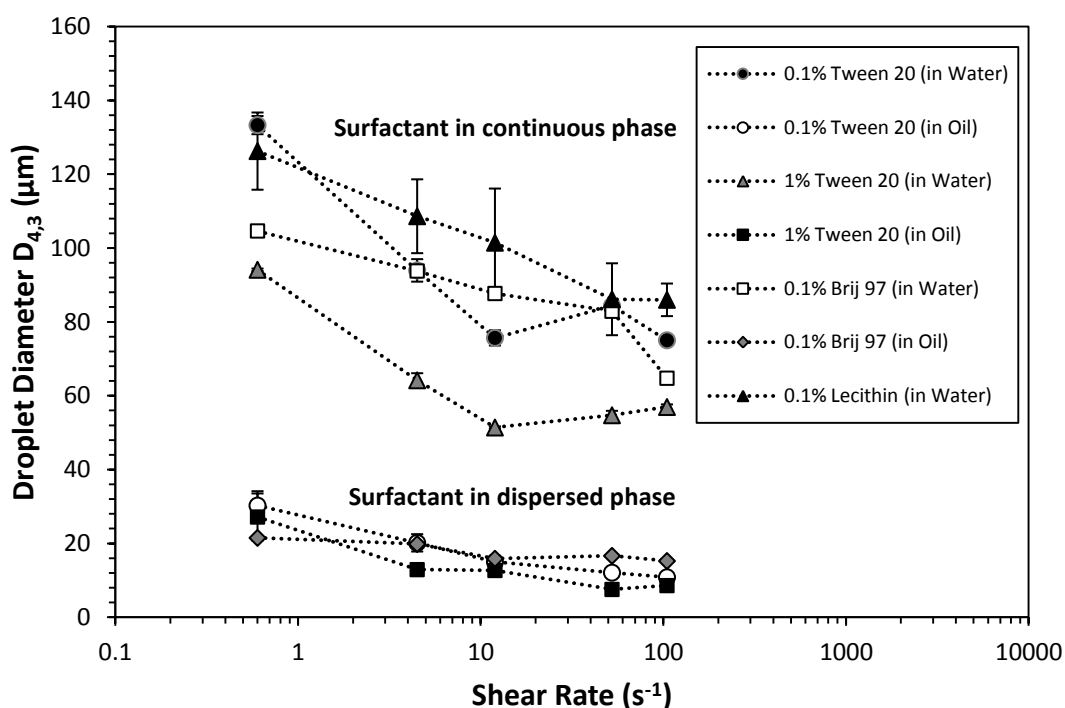


Fig. 5.14: The influence of shear rate on the mean droplet size for different surfactant positions. A transmembrane pressure of 0.5 bar is applied. The dotted lines are drawn to guide the eye across the data set. The error bars represent one standard deviation of a triplicate of experimental runs.

Fig. 5.15 shows droplet formation images for low ($100 \mu\text{l min}^{-1}$) and high ($1000 \mu\text{l min}^{-1}$) injection rates under quiescent continuous phase conditions (i.e. zero shear) using a Goniometer. Very small droplets can be produced from the needle (representative of a pore channel) with 1 wt. % Tween 20 (o) and a low injection rate applied. In this case, the droplet detaches almost simultaneously as it forms since buoyancy overcomes the low IFT holding the droplet at the needle outlet. For RME, the drag force will inevitably lead to an even earlier detachment but perhaps

reduce the extent of the size difference between the systems. To paraphrase, it is hypothesised that if the shear rate was increased to much greater values than 104.7 s^{-1} , the droplet size difference between the observed systems may be minimal. However, care is required when selecting operating parameters such as the applied TMP and shear rate in conjunction with inherent system properties such as IFT and viscosity in order to prevent chaotic jetting phenomena.

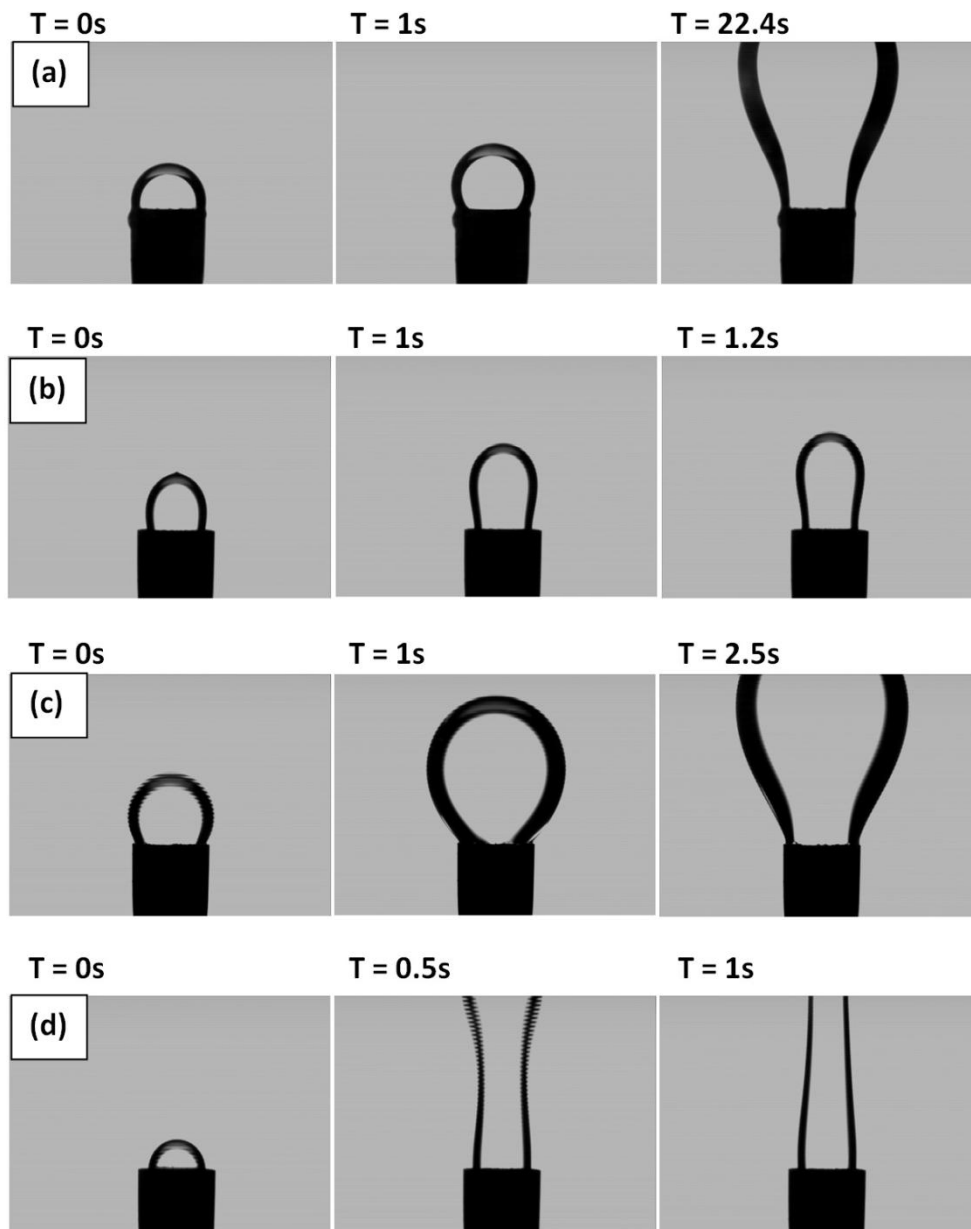


Fig. 5.15: Images of droplet formation and initial detachment stages from a 1.8 mm diameter needle under quiescent continuous phase conditions. Sunflower oil, water and 1 wt. % Tween 20 were used in all cases. The surfactant positioning and injection rate between low ($100 \mu\text{l min}^{-1}$) and high ($1000 \mu\text{l min}^{-1}$) were varied as follows: (a) low & in water, (b) low & in oil, (c) high & in water, (d) high & in oil.

5.10 Pre-mix Rotating Membrane Emulsification

A number of publications have altered the approach of membrane emulsification by passing coarse emulsions through the membrane rather than pure dispersed phase (Surh *et al.*, 2008; Vladisavljevic *et al.*, 2004a). The mechanism of droplet formation differs with droplets breaking down due to shear stresses elongating and compressing the droplets within the pore channel. Pre-mix membrane emulsification has been suggested to offer additional benefits such as high dispersed phase flux and lower energy consumption for producing high volume fraction emulsions (Nazir *et al.*, 2010). The logic underlining this approach is that droplets upon leaving pore outlets are already stabilised by surfactant provided within the initial coarse emulsion and therefore nullifies coalescence effects. If this is the case, this logic would also be valid with the surfactant being supplied within the dispersed phase as discussed in the previous section. To test this hypothesis, an initial emulsion of 20 vol % dispersed phase was formed either with Tween 20 within the continuous phase (w) or dispersed phase (o) using the conventional RME approach. Each of these emulsions was then passed through the same, cleaned membrane into distilled water a further three times to observe the extent of droplets being broken down within the pore channels. The results are presented in Fig. 5.16.

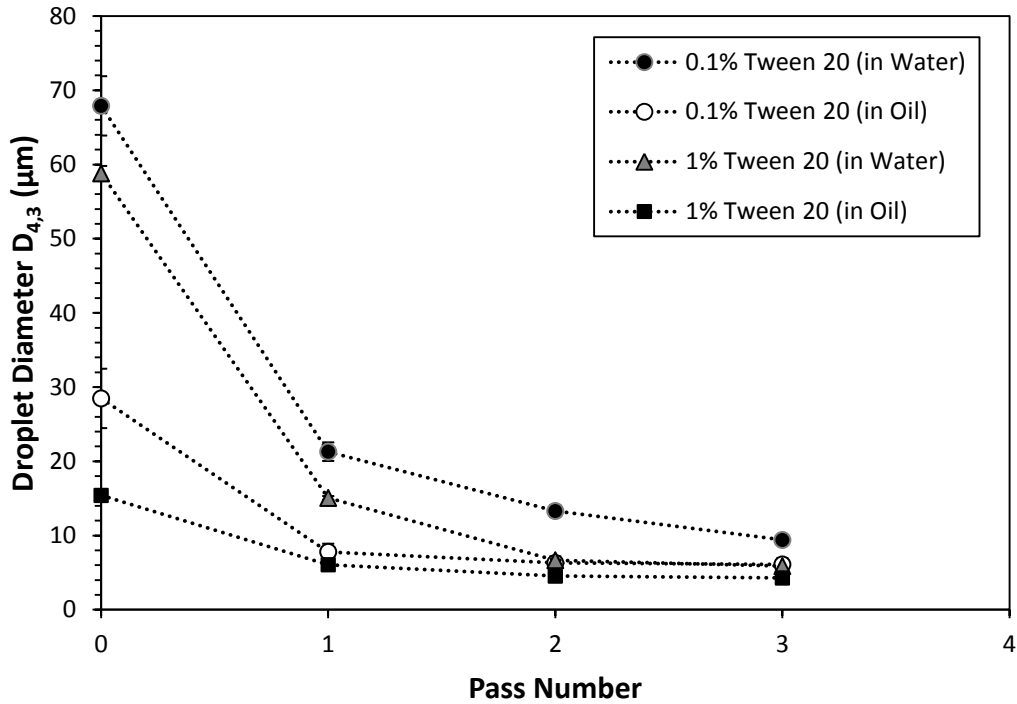


Fig 5.16: The influence of pass number on mean droplet size using sunflower oil, distilled water and 1 wt. % Tween 20. Pass 0 denotes the initial emulsion droplet size adopting the conventional RME approach. Pass 1-3 denotes the extent of droplet break up as the initial emulsion is passed through the membrane repeatedly. A transmembrane pressure of 0.5 bar and shear rate of 5.98 s^{-1} is applied in all cases. The dotted lines drawn are to guide the eye across the data set. The error bars represent one standard deviation of a triplicate of experimental runs.

As shown within the previous section, the initial emulsion droplet size (Pass 0) is lower with the Tween 20 in the dispersed phase due to the partitioning behaviour of the surfactant. What is interesting is the extent and rate of droplet size minimisation upon passing the emulsions through the membrane repeatedly (Pass 1 to 3). With the surfactant within the oil, the droplets experience only a small reduction in size beyond applying a single pass. With a more conventional use of surfactant, it was shown by Nazir *et al* (2011) that droplet size reduction is limited after three passes. Here, using 1 wt. % Tween 20 (o) as an example, the initial droplet size of $15.4 \mu\text{m}$ is broken down to $6.1 \mu\text{m}$, $4.5 \mu\text{m}$ and $4.3 \mu\text{m}$ upon applying further passes. If compared with 1 wt. % Tween 20 (w), the break down is much more prominent from $58.8 \mu\text{m}$ to $15.1 \mu\text{m}$, $6.7 \mu\text{m}$ and $5.9 \mu\text{m}$. With further passes, it is likely they will achieve the same droplet size value where the shear stresses are unable to deform droplets due to their high Laplace pressure. Overall, a much more efficient adsorption of

surfactant is achieved as demonstrated by 0.1 wt. % Tween 20 (o) reaching smaller diameters than 1 wt. % in the water phase. The point is, through applying the surfactant within the oil phase, the need of multiple passes to achieve sufficient break down to the minimum droplet size is eliminated. In fact, the very nature of adopting a pre-mix setup can be questioned since fouling is a severe problem (Trentin *et al.*, 2009; Surh *et al.*, 2008) as shown in Fig. 5.17. SPG membranes are known to be very effective for use within a pre-mix membrane emulsification setup. Since they have a structure of interconnected tortuous pore channels, this imparts much higher shear stresses to break up droplets than membranes with straight, perpendicular pore channels. On the other hand, the drawback to this is an increased likelihood of fouling and hence the dispersed phase flux will be negatively affected. This implies that the use of thin metallic membranes (such as silicon microsieves) may need to be implemented within a pre-mix setup to minimise fouling (Nazir *et al.*, 2011) and allow for more rigorous cleaning techniques with tailoring of process parameters (e.g. TMP) to impart higher shear.

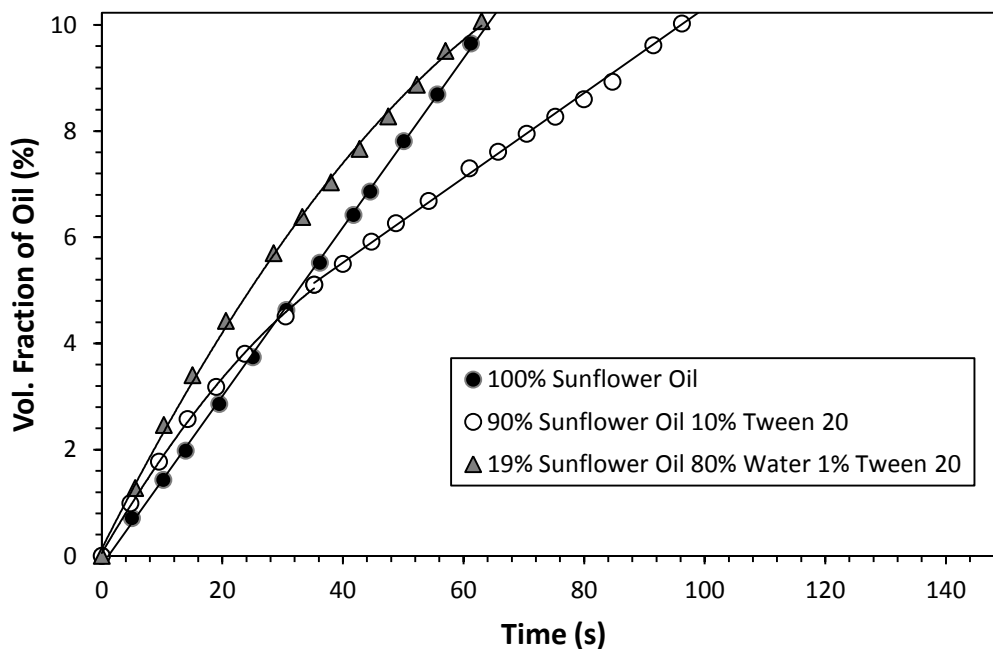


Fig. 5.17: Volume fraction of oil within the final emulsion during process operation at a transmembrane pressure of 0.5 bar and a shear rate of 5.98 s^{-1} . The percentages represent the mass composition of the dispersed phase only. Note: the 90% sunflower oil and 10% Tween 20 data set is representative of the 1 wt. % Tween 20 (o) system.

In order to compare flow behaviour between the dispersed phase systems used (pure SFO, oil with surfactant and a pre-emulsion), the graph is expressed as mass of oil added to the final emulsion since the objective is to reach a pre-defined quantity of this material. There is no doubt that the flux of a pre-emulsion is much higher than of pure oil, but a significant volume of that emulsion must pass through the membrane to arrive at the end point of the process. What is apparent is that the rate of mass transfer/addition for the pre-emulsion is not linear - that would be expected by Darcy's law. This suggests an increase in resistance to flow over time which is likely to be caused by fouling. In the case of droplets slightly larger in diameter than the membrane pore channel, the shear exerted within the internal structure may not be great enough to overcome the droplet Laplace pressure. As a consequence, the droplet cannot deform sufficiently enough to pass through and thus it becomes trapped within the membrane, causing a blockage. However, much larger droplets will be broken up by the shear within the pore channel whilst smaller droplets will pass through unopposed. The flow behaviour of pure SFO in contrast to a pre-emulsion obeys a linear addition of mass over time whilst a mixture of SFO and Tween 20 exhibits a slight reduction in the rate followed by a linear region. The surfactant may coat the membrane walls within pore channels during the initial stages of operation (and hence the flow behaviour) before the mixture acting as a bulk material. As expected the gradient of this linear region is lower than pure SFO since the viscosity is slightly higher. With the requirement to pass the pre-emulsion through the membrane further times to achieve sufficient break down of droplets, it may be therefore more efficient to operate using a dispersed phase with lower flux, but which ensures rapid adsorption of surfactant from a single pass i.e. using high HLB non-ionic surfactant within the oil. Subsequently, this limits the effect of fouling which will further reduce process efficiency.

5.11 Conclusions

A variety of emulsion systems stabilised by surfactants, particles and mixtures of the two were produced using a RME setup. The objective was to investigate how the interfacial behaviour governs the emulsion structure (i.e. droplet size) in conjunction with processing parameters (TMP and shear rate). For stable operation of RME, it is very important that the surfactant or particle adsorbs quickly, especially if operating at a high TMP paramount to greater emulsion production rates. This is to ensure coverage of the interface as it is generated to prevent coalescence at the membrane surface and allow for earlier droplet detachment (since the primary retention force of IFT is minimised). However, care is required to ensure jetting of the dispersed phase doesn't occur if the IFT is very low and the pore fluid velocity is high (e.g. 1% wt. SDS at 1.5 bar led to large, poly-dispersed droplets forming). The rate of transport towards the interface and subsequent adsorption depends primarily on physicochemical properties of the surfactant or particle used. For surfactant systems, such properties include the HLB number, molecular weight and the CMC. For particle systems, the particle radius and contact angle are important characteristics since these determine the adsorption energy. Interestingly, the presence of turbulent flow of the continuous phase was influential on producing smaller droplet sizes using particles (but surfactants were unaffected). This therefore suggests differences in the transport mechanism towards the droplet interface with surfactants relying on diffusion whilst particles on convection to increase the rate of collisions and hence the likelihood of adsorption.

The stabilisation mechanism provided by the material positioned at the droplet interface needs to be strong energetically. Assuming adsorption is sufficiently fast, electrostatic repulsion (demonstrated with the use of the anionic surfactant SDS) or steric repulsion (demonstrated with silica particles) between adjacent droplet interfaces can prevent coalescence. Utilising a combination of a surfactant alongside particles has a synergistic effect on droplet stabilisation with each providing a different function to the interface. The surfactant reduces the IFT to allow for early detachment

(by altering the point of force imbalance) whilst the particle provides a greater steric barrier to limit coalescence. The suggested mechanism of competitive adsorption has a slightly antagonistic effect on the IFT since particles do not reduce IFT to as great an extent as surfactants. Furthermore, some surfactant is likely to adsorb to the surface of the particle to reduce the concentration available for adsorption at the droplet interface. Irrespective of this matter, smaller droplets were produced by using both surfactants and particles together than each component separately.

Finally, a novel approach in which surfactant is supplied via the dispersed phase rather than its conventional positioning within the continuous phase was introduced. By allowing material to diffuse through the interface, this leads to a reduction in the IFT well below the equilibrium value which is highly beneficial to the RME process to allow early droplet detachment. However, this approach has only been successfully demonstrated for stabilising O/W droplets using high HLB non-ionic surfactants such as Tween 20 and Brij 97. When using a low HLB surfactant such as lecithin, droplets were not stabilised since due to its partition coefficient, remains primarily within the oil phase and hence does not diffuse out of the droplet to the extent of the high HLB surfactants. RME with surfactant within the dispersed phase compares favourably to a pre-mix emulsification setup since droplet size minimisation through multiple passes is achieved much earlier by ensuring rapid adsorption of surfactant. Furthermore, the effects of membrane fouling are avoided. Such an approach may therefore be advantageous for high production rate processing where the rate of surfactant adsorption is sufficiently fast compared to the rate of droplet interface generation.

Chapter 6:

Theoretical Modelling and Process Comparison

This chapter describes the development of models for rotating membrane emulsification based on findings within the previous two chapters. Comparisons are also made with a rotor-stator mixer and an ultrasonic probe device in terms of the rate of emulsion production and the energy consumption to assess the benefits of rotating membrane emulsification processing.

Data and discussions contained within this chapter are to be published within:

Lloyd, D.M., Norton, I.T., Spyropoulos, F. (2015). Process optimisation of Rotating Membrane Emulsification through the study of surfactant dispersions. *Journal of Food Engineering*, 166 316-324.

Lloyd, D.M., Norton I.T., Spyropoulos, F. (April 2014), Food-grade emulsion production using a low energy rotating membrane technology. *The 8th European Workshop on Food Engineering and Technology*, Quakenbrück, Germany (oral presentation).

Spyropoulos, F., Lloyd, D.M., Norton, I.T. (June 2015). A microstructural approach to optimising membrane emulsification: surfactant diffusion through the oil/water interface. *The 12th International Congress on Engineering and Food*, Quebec City, Canada (poster presentation).

6.1 Introduction

The aim of this chapter is to consider some of the theoretical concepts behind the rotating membrane emulsification process (RME); specifically related to coalescence at the membrane surface and the droplet size produced for a given set of conditions. The application of the models developed will prove valuable if one was to design and operate this piece of equipment. In addition, RME is compared to a rotor-stator high shear mixer (HSM) and an ultrasonic probe (SON). This is with regards to their capability to produce similar size droplets based on the emulsion rate of production and the energy input. Such a comparison evaluates whether producing emulsions with rotating membrane emulsification is as beneficial as suggested by other authors.

6.2 Model to Estimate the Probability of Coalescence

The likelihood of droplet coalescence during membrane emulsification is an important consideration since the presence or absence of this phenomenon may have a detrimental effect on the capability of the process to produce uniform droplet sizes. Coalescence has been shown to occur as a result of droplet contact on the membrane surface (Abrahamse *et al.*, 2002; Vladislavljevic *et al.*, 2004b). During expansion of the droplet interface, this provides an opportunity for droplet coalescence in contacting areas insufficiently covered by surfactant. Coalescence is less of an issue within the continuous phase as droplets reside with low collision energies. One of the key parameters contributing to the occurrence of coalescence (or not), as demonstrated by the work of Timgren *et al.* (2009) is membrane porosity. Membrane porosity to a large extent determines the distance between adjacent active pores, with smaller distances potentially leading to interactions between forming or just formed droplets. This emphasises the requirement for models that can predict coalescence to aid membrane design.

There are a couple of rough estimates on the maximum porosity value to avoid coalescence for a given droplet size to pore size ratio. Abrahamse *et al.* (2001) suggested a maximum porosity of

0.015 for producing 33 μm diameter droplets from a 5 μm diameter pore (ratio of 6.6). Schroder *et al.* (1998) calculated a porosity value of 0.3 for droplets a ratio of 1.6 times larger than the pore. Lepercq-Bost *et al.* (2010) took these observations and developed a model that estimated the risk of coalescence based on the operating conditions. A ceramic membrane ($\alpha\text{-Al}_2\text{O}_3$) was used so the effective membrane porosity increased with applied transmembrane pressure (TMP). The hypothesis behind the model was that in the event that one other pore was active within close proximity to the forming reference droplet, coalescence would occur. Whilst this assumption was supported by experimental droplet size distribution data, the model did not quantify a numerical probability value but stated a 'yes or no' likelihood. However, it still serves as a useful tool to determine the maximum effective porosity (due to the applied pressure) to create narrow droplet size distributions as quickly as possible. The percentage of active pores relies upon experimental determination of the relationship between dispersed phase flux and pressure prior to model application.

Here, a slightly more involved model has been developed for coalescence prediction. It is insufficient to simply state that coalescence does or does not occur considering it may happen to a minor extent with a minimal effect on the droplet size distribution. The distribution of active pores across the membrane surface is the most important consideration to both of these models; the two extreme cases are an equidistant distribution or a completely random distribution of pores producing droplets. For metallic materials, the pore spacing is controllable and the majority of pores are active i.e. droplets are formed as a regular array. For materials such as SPG and ceramics, the latter case of random activation is more applicable and therefore a more complex model is required to account for this.

The model presented here is derived for an SPG membrane of 6.1 μm pore diameter as used within Chapters 4 and 5. Firstly, the fraction of active pores at a specific TMP needs to be calculated (using Eq. 4.3 in section 4.2.2). This requires experimental determination of the dispersed phase flux

behaviour to find the membrane permeability. The average porosity of an SPG membrane is 0.56 (Vladisavljevic *et al.*, 2005). The porosity value is needed to solve for the active pore fraction using Eq. 4.2. Next, the total number of pores on the membrane surface requires estimation. Vladisavljevic *et al.* (2005) concluded that for SPG membranes, the total number of pores per unit area was inversely proportional to the square of the mean pore size:

$$n_{p,t} = \frac{0.56A_m}{d_p^2} \quad (\text{Eq. 6.1})$$

where $n_{p,t}$ is the total number of pores on the membrane surface, A_m is the membrane surface area covered by pores and d_p is the pore diameter. Therefore the number of pores active at a specific moment in time during operation ($n_{p,a}$) is:

$$n_{p,a} = \alpha n_{p,t} \quad (\text{Eq. 6.2})$$

where α is the fraction of active pores at a given TMP. Coalescence is likely to happen if the distance between forming droplets ($L_{x,a}$) is small enough such that the forming interfaces come into contact as shown in Fig. 6.1. Therefore, the likelihood of this event occurring requires consideration.

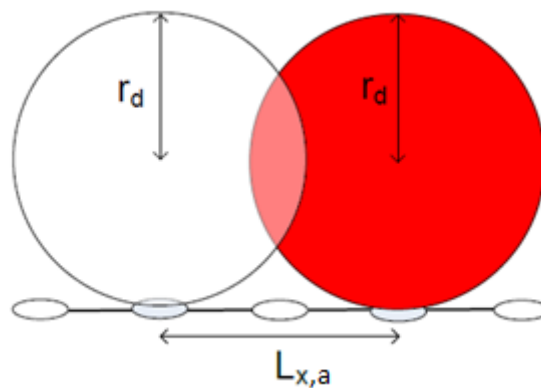


Fig. 6.1: A schematic representation of two droplets forming at adjacent active pores. In this case, $L_{x,a} < 2r_d$ indicating coalescence is likely due to droplet interface contact during expansion.

In the case of an even distribution of active pores, the distance between adjacent active pores can be found relatively easily. By dividing the membrane surface into a series of equilateral triangular

segments consisting of a pore at each vertex, the length of each side defines the distance between adjacent pore centre points (Fig. 6.2).

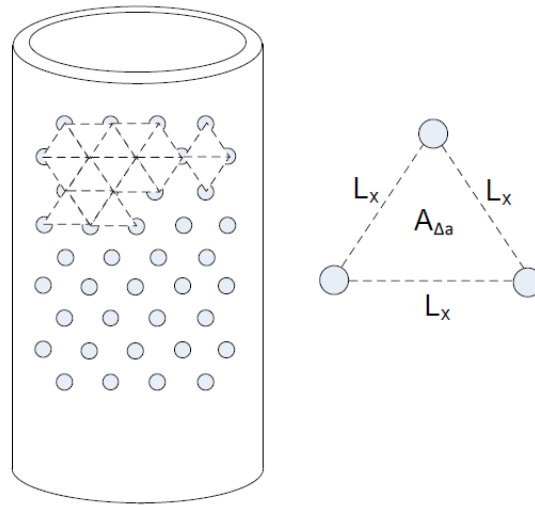


Fig. 6.2: The basis for calculation of the average distance between pores across the membrane surface assuming a triangular array.

If one of these segments is formed by three active pores, the number of segments ($x_{\Delta,a}$) across the membrane surface (Pach and Pinchasi, 2003) is:

$$x_{\Delta,a} = n_{p,a} - 2 \quad (\text{Eq. 6.3})$$

And therefore the area of one segment ($A_{\Delta,a}$):

$$A_{\Delta,a} = \frac{A_m}{x_{\Delta,a}} \quad (\text{Eq. 6.4})$$

The length of each side calculated for an equilateral triangle is the average distance between the centre of each active pore ($L_{x,a}$):

$$A_{\Delta,a} = L_{x,a}^2 \frac{\sqrt{3}}{4} \quad (\text{Eq. 6.5})$$

$$L_{x,a} = \sqrt{\frac{4A_{\Delta,a}}{\sqrt{3}}} \quad (\text{Eq. 6.6})$$

If $L_{x,a}$ is less than the diameter of the droplet, coalescence may occur. This is the basis of the Lepercq-Bost model. However, the approach is inappropriate if the active pores are not distributed in this way.

In the case of a random active pore distribution, a similar approach is required to determine the spacing between all pores on the membrane surface. Eq. 6.1 to Eq. 6.6 can be applied but instead by using the total number of pores ($n_{p,t}$) rather than the number of active pores ($n_{p,a}$). The next step is to assume a theoretical droplet diameter for a droplet attached to the membrane surface. There will be a number of pores within close proximity of this droplet, more so if the droplet is large. Since coalescence is assumed to occur if the distance between forming droplets is less than the droplet diameter (d_d), there is a proximity zone where formation of another droplet will induce coalescence. The cross-sectional area of this zone ($A_{d,p}$) is defined as:

$$A_{d,p} = \pi(d_d^2) \quad (\text{Eq. 6.7})$$

There are a number of pores within this proximity zone. The average number of segments ($x_{\Delta,p}$) and hence pores ($n_{p,p}$) nearby to a forming droplet:

$$x_{\Delta,p} = \frac{A_{d,p}}{A_{\Delta,t}} \quad (\text{Eq. 6.8})$$

$$n_{p,p} = x_{\Delta,p} + 2 \quad (\text{Eq. 6.9})$$

where $A_{\Delta,t}$ is the area of one segment formed by three adjacent pores. For a given active pore fraction, the number of pores that are active at any one moment and therefore the likelihood that one of the pores within the proximity zone will be active can be calculated. The number of pores active is solved by Eq. 4.1 to Eq. 4.3. Assuming all droplets have the same droplet formation time, the maximum number of pores that could be active ($n_{p,ac}$) would be realised if all other droplets

begin to form from previously inactive pores at the midpoint of droplet formation of the reference droplet (i.e. completely out of phase frequency):

$$n_{p,ac} = 2n_{p,a} - 1 \quad (\text{Eq. 6.10})$$

The probability of a randomly chosen pore on the membrane surface being active (P_{active}) is therefore:

$$P_{active} = \frac{n_{p,ac}}{n_{p,t}} \quad (\text{Eq. 6.11})$$

With $n_{p,p}$ number of pores being active and the probability of any single pore being active is P_{active} , the probability of at least one pore being active within the proximity zone and hence coalescence occurring ($P_{coalescence}$) is:

$$P_{coalescence} = 1 - [(1 - P_{active})^{n_{p,p}}] \quad (\text{Eq. 6.12})$$

To demonstrate the implications of these models, the following input parameters shown in Table 6.1 are used for SPG membranes:

Table 6.1: Parameter values applied within model of droplet coalescence

Parameter	Value
Membrane Surface Area (A_m)	0.00141 (m ²)
Membrane Pore Diameter (d_p)	6.1×10^{-6} (m)
Active Pore Fraction (α)	Assumed Variable
Droplet Diameter (d_d)	Assumed Variable

For equidistant pore distribution, applying Eq. 6.1 to Eq. 6.6 yields the following results (Table 6.2):

Table 6.2: Distance between active pores assuming an even distribution of these pores across the membrane surface, for a given active pore fraction.

Active Pore Fraction, α (%)	Distance between Adjacent Active Pores, $L_{x,\alpha}$ (μm)
0.01	1240
0.1	392
1	124
5	55.4

This means that if the droplet diameter is larger than the distance between adjacent active pores, coalescence may occur. Considering the distances are relatively large compared to the droplet size data shown in Chapters 4 and 5 (except at the highest active pore fractions), this indicates coalescence is unlikely. However, this is an idealised case since the pores are spaced as far away from each other as possible.

For a random active pore distribution, applying Eq. 6.1 to Eq. 6.12 for all pores shows there are 2.13×10^7 pores on the membrane surface with each spaced on average $12.4 \mu\text{m}$ away from each other. As the theoretical diameter of the droplet becomes larger, more pores are located in the proximity zone increasing the likelihood of coalescence. Similarly, with a higher active pore fraction the probability of one of these pores being active is higher which also increases coalescence phenomena. This is shown in Fig. 6.3:

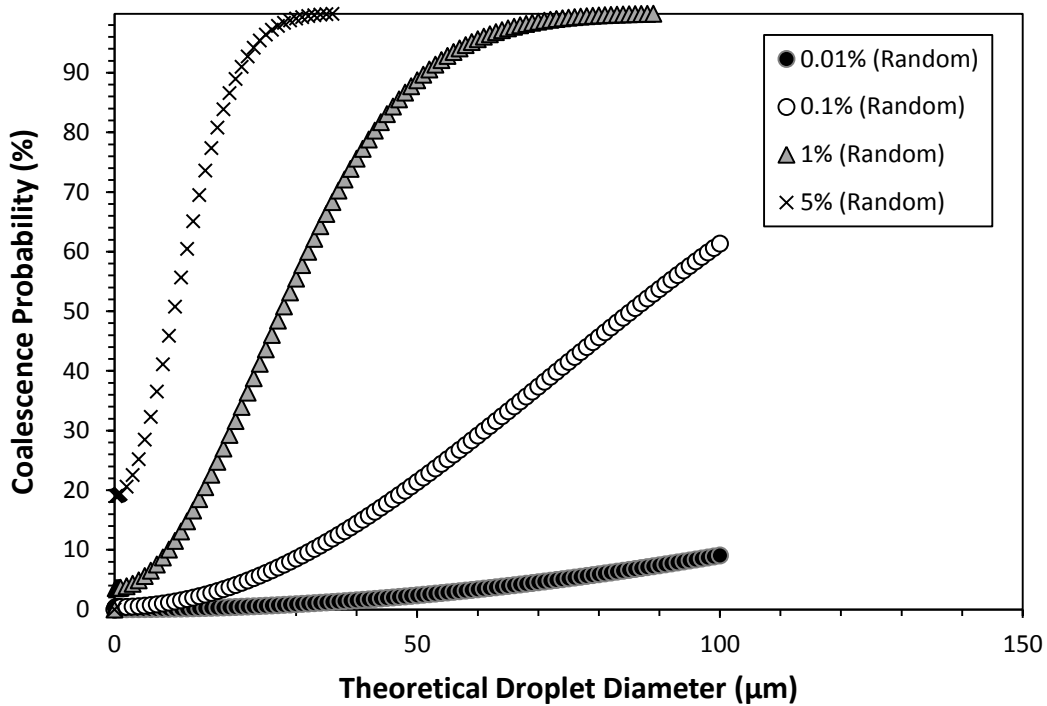


Fig. 6.3: The probability of coalescence for active pores randomly distributed on the membrane surface as a function of theoretical droplet diameter.

Applying the coalescence probability models with the data shown in section 4.2, the effect of TMP between 0.1-1.8 bar found 0.9-2.7 % of pores to be active based on the dispersed phase flux measurements. If these pores were evenly distributed, the distance separating them would be between 75.4 μm and 131 μm. All droplet sizes were greater than 51.4 μm (0.5 bar, 2000 RPM) which means in the case of completely random distribution, even with the lowest active pore fraction (0.9%) coalescence would occur in roughly 80+% of cases. This therefore clearly suggests that coalescence has occurred to some extent and the droplets were likely to have been smaller but had in fact coalesced during processing. The final measured sizes ranged between 51.4-103 μm.

6.3 Application of the Force Balance Model to Predict Droplet Size

It was discussed within Section 2.2.3 that a droplet will begin to detach from the membrane surface due to an imbalance of forces (Peng and Williams, 1998). If these forces can be identified and then calculated, the droplet size can be predicted at least at the end of the growth stage i.e. at the point of detachment. It was highlighted that the size will increase due to additional material being contributed to the droplet via its neck; this is a function of the dispersed phase flux and the droplet detachment time (Eq. 2.8). Therefore, it is expected that such a force balance model would under-predict the droplet size unless i) the dispersed phase flux is low or ii) the droplet detachment time is short. A force balance model applicable to rotating membrane emulsification is discussed and evaluated within this section.

There are a number of forces that are common within a range of membrane emulsification approaches. The adhesive force holding a forming droplet at the pore outlet is the interfacial tension force (F_γ). The force can be calculated assuming a spherical pore:

$$F_\gamma = 2\pi\gamma r_p \quad (\text{Eq. 6.13})$$

where γ is the interfacial tension and r_p is the pore radius. It is important to note that there is a time dependency on the value of interfacial tension between the organic and the aqueous phase. The adsorption of surfactant molecules decreases the interfacial tension whilst the expanding nature of the interface depletes the surfactant coverage, increasing interfacial tension. It is therefore complicated to predict the interfacial tension of a growing droplet over time so static interfacial tension values are adopted (Schroder *et al.*, 1998). Approaches to use dynamic values are difficult to use, requiring mathematical simulations to apply (De Luca *et al.*, 2004; De Luca and Drioli, 2006). Therefore, in this case a static value is applied.

The drag force (F_R) is the dominant detachment force enabling individual droplets to be produced. It is calculated by considering the force exerted by fluid flow on a rigid sphere:

$$F_R = k_x(6\pi r_d \mu_c v_c) \quad (\text{Eq. 6.14})$$

where k_x is the wall correction factor, μ_c is the continuous phase viscosity and v_c is the velocity difference between the continuous phase and the membrane surface. The wall correction factor usually adopted is 1.7 (O'Neil, 1964). It was suggested earlier within this thesis (section 4.6.1) that k_x may vary as a function of viscosity since droplets are not rigid spheres but they can be deformed altering the drag coefficient (Timgren *et al.*, 2008; Egidi *et al.*, 2008).

The two other universally recognised forces are the buoyancy force (F_{BG}) and the inertial force (F_I). The former is induced by density differences between the two phases (Eq. 6.15) whilst the latter is the result of the linear momentum of the dispersed phase upon leaving the pore channel (Eq. 6.16):

$$F_{BG} = \frac{4}{3} \pi r_d^3 (\rho_c - \rho_d) g \quad (\text{Eq. 6.15})$$

$$F_I = \rho_d \overline{v_d^2} A_n \quad (\text{Eq. 6.16})$$

where ρ_c and ρ_d are the densities of the continuous and dispersed phases respectively, g is the gravitational field strength, $\overline{v_d}$ is the average velocity of dispersed phase within the pore channel (which depends on the TMP) and A_n is the cross-sectional area of the droplet neck. Other forces that should theoretically be considered are the dynamic lift force (F_{DL}) and the static pressure force (F_{stat}) defined by Eq. 6.17 and Eq. 6.18 (Schroder *et al.*, 1998):

$$F_{DL} = k_y \frac{\tau_w^{1.5} d_d^3 \sqrt{\rho_c}}{\mu_c} \quad (\text{Eq. 6.17})$$

$$F_{stat} = P_d^0 A_n \quad (\text{Eq. 6.18})$$

where k_y is the lift coefficient, τ_w is the shear stress at the membrane wall and P_d^0 is the pressure difference between the dispersed and continuous phase. The dynamic lift force is the perpendicular component of the surface force experienced by object within a fluid flow field (with drag force being the parallel component). The lift coefficient was debated by Timgren *et al.* (2008) to vary as a

function of Reynolds number so it may be higher than the value of 0.761 which is typically used within this equation. The static pressure force is caused by the difference in internal pressure of the droplet and the continuous phase. The internal pressure comprises of i) a fraction of the applied pressure upstream after the pressure drop across the membrane due to frictional losses and ii) a modified Laplace pressure value for a droplet attached to the membrane surface. This was determined by Abrahamse *et al.* (2001) as:

$$P_{LP}^* = \frac{4\gamma}{\sqrt[3]{6V_{dr}\pi}} \quad (\text{Eq. 6.19})$$

where P_{LP}^* is the estimated Laplace pressure for a non-spherical droplet and V_{dr} is the droplet volume. It was shown via simulation that the cumulative effect on the internal droplet pressure was a reduction over the initial stages of droplet formation as the droplet grows in size. The Laplace pressure can be considered to be the main component of this value since the pressure drop across the pore channel is often large.

Finally, with rotating membrane emulsification an additional centripetal force (F_c) requires consideration. This force hinders droplet detachment if the dispersed phase density is lower than the continuous phase. The centripetal force acting on a spherical droplet can be estimated using Eq. 6.20:

$$F_c = \frac{m_d v_{dr}^2}{r_1} \quad (\text{Eq. 6.20})$$

where m_d is the mass of the droplet and r_1 is the membrane radius. The tangential velocity of the droplet (v_{dr}) equals:

$$v_{dr} = \frac{2\pi(r_1 + r_d)n_1}{60} \quad (\text{Eq. 6.21})$$

where n_1 is the rotations per minute of the membrane. The presence of a ‘push off’ force hypothesised by Egidi *et al.* (2008) and Kosvintsev *et al.* (2008) has not been included since droplet formation is extremely unlikely to occur as a regular array when using SPG membranes. The force balance model for rotating membrane emulsification therefore takes the final form shown in Eq. 6.22 and visually represented in Fig. 6.4:

$$F_Y + F_c = F_R + F_{BG} + F_I + F_D + F_{stat} \quad (\text{Eq. 6.22})$$

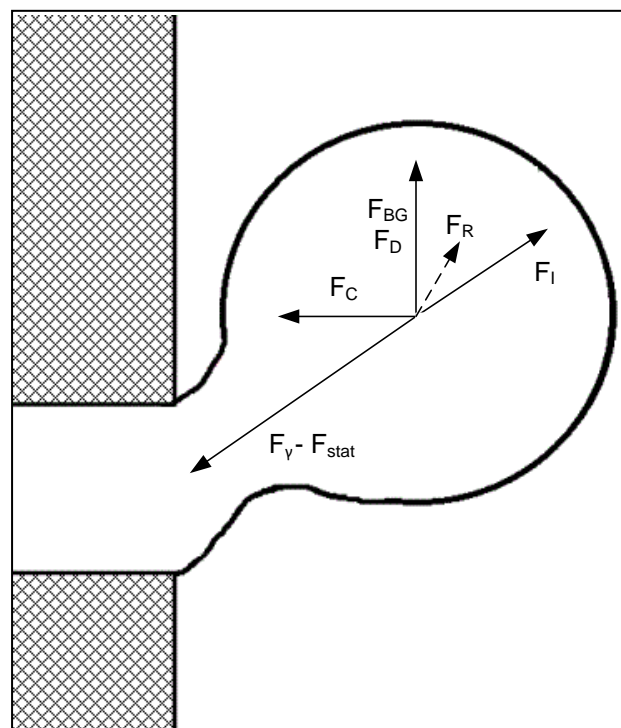


Fig. 6.4: A schematic representation of the forces acting on a droplet at the point of detachment from the membrane surface.

As is seen by observing Eq. 6.13 to Eq. 6.20, the magnitude of the forces changes with an increase in droplet size; the detachment forces are greater for larger droplets. Eventually a droplet will reach a size where the interfacial tension force is overcome. This can be seen by solving the force balance for an example case; the input parameters used are listed in Table 6.3:

Table 6.3: Parameter values applied within the force balance model example.

Parameter	Value	Parameter	Value
Transmembrane Pressure	0.5 (Bar)	Pore Diameter	6.1 (μm)
Rotational Speed	1000 (RPM)	Membrane Diameter	10 (mm)
Vessel Diameter	60 (mm)	Membrane Thickness	1 (mm)
Interfacial Tension	4.8 (mN m^{-1})	Tortuosity Factor	1.25
Dispersed Phase Viscosity	0.066 (Pa s)	Drag Coefficient	1.7
Dispersed Phase Density	919 (kg m^{-3})	Lift Coefficient	0.761
Continuous Phase Viscosity	0.0015 (Pa s)	Gravitational Field Strength	9.81 (N kg^{-1})
Continuous Phase Density	999 (kg m^{-3})		

The magnitude of the sum of the detachment and retaining forces as a function of a theoretical droplet size is shown in Fig. 6.5 whilst a breakdown of the individual component forces is shown in Fig. 6.6:

Fig. 6.6:

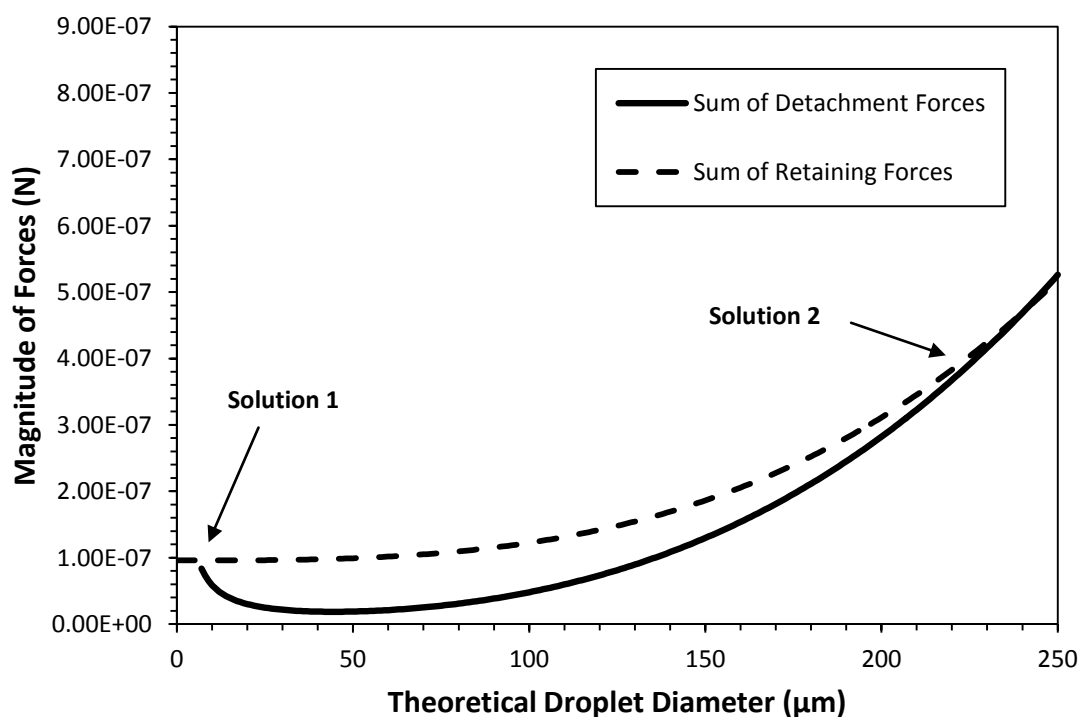


Fig. 6.5: Relationship between droplet diameter and the magnitude of detachment and retaining forces based on the conditions listed in Table 6.3.

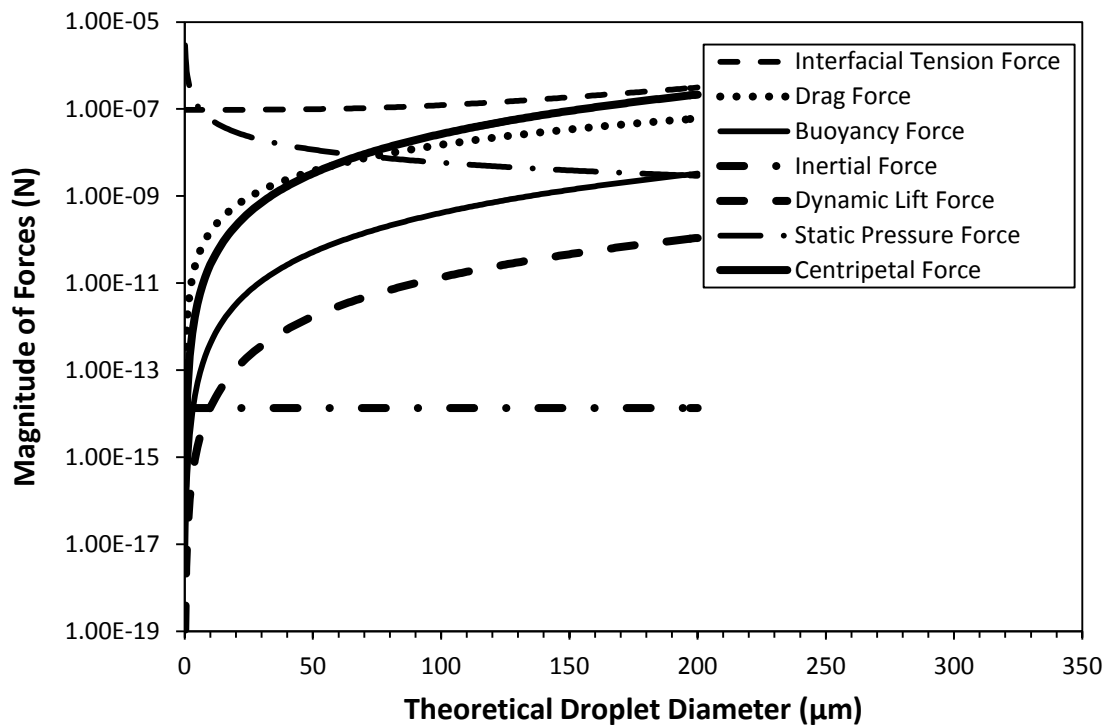


Fig. 6.6: A more detailed breakdown of the acting forces on a droplet as it grows based on the conditions listed in Table 6.3.

From Fig. 6.5., it is clear there are two solutions given where the detachment and retaining forces intersect. Solution 1 equals the membrane pore diameter; this is an imaginary solution. As the droplet begins to form, the interfacial tension will be higher than the equilibrium value used in this instance. Furthermore, it is likely the Laplace pressure and therefore the static pressure force is overestimated since only a small portion of the dispersed phase is in contact with the continuous phase. However, as the droplet begins to protrude into the continuous phase, the static pressure value becomes more accurate (decreasing as the droplet grows in volume). Solution 2 is the real value; in this example case it is 236 μm which was found via iteration. This is likely to be an over-prediction of the size produced, even more so considering the volume increase during detachment has not been accounted for. Fig. 6.6, shows that the majority of the detachment forces increase as the droplet grows. The primary forces are the drag, buoyancy and static pressure forces. The inertial and dynamic lift forces are orders of magnitude lower so are typically negated from such force balance models. The interfacial tension force (although constant here) would be decreasing as

surfactant adsorbs at the interface. Models such as the one developed by Rayner *et al.* (2005) connecting the rate of droplet inflation with its surfactant coverage would be required to use dynamic rather than static interfacial tension values.

The force balance model was tested and compared to experimental data acquired and presented in Chapters 4 and 5. The four parameters investigated and shown within Fig. 6.7 were Transmembrane Pressure (a), Rotational Speed (b), Concentration of Tween 20 (c) and Interfacial Tension (d). Unless otherwise stated, the conditions listed in Table 6.3 are applied.

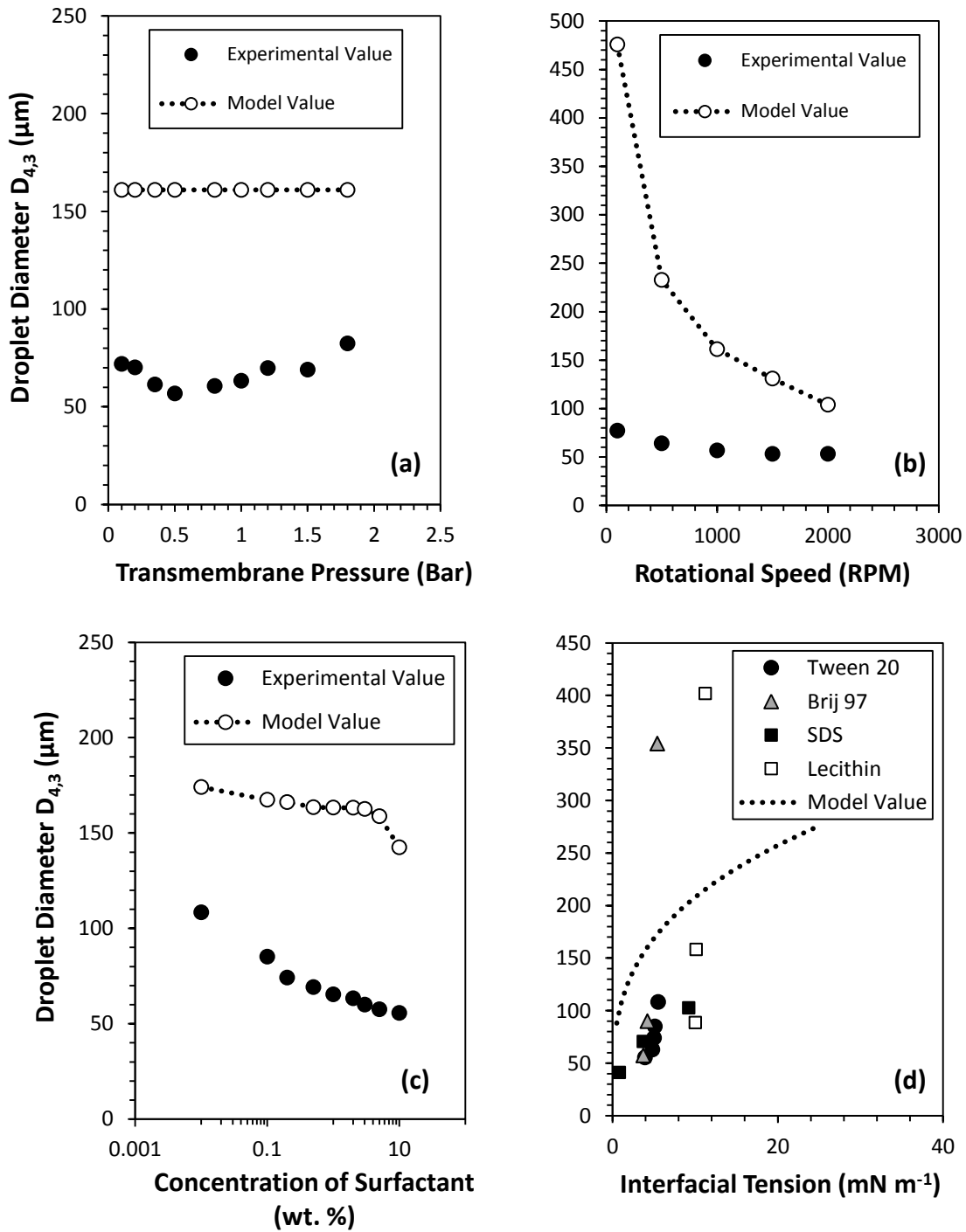


Fig. 6.7: Predicted droplet sizes compared to actual experimental data presented within Chapters 4 and 5. The parameters modified were (a) Transmembrane Pressure (b) Rotational Speed (c) Tween 20 concentration and (d) Interfacial Tension value.

There are a number of observations that can be made from Fig. 6.7. Firstly, the model is not able to distinguish the effects of TMP on droplet size. The pressure alters the inertial force, which from Fig. 6.6 is at least a couple of orders of magnitude lower than the other forces. The interfacial

tension force should also be influenced by pressure since as mentioned the surfactant will be depleted as the interface expands. However, in this case a static value is used. Similarly, the different behaviour for the surfactants (i.e. rate of diffusion and adsorption) is not discriminated; the interfacial tension value is insufficient information for prediction of the droplet size. Finally, in the majority of cases the force balance model significantly overestimates the droplet size produced. This is all the more surprising considering the volumetric contribution of dispersed phase during detachment is not accounted for, and furthermore that the equilibrium value of interfacial tension is used. The reason that droplets may be detaching earlier than expected is due to the mechanism proposed by Rayner *et al.* (2004); spontaneous transformation-based droplet formation. This is a likely phenomenon especially if tortuous pore channels imperative of SPG membranes are used. The detachment forces may deform the droplet to a non-spherical, higher energy state with the interfacial energy then acting to detach the droplet. The detachment forces then act to accelerate the detached droplet away from the membrane surface to reduce coalescence phenomena. Perhaps derivation of an interfacial energy driving force (to induce detachment) is required to improve model accuracy. The force balance model in its current form serves as a useful, easy-to-apply tool for predicting rotating membrane process behaviour rather than accurately determining the droplet size produced. More rigorous computational-based modelling processes should be used in conjunction with the force balance model to increase accuracy.

6.4 Process Comparison on the Basis of Production Rate

One of the primary limitations of membrane emulsification relates to its ability to produce emulsions at a rate competitive with other processes. This is due to the low dispersed phase flux typically required to produce small, mono-dispersed droplet sizes. If membrane emulsification cannot match the capability of current implemented processes within industry i.e. production of comparable droplet sizes at a similar rate, irrespective of the energy savings the business case will not be answered. The loss of production rate is far more likely to damage potential income than save

cost through reduction in energy consumption. Therefore, the capabilities of alternative processes (to membrane emulsification) require exploration prior to comparison to the RME process to determine whether RME can be competitive.

For batch processing, the production rate can be altered simply by changing the processing time or the quantity of material processed in a single operation i.e. the batch size. In this instance, the former is investigated. The processes used were a rotor-stator high shear mixer (HSM) and an ultrasonic probe (SON). An intermediate rotational speed (6000 RPM) or tip velocity (5.5 m s^{-1}) were selected and the processing time was varied between 10-600 seconds (these times were similar to the RME operating times measured in Chapter 4 and 5). The emulsions produced were all 10 v/v % SFO stabilised by 1 wt. % surfactant; these were Tween 20 either in the aqueous (w) or organic (o) phase or SDS. The results are shown in Fig. 6.8:

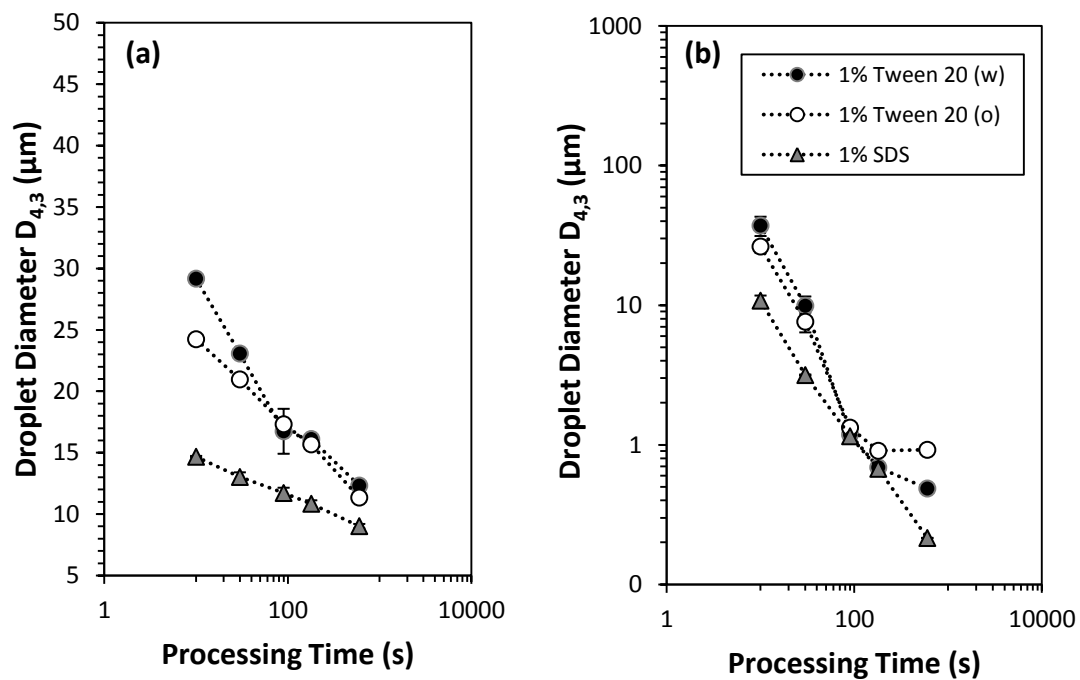


Fig. 6.8: The effect of processing time on the emulsion droplet size produced using: (a) Rotor-stator high shear mixer (HSM) at 6000 RPM and (b) Ultrasonic probe (SON) at 5.5 m s^{-1} tip speed.

It is clear that with increasing processing time, the droplet size decreases. This is explained simply by the droplet experiencing continual break up within regions of shear (cavitation) for a longer period. As the droplet becomes smaller, the Laplace pressure increases significantly such that the droplet is able to resist deformation and hence break-up. It is apparent that the droplet size decrease with SON is much more dramatic than for the HSM; using Tween 20 (w) as an example, SON droplet sizes decrease from 37.3 μm to 0.5 μm whereas for HSM, the decrease is 29.2 μm to 12.3 μm . SON is a higher energy process (as will be discussed further in Section 6.5) which enables the formation of sub-micron droplets. A slight plateau in droplet size can be observed for SON when using Tween 20 at the longer processing times; it is possible that the surfactant available for adsorption has been exhausted and therefore the system is incapable of stabilising a greater interfacial area. An alternative explanation would be that the Tween 20 cannot adsorb sufficiently quickly to prevent droplet coalescence (i.e. the 'back-reaction'). In the case of SDS, the surfactant can quickly stabilise droplets as small as 0.2 μm aided by electrostatic repulsion to keep droplets as separate entities. The IFT of SDS systems is lower which facilitates easier break-up of droplets. The effect of surfactant positioning is minimal compared to membrane emulsification processing (except at the shortest processing times). The repeated break-up of droplets means the primary surfactant transport mechanism is convection. As such, the system is mechanically forced to approach the equilibrium IFT value of which surfactant positioning does not make a difference, so droplet break-up towards the end of the process occurs to a similar extent.

Re-plotting the above data as production rate and comparing to RME data presented in Chapter 5 (where the TMP is used to control the production rate), it can be observed within Fig. 6.9 that generally the droplet size for all processes increases as the production rate is increased from 0.7-39.7 kg h^{-1} . Ideally, the production rate should be high from a manufacturer's perspective to create more emulsion product. Although SON is able to produce sub-micron droplet sizes, this advantage is lost at higher production rates $> 4.4 \text{ kg h}^{-1}$. What is important to note is that by positioning the surfactant in the dispersed phase for RME i.e. 1 wt. % Tween 20 (o), the droplet sizes

are in a similar range to HSM and SON even at production rates above 8.0 kg h^{-1} . This is despite a much lower energy input. Thus, ensuring the rapid adsorption of surfactant is paramount if RME is to be competitive with other processes (at least for small-scale processing).

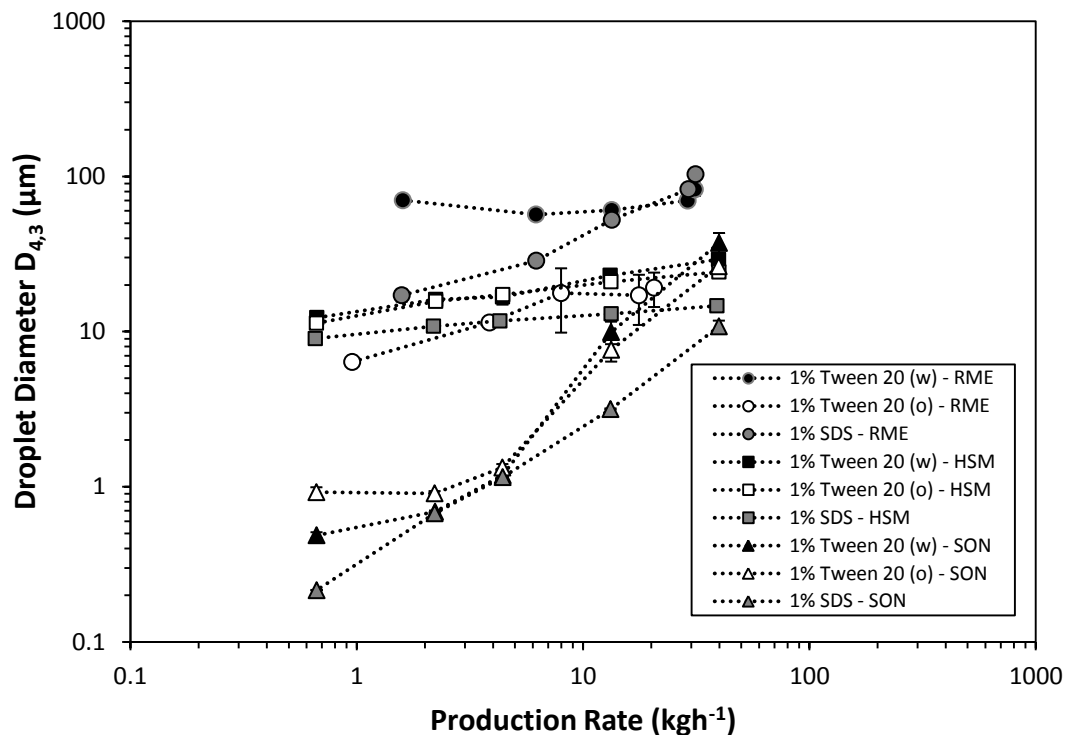


Fig. 6.9: The effect of varying processing time and subsequently the production rate on the emulsion droplet size produced. Power consumption: Rotating Membrane Emulsification (RME) = 16.4 W, Rotor-stator High Shear Mixer (HSM) = 70.9 W, Ultrasonic Probe (SON) = 102.2 W.

6.5 Process Comparison on the Basis of Energy Consumption

It is widely reported that membrane emulsification utilises energy to produce emulsions in a much more efficient manner due to the avoidance of repeated droplet break up and re-coalescence (Gijsbertsen-Abrahamse *et al.*, 2004; Jafari *et al.*, 2008; Charcosset, 2009). However, this efficiency is yet to be determined for production of emulsions that match both the droplet size and the throughput. Whilst RME may be able to produce very small droplet sizes in a controlled way (generally under low TMP conditions), the long operation times mean the energy savings may be lost

(Joscelyne and Tragardh, 2000). The idea behind the following experiments was to demonstrate the process energy efficiency of the RME process in comparison with the HSM and SON processes.

The energy input during processing can be dramatically modified by altering the speed of which the mechanical workings that impart shear/cavitation operate at. For HSM, this is quantified typically by the rotational speed and for SON, the tip velocity can be used (a function of the % of the maximum amplitude for a fixed oscillation frequency). The droplet size data of the 10 vol. % SFO in water emulsions is shown in Fig. 6.10:

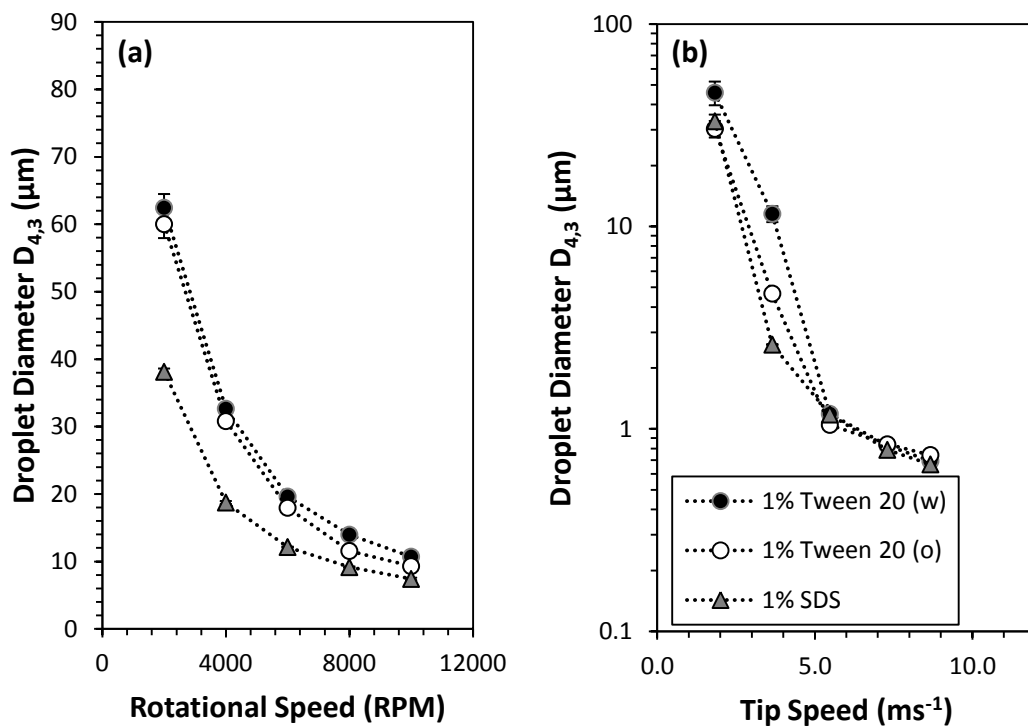


Fig. 6.10: The effect of varying the process mechanical speed on the resulting emulsion droplet size. For the HSM (a), this was rotational speed of the rotor and for SON (b), this was the tip speed. The processing time (90 seconds) and batch size (110 ml) were kept constant.

From theoretical discussions, it is unsurprising that with greater mechanical speeds, droplets are broken-up more to be smaller. This occurs until a minimum droplet size is produced of which the energy input is unable to overcome the Laplace pressure. It is clear from Fig. 6.10 (b) that the amount of surfactant used can stabilise the interfacial area resulting from droplet sizes $< 1 \mu\text{m}$. This

therefore suggests for the HSM, the surfactant is yet to be exhausted for droplet sizes $< 10 \mu\text{m}$ and that the shear forces are limiting factor enabling further break-up.

Fig. 6.11 shows the amount of energy input per volume to formulate an emulsion against the droplet diameter achieved. The emulsion production rate was between $3.7\text{-}6.2 \text{ kg h}^{-1}$. With consideration against RME data shown in Chapter 5, it can be seen that RME is further towards the left side of scale; the energy densities are orders of magnitude lower than HSM and SON with values between 3.2×10^3 and $3.0 \times 10^4 \text{ kJ m}^{-3}$. For HSM and SON, the energy densities were between 2.1×10^4 and $1.5 \times 10^5 \text{ kJ m}^{-3}$.

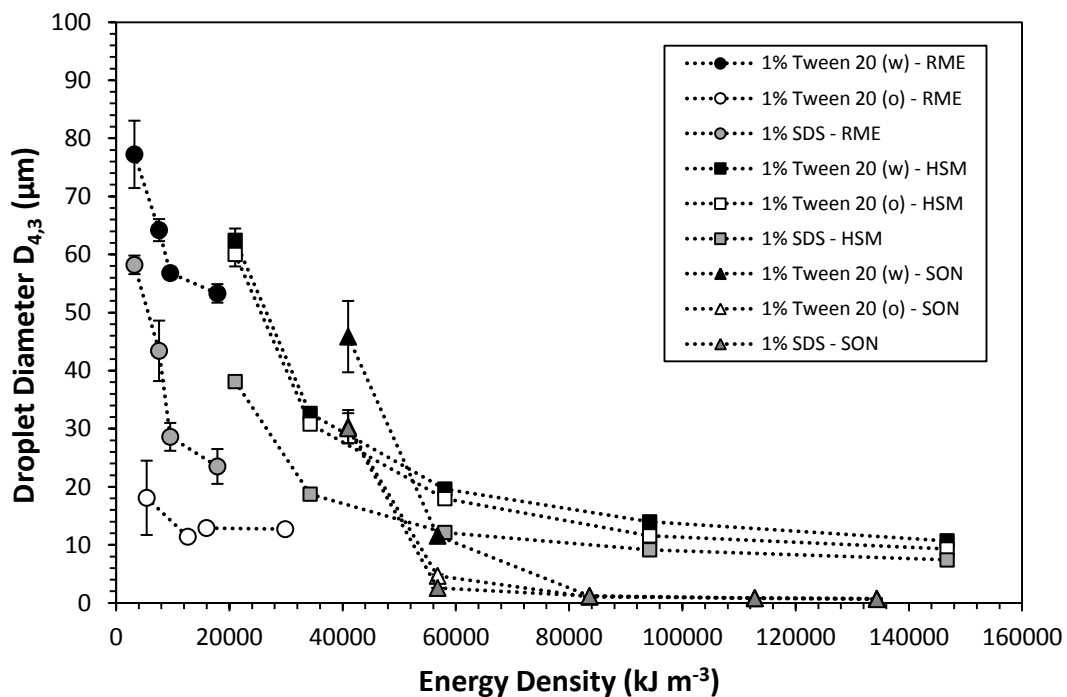


Fig. 6.11: The energy density utilised to produce emulsions containing 10 vol. % sunflower oil at a rate between 3.7 kg h^{-1} to 6.2 kg h^{-1} (depending on dispersed phase viscosity in case of RME).

What is important to notice is that although droplet sizes with 1 wt. % Tween 20 (w) and 1 wt. % SDS are generally larger for the RME process, if rapid adsorption of surfactant can be realised as in the case of 1 wt. % Tween 20 (o), the droplet sizes produced is able to at least match those of the other processes at much less energy input. For an O/W emulsion stabilised by 1 wt. % Tween 20,

RME can form droplet sizes between 11.4-18.1 μm with energy densities values $<3.0 \times 10^4 \text{ kJ m}^{-3}$. For HSM, this region is obtained with energy density values $>5.8 \times 10^4 \text{ kJ m}^{-3}$. For SON, approximately $>5.0 \times 10^4 \text{ kJ m}^{-3}$ is needed. This therefore emphasises the potential of RME for production of emulsions in a more energy efficient manner without necessarily compromising the dispersed phase flux and hence production rate. Another further consideration is the energy wasted as thermal energy input. For RME there was no change in the sample temperature as a consequence of processing. For HSM the bulk temperature (per 110 ml) increased by 0.7-3.8°C whilst for SON this value was between 3.0-18.4°C (not accounting for heat losses). Hence, both the HSM and SON demonstrate potential unsuitability for certain ingredients (e.g. possible protein denaturisation) if one considers localised temperatures may far exceed those of the bulk temperature (alongside the energy being wasted in the form of heat). Whether this energy advantage is upheld for more concentrated emulsion systems remains to be seen, but it is hypothesised this is unlikely given the energy consumption will scale at best with linear behaviour against the processing time required.

6.6 Conclusions

A number of models relating to droplet coalescence and droplet size prediction have been derived and tested within this chapter. In addition, rotating membrane emulsification has been compared to a rotor-stator high shear mixer and an ultrasonic probe both on the basis of emulsion production rate or energy consumption versus the droplet size. From this work, a number of conclusions can be drawn.

Firstly, the probability of coalescence can be predicted for non-regular array membrane materials (e.g. SPG) by considering the two extreme cases of active pore distribution; equidistant and random. Applying the derived model to data obtained in Chapter 4, the former case suggested coalescence to be unlikely whilst the latter suggested it would occur in at least 80% of droplet formation instances. Since active pore distributions with SPG membranes are randomised, this implies coalescence is likely and hence explains the relatively large droplet to pore size ratio obtained (8.6-17.2).

Secondly, a force balance model was adapted for rotating membrane emulsification. The primary forces enabling droplet detachment are the drag, buoyancy and static pressure forces. Comparing against a range of processing and formulation parameters, the model over-predicted the droplet size in the majority of cases. This is despite not accounting for further addition of dispersed phase as the droplet detaches and also applying a static, equilibrium interfacial tension value. It is therefore suggested that the spontaneous transformation-based droplet formation mechanism plays a role in enabling earlier droplet detachment. This may need to be included for future models. However, the model in its current form can still be applied as a simple process optimisation tool.

Finally, comparing rotating membrane emulsification to other processes reveals that by ensuring rapid, efficient adsorption of surfactant (namely through positioning a high HLB non-ionic surfactant within the dispersed phase), this enables rotating membrane emulsification to be highly

competitive. This is on the basis of producing comparable droplet sizes at a similar rate of production (8-20 kg h⁻¹) for 10 vol. % dispersed phase O/W emulsions. The advantage of energy efficiency is maintained whilst minimum thermal stress is imparted on the emulsion structure. The findings therefore reflect favourably on rotating membrane emulsification and its potential for exploitation within industry, at least for the production of dilute emulsion systems (< 10 vol. % dispersed phase).

Chapter 7:

Operation using a Pilot-scale Rotating Membrane Emulsification Device

This chapter discusses initial findings using a novel, pilot-scale rotating membrane emulsification device for batch sizes greater than 8 kg. A recommended design procedure is outlined from findings made across the two process scales investigated within this thesis.

Discussion contained within this chapter has been published within:

Spyropoulos, F., Lloyd, D.M., Hancocks, R.D., Pawlik, A.K. (2014). Advances in Membrane Emulsification. Part B: Recent developments in Modelling and Scale-up approaches. *Journal of the Science of Food and Agriculture*, 94 (4) 628-638.

7.1 Introduction

The aim of this chapter is to investigate the capabilities of a pilot-scale RME device as a proof of concept. Since the inception of membrane emulsification at the start of the 1990s (Nakashima *et al.*, 1991), the process has been demonstrated to offer numerous benefits over conventional emulsification techniques as evident in the previous chapters. Advantages such as less energy consumption, lower shear, a more efficient use of surfactant, good process repeatability and a significant level of control over droplet size are typically cited in literature (Joscelyne and Tragardh, 2000; Charcosset *et al.*, 2004; Gijsbertsen-Abrahamse *et al.*, 2004). Yet, to date there is only one documented case of using membrane emulsification industrially; ‘Yes light’, a low fat butter substitute by Moringa Milk Industry in Japan. It is therefore very surprising that the process has not been exploited further. This can possibly be attributed to a lack of validated scale-up theories and approaches. The research conducted using this pilot-scale RME device should therefore enable the development of such approaches as one shifts across different scales of production.

The approach adopted here is to use both a greater membrane effective surface area (97.4 cm²) within a larger vessel (12 litres maximum capacity). Given the working volume of continuous phase was around 8 litres, very dilute emulsions of less than 1 vol. % dispersed phase of SFO were produced in order to conserve material (this was still around 70 g of oil per experimental run). A laser drilled stainless steel membrane of 26 µm was used since fragile materials such as SPG and ceramic membranes would be unlikely to withstand the mechanical stresses during operation. The applied TMPs investigated were much higher than the capabilities of the small-scale device (up to 4 bar). Additionally, the rotational speed could be altered to values between 100 and 4000 RPM, corresponding to shear rates between 2.23 s⁻¹ and 89.1 s⁻¹. For very high ratios of TMP to capillary pressure, the shear rate needs to be high for stable emulsion droplet production.

7.2 Effect of Transmembrane Pressure

Fig. 7.1 shows the resultant droplet diameter stabilised by 1 wt. % Tween 20 (within the continuous phase) with variation in the TMP. The rotational speed was held constant at 1000 RPM which applied a shear rate at the membrane surface of 22.3 s^{-1} .

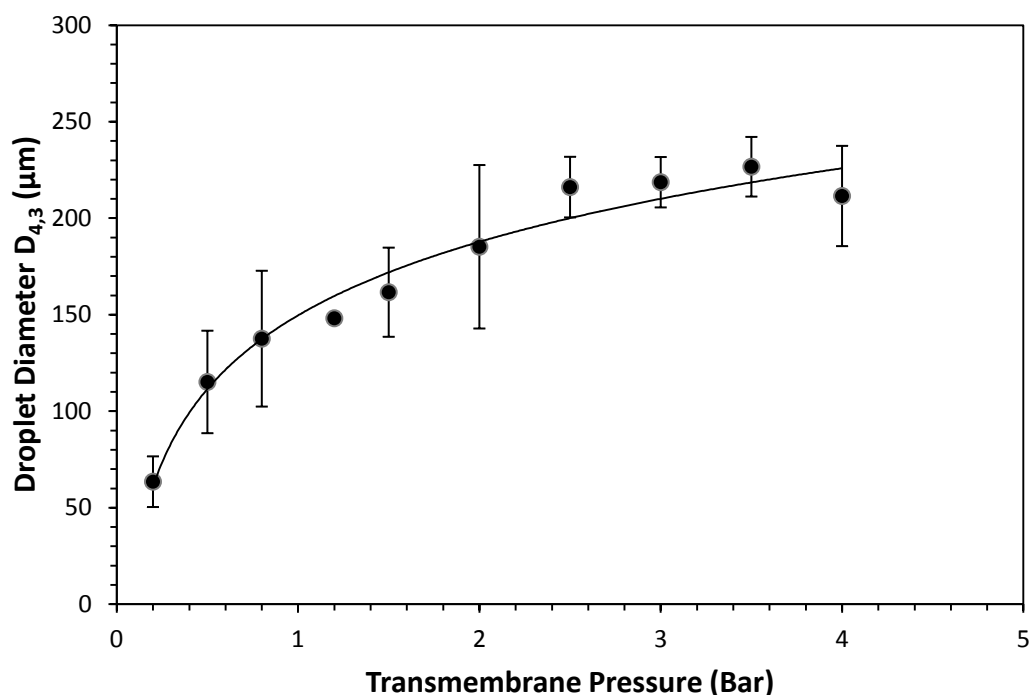


Fig. 7.1: The effect of transmembrane pressure on the mean droplet size using a pilot-scale rotating membrane emulsification device. The emulsions are approximately 1 vol. % sunflower oil stabilised by 1 wt. % Tween 20 within the continuous phase. The error bars represent one standard deviation of a triplicate of experimental runs.

It is apparent that the relationship between TMP and droplet size is different from that seen when using an SPG membrane (e.g Fig 4.4 in section 4.2.1). In this case, larger droplet diameters are produced at higher TMPs. For example, at 0.2 bar the droplet diameter is $63 \mu\text{m}$ whereas at 2.5 bar the size is $216 \mu\text{m}$. This is attributed to the greater rate of droplet inflation relative to the rate of IFT decrease to enable detachment. The coalescence region is not observed at low pressures (as was the case using the SPG membranes) because the pore spacing is sufficiently wide (0.5 mm or $500 \mu\text{m}$) such that droplets will not interact during formation. This emphasises the advantage of

membranes consisting of a regular array of pores since the spacing between adjacent pores can be controlled to limit coalescence phenomena. In the absence of coalescence, this relationship between droplet size and TMP is expected (Wagdare *et al.*, 2010). It is evident that the error bars across the data set are generally large indicating droplet formation is not a uniform process. However, this is likely to be due to the wide pore size distribution from drilling inaccuracy during fabrication of the membrane. Additionally, considering the dispersed phase flux behaviour shown in Fig. 7.2, the values presented corresponds to pore fluid velocities up to 0.017 m s^{-1} i.e. an order of magnitude higher than with the SPG membranes. As a consequence, the dispersed phase capillary number is likely to be sufficiently high (>0.056) even at the lowest TMPs such that jetting could occur and hence droplet formation is unstable and erratic. The flux increases between $4.7\text{-}123.2 \text{ L m}^{-2} \text{ h}^{-1}$ at a rate directly proportional to the TMP to the power of 1.05. It was expected the relationship would be linear (i.e. a power coefficient of 1.00) since the membrane consists of rigid, straight-through pore channels. This therefore suggests that there is a very slight increase in membrane permeability associated with activation of pores.

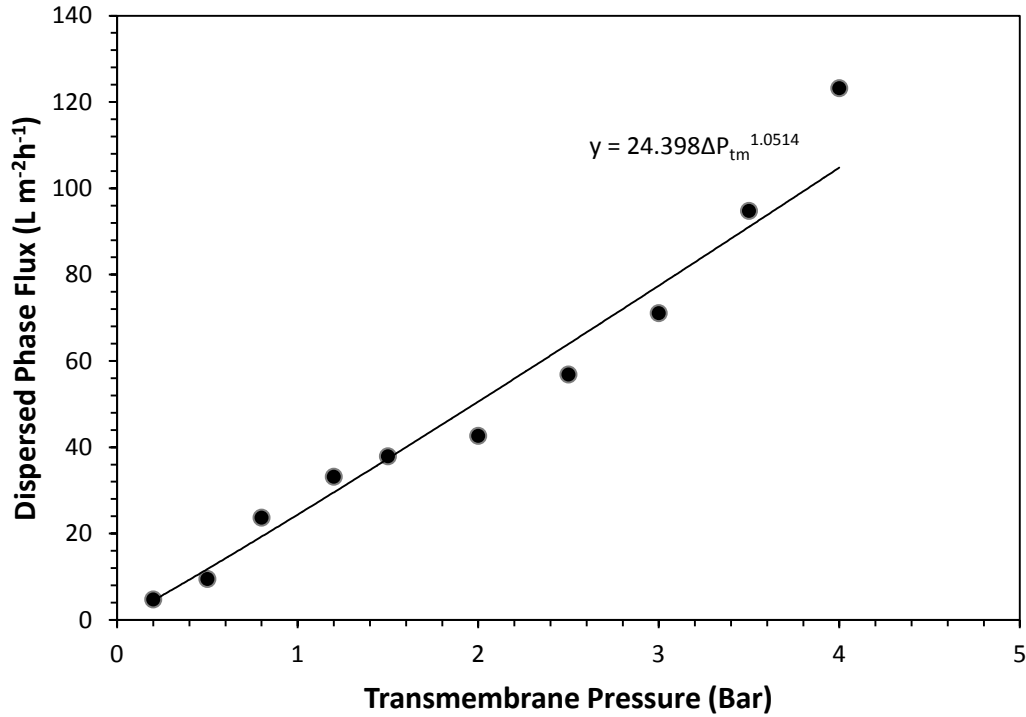


Fig. 7.2: Influence of transmembrane pressure on the dispersed phase flux at 1000 RPM for a 26 μm pore diameter, stainless steel membrane.

7.3 Effect of Rotational Speed

The effect of membrane rotational speed on the emulsion droplet size is shown in Fig. 7.3 at a TMP of 0.5 bar and 1 wt. % Tween 20 within the continuous phase. This TMP value was selected in order to add the dispersed phase sufficiently quickly whilst also being just below the jetting point. As the rotational speed was increased from 100 RPM to 4000 RPM, this increased the shear rate linearly from 2.23 s^{-1} to 89.1 s^{-1} . As a consequence, the droplet diameter decreased due to higher drag force to aid droplet detachment from the membrane surface. In all cases, Taylor vortices were present since under the lowest rotational speed of 100 RPM and annular gap width of 0.1m (fixed), the Taylor number exceeded 2700 indicating turbulent flow behaviour.

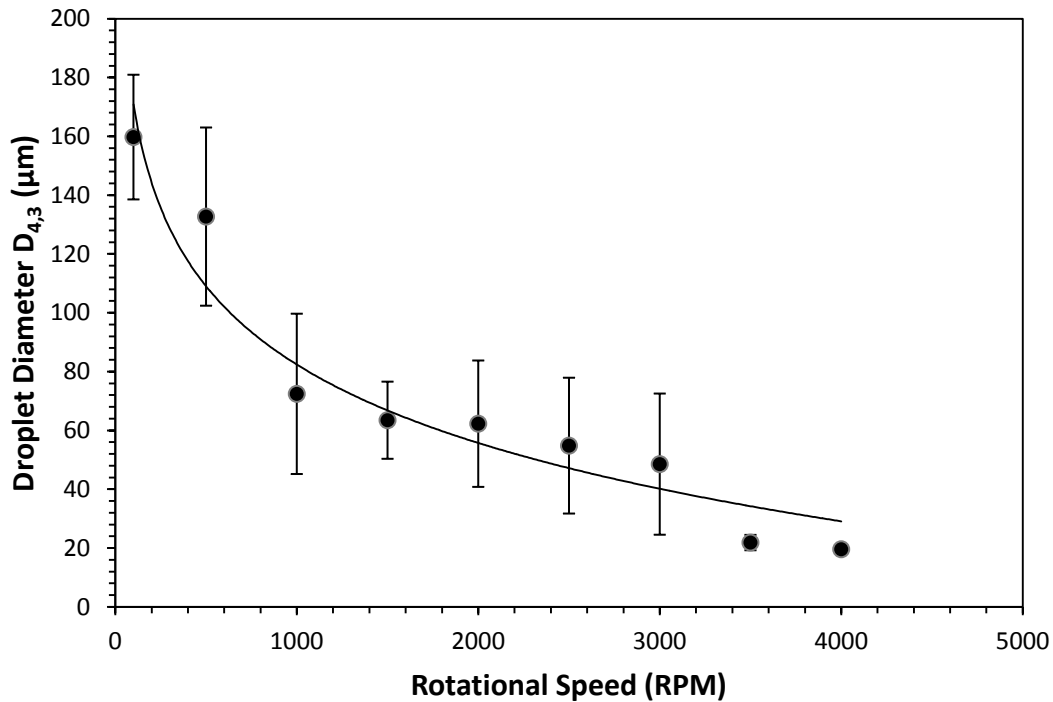


Fig. 7.3: The influence rotational speed on the mean droplet size at a transmembrane pressure of 0.5 bar. The emulsions are 1 vol. % sunflower oil stabilised by 1 wt. % Tween 20 within the continuous phase. The error bars represent one standard deviation of a triplicate of experimental runs.

Interestingly, at rotational speeds greater than 3500 RPM, the droplet size produced was between 19.6-21.9 μm . This indicates with sufficiently high detachment forces, the droplet diameter formed can be smaller than the pore diameter. Vladisavljevic and Williams (2006) also produced droplets smaller than the pore diameter with RME using a laser drilled stainless steel membrane of 100 μm pore diameter. This was the case specifically when operating at faster speeds or with a viscous continuous phase; both significantly applying high shear stress at the membrane surface. Oh et al. (2011) produced nano-sized droplets that were 25 times smaller than the pore diameter (2.5 μm SPG membrane) using a stirred-cell configuration, low TMP and a very high concentration of surfactant. These findings therefore indicate that the droplet size to pore size ratio minimum is much lower than the typically cited value of 2 (Joscelyne and Tragardh, 2000) if the detachment forces are very high or the IFT retention force is low.

7.4 Comparison with Small-scale Rotating Membrane Device

In order to develop the theoretical understanding on how to design the RME process, a comparison between a small-scale and pilot-scale device needs to be undertaken. For this, the processing parameters of TMP and rotational speed are considered to alter the flow behaviour for each of the two scales. The membrane parameters (e.g. pore diameter, porosity) ideally need to be very similar if not identical in order to draw comparison on the droplet formation mechanisms induced by this flow behaviour. Ultimately, this study aims to answer questions related to the physical constraints of the process e.g. how big or how fast does the process need to be to achieve desired outputs such as droplet size and dispersed phase flux?

A stainless steel membrane with almost identical pore size (25 μm) and matching pore spacing (0.5 mm) was tested on the small-scale device. This therefore had similar properties to the pilot-scale stainless steel membrane. The active surface areas of two membranes were 15.7 cm^2 and 97.4 cm^2 which were due to the differences in membrane diameter; 10 and 62 mm respectively. Emulsions of 1 vol. % of dispersed phase stabilised by 1 wt. % Tween 20 were produced across a range of TMPs between 0.2 and 1.5 bar as shown in Fig. 7.4. The rotational speed was held constant at 1000 RPM allowing for the results to be comparable with Fig. 7.1 in section 7.2. Firstly, it is apparent that the relationship between droplet diameter and TMP is very similar to the one observed with the pilot-scale device. Larger droplet diameters are produced with increasing TMP as would be expected in the absence of coalescence at the membrane surface. Secondly, the droplet diameters are significantly larger across a similar TMP range for the small-scale device. The droplet size varies between 240-302 μm between 0.2 bar to 1.5 bar, whilst for the pilot-scale the range is 63.5-162 μm . This therefore suggests that the scaling of the RME process is not simply achieved through matching the RPM.

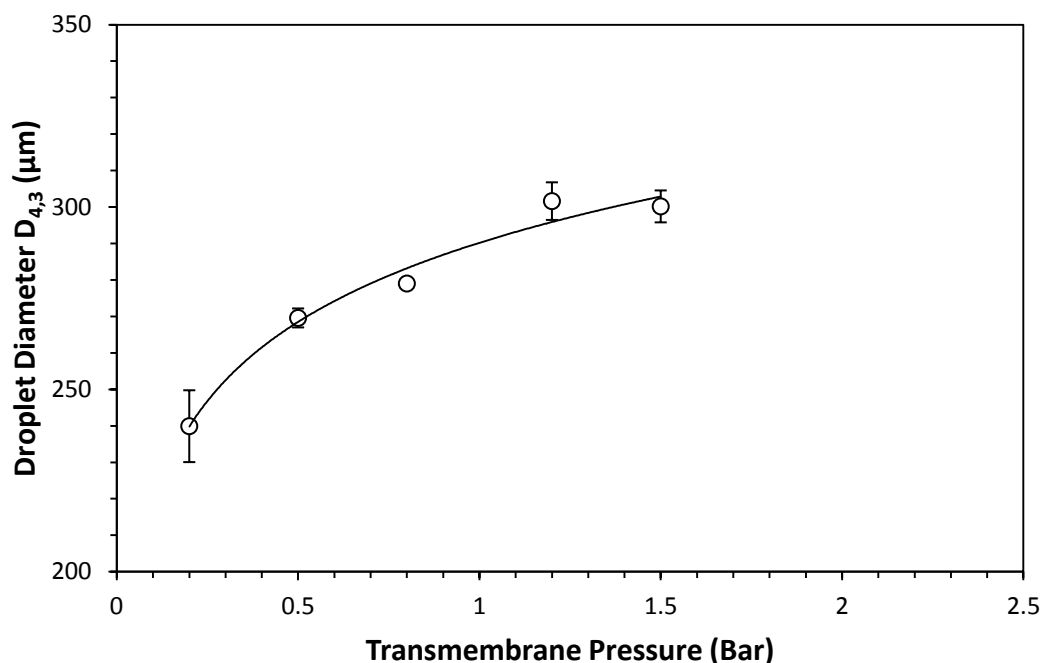


Fig. 7.4: The effect of transmembrane pressure on the mean droplet size using a small-scale rotating membrane emulsification device with a stainless steel membrane. The rotational speed is 1000 RPM and the annular gap width is 25 mm. The emulsions are 1 vol. % sunflower oil stabilised by 1 wt. % Tween 20 within the continuous phase. The error bars represent one standard deviation of a triplicate of experimental runs.

Droplet formation for membrane emulsification as previous discussed in the previous chapters is attributed to an imbalance of forces. For RME, the primary force inducing detachment is the drag force but on the other hand, the centripetal force hinders detachment. Whilst the magnitude of these forces are heavily dependent on the rotational speed with higher speeds resulting in greater force, this term does not appear in the derived equations for each of these forces. This is why matching the rotational speed across the two scales does not yield similar droplet sizes. Instead, the magnitude of these forces is indebted specifically to the velocity that the droplet moves at whilst attached to the membrane surface. The difference between the droplet velocity and membrane surface velocity is negligible given droplet diameters are orders of magnitude smaller than the membrane diameter. At a fixed rotational speed (RPM), the membrane surface of the pilot-scale device is required to move with greater velocity as its circumference is more than six times greater than the small-scale device. Alternatively, one might consider that matching the shear rate at the membrane surface may consequently result in similar droplet sizes. As was apparent in

Chapter 4, the flow behaviour of the continuous phase (whether Taylor vortices can form) is strongly related to the annular gap width alongside the rotational speed. The annular gap width for the small-scale and pilot-scale devices was 25 mm and 69 mm respectively. In order to match the membrane surface velocity and shear rate for the two systems, the small-scale device was operated at 2000 RPM whilst the pilot-scale device was set at 322 RPM (matched velocity) and 537 RPM (matched shear rate). This is summarised in Table 7.1:

Table 7.1: Details of experimental configurations investigated across the small-scale and pilot-scale rotating membrane emulsification devices.

Scale	Matched RPM		Matched Surface Velocity		Matched Shear Rate	
	Small	Pilot	Small	Pilot	Small	Pilot
Relevant Figure	Fig. 7.4	Fig. 7.1	Fig. 7.5 (a)		Fig. 7.5 (b)	
Rotational Speed (RPM)	1000	1000	2000	322	2000	537
Membrane Surface Velocity (m s^{-1})	0.52	3.25	1.05	1.05	1.05	1.75
Shear Rate (s^{-1})	5.98	22.3	12.0	7.18	12.0	12.0

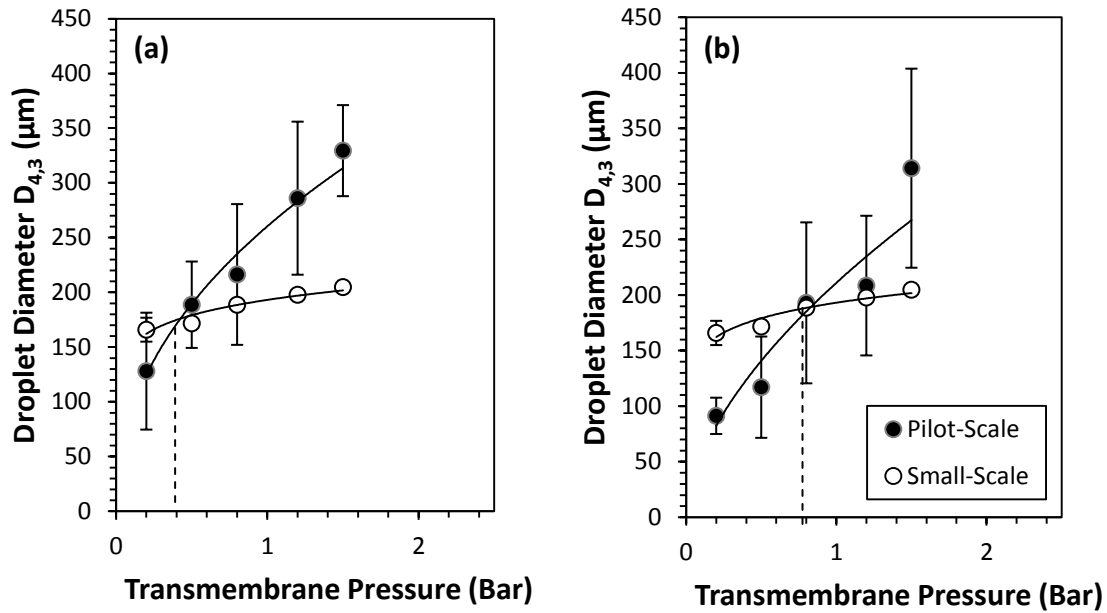


Fig. 7.5: The effect of transmembrane pressure on the mean droplet size for matched membrane surface velocity (a) and matched shear rate (b). The emulsions are 1 vol. % sunflower oil stabilised by 1 wt. % Tween 20 within the continuous phase. The error bars represent one standard deviation of a triplicate of experimental runs.

The effect of TMP on droplet diameter is shown for a matched membrane velocity of 1.05 m s^{-1} (Fig. 7.5 [a]) and matched shear rate of 12.0 s^{-1} (Fig. 7.5 [b]). Irrespective of the scalable parameter used, the droplet diameter increases with increasing TMP. However, it is apparent there is a transitional point in which droplet diameters produced using the pilot-scale device are larger than those by the small-scale device. It is hypothesised that given the membrane parameters are very similar and the formulation parameters are the same, that the transitional point is connected to the flow behaviour of both the dispersed phase and the continuous phase. Furthermore, that as the applied TMP is extended beyond this threshold pressure value, that jetting occurs for pilot-scale operation but not for the small-scale explaining the larger droplet sizes. As shown by Pathak (2011), jetting is a function of the flow of both phases. The transitional point shifts as a function of rotational speed of the pilot-scale device with jetting more probable when operating at low speed and hence a more stationary continuous phase. At 322 RPM and 537 RPM, the transitional TMPs are 0.39 bar and 0.64 bar respectively, whilst at 1000 RPM, the curves do not intersect at all. This

therefore requires consideration since jetting is unfavourable, although operation at a TMP just below the point of jetting is advantageous in maximising the rate of stable droplet production.

The scalable parameters of membrane surface velocity (Fig. 7.6 [a]) and shear rate (Fig. 7.6 [b]) were investigated further for a fixed TMP of 0.5 bar across the two scales. This was achieved by varying the rotational speed of the membrane between 100-2000 RPM for the small-scale device and 100-4000 RPM for the pilot-scale device (as with Fig. 7.3). In both instances, increasing the velocity or shear rate results in a decrease to a size independent of the scalable parameter used. The droplet diameter limit is governed primarily by the interfacial tension between the oil/water interface, the viscosity of the respective phases and the pore diameter. Inspection of the two curves reveals the most suitable scalable parameter is membrane surface velocity. There is a smoother transition from small-scale to large-scale emulsion production (at a given TMP) as shown by the R^2 values. However, this would require further investigation (perhaps at another scale of production) in order to validate this suggestion.

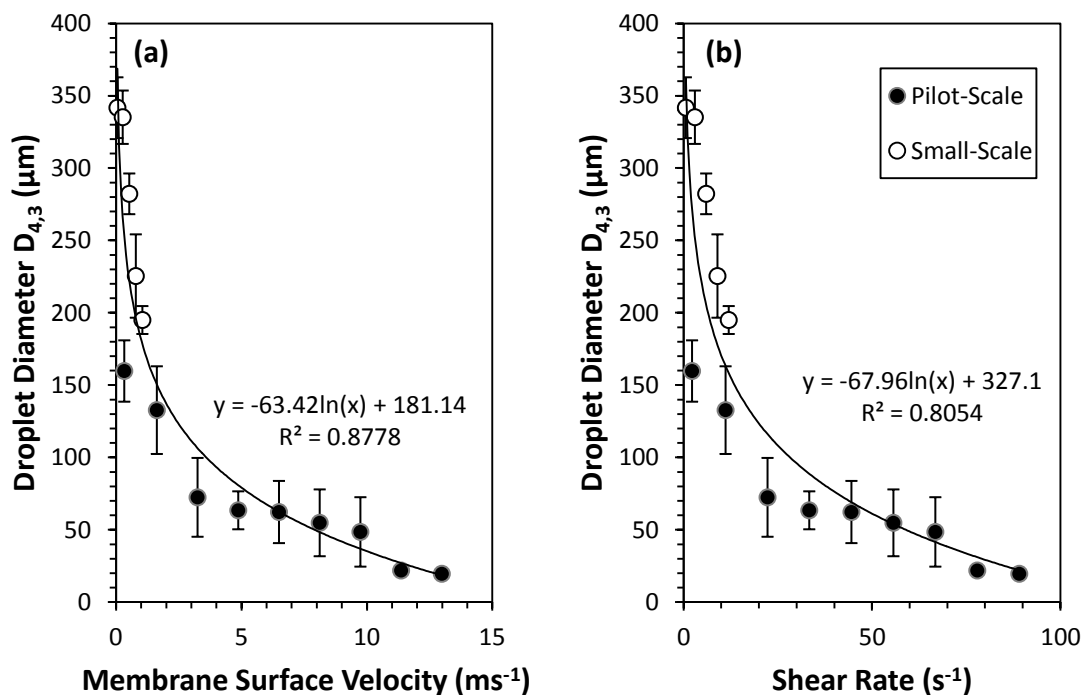


Fig. 7.6: The effect of Membrane surface velocity (a) and Shear rate (b) on the mean droplet size produced. The emulsions are 1 vol. % sunflower oil stabilised by 1 wt. % Tween 20 within the continuous phase. The error bars represent one standard deviation of a triplicate of experimental runs.

7.5 Effect of Surfactant Type/Concentration

As was shown within the previous section, for the pilot-scale RME device the droplet size tends to a minimum value with increasing rotational speed/shear rate/membrane surface velocity. At this point, the droplet size is limited by factors such as the IFT holding the droplet at the membrane surface. This was therefore investigated further by altering the surfactant type and concentration to modify the IFT, allowing for exploration of the process limit to form droplets smaller than the membrane pore diameter. The process parameters were optimised with a TMP of 0.5 bar and a rotational speed of 4000 RPM in order to minimise the droplet diameter whilst also achieving reasonable dispersed phase flux. The non-ionic surfactant Tween 20 was compared to anionic SDS (within the continuous phase) since the latter imparts the droplet interface with a negative electrostatic charge which can minimise possible droplet coalescence. The concentration of surfactant ranged between 0.01-2 wt. % to alter the rate of IFT decrease as shown within Chapter 5.

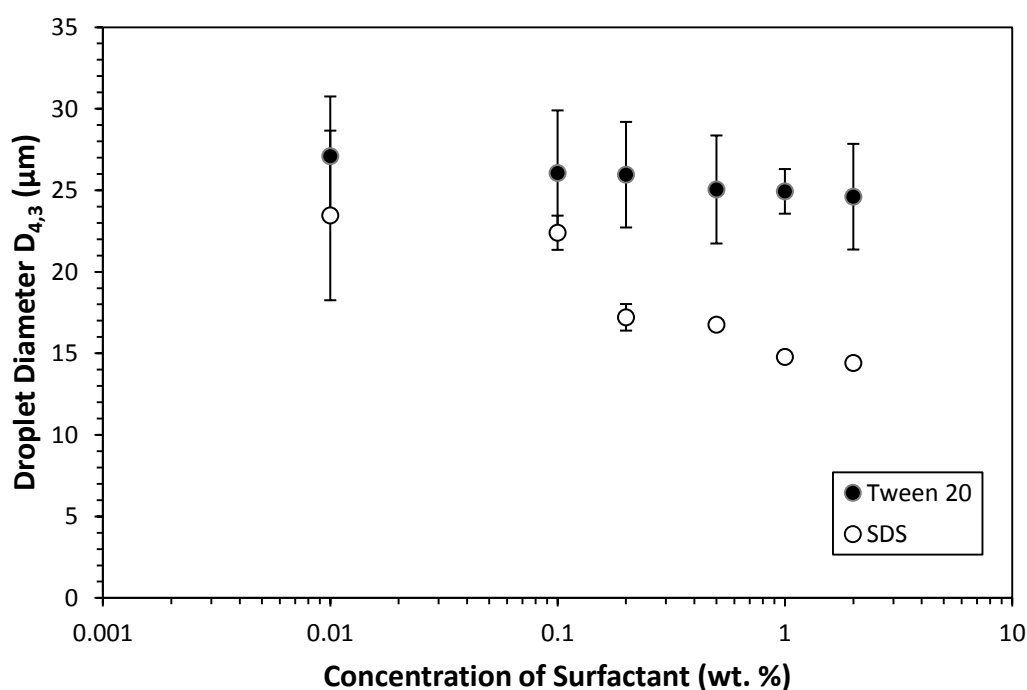


Fig. 7.7: The effect of surfactant concentration on the mean droplet size for different surfactant types positioned within the aqueous continuous phase. The emulsions are 1 vol. % sunflower oil in water. The transmembrane pressure is 0.5 bar and the shear rate is 89.1 s^{-1} . The error bars represent one standard deviation of a triplicate of experimental runs.

Under these optimised processing conditions, it is illustrated within Fig. 7.7 that with increasing Tween 20 concentration, a very slight decrease in droplet diameter is observed (from 27.1 μm to 24.6 μm ; a decrease of 9.2%). For SDS, a sudden drop in droplet size can be seen at 0.2 wt. % which is close to the CMC (0.22 wt. %). Below 0.2 wt. % of SDS, larger droplets between 22.4-23.5 μm are produced since the surfactant monomer is depleted from the continuous phase over time and so the IFT is higher. At an SDS concentration beyond the CMC, again a minimal decrease in size is evident from 17.2 μm at 0.2 wt. % to 14.4 μm at 2 wt. % (decrease of 16.3%). Generally, SDS produces smaller droplet sizes than Tween 20 since the IFT is lower as was observed in Fig. 5.3. Furthermore, the effect of increasing concentration relative to droplet size reduction is minimal compared to operation at the small-scale (Fig. 5.2). This is due to the dominance of the detachment forces over the retaining IFT force such that small variations in the IFT force have a negligible effect.

7.6 Effect of Surfactant Positioning

It has been previously shown that positioning non-ionic, high HLB surfactants within the dispersed phase (as opposed to their conventional positioning within the continuous phase) is advantageous if the aim is to produce small droplets. In this case, blending surfactant with oil was demonstrated to reduce the IFT of the system very quickly to a value below the equilibrium IFT (measured at long time scales). As a consequence, droplets could detach very early from the membrane surface at a smaller diameter since the surfactant moves towards the interface quickly due to its partitioning coefficient. This concept was investigated (using Tween 20) for the pilot-scale device to examine whether this advantage is still upheld. For modification of the TMP between 0.2 and 4 bar, the rotational speed was constant at 1000 RPM (Fig. 7.8 [a]) whilst for the study of rotational speed effects, the TMP was set at 0.5 bar (Fig. 7.8 [b]).

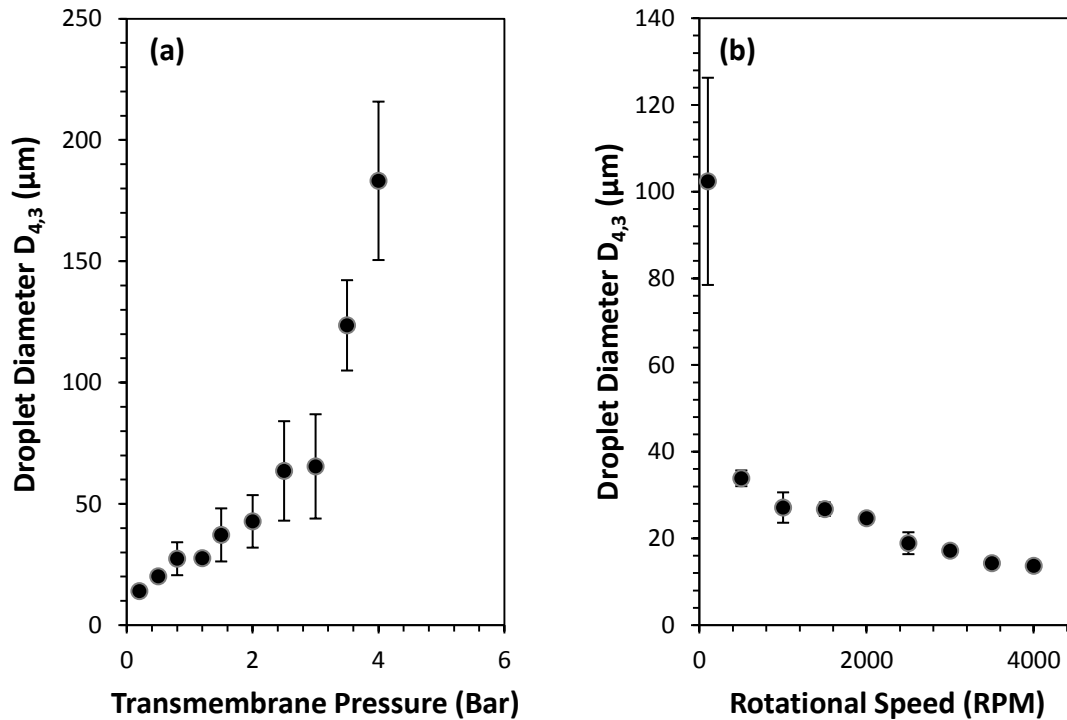


Fig. 7.8: The effect of transmembrane pressure (a) and rotational speed (b) on the mean droplet size using a pilot-scale rotating membrane emulsification device. The emulsions are approximately 1 vol. % sunflower oil stabilised by 1 wt. % Tween 20 within the dispersed phase. The error bars represent one standard deviation of a triplicate of experimental runs.

It is clear that positioning the surfactant within the dispersed phase (o) using the pilot-scale RME device generally forms small droplets compared to when Tween 20 is within the continuous phase (w) as shown in section 7.2 and 7.3. Focussing on Fig. 7.8 (a) the droplet size increases at higher TMP as expected when coalescence is minimised. Across the TMP range, droplet sizes between 14.0 μm and 183 μm are produced which are smaller than with Tween 20 (w) as was shown in Fig. 7.1 (63.5-212 μm). This is due to differences in the IFT between the two systems. Whilst the IFT is lower for the Tween 20 (o), jetting did not occur until the TMP exceeded 3 bar in which the droplet size increased rapidly with large variation between experimental runs (wide error bars). The viscosity increase caused by blending Tween 20 with the dispersed phase results in a greater resistance to flow and hence a lower pore fluid velocity. In the case of modifying the rotational speed (Fig. 7.8 [b]), again the droplet diameter is much smaller with Tween 20 (o); between 13.7-102 μm , compared to Tween 20 within the continuous phase (19.6-160 μm). Droplet detachment is achievable under low shear if the IFT force holding the droplet is small such that even at a speed of

1500 RPM for example, droplets roughly the same diameter as the pore diameter (26.8 μm) could be created. For Tween 20 (w), the rotational speed had to exceed 3000 RPM for the droplet size to pore size ratio to equal 1. This suggests that by using surfactant in this way, processing can be undertaken at a lower rotational speed (and hence less energy consumption) since inducing droplet detachment is much easier.

7.7 Energy Considerations

Within Chapter 6, it was demonstrated that a small-scale RME device could be competitive with both a rotor-stator mixer and an ultrasonic probe for emulsion production. This is on the basis of droplet size and production rate whilst using less energy. It is expected that a pilot-scale device will require a greater energy input in order to rotate a much larger, heavier cylindrical membrane. As such, questions could arise as to whether the energy advantage is upheld as a consequence of up-scaling. Therefore, this clearly required consideration. The energy input (and hence energy density) was modified by altering the rotational speed at a TMP of 0.5 bar i.e. using the data presented in Fig. 7.3 and Fig. 7.8 (b) for a production rate of 10 kg h^{-1} . The results are shown below in Fig. 7.9.

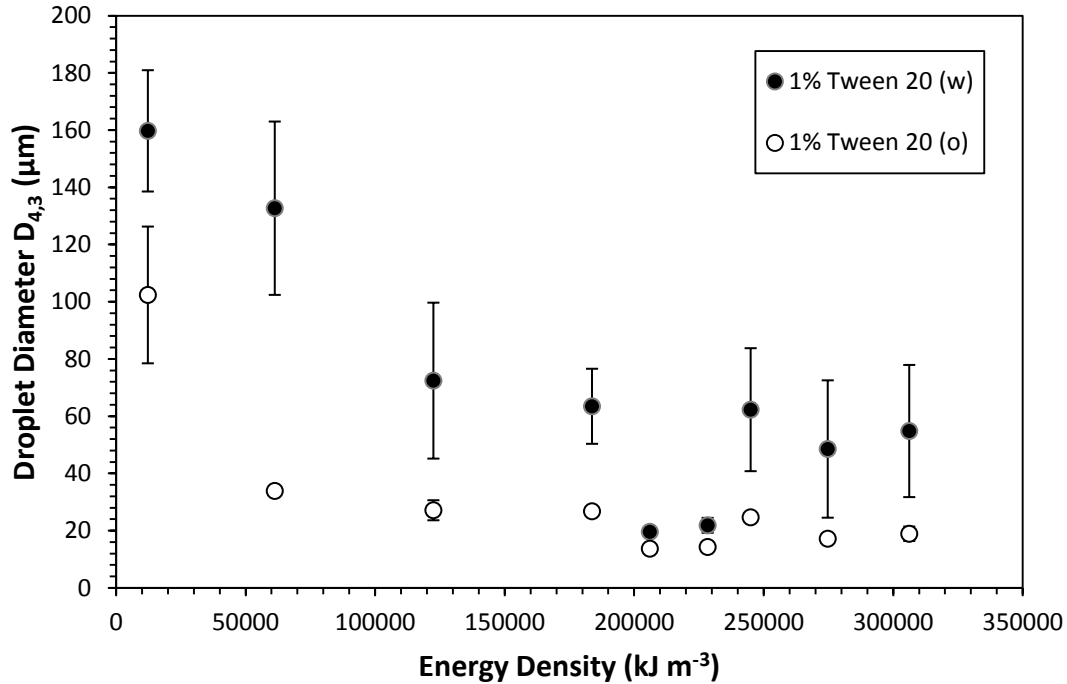


Fig. 7.9: The energy density utilised to produce emulsions containing ≈ 1 vol. % sunflower oil at a rate of 10 kg h^{-1} . A constant TMP of 0.5 bar is applied whilst the rotational speed is varied between 100-4000 RPM.

As observed with the small-scale processes, generally increasing the amount of energy input to form the emulsion results in the production of smaller droplet sizes. Surprisingly, rotational speeds of 3500-4000 RPM utilise less energy than 2000-3000 RPM as was specified by the power curve provided by the manufacturer. However, this concept is similar to a motorised vehicle engine in which there is an optimum speed to travel at for maximum fuel efficiency based on rotational frequency. It is therefore apparent that operating at speeds greater than 3500 RPM is beneficial both in maximising the membrane surface velocity and hence the drag force required to enable droplet detachment, but also to operate more energy efficiently. By utilising the surfactant within the dispersed phase, this suggests that operating at even lower speeds (≈ 1000 RPM) allows for the production of droplet sizes smaller than when positioned within the continuous phase. Operation at very high rotational speeds may therefore be unnecessary when the role of interfacial tension minimisation to enable detachment is more critical. The energy density range investigated (1.2×10^4 to $3.1 \times 10^5 \text{ kJ m}^{-3}$) is broader than the values explored at the small-scale. Despite non-optimised

processing and membrane parameters (large pore diameter, low porosity), RME still maintains the potential to be more energy efficient than other emulsification processes although perhaps not to the extent as observed at the small-scale. A more rigorous study is required using smaller pore, higher porosity membranes is required in order to fully explore the capabilities of the pilot-scale device and its advantage over other emulsification methods.

7.8 Recommended Procedure for Process Design

Analysis of the experimental data presented within this thesis has allowed for a significant understanding of the processing mechanisms involved within rotating membrane emulsification. Combining this work within the existing knowledge contained within the literature enables the inception of a possible procedure to design such a piece of equipment. However, in order to implement such a guide relies upon the desired droplet size and production rate (i.e. dispersed phase flux) to be specified. Furthermore, the physicochemical properties of the emulsion system (e.g. interfacial tension, dispersed phase viscosity) and the membrane pore activation behaviour under applied pressure must be well characterised. Assuming these input parameters are known, the following procedure is recommended:

1. Select a membrane with the appropriate pore size and surface properties

Ensure the pores are sufficiently small to form the desired droplet size. Emulsion droplets for O/W emulsions can be between a ratio of 1-15 times larger than the pore diameter. If the surfactant adsorption kinetics is fast or the interfacial tension is low, a larger pore size may be suitable since the droplet to pore size ratio is likely to be lower.

It is also important that hydrophilic charged membranes are used for O/W emulsion production and hydrophobic charged membranes for W/O emulsions to ensure the dispersed phase does not wet the membrane surface and potentially cause coalescence.

2. Check pore spacing is suitable between adjacent forming droplets

Steric hindrance of droplets as they are forming can result in a much less controlled emulsion microstructure. It is recommended that the pore spacing is either 1.5 times the desired droplet diameter (to consider possible droplet distortion due to detachment forces) or 10 times the pore diameter; whichever is the larger value to reduce the probability of coalescence. For materials with random pore activation (e.g. glass and ceramic membranes), more care is required since pores are very unlikely to be evenly distributed so evaluate whether the distance between active pores will be great enough under the likely TMP range to be applied.

3. Evaluate the transitional point from dripping to jetting droplet formation mechanism

For well controlled droplet production, droplets must form within the dripping regime. Although the exact transitional point can vary depending on the Weber and Ohnesorge numbers of the continuous phase, calculation of the Capillary number for the dispersed phase using Eq. 2.10 can determine whether jetting is likely. An approximate value of critical Capillary number is 0.056 (Sugiura *et al.* 2002). Therefore substituting the threshold value alongside the system interfacial tension and the dispersed phase viscosity and then rearranging yields the pore fluid velocity that would instigate jetting. Operating below this point is favourable in producing narrow droplet size distributions.

4. Calculate the volumetric flow rate of dispersed phase required

For a specified production rate (kg h^{-1}) and dispersed phase volume fraction, the volumetric flow rate ($\text{m}^3 \text{h}^{-1}$) can be found. This may involve converting between mass and volume using the density of the respective phases.

5. Calculate the membrane surface area required

With the dispersed phase volumetric flow rate specified and membrane properties and behaviour known, the membrane surface area needed to achieve the necessary flow rate can be calculated as a function of TMP. This is possible by equating Darcy's law to the rate of mass transfer required and rearranging. The pore channel length (L_p) and membrane permeability (K) may require solving using Eq. 2.15 and Eq. 4.2 respectively. It is important to check that the pore fluid velocity does not exceed the value found in step 3. This can be estimated by using Eq. 2.19. If the membrane dimensions are too large, a higher TMP may be required as well as possible reconsideration of the membrane parameters i.e. thickness, pore spacing, pore diameter etc.

6. Consider the aspect ratio of the membrane cylinder

There are a range of options available for ensuring the membrane has the required surface area. Both the membrane length (h_1) and diameter (d_1) are possible variables that can be altered. It is recommended that short membranes of wide diameter are more suitable since the pressure drop of the dispersed phase inside the centre of the tube will be less and the membrane surface velocity to induce droplet detachment will be greater. However, it is vital to consider the likely dimensions of the emulsification vessel of which the membrane is to be situated in, as well as the power requirements of the motor needed to rotate the membrane-mounted shaft.

7. Consider the likely range of rotational speeds to be applied

The range of rotational speeds to be used to control the droplet size depends on the power of the motor and the scale of operation. Higher rotational speeds are more capable of producing smaller droplets and therefore reducing the droplet to pore size ratio. However, the maximum speed to be incorporated within the design will depend on mechanical constraints as well as capital costs, energy consumption etc.

8. Calculate the required dimensions of the emulsification vessel

For the minimum rotational speed, it is important for Taylor vortices to form in order to produce the smallest droplets and a narrow size distribution. Thus, the Taylor number must exceed 41.3. This can be ensured by selecting a suitable emulsification vessel radius. In one respect, the gap size should be small to apply the highest shear at the membrane surface. On the other hand, it is vital that the radius is large enough for the vortices to form within the continuous phase flow. Substituting $Ta = 41.3$ into Eq. 2.22 and rearranging can find the minimum vessel radius (r_2) required. The height of the vessel must be greater than the height of the membrane to ensure all pores are submerged within the continuous phase. In addition, there must be sufficient volume for the dispersed phase to be added without overfilling the vessel.

9. Check industrial applicability of design parameters and scale-up considerations

As a final step, it is necessary to check all calculations are mathematically correct, logical and realistic. The operating time will depend on the volume of dispersed phase to be added to the emulsification vessel and the TMP applied. The droplet size can be controlled by modifying the membrane surface velocity, TMP (at the expense of throughput) or the surfactant concentration (provided jetting of the dispersed phase does not occur). Scale-up can be undertaken by matching the membrane surface velocity provided all other operating parameters are similar. The throughput should scale proportionally with the membrane surface area. Further process optimisation is possible with the use of ionic surfactants to reduce coalescence likelihood or by incorporating high HLB non-ionic surfactants within the dispersed phase. In the latter case, care must be taken to ensure sufficient dispersed phase flux without jetting due to low IFT values.

An example calculation following the above procedure is shown within Appendix A.

7.9 Conclusions

A pilot-scale RME device has been investigated to produce O/W emulsions. Emulsion droplet sizes between 13.7-160 μm were produced using a laser-drilled stainless steel membrane of pore diameter 26 μm . A few key processing and formulation parameters were studied to see their impact on the emulsion microstructure. Furthermore, a procedure to design a RME device based on experimental observations and theory has been outlined and suitable scalable parameters were identified.

For pilot-scale production, it is recommended to use metallic membranes due to the high mechanical forces exerted on the membrane itself due to pressure and rotation. A benefit to using metal material is that the pore spacing can be controlled and therefore selected to minimise coalescence phenomena; an issue problematic for SPG membranes. As a consequence, it was observed that increasing TMP between 0.2 and 4 bar increased the droplet size only. This relationship was more complex as discussed within Chapter 4. However, careful operation is required to avoid droplet formation through jetting under very high TMPs (but also under low shear rates). For the dispersed phase flux, minimal variation in the active pore fraction as a function of TMP was seen due to the use of straight-through pore channels. Flux values between 4.7-123.2 $\text{L m}^{-2} \text{h}^{-1}$ were recorded.

Modifying the rotational speed between 100-4000 RPM demonstrated a similar relationship (seen previously) of decreasing droplet size exponentially to a minimum value. Thus, observations made both earlier within this thesis and in other literature are relevant to pilot-scale operation since the trends at the small-scale are similar. For sufficiently high rotational speeds (>3500 RPM), droplets smaller than the pore diameter can be produced even without reducing the IFT to small values (i.e. positioning non-ionic high HLB surfactants in the dispersed phase). The IFT is less important when greater detachment forces are exerted on the droplet and hence subtle variations in the retention force have a minimal influence on the final droplet size achieved. Importantly, it was

discovered that simply matching the rotational speed of the membrane does not yield similar droplet sizes. Instead, the membrane surface velocity requires consideration with wider diameter membranes able to potentially exert much greater drag force on a forming droplet (even at a lower RPM).

Pilot-scale operation of RME is not as advantageous as expected in terms of energy consumption as was seen at the small-scale. This is due to the much greater force required to rotate a heavier membrane at high speeds. Another limitation for the process relates to the properties of the membrane itself. For metallic membranes, current technology to produce the pores is unable to deliver very small pore diameters with high precision (although rapid progress is being made). Additionally, it is evident that thin-walled (but mechanically strong) membranes are necessary to achieve sufficiently high dispersed phase flux for emulsion production on an industrial scale. However, this is likely to be recognised in future with advancements in material science (e.g. nano-reinforced metal composites) and therefore this limitation can be overcome.

Chapter 8:

Conclusions

The objectives of this thesis were to further understanding of the processing mechanisms involved during rotating membrane emulsification, such that they are well understood and therefore can be optimised. In addition, the aim was to investigate the capabilities of a pilot-scale rotating membrane emulsification device to help generate a procedure of how one might design and up-scale such a piece of equipment.

A wide range of emulsion droplet sizes were formulated via manipulation of the processing and formulation parameters. This approach enabled the development of a fundamental understanding of how such parameters can control both the emulsion microstructure and the rate of production.

The main conclusions from the results chapters are summarised:

1. Alteration of membrane emulsification processing parameters can induce multiple contributing effects that influence the final droplet size created.

It is important to consider a number of processing effects that can occur during operation; imparted by the fluid flow and interfacial behaviour of the two phases. These include the possibilities of coalescence on the membrane surface if droplets form within close proximity of each other, remain at the surface for a prolonged time period (due to low shear for example) or are not displaced away from the membrane surface upon detachment (due to a high viscosity continuous phase). Spontaneous transformation-based droplet formation may occur if the O/W interfacial tension is high and non-circular pore membranes are used imperative of porous glass (e.g. SPG) and ceramic materials. Droplets distorted by externally acting forces detach earlier than expected to become spherical and hence achieve a lower thermodynamically energetic state. In this instance, the interfacial tension almost solely dictates the point of droplet detachment with minimal influence of processing parameters; as such this may be referred to as droplets reaching their 'natural' detachment size. Droplet formation can also occur through break up of liquid jets if the dispersed

phase fluid velocity is too high (typically controlled by the transmembrane pressure) or the O/W interfacial tension is low; both factors can be quantified by the dimensionless dispersed phase Capillary number. This approach generally leads to production of poly-dispersed emulsions of larger droplet sizes rather than droplets of a single size; thus processing in this way is less controllable and more chaotic. The occurrence of Taylor vortices is observed to be beneficial for rotating membrane emulsification processing for production of smaller droplet sizes. Operating under high enough rotational speeds or larger diameter emulsification vessels enables their formation, which subsequently aids droplet detachment and displace droplets away from the membrane surface.

2. The behaviour of the material used to stabilise the droplet interface strongly determines the droplet size formed.

The rapid adsorption of the material (surfactant/particle) at the droplet interface is necessary to minimise droplet coalescence and allow for earlier droplet detachment. The transport of material towards the interface is also critical and depends on its physicochemical properties. Generally, surfactants adsorb faster than particles due to their lower minimum energy of adsorption and their smaller size (which aids mobility towards the interface due to less hydrodynamic resistance). Hence, surfactant transport is determined by diffusion whereas convection is more relevant for particle systems. Stabilisation of a droplet interface combining both surfactants and particles is seen to synergistically benefit droplet formation since each provide a different role; the surfactant which adsorbs first lowers the interfacial tension holding the droplet at the membrane surface whilst the particle provides a greater steric barrier to minimise coalescence..

3. Surfactant diffusion through a forming droplet interface can enhance process efficiency.

The movement of non-ionic surfactants through a droplet interface (demonstrated with Tween 20 and Brij 97) can lower the interfacial tension below the equilibrium value and thus a droplet is able to detach very early from the membrane surface. This approach requires the use of a surfactant that

is soluble in both phases, but preferential to the opposing phase that it is positioned in e.g. high HLB Tween within the oil phase. Hydrolysed lecithin (low HLB) demonstrated the opposite behaviour with smaller droplets when positioned within the aqueous phase, hence indicating this phenomenon to be implicit to the partition coefficient of the surfactant. Applying this approach allows for direct membrane emulsification to be competitive with a pre-mix configuration without suffering from fouling due to droplet break up within the pores (as in the latter case). This therefore is advantageous for emulsion production containing small droplets at greater rates than through applying the conventional approach.

4. Theoretical models for rotating membrane emulsification are useful for process optimisation rather than accurate prediction.

Models to estimate either droplet coalescence or droplet size prediction (based on a force balance model) were derived for rotating membrane emulsification. For droplet coalescence modelling, two cases representing the extremities of active pore distribution were considered; even distribution or random distribution. Application of the model to experimental data revealed coalescence was likely to be the cause of the large droplet sizes produced. For the force balance model, the predicted droplet size was always greater than the measured size despite not accounting for dispersed phase addition as the droplet detaches. The over-prediction in size is hypothesised to be due to an additional force yet to be included in any force balance model, but based on thermodynamically induced detachment (i.e. spontaneous transformation-based droplet formation mechanism). However, the model does predict the general trend and therefore can be applied as a process optimisation tool.

5. Rotating membrane emulsification is a more energy efficient process than both a rotor-stator high shear mixer and an ultrasonic probe under the condition of matching emulsion droplet size and production rate.

Comparison between the processes found rotating membrane emulsification has the potential to produce similar droplet sizes with a fraction of the energy input. By ensuring the interfacial tension decreases rapidly with surfactant diffusion through the droplet interface, rotating membrane emulsification can be operating at higher production rates without compromising its ability to create small droplets. This is therefore a significant process optimisation approach which considers both droplet size minimisation and dispersed phase flux maximisation in tandem. However, it is likely that producing more concentrated emulsions (greater than 10 vol. % dispersed phase) that the energy advantage will be lost since the energy consumption scales linearly with operating time.

6. Rotating membrane emulsification can be successfully operated at a pilot-scale of production.

The capabilities of a pilot scale device were tested to produce O/W emulsions using a laser drilled stainless steel membrane. This membrane material is more suited to larger scale operation due to the high mechanical forces exerted by either the transmembrane pressure or the rotational motion applied. For metallic membranes formed in this way, the pore spacing can be selected to be great enough such that coalescence between adjacent forming droplets is eliminated. The pilot-scale operation demonstrated similar trends to those observed at the small-scale indicating process phenomena to be relevant irrespective of the scale. The interfacial tension plays a less significant role in determining the droplet size formed since the forces inducing detachment (e.g. drag force) are much greater. Scaling up rotating membrane emulsification into a pilot-scale device was found to not be as advantageous in energy efficiency due to the force required to rotate a larger membrane. Comparison across two scales of operation highlighted the likely scalable parameters to be the membrane surface area (more pores form more droplets in a linear manner) and membrane surface velocity (a key variable altering the magnitude of the detachment forces).

7. Rotating membrane emulsification can be designed by applying the relevant equations and considering the process mechanisms that can impact on emulsification performance.

A proposed design procedure was outlined with discussion of the important considerations at each step. This was based on both theoretical understanding of the process and experimental findings that are presented within the thesis. For example, it may be extremely useful to incorporate computational modelling (e.g. lattice Boltzmann simulations) in order to both validate and improve the procedure for scale-up and thus industrially relevant applications.

Chapter 9:

Future Work

The research presented here has uncovered a number of areas related to rotating membrane emulsification that would be very interesting to explore. These are suggested below:

9.1 Operation as a continuous process

At present, rotating membrane emulsification is operated as a semi-continuous process; the dispersed phase is gradually added to a fixed amount of continuous phase. An alternative approach would be to flow continuous phase into the emulsification vessel as the dispersed phase is added, whilst allowing emulsion product to leave. This would be very interesting especially if the process is to be implemented within industry. Continuous processes are generally more capable of achieving higher production rates and are also much easier to automate the control. However, continuous operation would be challenging since the dispersed phase volume fraction of the exiting emulsion is determined by the ratio of the continuous and dispersed phase inlet flow rates and the residence time within the emulsification vessel. The droplet size would have to be controlled by the rotational velocity, surfactant type/concentration (etc.) rather than the transmembrane pressure. The continuous phase flow behaviour would also be more complex with streams of material entering and leaving the emulsification vessel; this could possibly be overcome with careful design of the entry and exit points. A possible adaptation may also include the use of static mixers within the emulsification vessel to control the flow profile and hence shear better in the case of continuous production. Sufficient mixing would also be required to ensure the emulsion siphoned off is homogeneous in consistency. In this instance, qualitative checks with tools such as CFD modelling would be extremely useful.

9.2 Effect of Temperature

Whilst a number of processing parameters were investigated, another parameter that could be considered would be the temperature of the dispersed and continuous phases. With the low dispersed phase flux being the primary limitation of membrane emulsification processing, perhaps

this could be enhanced by heating the dispersed phase to lower the viscosity (Joscelyne and Tragardh, 2000). This may be compensated with a much cooler continuous phase to ensure the emulsion is not destabilised by the thermal energy input. The temperature might also be used to alter the interfacial tension and viscosities of the system to control the droplet diameter produced. It may be possible to crystallise material e.g. fat via flash cooling of the droplets as they form but it is anticipated this would risk fouling of the membrane pores.

9.3 Further study of Surfactant Diffusion through an Interface

A good continuation of the study of surfactant positioning would be to explore W/O emulsion production by adopting a similar approach. It was demonstrated that positioning high HLB non-ionic surfactants within the dispersed phase could produce much smaller oil droplet sizes. If surfactant diffusion to lower the interfacial tension below the equilibrium value is responsible, it is expected that a low HLB non-ionic surfactant positioned within a forming water droplet would show similar behaviour. In addition to this, it would be interesting to observe these effects for multiple surfactant or surfactant-particle systems. For example, a non-ionic surfactant within the dispersed phase and particles positioned within the continuous phase. It would also be useful to undertake studies of long-term emulsion stability (rather than just the initial size produced) in order to better understand the dynamic behaviour of such systems.

9.4 Bi-modal Emulsion Production

In the majority of cases, mono-dispersed droplet size production is desired in order to ensure high stability (Walstra, 2003). However, bi-modal or multi-modal distributions with distinct narrow peaks may also be produced by altering the rotational velocity of the process mid-operation. Droplets forming either side of this modification to the operating conditions would detach at different sizes. This may be advantageous for achieving a particular emulsion viscosity or the delivery of an active ingredient with variation in the release rate for example.

Appendix A: Example Case for Design Procedure

An O/W emulsion containing droplets of 10 μm (2 vol. % dispersed phase) is required to be produced at a rate of 50 kg h^{-1} . The equilibrium IFT between the oil and water with a pre-determined surfactant type and concentration is 5 mN m^{-1} . Suggest a suitable design configuration.

ASSUMPTION: Stainless steel membrane, triangular array of pores. Straight through channels i.e. membrane tortuosity (τ) = 1. Active pore fraction (α) constant = 1. Membrane thickness (L_m) = 0.1 mm.

1. 1 μm pore diameter would be suitable assuming a droplet to pore size ratio of 10.
2. With droplets of 10 μm diameter, a pore spacing of 15 μm should limit steric hindrance of adjacent forming droplets.

Dynamic viscosity (μ_d) of SFO at 20°C = 0.066 Pa s. The dispersed phase is Newtonian.

$$3. \quad Ca_d = \frac{\mu_d v_d}{\gamma} \quad \Rightarrow \quad v_d = \frac{Ca_d \gamma}{\mu_d} = \frac{0.056 \times 0.005}{0.066} \quad \Rightarrow \quad v_d = 4.2 \times 10^{-3} \text{ m s}^{-1}$$

Therefore the dispersed phase fluid velocity in the pore must not exceed this value.

Densities of dispersed (ρ_d) and continuous (ρ_c) phases at 20°C are 920 kg m^{-3} and 1000 kg m^{-3} respectively.

$$4. \quad \rho_{emulsion} = (0.02 \times \rho_d) + [(1 - 0.02) \times \rho_c] = (0.02 \times 920) + (0.98 \times 1000)$$

$$\Rightarrow \quad \rho_{emulsion} = 998.4 \text{ kg m}^{-3}$$

$$Q_{emulsion} = \frac{\dot{M}_{emulsion}}{\rho_{emulsion}} = \frac{100}{998.4} \quad \Rightarrow \quad \dot{Q}_{emulsion} = 0.1 \text{ m}^3 \text{ h}^{-1}$$

$$Q_d = 0.02 \times \dot{Q}_{emulsion} = 0.02 \times 0.1 \quad \Rightarrow \quad Q_d = 2 \times 10^{-3} \text{ m}^3 \text{ h}^{-1}$$

$$5. \quad J_d = \frac{K \Delta P_{tm}}{\mu_d L_p} = \frac{\dot{M}_d}{\rho_d A_m} \quad \Rightarrow \quad A_m \Delta P_{tm} = \frac{\dot{M}_d \mu_d L_p}{K \rho_d}$$

$$\dot{M}_d = \frac{M_d}{t_p} = Q_d \rho_d = 2 \times 10^{-3} \times 920 \Rightarrow \dot{M}_d = 1.84 \text{ kg h}^{-1}$$

$$L_p = L_m \tau = 0.1 \times 10^{-3} \times 1 \Rightarrow L_p = 0.1 \times 10^{-3} \text{ m}$$

On the basis of 1m × 1m sheet of membrane material with triangular array of 1 μm diameter pores spaced 15 μm apart:

$$A_\Delta = L_x^2 \frac{\sqrt{3}}{4} = (15 \times 10^{-6})^2 \times \frac{\sqrt{3}}{4} \Rightarrow A_\Delta = 9.74 \times 10^{-11} \text{ m}^2$$

$$x_\Delta = \frac{A_{total}}{A_\Delta} = \frac{1}{9.74 \times 10^{-11}} \Rightarrow x_\Delta = 1.03 \times 10^{10} \approx n_p$$

$$A_{void} = \pi r_p^2 n_p = \pi \times (0.5 \times 10^{-6})^2 \times (1.03 \times 10^{10}) \Rightarrow A_{void} = 8.06 \times 10^{-3} \text{ m}^2$$

$$\phi = \frac{A_{void}}{A_{total}} = \frac{8.06 \times 10^{-3}}{1} \Rightarrow \phi = 0.00806$$

$$K = \alpha d_p^2 \phi^{1.5} = 1 \times (1 \times 10^{-6})^2 \times 0.00806^{1.5} \Rightarrow K = 7.24 \times 10^{-16} \text{ m}^2$$

$$A_m \Delta P_{tm} = \frac{\dot{M}_d \mu_d L_p}{K \rho_d} = \frac{1.84 \times 0.066 \times (0.1 \times 10^{-3})}{(7.24 \times 10^{-16}) \times 920} \Rightarrow A_m = \frac{1.82 \times 10^7}{\Delta P_{tm}}$$

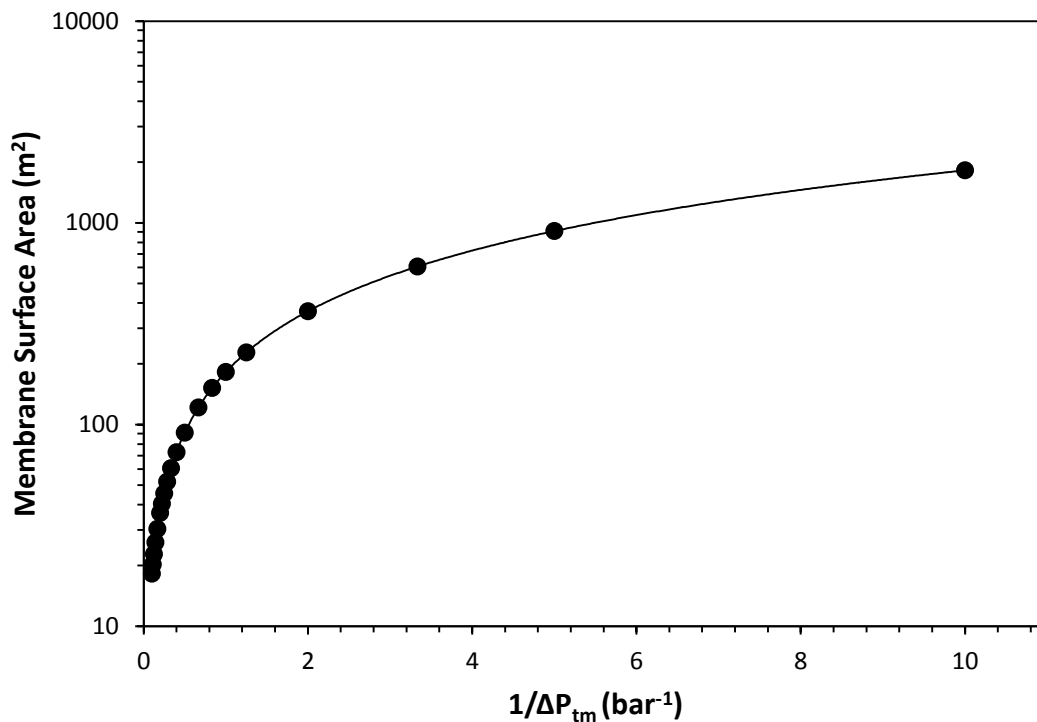


Fig. A1: Membrane surface area required based on the selected Transmembrane Pressure.

Table A1: Possible solutions for membrane surface area required based on selected Transmembrane Pressure.

Transmembrane Pressure (Bar)	Membrane Surface Area (m ²)	Pore Fluid Velocity (m s ⁻¹)
1	182.0	3.03×10^{-7}
2	91.0	7.57×10^{-7}
5	36.4	1.89×10^{-6}
10	18.2	3.79×10^{-6}

Pore fluid velocity across range of TMPs does not exceed value that would cause jetting ($4.2 \times 10^{-3} \text{ m s}^{-1}$).

ASSUMPTION: Transmembrane Pressure of 8 bar deemed suitable in conjunction with a membrane surface area of 22.8 m². A cylindrical membrane is used.

$$6. \quad A_m = \pi d_1 h_1 \quad \Rightarrow \quad d_1 h_1 = \frac{A_m}{\pi} = \frac{22.8}{\pi} \quad \Rightarrow \quad d_1 h_1 = 7.257$$

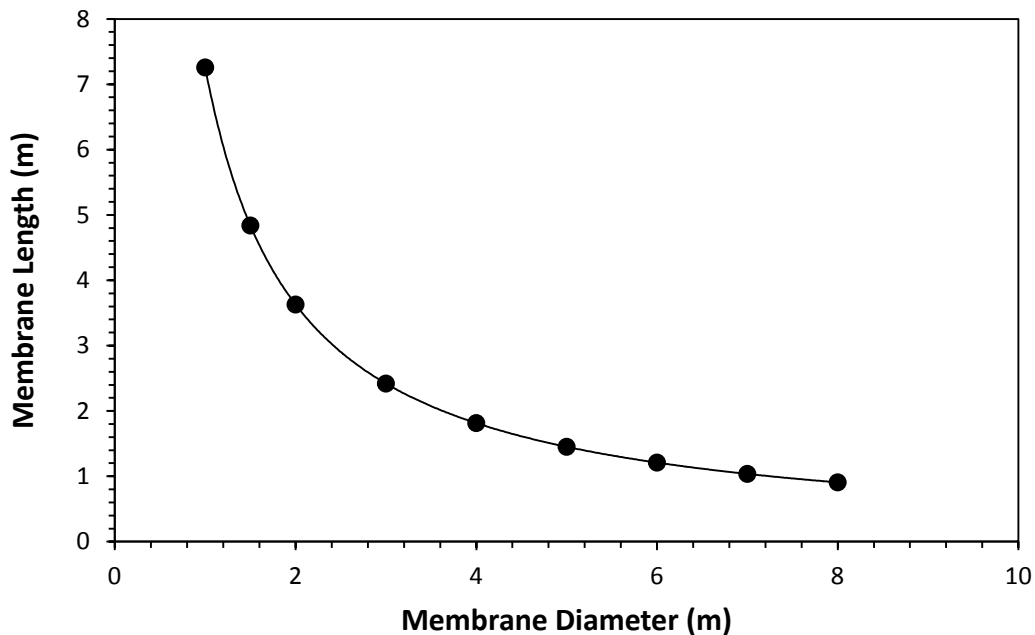


Fig. A2: Possible dimensions for a cylindrical membrane for the chosen surface area of 22.8 m².

A suitable arrangement may be a 1.5 m diameter ($r_1 = 0.75 \text{ m}$) membrane of 4.8 m length (h_1) to provide the surface area of 22.8 m².

ASSUMPTION: The dimensions are suitable but the motor is only sufficiently powerful to operate at rotational speeds between 50-400 RPM.

$$7. \quad v_1 = \frac{\pi d_1 n_1}{60} = \frac{\pi \times 1.5 \times n_1}{60} \Rightarrow \quad v_1 = 3.9 \text{ to } 31.4 \text{ m s}^{-1}$$

Dynamic viscosity (μ_c) of the continuous phase at 20°C = 0.0013 Pa s. The solution is Newtonian.

$$8. \quad Ta = \omega_1 r_1 (r_2 - r_1) \frac{\rho_c}{\mu_c} \sqrt{\frac{2(r_2 - r_1)}{r_1 + r_2}} = 41.3$$

$$\Rightarrow \quad \frac{50}{60} \times 0.75 \times (r_2 - 0.75) \times \frac{1000}{0.0013} \times \sqrt{\frac{2(r_2 - 0.75)}{0.75 + r_2}} = 41.3 \Rightarrow \text{Solve iteratively for } r_2$$

$$\Rightarrow \quad r_2 \text{ minimum} > 0.752 \text{ m}$$

ASSUMPTION: An emulsification vessel diameter of 2 m is selected and the vessel is cylindrical; hence a concentric cylinder configuration. Initially, the vessel height (h_2) equals the membrane height (h_1).

$$V_c = \pi r_2^2 h_1 - \pi r_1^2 h_1 = (\pi \times 1^2 \times 4.8) - (\pi \times 0.75^2 \times 4.8) \Rightarrow V_c = 6.6 \text{ m}^3$$

Therefore the required volume is the nominal emulsification vessel volume (V_c) plus the volume of dispersed phase needed to be added to form the emulsion, multiplied by a safety factor (1.2) to prevent overfilling.

$$V_2 = (V_c + 0.02V_c) \times 1.2 = (1.02 \times 6.6) \times 1.2 \Rightarrow V_2 = 8.08 \text{ m}^3$$

ASSUMPTION: The membrane height (h_1) will now equal the required emulsification vessel height (h_2).

$$V_2 = \pi r_2^2 h_2 - \pi r_1^2 h_2 = h_2 (\pi r_2^2 - \pi r_1^2)$$

$$h_2 = \frac{V_2}{(\pi r_2^2 - \pi r_1^2)} = \frac{8.08}{[(\pi \times 1^2) - (\pi \times 0.75^2)]} \Rightarrow h_2 = 5.88 \text{ m}$$

To summarise:

Processing Parameters		
Transmembrane Pressure	8	bar g
Rotational Speed	50-400	RPM

Membrane Parameters		
Material	SS	
Surface Area of Porous section	22.8	m ²
Pore Diameter	1	µm
Pore Spacing	15	µm
Membrane Thickness	0.1	mm
Membrane Diameter	1.5	m
Membrane Height	5.88	m
Total Membrane Surface Area	27.7	m ²

Vessel Parameters		
Operating Volume of Vessel	8.08	m ³
Vessel Diameter	2	m
Vessel Height	5.88	m

Chapter 10:

References

-
- Abrahamse, A.J., van der Padt, A., Boom, R.M. (2001).** Process fundamentals of membrane emulsification: simulation with CFD. *Journal of the American Institute of Chemical Engineers*, 47 (6) 1285-1291.
- Abrahamse, A.J., van Lierop, R., van der Sman, R.G.M., van der Padt, A., Boom, R.M. (2002)** Analysis of droplet formation and interactions during cross-flow membrane emulsification. *Journal of Membrane Science*, 204 (1-2) 125-137.
- Ambrawaneswaran, B., Subramani, H.J., Phillips, S.D., Basaran, O.A. (2004)** Dripping-Jetting Transitions in a Dripping Faucet. *Physical Review Letters*, 93 (3) 034501.
- Aryanti, N., Hou, R., Williams, R.A. (2009).** Performance of rotating membrane emulsifier for production of coarse droplets. *Journal of Membrane Science*, 326 (1) 9-18.
- Baier, G., Graham, M.D., Lightfoot, E.N. (2000).** Mass transport in a novel two-fluid Taylor vortex extractor. *Journal of the American Institute of Chemical Engineers*, 46 (12) 2395-2407.
- Ban, S., Kitahara, M., Yamasaki, A. (1994).** Preparation of O/W emulsions with poly (oxyethylene) hydrogenated castor-oil by using SPG membrane emulsification method. *Nippon Kagaku Kaishi*, 8 734-742.
- Bancroft, W.D. (1912).** The Theory of Emulsification III. *The Journal of Physical Chemistry*, 16 475-512.
- Binks, B.P., Lumsdon, S.O. (1999).** Stability of oil-in-water emulsions stabilised by silica particles. *Physical Chemistry Chemical Physics*, 2 3007-3016.
- Binks, B.P. (2002).** Particles as surfactants – similarities and differences. *Current Opinion in Colloid & Interface Science*, 7 (1-2) 21-41.
- Binks, B.P., Desforges, A., Duff, D.G. (2007).** Synergistic stabilization of emulsions by a mixture of surface-active nanoparticles and surfactant. *Langmuir*, 23 1098-1106.
- Binks, B.P., Rodrigues, J.A. (2007).** Enhanced stabilization of emulsions due to surfactant-induced nanoparticle flocculation. *Langmuir*, 23 7436-7439.
- Bouzerar, R., Ding, L., Jaffrin, M.Y. (2000).** Local permeate flux-shear-pressure relationships in a rotating disk microfiltration module: implications for global performance. *Journal of Membrane Science*, 170 (1) 127-141.
- Boyd, J., Parkinson, C., Sherman, P. (1972).** Factors Affecting Emulsion Stability, and the HLB Concept. *Journal of Colloid and Interface Science*, 41 (2) 359-370.
- Brian, B.W., Chen, J.C. (1987).** Surface tension of solid-liquid slurries. *Journal of the American Institute of Chemical Engineers*, 33 (2) 316-318.
- Charcosset, C., Limayem, I., Fessi, H. (2004).** The membrane emulsification process – a review. *Journal of Chemical Technology and Biotechnology*, 79 (3) 209-218.

Charcosset, C. (2009). Preparation of emulsions and particles by membrane emulsification for the food processing industry. *Journal of Food Engineering*, 92 (3) 241-249.

Charles, G.E., Mason, S.G. (1960). The coalescence of liquid drops with flat liquid/liquid interfaces. *Journal of Colloid Science*, 15 (3) 236-267.

Cheng, C., Chu, L., Xie, R. (2006). Preparation of highly monodisperse W/O emulsions with hydrophobically modified SPG membranes. *Journal of Colloid and Interface Science*, 300 (1) 375-382.

Christov, N.C., Danov, K.D., Danova, D.K., Kralchevsky, P.A. (2008). The drop size in membrane emulsification determined from the balance of capillary and hydrodynamic forces. *Langmuir*, 24 (4) 1397-1410.

Conley, R.F. (1996). Practical dispersion: a guide to understanding and formulating slurries. *Wiley-VCH, Inc.*, 1-447.

Debye, P. (1947). Molecular-weight determination by light scattering. *Journal of Physical Chemistry*, 51 (1) 18-32.

De Luca, G., Sindona, A., Giorno, L., Drioli, E. (2004). Quantitative analysis of coupling effects in cross-flow membrane emulsification. *Journal of Membrane Science*, 229 199-209.

De Luca, G., Drioli, E. (2006). Force balance conditions for droplet formation in cross-flow membrane emulsifications. *Journal of Colloid and Interface Science*, 294 436-448.

De Luca, G., Di Renzo, A., Di Maio, F.P., Drioli, E. (2007). Modelling droplet formation in cross-flow membrane emulsification. *Desalination*, 199 177-179.

De Luca, G., Di Maio, F.P., Di Renzo, A., Drioli, E. (2008). Droplet detachment in cross-flow membrane emulsification: Comparison among torque- and force-based models. *Chemical Engineering and Processing: Process Intensification*, 47 (7) 1150-1158.

Dijke, K., Veldhuis, G., Schroen, K. (2009). Parallelized edge-based droplet generation (EDGE) devices. *Lab on a Chip*, 9, 2824-2830.

Dimitrov, D.S., Panaiotov, I., Richmond, P., Ter-Minassian-Saraga, L. (1978). Dynamics of insoluble monolayers: I. Dilatational or elastic modulus, friction coefficient, and Marangoni effect for dipalmitoyl lecithin monolayers. *Journal of Colloid and Interface Science*, 65 (3) 483-494.

Dragosavac, M.M., Sovilj, M.N., Kosvintsev, S.R., Holdich, R.G., Vladisavljevic, G.T. (2008). Controlled production of oil-in-water emulsions containing unrefined pumpkin seed oil using stirred cell membrane emulsification. *Journal of Membrane Science*, 322 (1) 178-188.

-
- Drelich, A., Gomez, F., Clause, D., Pezron, I. (2010).** Evolution of water-in-oil emulsions stabilized with solid particles: Influence of added emulsifier. *Colloids and Surfaces A: Physicochemical and Engineering Aspects*, 365 171-177.
- Du, K., Glogowski, E., Emrick, T., Russell, T.P. (2010).** Adsorption Energy of Nano- and Microparticles at Liquid-Liquid Interfaces. *Langmuir*, 26 (15) 12518-12522.
- Egidi, E., Gasparini, G., Holdich, R.G., Vladisavljevic, G.T., Kosvintsev, S.R. (2008).** Membrane emulsification using membranes of regular pore spacing: Droplet size and uniformity in the presence of surface shear. *Journal of Membrane Science*, 323 (2) 414-420.
- Eisner, V. (2007).** Emulsion Processing with a Rotating Membrane (ROME). *PhD Thesis, ETH Zurich, Switzerland*, 1-112.
- Ferrari, M., Liggieri, L., Ravara, F., Amodio, C., Miller, R. (1997).** Adsorption kinetics of alkylphosphine oxides at water/hexane interface: 1. Pendant drop experiments. *Journal of Colloid and Interface Science*, 186 (1) 40-45.
- Garces, R., Martinez-Force, E., Salas, J.J., Venegas, M. (2009).** Current advances in sunflower oil and its applications. *Lipid Technology*, 21 (4) 79-82.
- Gassin, P., Champory, R., Martin-Gassin, G., Dufreche, F., Diat, O. (2013).** Surfactant transfer across a water/oil interface: A diffusion/kinetics model for the interfacial tension evolution. *Colloids and Surfaces A: Physicochemical and Engineering Aspects*, 436 1103-1110.
- Gijsbertsen-Abrahamse, A.J., van der Padt, A., Boom, R.M. (2004).** Status of cross-flow membrane emulsification and outlook for industrial application, *Journal of Membrane Science*, 230 149-159.
- Glaser, N., Adams, D.J., Boker, A., Krausch, G. (2006).** Janus Particles at Liquid-Liquid Interfaces. *Langmuir*, 22 5227-5229.
- Griffin, W.C. (1949).** Classification of Surface-Active Agents by 'HLB'. *Journal of the Society of Cosmetic Chemists*, 1 (5) 311-326.
- Griffin, W.C. (1954).** Calculation of HLB values of Non-Ionic Surfactants. *Journal of the Society of Cosmetic Chemists*, 5 (4) 249-256.
- Guillot, S., Bergaya, F., de Azevedo, C., Warmont, F., Tranchant, J.F. (2009).** Internally structured pickering emulsions stabilized by clay mineral particles. *Journal of Colloid and Interface Science*, 333 (2) 563-569.
- Hancocks, R.D. (2011).** Controlled Emulsification using Microporous Membranes. *PhD Thesis, University of Birmingham, UK*. 1-177.
- Hancocks, R.D., Spyropoulos, F., Norton, I.T. (2013).** Comparisons between membranes for use in cross flow membrane emulsification. *Journal of Food Engineering*, 116 (2) 382-389.

Hansson, J., Karlsson, J.M., Haraldsson, T., Brismar, H., van der Wijngaart, W., Russom, A. (2012). Inertial microfluidics in parallel channels for high-throughput applications. *Lab on a Chip*, 12 4644-4650.

Hassander, H., Johansson, B., Tornell, B. (1989). The mechanism of emulsion stabilization by small silica (Ludox) particles. *Colloids and Surfaces*, 40 (93-105).

Jafari, S.M., Assadpoor, E., He, Y., Bhandari, B. (2008). Re-coalescence of emulsion droplets during high-energy emulsification. *Food Hydrocolloids*, 22 (7) 1191-1202.

Joscelyne, S., Tragardh, G. (2000). Membrane emulsification – a literature review. *Journal of Membrane Science*. 169 (1) 107-117.

Katoh, R., Asano, Y., Furuya, A., Sotoyama, K., Tomita, M. (1996). Preparation of food emulsions using a membrane emulsification system. *Journal of Membrane Science*, 113, 131-135.

Katoh, R., Asano, Y., Furuya, A., Sotoyama, K., Tomita, M., Okongi, S. (1997). Preparation of food emulsions using a membrane emulsification system 3. A method of preventing dispersed droplets from crushing using a membrane emulsification system. *Nippon Shokuhin Kagaku Kokaku Kaishi*, 44 (3) 233-237.

Kelder, J.D.H., Janssen, J.J.M., Boom, R.M. (2007). Membrane emulsification with vibrating membranes: A numerical study. *Journal of Membrane Science*, 304 (1-2) 50-59.

Kim, J., Cote, L.J., Kim, F., Yuan, W., Shull, K.R., Huang, J. (2010). Graphene Oxide Sheets at Interfaces. *Journal of the American Chemical Society*, 132 8180-8186.

Kobayashi, I., Mitsutoshi, M., Chun, K., Kikuchi, Y., Fujita, H. (2002) Silicon array elongated through-holes for monodisperse emulsion droplets. *Journal of the American Institute of Chemical Engineers*, 48 (8) 1639-1644.

Kobayashi, I., M. Nakajima, Mukutaka, S. (2003). Preparation characteristics of oil-in-water emulsions using differently charged surfactants in straight-through microchannel emulsification. *Colloids and Surfaces A: Physicochemical and Engineering Aspects*, 229 (1-3) 33-41.

Kobayashi, I., Mukutaka, S., Nakajima, M. (2005). Effects of type and physical properties of oil phase on oil-in-water emulsion droplet formation in straight-through microchannel emulsification, Experimental and CFD studies. *Langmuir*, 21 5722-5730.

Kobayashi, I., Neves, M.A., Uemura, K., Nakajima, M. (2011). Production characteristics of uniform large soybean oil droplets by microchannel emulsification using asymmetric through-holes. *Procedia Food Science*, 1 123-130.

Kosvintsev, S.R., Gasparini, G., Holdich, R.G. (2008). Membrane emulsification: Droplet size and uniformity in the absence of surface shear. *Journal of Membrane Science*, 313 (1-2) 182-189.

Kuiper, S., van Rijn, C.J.M., Nijdam, W., Elwenspoek, M.C. (1998). Development and applications of very high flux microfiltration membranes. *Journal of Membrane Science*, 150 1-8.

Kukizaki, M. (2009). Shirasu porous glass (SPG) membrane emulsification in the absence of shear flow at the membrane surface: Influence of surfactant type and concentration, viscosities of dispersed and continuous phases, and transmembrane pressure. *Journal of Membrane Science*, 327 (1-2) 234-243.

Kutuzov, S., He, J., Tangirala, R., Emrick, T., Russell, T.P., Boker, A. (2007). On the kinetics of nanoparticle self-assembly at liquid/liquid interfaces. *Physical Chemistry Chemical Physics*, 9 6351-6358.

Lambrich, U., Schubert, H. (2005). Emulsification using microporous systems. *Journal of Membrane Science*, 257 (1-2) 76-84.

Lathrop, D.P., Fineberg, J., Swinney, H.L. (1992). Transition to shear-driven turbulence in Couette-Taylor flow. *Physical Review A*, 46 (10) 6390-6405.

Lee, S., Lueptow, R.M. (2001). Rotating reverse filtration for space mission wastewater: membrane properties and operating conditions. *Journal of Membrane Science*, 182 (1-2) 77-90.

Lepercq-Bost, E., Giorgi, M., Isambert, A., Arnauld, C. (2008). Use of the capillary number for the prediction of droplet size in membrane emulsification. *Journal of Membrane Science*, 314 (1-2) 76-89.

Lepercq-Bost, E., Giorgi, M., Isambert, A., Arnauld, C. (2010). Estimating the risk of coalescence in membrane emulsification. *Journal of Membrane Science*, 357 (1-2) 36-46.

Levine, S., Bowen, B.D., Partridge, S.J. (1989). Stabilization of emulsions by fine particles II. Capillarity and van der Waals forces between particles. *Colloids and Surfaces*, 38 345-364.

Liggieri, L., Ravara, F., Amodio, C., Miller, R. (1997). Adsorption kinetics of alkylphosphine oxides at water/hexane interface: 2. Theory of the Adsorption with Transport across the Interface in Finite Systems. *Journal of Colloid and Interface Science*, 186 (1) 46-52.

Lloyd, D.M., Spyropoulos, F., Norton, I.T. (2014). Processing effects during rotating membrane emulsification. *Journal of Membrane Science*, 466 8-17.

Lloyd, D.M., Spyropoulos, F., Norton, I.T. (2015). Process optimisation of Rotating Membrane Emulsification through the study of surfactant dispersions. *Journal of Food Engineering*, 166 316-324.

Manga, M.S., Cayre, O.J., Williams, R.A., Biggs, S., York, D.W. (2012). Production of solid-stabilised emulsions through rotating membrane emulsification: Influence of particle adsorption kinetics. *Soft Matter*, 8 1532-1538.

Matos, M., Suarez, M.A., Gutierrez, G., Coca, J., Pazos, C. (2013). Emulsification with microfiltration ceramic membranes: A different approach to droplet formation mechanism. *Journal of Membrane Science*, 444 345-358.

-
- McClements**, D.J. (2011). Edible nanoemulsions: fabrication, properties, and functional performance. *Soft Matter*, 7 2297-2316.
- Meyer**, R.F. (2010) The Physics of Membrane Emulsification and Applications for Controlled Drug Delivery. *PhD Thesis, University of Pennsylvania, US*. 1-124.
- Midmore**, B.R. (1998). Preparation of a novel silica-stabilized oil/water emulsion. *Colloids and Surfaces A: Physicochemical and Engineering Aspects*, 132 (2-3) 257-265.
- Nakashima**, T., Shimizu, M., Kukizaki, M. (1987). U.S. Patent number 4657875.
- Nakashima**, T., Shimizu, M., Kukizaki, M. (1991). Membrane emulsification by microporous glass. *Key Engineering Materials*, 61-62 513-516.
- Nakashima**, T., Shimizu, M. (1993). Liquid permeability of porous glass membrane and its microstructure. *Journal of the Ceramic Society of Japan*, 101 (5) 528-532.
- Nakashima**, T., Shimizu, M., Kukizaki, M. (1994). U.S. Patent number 5326484.
- Nakashima**, T., Shimizu, M., Kukizaki, M. (2000). Particle control of emulsion by membrane emulsification and its applications. *Advanced Drug Delivery Reviews*, 46 (1) 47-56.
- Nazir**, A., Schroen, K., Boom, R. (2010). Premix emulsification: A review. *Journal of Membrane Science*, 362 (1-2) 1-11.
- Nazir**, A., Schroen, K., Boom, R. (2011). High-throughput premix membrane emulsification using nickel sieves having straight-through pores. *Journal of Membrane Science*, 383 (1-2) 116-123.
- O'Brien**, F.J., Harley, B.A., Waller, M.A., Yannas, I.V., Gibson, L.J., Prendergast, P.J. (2007). The effect of pore size on permeability and cell attachment in collagen scaffolds for tissue engineering. *Technology and Health Care*, 15 (1) 3-17.
- Oh**, D.H., Balakrishnan, P., Oh, Y., Kim, D., Yong, C.S., Choi, H. (2011). Effect of process parameters on nanoemulsion droplet size and distribution in SPG membrane emulsification. *International Journal of Pharmaceutics*, 404 (1-2) 191-197.
- O'Neil**, M.E. (1964). A slow motion of viscous liquids caused by a slowly moving solid sphere. *Chemical Engineering Science*, 23 (67-74).
- Pach**, J., Pinchasi, R. (2003). How many unit equilateral triangles can be generated by N points in convex position. *The American Mathematical Monthly*, 110 (5) 400-406.
- Pathak**, M. (2011). Numerical simulation of membrane emulsification: Effect of flow properties in the transition from dripping to jetting. *Journal of Membrane Science*, 382 (1-2) 166-176.

Paul, E. L., Atiemo-Obeng, V.A., Kresta, S.M. (2004). Handbook of Industrial Mixing: Science and Practice. Vol. 1, *John Wiley and Sons. Inc.*, 1-1377.

Pawlik, A.K., Norton, I.T. (2012). Encapsulation stability of duplex emulsions prepared with SPG cross-flow membrane, SPG rotating membrane and rotor-stator techniques – A comparison. *Journal of Membrane Science*, 415-416 459-468.

Pawlik, A.K., Norton, I.T. (2013). SPG rotating membrane technique for production of food grade emulsions. *Journal of Food Engineering*, 114 530-537.

Peng, S.J., Williams, R.A. (1998). Controlled Production of Emulsions Using a Crossflow Membrane: Part I: Droplet Formation from a Single Pore. *Chemical Engineering Research and Design*, 76 (8) 894-901.

Pichot, R., Spyropoulos, F., Norton, I.T. (2009). Mixed-emulsifier stabilised emulsions: Investigation of the effect of monoolein and hydrophilic silica particle mixtures on the stability against coalescence. *Journal of Colloid and Interface Science*, 329 (2) 284-291.

Pichot, R., Spyropoulos, F., Norton, I.T. (2010). O/W emulsions stabilised by both low molecular weight surfactants and colloidal particles: The effect of surfactant type and concentration. *Journal of Colloid and Interface Science*, 352 (1) 128-135.

Pichot, R., Spyropoulos, F., Norton, I.T. (2012). Competitive adsorption of surfactants and hydrophilic silica particles at the oil-water interface: Interfacial tension and contact angle studies. *Journal of Colloid and Interface Science*, 377 (1) 396-405.

Pickering, S.U. (1907). Emulsions. *Journal of the Chemical Society*, 91 2001-2021.

Rayner, M., Tragardh, G., Tragardh, C., Dejmek, P. (2004). Using the Surface Evolver to model droplet formation processes in membrane emulsification. *Journal of Colloid and Interface Science*, 279 (1) 175-185.

Rayner, M., Tragardh, G., Tragardh, C. (2005). The impact of mass transfer and interfacial expansion rate on droplet size in membrane emulsification processes. *Colloids and Surfaces A: Physicochemical and Engineering Aspects*, 266 1-17.

Santos, J., Vladislavljevic, G.T., Holdich, R.G., Dragosavac, M.M., Munoz, J. (2015). Controlled production of eco-friendly emulsions using direct and premix membrane emulsification. *Chemical Engineering Research and Design*, 98 59-69.

Schadler, V., Windhab, E.J. (2006). Continuous membrane emulsification by using a membrane system with controlled pore distance. *Desalination*, 189 (1-3) 130-135.

Scheele, G.F., Meister, B.J. (1968). Drop formation at low velocities in liquid-liquid systems: Part I. Prediction of drop volume. *Journal of the American Institute of Chemical Engineers*, 14 (1) 9-15.

-
- Schroder**, V., Behrend, O., Schubert, H. (1998) Effect of Dynamic Interfacial Tension on the Emulsification Process Using Microporous Ceramic Membranes. *Journal of Colloid and Interface Science*, 202 (2) 334-340.
- Schroder**, V. Schubert, H. (1999). Production of emulsions using microporous, ceramic membranes. *Colloids and Surfaces A: Physicochemical and Engineering Aspects*, 152 (1-2) 103-109.
- Spyropoulos**, F., Hancocks, R.D., Norton, I.T. (2011). Food-grade emulsions prepared by membrane emulsification techniques. *Procedia Food Science*, 1 920-926.
- Spyropoulos**, F., Lloyd, D.M., Hancocks, R.D., Pawlik, A.K. (2014). Advances in Membrane Emulsification. Part B: Recent developments in Modelling and Scale-up approaches. *Journal of the Science of Food and Agriculture*, 94 (4) 628-638.
- Sugiura**, S., Nakajima, M., Iwamoto, S., Seki, M. (2001). Interfacial Tension Driven Monodispersed Droplet Formation from Microfabricated Channel Array. *Langmuir*, 17 (18) 5562-5566.
- Sugiura**, S., Nakajima, M., Kumazawa, N., Iwamoto, S., Seki, M. (2002). Characterization of spontaneous transformation-based droplet formation during microchannel emulsification. *The Journal of Physical Chemistry B*, 106 (36) 9405-9409.
- Surh**, J., Jeong, Y.G., Vladisavljevic, G.T. (2008). On the preparation of lecithin-stabilized oil-in-water emulsions by multi-stage premix membrane emulsification. *Journal of Food Engineering*, 89 (2) 164-170.
- Suzuki**, K., Fujiki, I., Hagura, Y. (1998). Preparation of corn oil/water and water/corn oil emulsions using PTFE membranes. *Food Science and Technology International Tokyo*, 4 (2) 164-167.
- Tadros**, T.F. (2005). Applied Surfactants. *Wiley-VCH Verlag GmbH & Co.*, 1-631.
- Tangirala**, R., Revanur, R., Russell, T.P., Emrick, T. (2007). Sizing Nanoparticle-Covered Droplets by Extrusion through Track-Etch Membranes. *Langmuir*, 23 (3) 965-969.
- Taylor**, G.I. (1923). Stability of a Viscous Liquid Contained between Two Rotating Cylinders. *Philosophical Transactions of the Royal Society of London. Series A. Containing Papers of a Mathematical or Physical Character*, 223 289-343.
- Timgren**, A., Tragardh, G., Tragardh, C. (2008). Application of the PIV technique to measurements around and inside a forming drop in liquid-liquid system. *Experiments in Fluids*, 44 (4) 565-575.
- Timgren**, A., Tragardh, G., Tragardh, C. (2009). Effects of pore spacing on drop size during cross-flow membrane emulsification – a numerical study. *Journal of Membrane Science*, 337 (1-2) 232-239.
- Timgren**, A., Tragardh, G., Tragardh, C. (2010). A model for drop size prediction using cross-flow emulsification. *Chemical Engineering Research and Design*, 88 (2) 229-238.

-
- Trentin, A., Ferrando, M., Lopez, F., Guell, C. (2009).** Premix membrane O/W emulsification: Effect of fouling when using BSA as emulsifier. *Desalination*, 245 (1-3) 388-395.
- van Boekel, M.A.J.S., Walstra, P. (1981).** Effect of Couette flow on stability of oil-in-water emulsions. *Colloids and Surfaces*, 3 (2) 99-107.
- van der Graaf, S., Schroen, C.G.P.H., Boom, R.M. (2005).** Preparation of double emulsions by membrane emulsification – a review. *Journal of Membrane Science*, 251 (1-2) 7-15.
- van der Graaf, S., Nisisako, T., Schroen, C.G.P.H., van der Sman, R.G.M., Boom, R.M. (2006).** Lattice Boltzmann Simulations of Droplet Formation in a T-Shaped Microchannel. *Langmuir*, 22 (9) 4144-4152.
- van der Zwan, E.A., Schroen, C.G.P.H., Boom, R.M. (2008).** Premix membrane emulsification by using a packed layer of glass beads. *Journal of the American Institute of Chemical Engineers*, 54 (8) 2190-2197.
- van der Zwan, E., van der Sman, R., Schroen, K., Boom, R. (2009).** Lattice Boltzmann simulations of droplet formation during microchannel emulsification. *Journal of Colloid and Interface Science*, 335 112-122.
- Vladisavljevic, G.T., Schubert, H. (2002).** Preparation and analysis of oil-in-water emulsions with a narrow droplet size distribution using Shirasu-porous-glass (SPG) membranes. *Desalination*, 144 (1-3) 167-172.
- Vladisavljevic, G.T., Shimizu, M., Nakashima, T. (2004a).** Preparation of monodisperse multiple emulsions at high production rates by multi-stage premix membrane emulsification. *Journal of Membrane Science*, 244 (1-2) 97-106.
- Vladisavljevic, G.T., Lambrich, U., Nakajima, M., Schubert, H. (2004b).** Production of O/W emulsions using SPG membranes, ceramic α -aluminium oxide membranes, microfluidizer and a silicon microchannel plate-a comparative study. *Colloids and Surfaces A: Physicochemical and Engineering Aspects*, 232 (2-3) 199-207.
- Vladisavljevic, G.T., Williams, R.A. (2005).** Recent developments in manufacturing emulsions and particulate products using membranes. *Advances in Colloid and Interface Science*, 113 (1) 1-20.
- Vladisavljevic, G.T., Shimizu, M., Nakashima, T. (2005).** Permeability of hydrophilic and hydrophobic Shirasu-porous-glass (SPG) membranes to pure liquids and its microstructure. *Journal of Membrane Science*, 250 (1-2) 69-77.
- Vladisavljevic, G.T., Williams, R.A. (2006).** Manufacture of large uniform droplets using rotating membrane emulsification. *Journal of Colloid and Interface Science*, 299 (1) 396-402.
- Vladisavljevic, G.T., Kobayashi, I., Nakajima, M., Williams, R.A., Shimizu, M., Nakashima, T. (2007).** Shirasu Porous Glass membrane emulsification: Characterisation of membrane structure by high-resolution X-ray microtomography and microscopic observation of droplet formation in real time. *Journal of Membrane Science*, 302 (1-2) 243-253.

-
- Vladisavljevic**, G.T., Kobayashi, I., Nakajima, M. (2008). Generation of highly uniform droplets using asymmetric microchannels fabricated on a single crystal silicon plate: Effect of emulsifier and oil types. *Powder Technology*, 183 (1) 37-45.
- Wagdare**, N.A., Marcelis, A.T.M., Boen Ho, O., Boom, R.M., van Rijn, C.J.M. (2010). High throughput vegetable oil-in-water emulsification with a high porosity micro-engineered membrane. *Journal of Membrane Science*, 347 (1-2) 1-7.
- Walstra**, P., Smulders, P.E.A. (1998), Emulsion formation. in *Modern aspects of emulsion science*. Cambridge: Royal Society of Chemistry.
- Walstra**, P. (2003). Physical Chemistry of Foods. *Marcel Dekker Inc.*,
- Whitby**, C.P., Fornasiero, D., Ralston, J. (2008). Effect of oil soluble surfactant in emulsions stabilised by clay particles. *Journal of Colloid and Interface Science*, 323 (2) 410-419.
- Williams**, R.A., Peng, S.J., Wheeler, D.A., Morley, N.C. Taylor, D., Whalley, M., Houldsworth, D.W. (1998). Controlled Production of Emulsions Using a Crossflow Membrane: Part II: Industrial Scale Manufacture. *Chemical Engineering Research and Design*, 76 (8) 902-910.
- Wu**, J., Jing, W., Xing, W., Xu, N. (2006). Preparation of W/O emulsions by membrane emulsification with a mullite ceramic membrane. *Desalination*, 193 381-386.
- Vignati**, E., Piazza, R., Lockhart, T.P. (2003). Pickering Emulsions: Interfacial Tension, Colloidal Layer Morphology, and Trapped-Particle Motion. *Langmuir*, 19 6650-6656.
- Yilmaz**, G., Jongboom, R.O.J., van Soest, J.J.G., Feil, H. (1999). Effect of glycerol on the morphology of starch-sunflower oil composites. *Carbohydrate Polymers*, 38 (1) 33-39.
- Yasuno**, M., Nakajima, M., Iwamoto, S., Maruyama, T., Sugiura, S., Kobayashi, I., Shono, A., Satoh, K. (2002). Visualization and characterization of SPG membrane emulsification. *Journal of Membrane Science*, 210 (1) 29-37.
- Yuan**, Q., Aryanti, N., Hou, R., Williams, R.A. (2009). Performance of slotted pores in particle manufacture using rotating membrane emulsification. *Particuology*, 7 (2) 114-120.
- Zhu**, J., Barrow, D. (2005). Analysis of droplet size during crossflow membrane emulsification using stationary and vibrating microchannel silicon nitride membranes. *Journal of Membrane Science*, 261 (1-2) 136-144.